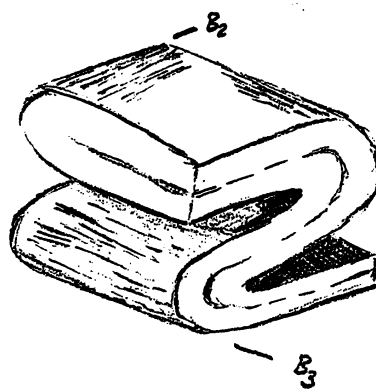


**Mesozoic fold structure of the Otago  
and Alpine Schist Belt  
and its implications  
on the tectonic evolution of  
South Island, New Zealand**



**Maren E. Tünker**

**Mesozoic fold structure of the Otago and Alpine Schist Belt  
and its implications on the tectonic evolution of  
South Island, New Zealand**

Dissertation zur Erlangung des Grades

“Doktor der Naturwissenschaft”

am Fachbereich Geowissenschaften  
der Johannes Gutenberg – Universität in Mainz

Maren Edda Tünker,  
geboren am 19.07.1971  
in Mülheim an der Ruhr

Mainz, Mai 2002

## Erklärung

Ich versichere hiermit, die vorliegende Arbeit selbstständig und nur unter Verwendung der angegebenen Quellen und Hilfsmittel verfasst zu haben.

All views and results presented in this thesis are those of the author, Maren Tünker, unless stated otherwise.

Mainz, Mai 2002

Tag der mündlichen Prüfung: 06.01.2003

## Summary

Re-investigation into the Mesozoic fold structure of the Otago Schist, South Island, New Zealand reveals two successive resembling, asymmetric open to close fold generations with wavelength and amplitude at km-scale ( $F_2$ ,  $F_3$ ) instead of previously assumed nappe or half-folds. Second generation's folds ( $F_2$ ) verge to the NE and the third ones ( $F_3$ ) to the NW. Mesofolds of both generations with a wavelength of dm-scale grow in amplitude and tightness towards the respective major hinge zone on the upper long limb. The asymmetry of the regional folds causes that the recumbent, tight to isoclinal mesofolds of the short limb are disrupted by boudinage on the succeeding lower long limb of the regional fold. This zone of predominant boudinage misleads previous workers to the interpretation of „high strain zones“ or thrust zones. The asymmetric fold style and the resulting boudinage of the long limbs reflect that the shortening direction has a steep plunge either to the NE ( $F_2$ ) or to the NW ( $F_3$ ). Both interfering regional folds with their almost orthogonal oriented fold axes display an intermediate type 1/ type 2 interference pattern, which can be best described as a broad nose structure. The regional fold pattern is variable within the Otago Belt, because the superposed third fold generation grows in amplitude from the SE to the NW, becoming the dominant fold generation in the northwestern Otago Schist Belt.

The superposition of the third fold generations on the second one results in the deformation of the parasitic folds of both fold generations. Where one regional fold generation dominates, all the parasitic hinge lines of this fold generation plunge in the same direction following Pumpelly's law. Interfering major upper long limbs of both asymmetric regional folds cause a variable type 1 to type 2 interference pattern of the parasitic folds depending on their tightness. However, where both regional hinge zones intersect, strain localisation causes the parasitic hinge lines of both generations to rotate towards each other and the interference pattern changes from type 2 to type 3. The orientation of the resulting conical noncylindrical parasitic folds does not stringently imply the orientation of the regional fold axes anymore. But the change from orthogonal to almost coaxial orientation of the interfering parasitic folds infers that the superposed shortening direction is not subparallel but almost enclosing an angle of  $30^\circ$  to the second fold axis to the E.

The Mesozoic fold structure overprints the first object lineation  $L_1$ , which develops syn-deformational and subparallel to intrafolial  $F_1$  folds under moderate high pressure metamorphic conditions. The refolded  $L_1$  lineation rotates within the short limbs of the parasitic folds towards the respective fold axis ( $B_2/B_3$ ), whereas it comes to lie at a higher angle to the fold axis on the parasitic fold limbs (type 2 geometry of Ghosh & Chatterjee (1985)).  $L_1$  is generally strengthened on the short limbs displaying an N-S to NE-SW trend. However, reconstruction of the refolded linea-

tion patterns reveals that the initial rectilinear  $L_1$  trends in ENE-WSW direction on the main foliation  $S_1$ .

The Cenozoic overprint of the transpressional Alpine Fault System causes a two-sided fold and thrust belt. The Mesozoic fold structure ( $F_2/F_3$ ) is folded in N-NE trending long wavelength syn- and antiforms. At the tip line of the reverse faults, the Mesozoic fold structure is steepened and shortened orthogonal to the previous main foliation resulting in strongly foliated rocks. The former inclined to recumbent Mesozoic mesofolds are rotated to upright folds, where the fold axis is subparallel to the Cenozoic fold axis, or to vertical folds, where the fold axis is oblique to the Cenozoic fold axis. In the Otago Belt, the fold and thrust belt is widely spaced, where the foliation remains flat and only rotates to a steeper dip in the vicinity of a reverse fault. Towards the Alpine Fault the fold and thrust belt gets continuously more narrowly spaced. In the Alpine Belt the upright Cenozoic fold structure can be subdivided in extensive zones of steeply dipping foliation, respectively the limbs and synforms of the steepened folds adjacent to the reverse faults, and antiforms, where the Mesozoic foliation remains flat. Consequently the Cenozoic structure of the Otago and Alpine Belt reflects an asymmetric large scale flower structure with an uplifted and tilted western wing in the vicinity of the Alpine Fault.

## Zusammenfassung

Erneute Untersuchungen der mesozoischen Faltenstruktur des Otago Schiefergürtels, Südinsel, Neuseeland, zeigen, dass diese aus zwei aufeinander folgenden, ähnlichen, asymmetrischen, offenen bis mäßig engen Großfaltengenerationen im km-Größenbereich besteht anstatt aus den vorher angenommenen Decken- oder Halbfalten. Großfalten der zweiten Generation vergieren nach Nordost ( $F_2$ ), der dritten Faltengeneration ( $F_3$ ) nach Nordwest. Asymmetrische, offene Kleinfalten mit einer Wellenlänge im dm-Bereich wachsen in der Amplitude auf dem Langschenkel der Großfalte zu symmetrischen, liegenden, engen bis isoklinalen Kleinfalten im Scharnier. Selten zeigen die liegenden Kleinfalten auf dem Kurzschenkel einen Wechsel der Vergenz an. Die Asymmetrie der Großfalten führt dazu, dass die engen, liegenden Kleinfalten auf dem folgenden liegenden Langschenkel boudiniert werden. Diese Zone mit vorherrschender Boudinage wurde von vorherigen Bearbeitern als "starke Verformungszone" oder Überschiebungszone missdeutet. Der asymmetrische Faltenstil und die daraus entstandene Boudinage am Übergang vom Kurz- zum Langschenkel der Großfalte widerspiegeln eine steil einfallende Verkürzungsrichtung entweder nach Nordost ( $F_2$ ) oder Nordwest ( $F_3$ ). Die annähernd orthogonal orientierten Faltenachsen beider Großfaltengenerationen beschreiben ein Interferenzmuster zwischen dem ersten und zweiten Typ, abhängig vom Öffnungswinkel der Großfalten beider Generationen. Das Interferenzmuster variiert im Otago Schiefergürtel, weil die überprägende, dritte Faltengeneration in der Amplitude vom Südosten zum Nordwesten wächst. Im Nordwesten des Otago Schiefergürtels ist die dritte Faltengeneration ( $F_3$ ) dominant.

Die Überprägung der dritten Faltengeneration auf die zweite beeinflusst die Orientierung der Kleinfalten beider Generationen aller Ordnungen. Wo eine Großfalte dominiert, widerspiegelt die Raumlage der Kleinfalten Pumpellys Gesetz folgend die Orientierung der vorherrschenden Großfalte. Auf den Langschenkeln beider Großfaltengenerationen verfallen sich die Kleinfalten im Interferenzmuster des ersten bis zweiten Typs, abhängig vom Öffnungswinkel der Kleinfalten. Wo jedoch zwei Scharniere beider Großfaltengenerationen aufeinander treffen, führt der erhöhte Verformungsdruck dazu, dass die Faltscheitellinie der Kleinfalten beider Generationen aufeinander zu rotieren und somit das Interferenzmuster vom zweiten zum dritten Typ wechselt. Die Orientierung der hieraus entstandenen konischen, nichtzylindrischen Kleinfalten widerspiegelt nicht unbedingt mehr die Raumlage der Großfalten. Aber der Wechsel vom orthogonalen zum koaxialen Interferenzmuster der Kleinfalten lässt folgern, dass die überprägende Verkürzungsrichtung der dritten Faltengeneration ( $F_3$ ) nicht subparallel zur zweiten Faltenachse ( $B_2$ ) ist, sondern einen Winkel von rund  $30^\circ$  in östlicher Richtung einschließt.

Die mesozoischen Faltenstruktur überprägt die erste Objektlineation  $L_1$ , welche sich subparallel zur Faltenachse ( $B_1$ ) der ersten intrafolialen Falten ( $F_1$ ) unter mäßigen Hochdruck- Metamorphosebedingungen bildete. Die verfaltete erste Lineation  $L_1$  rotiert auf dem Kurzschenkel der Kleinfalten zu und auf den Langschenkel weg von der jeweiligen Faltenachse ( $B_2, B_3$ ).  $L_1$  wird verstärkt auf dem Kurzschenkel und zeigt hier eine vorherrschende N-S bis NE-SW verlaufende Richtung. Rekonstruktionen dieses verfalteten Lineationsmusters zeigen jedoch, dass  $L_1$  vor der Verfaltung geradlinig in ENE-WSW Richtung auf der Hauptschieferung  $S_1$  verlief.

Das känozoisch entstandene, transpressionale Alpine Störungssystem bildet einen zweiseitigen Falten- und Überschiebungsgürtel im Otago und im Nordwesten anschließenden Alpen Schiefergürtel. Die mesozoischen Falten generationen ( $F_2, F_3$ ) sind in N-NE verlaufenden, großmaßstäblichen Mulden- und Sattelstrukturen verfaltete. An der Überschiebungsfront wird die mesozoische Faltenstruktur verkippt und verkürzt. Vorher geneigte bis liegende, mesozoische Kleinfalten werden zu aufrechten Falten rotiert, wenn die Faltenachse ( $B_2, B_3$ ) subparallel zur känozoischen Faltenachse orientiert ist. Kleinfalten, deren Faltenscheitellinie ( $B_2, B_3$ ) einen großen Winkel zur känozoischen Faltenachse einnehmen, werden zu annähernd vertikalen Falten verkippt. Im Otago Schiefergürtel liegen die Störungszonen so weit auseinander, dass die Hauptfoliation  $S_1$  vorwiegend flach einfallend bleibt und nur lokal an den Überschiebungsfronten verkippt wird. Zur Alpen Störung hin werden die Störungszonen engständiger. Im Alpen Schiefergürtel kann die känozoische Faltenstruktur in ausgedehnte Bereiche mit steil einfallender Foliation, die die Schenkel und Mulden in der Nähe der versteilten Überschiebungen darstellen, und in Sättel, wo die ursprünglich subhorizontale Raumlage der mesozoischen Faltenstruktur erhalten blieb, unterschieden werden. Die känozoische Struktur des Otago und Alpen Schiefergürtels widerspiegelt ein asymmetrisches, großmaßstäbliches Störungssystem, das einen an einen Palmenbaum erinnert, wobei der westliche Teil des Störungssystemes verkippt wurde.

## **Content**

<b>Summary</b>	<b>3</b>
<b>Zusammenfassung</b>	<b>5</b>
<b><i>Chapter 1</i></b>	
Haere Mai Aotearoa	<b>8</b>
Background, problems and aims – or why am I here?	<b>12</b>
<b><i>Chapter 2</i></b>	
Regional folds and their implications on the tectonic evolution of the Otago Schist Belt	<b>16</b>
<b><i>Chapter 3</i></b>	
Do parasitic folds predict the orientation of a larger fold?	<b>48</b>
<b><i>Chapter 4</i></b>	
Superposed folding of an early lineation – is it possible to reconstruct the initial rectilinear orientation?	<b>66</b>
<b><i>Chapter 5</i></b>	
Tilting of regional folds in a superposed fold and thrust belt- a continuous tectonic concept for the Otago and Alpine Schist Belt	<b>85</b>
<b><i>Chapter 6</i></b>	
Late Paleozoic to Cenozoic tectonic development of South Island, New Zealand	<b>112</b>
<b><i>Appendix</i></b>	
Mathematica subprogram written by Moore & Johnson (2000)	<b>130</b>
<b>References</b>	<b>141</b>
<b>Acknowledgement</b>	<b>157</b>
<b>Curriculum Vitae/ Lebenslauf</b>	<b>158</b>



# Chapter 1

## Haere Mai Aotearoa – Welcome in the Land of the Long White Cloud

The name Aotearoa was given especially for the North Island of New Zealand by the first Maori arrivals. They left Hawaiiki – the homeland of the Polynesian – on their voyage of discovery to Aotearoa (the Land of the Long White Cloud). Dozens of Maori myths are known from the creation of earth and sky, the birth of gods and the development of biota. To introduce the reader to see New Zealand with the eyes of the Maori, two myths are chosen, which describe the creation of New Zealand.



*Fig. 1.1: North and South Island of New Zealand*

### *The story of creation*

In the beginning there was nothing. All was darkness (Te Po). Out of the first glimmer of light (Te Ao), long standing light (Te Aoturoa) emerged until it stood in all quarters. Encompassing everything was a womb of emptiness, an intangible void (Te Kore – the Nothingness). This void was intense in its search for procreation. Finally it reached its ultimate boundaries and became a parentless void (Te Korematua) but with potential for life. And so Te Maku, moisture, emerged and coupled with Mahoranuiatea, a cloud that grew from the dawn. From this union came Raki, the heavens or the Sky father, who coupled with Poharua Te Po, the breath of life found in the womb of darkness. The first child in this chain of creation was Aoraki, the cloud in the sky.



**Fig. 1.2:** **a)** *The celestial brothers sit on their canoe turning to stone and earth in the process (drawing taken from a hand-out of the Department of Conservation 1999).* **b)** *The majestic calm of the setting sun belies the power and sometimes aggressive nature of New Zealand's highest peak, Mount Cook (3754m). Mount Tasman to the left (taken from kiwivista postcard).*

At this time there was no Aotearoa. The waters of Kiwa rolled over the place now occupied by New Zealand - the South Island, the North Island and Stewart Island. No sign of land existed. Raki (the Sky father) wedded Papa-tua-nuku (the Earth Mother). After the marriage, some of the Sky children came down to greet their father's new wife. Among the celestial visitors four sons of Raki who were named Ao-raki (Cloud in the sky), Raki-roa (Long Raki), Raki-rua (Raki the second), and Raraki-roa (Long Unbroken Line). They came down in a canoe, which was known as Te Waka O Aoraki (Aoraki's canoe). They cruised around the Earth Mother - Papa-tua-nuku, who lay as one body in a huge continent known as Hawaiiiki. Then, keen to explore, the voyagers set out to sea, but no matter how far they travelled, they could not find land. They decided to return to their celestial home, but the incantation, a karakia, which should have lifted the waka (canoe) back to the heavens failed and the canoe fell back into the sea and turned over onto its side, turning to stone and earth in the process. The waka listed and settled with the western side much higher out of the water than the east. Thus the whole waka formed the South Island, hence the name: Te Waka O Aoraki. Aoraki and his brothers clambered on to the high side and were turned to stone. They are still there today. Aoraki is the highest mountain of South Island known as Mount Cook, and his brothers are the next highest peaks near him - Rakiroa (Mount Dampier), Rakirua (Mount Teichelmann), and Rarakiroa (Mount Tasman).

(Taken from a hand-out of the Department of Conservation 1999)

### *Te Ika A Maui - The fish of Maui*

Maui was a demi-god, who lived in Hawaiiiki. He was the youngest of four brothers. They were jealous of him and afraid of his magic powers. One night he heard his brothers talking about going fishing and they decided to go without him. It is known that Maui was not a good fisherman. His brothers were much more skilled. Some say that Maui stole the fishing of his brothers. Maui proceeded to hide in the canoe. Early the next morning the brothers sneaked down to the sea at dawn and thought to get away before Maui saw them. When they had been paddling for quite a while Maui left his hideout. The brothers grumbled and were resentful of Maui. They would not share their bait. Not to be defeated Maui punched his own nose and smeared the curdled blood onto his fishhook - the magic jawbone of his grandmother that he had brought along. It hung in the air for a moment and then sunk down deep into the ocean. Chanting a spell of power, he commanded the hook to catch a big fish. The hook lodged itself into a magnificent great fish. Maui pulled and the fish pulled. They had a great battle. Maui called his brothers for assistance. But they were scared and they begged him to let the fish go. Maui refused and began to chant an incantation, a karakia, to help him land his fish. There it lay this glorious fish. The brothers jumped upon its back and gazed in awe. Maui said they should not pound his fish and he dived into the ocean to thank Tangaroa, the God of the sea, for this bounty. But of course his greedy brothers started hacking away at the magnificent great fish. Wherever they could, they cut great

valleys and formed mountains. Te Ika A Maui – Maui's fish is the name of North Island. If you look closely at the map of North Island, you will see that it is shaped much like a giant fish, maybe a stingray, the mouth in the south and the tail fin in the north.

Maui also fished up the South Island, which is known as Te Waka a Maui (the canoe of Maui). Stewart Island, which lies at the very bottom of New Zealand, is known as Te Punga O Te Waka A Maui (Maui's anchor), as it was the anchor which held Maui's waka as he was pulling in the giant fish.

(Compiled from different websites: [www.history-nz.org](http://www.history-nz.org), [www.kiwianaz-site.cityslide.com](http://www.kiwianaz-site.cityslide.com), [www.mauigate-way.com/~rw/myths1.htm](http://www.mauigate-way.com/~rw/myths1.htm))

## Background, problems and aims – or why am I here?

### 1.1. Short introduction to South Island, New Zealand

Two active continental margins with opposite subduction polarity occur at each end of South Island, New Zealand (fig. 1.3). In the north, on the eastern side of the North Island, the Pacific plate is subducted under the Australia plate at the Hikurangi Trench, which continues further north into the Kermadec Trench. In the south, relative young oceanic crust of the Australia plate is subducted at the Puysegur Trench. In the southwest Pacific region, the oceanic crust of both the Australia and Pacific plate obtains a Late Cretaceous age determined by the magnetic anomaly lineation number 33 (= 77Ma; Kamp 1986b). The link between these two margins, the dextral transcurrent Alpine Fault, causes a zone of advanced and active, oblique continental collision (Kamp et al. 1989, Norris et al. 1990, Koons & Henderson 1995, Casas et al. 2001). The crust involved in this collision has a long history of vertical and horizontal mobility.

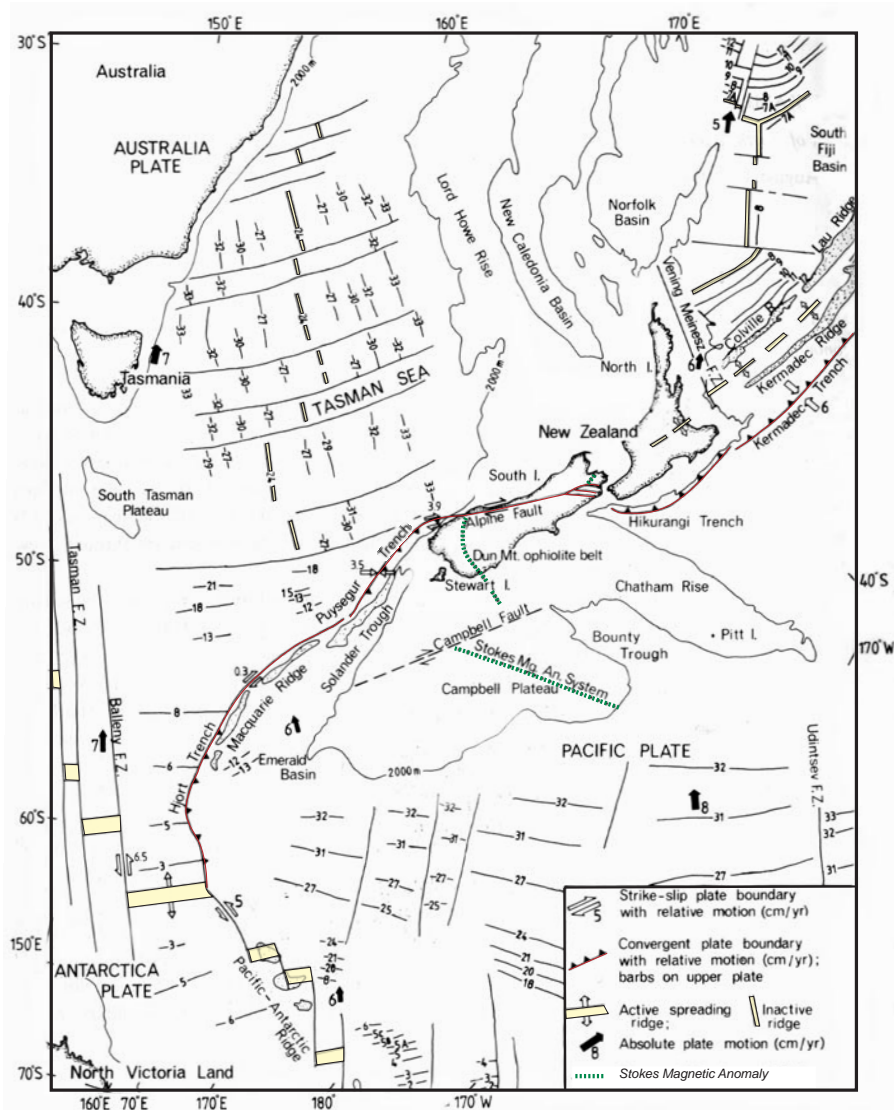


**Fig. 1.3:** Map of the southwest Pacific region showing the present-day changing tectonic character of the Australia-Pacific plate boundary (based on Kamp 1986b, Figure 1).

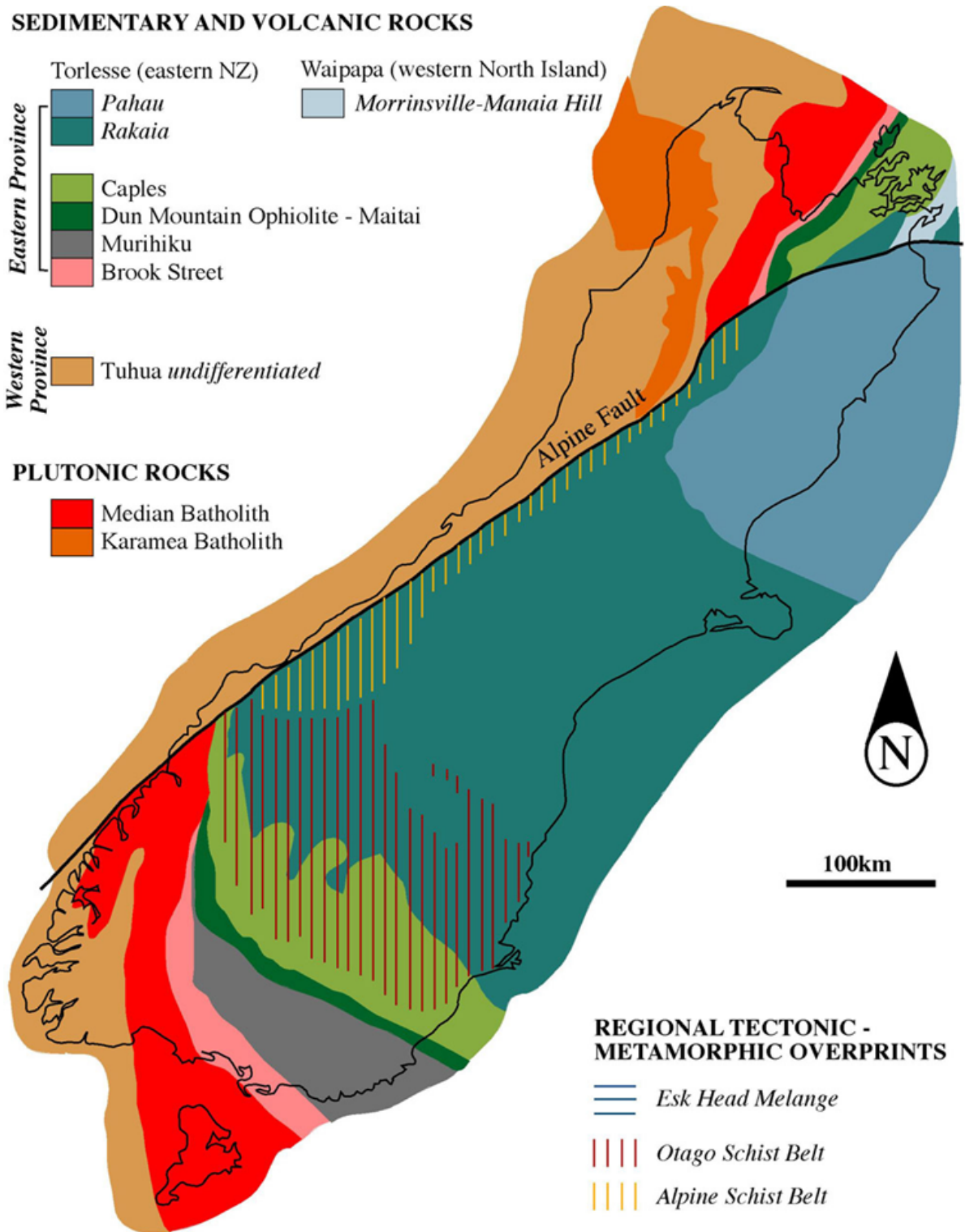
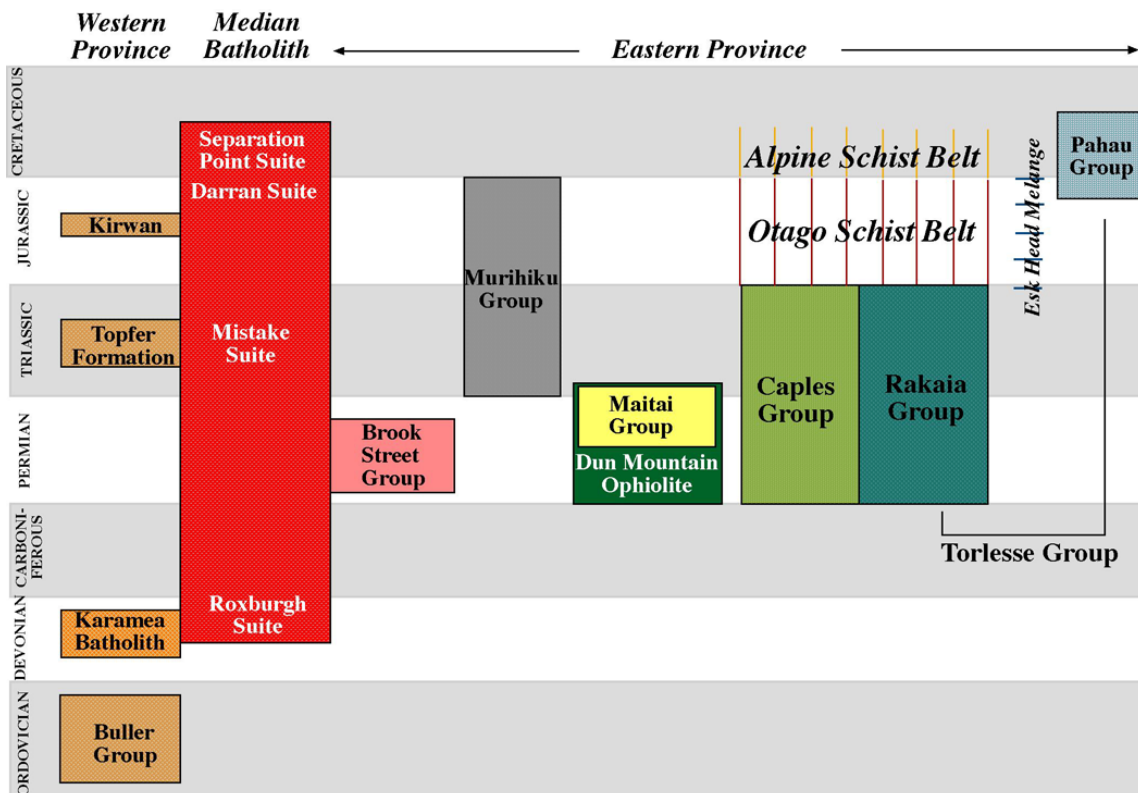


Fig. 1.4: Tectonostratigraphy of the South Island, New Zealand (based on Turnbull 2000, Figure 3)

The Western Province (fig. 1.4, 1.5), which comprises mainly Paleozoic rocks at the western side of South Island, is related to Gondwana margin (Mortimer 1995, Mortimer et al. 1999b). Both the Median Batholith and the Eastern Province form in a long-lived and evolving subduction zone along the Late Paleozoic-Mesozoic margin of Gondwana. The Median Batholith intrudes into both the Western and the Eastern Province comprising calc-alkaline to adakitic magmatic rocks (Mortimer et al. 1999b). The Eastern Province (fig. 1.4, 1.5) consists of different Late Paleozoic to Mesozoic rocks (e.g. Coombs et al. 1976, Kimbrough et al. 1992, Mortimer 1993b): both the Permian volcanic arc and basin complex of the Brook Street Group and the Permian-Early Triassic ophiolite sequence and related sediments of the Dun Mountain – Maitai Group are overlain by the forearc basin fill of the Murihiku Group. To the north occur the volcanoclastic sediments of the Caples Group and the quartzofeldspathic sediments of the Rakaia Group (older Torlesse, fig. 1.4, 1.5). Both sedimentary groups are considered to be evolved as a Permian-Jurassic accretionary complex. The metamorphosed and highly deformed parts are subdivided into the Otago and the Alpine Schist Belt (fig. 1.4, 1.5). The Esk Head Melange separates the Rakaia Group (older Torlesse) from the Pahau Group (younger Torlesse). The Pahau Group builds up a Late Jurassic-Early Cretaceous accretionary complex (fig. 1.4, 1.5).



**Fig. 1.5:** Schematic summary of units comprising the Western and Eastern Province and the Median Batholith (time axis not to scale, based on Mortimer 1995, Figure 2 and Turnbull 2000, Figure 10). The sedimentary and volcanogenic formations of the Western Province are further differentiated showing the chronology.

## 1.2. Questionnaire

My thesis focuses on the tectonic evolution of the Caples and Rakaia Group (older Torlesse). Several studies about this topic are published over the last decades reflecting changing theories and advanced techniques. But studying this literature, one question arises from another. There always remains the question of the juxtaposition of the Caples and Rakaia Group. Is the sedimentation area of both groups continuous (e.g. Korsch & Wellman 1988, Mortimer & Roser 1992) or do both groups amalgamate during a collisional event in a subduction process (e.g. Coombs et al. 1976, Norris & Craw 1987)? Moreover, can both groups be classified as terranes (e.g. Coombs et al. 1976, Norris & Craw 1987)? My attempt to answer these questions is summarised in *chapter 2 and 6*.

The main focus of my thesis is the Mesozoic fold structure of the Caples and Rakaia Group within the Otago Schist Belt. Especially the interpretations of this fold structure reflect the changing theories over the last decades – from recumbent macroscopic folds (Means 1966, Wood 1978) via nappe folds (Craw 1985, Cox 1991) to a- type folds (Mortimer 1993b) and recently sheath folds (Gray et al. 1995). An overview on the development of the regional folds is given in *chapter 2*, whereas *chapter 3* is a closer look at the relationship between parasitic and macroscopic folds. Focussing on the problem: what happens to the parasitic folds of an early and a superposed generation when both regional folds of these generations intersect?

The effect of an early lineation on the Mesozoic fold structure is dealt with in *chapter 4*. Can the initial rectilinear orientation of the early lineation be reconstructed? And what is the trend of this initial orientation?

Another point, what happens to the Mesozoic fold structure in the Cenozoic? In *chapter 5* the influence of the Late Cenozoic Alpine transpressional fault system on the Mesozoic fold structure is discussed. On the one hand the known Mesozoic fold structure of the Otago Belt is compared to the Alpine fold structure to solve the question, whether both experience the same development during Mesozoic times. On the other hand the comparison shows the different extent of the Cenozoic deformation in the Otago and Alpine Belt. A long-discussed problem in regional tectonics of South Island is the bending of the Eastern Province rocks towards the Alpine Fault. Are the Eastern Province rocks bent by collisional events during Mesozoic times (Wood 1978, Kamp 1987) or by the dextral movement on the Alpine Fault (Hunt 1978, Korsch & Wellman 1988, Sutherland 1999)?

*Chapter 6* concludes the results of my thesis and presents the renewed tectonic evolution of the Otago and Alpine Belt in relation to the regional geology of the South Island.

This thesis is written form of papers, only the regional context is omitted in chapter 3 and 4 because it has been easier for me to focus on the diverse topics of my thesis.



## Chapter 2

*“groß ist nur was man nicht erkennen kann und größer noch was man nicht begreift”  
(Sven Regener 2001)*



*View over the Manorburn Valley towards the Upper Manorburn Dam – the valley coincides here with a vergence boundary of the second fold generation (NE vergent folds to the S (right) and SW vergent folds to the N (left)).*



*(see caption next side)*

## Chapter 2

*View from the Coronet Peak ski station towards the S showing the northern and western flank of the Remarkables Mountains (on the eastern or left hand side), the Kelvin Heights and the Lake Wakatipu (on the western or right hand side). The northern flank of the Remarkables outline a regional fold of the second generation, whereas the western flank displays a regional fold of the superposed third fold generation.*

*The Maori gave these mountains the name of Kawarau, now given to the outlet river of the Lake Wakatipu. Pakiwaitara (legends) talk of monsters in unknown lands beyond this range and atua (gods) that inhabited the peaks. Traditionally it was inappropriate to climb to the mountain tops as you would then be placing yourself higher than the gods whose domain it was.*



*View from the Treble Cone ski station over the Matukituki Valley towards the Lake Wanaka – a view over a vergence boundary of the third fold generation (SE vergent folds at the ski station and NW vergent folds down in the Matukituki Valley).*

## **Regional folds and their implications on the tectonic evolution of the Otago Schist Belt**

### **Abstract**

Re-examination of the Mesozoic fold structure in the Otago Schist Belt reveals two successive fold generations with wavelength and amplitude at km-scale ( $F_2$ ,  $F_3$ ). Mesofolds of both resembling generations with a wavelength of dm-scale grow in amplitude and tightness towards the respective major hinge zone on the upper long limb. Tight to isoclinal mesofolds of the short limb are disrupted by boudinage on the succeeding lower long limb of the regional fold. The change of appearance, vergence and interlimb angle of parasitic mesofolds outlines open to close asymmetric regional folds, second generation's folds ( $F_2$ ) verge to the NE and the third ones ( $F_3$ ) to the NW, both developed by a combined buckling and flattening process. Both interfering regional folds with their almost orthogonal oriented fold axes display an intermediate type1/ type 2 interference pattern. The regional fold pattern is variable within the Otago Belt, because the superposed third fold generation grows in amplitude from the SE to the NW, becoming the dominant fold generation in the northwestern Otago Schist Belt.

### **2.1. Introduction**

Fold classification is based on geometric features, generally termed fold style (Ramsay 1967, Ramsay & Huber 1987, p. 309). Variations in fold style are invariably linked with differences in the mechanical origin of the structures and especially with the rheological state of the rocks during the folding process. Consequently, folds developed during one deformation phase in lithologic monotonous series of rock, as the Otago Schists, have a uniform style and can be grouped in one fold generation. Slight variations in amplitude, interlimb angle and frequency of folding display that folds are developed parasitically on the back of a macroscopic fold (Pumpelly et al. 1894, Turner & Weiss 1963, Ramsay & Huber 1987, p.320, 454).

Different fold generations are established by overprinting relationships (see Weiss 1959, Turner & Weiss 1963). This methodology is problematic in areas where more than one generation of structure has the same style or overlapping ranges of varying style (Park 1969, Williams 1985). In the Otago Schist Belt the same style of two fold generations leads to an underestimation of the extent of one fold generation. As a basic approach, measuring the orientation and vergence of folds can be a useful tool leading to the existence and orientation of an interference pattern (Ramsay 1967, pp. 520-553, Passchier et al. 1981, Williams 1985). The orientation analysis is used on the Mesozoic fold structure of the Otago Belt despite the fact that Craw (1985) notes that orientations of the folds are highly diverted and no distinct result can be expected. Certainly, various orientations occur, not only due to superposition of a younger fold generation on an older one, but as well within one fold generation. Diverted orientations result from:

- changing intensity and extent of one fold generation, especially on regional scale
- various thickness, extent or competence contrast of layers like extensional veins
- fanning of convergent/divergent axial fold planes

- refolding of early hinge lines leads to diverted orientations not only of the early hinge lines but as well of the superposed ones
- rotation of early lineations due to superposition of folds
- diverted hinge lines of parasitic folds due to superposition of larger folds, especially on regional scale

The analysis of the Mesozoic fold structure shows that the highly diverted orientations recorded by Craw (1985) display an interference pattern of two resembling folds. Although the orientation diverts somewhat on mesoscopic scale, the orientation of the regional folds of both generations exists over areas of large extent as previously Brown (1968) notes. Two main sets of folds are observed in the Otago Schist Belt, the first set with hinge lines trending NW-SE and the second superposed set with hinge lines trending NE-SW. Observed repetition of certain fold and interference patterns results in a new model of intersecting open to close asymmetric regional folds, the first set mainly verging to the NE and the second superposed set verging to the NW. Implications of the new model of regional folds on the tectonic evolution of the Otago Schist Belt are discussed.

### *2.1.1. Geological setting*

The Otago Schist Belt consists of Torlesse rocks in the northern and Caples rocks in the southern part forming an approximately 150km-wide two-sided arch (fig. 2.1a). Both rock types comprise Permian to Triassic greywacke and argillite, the Caples with a dominantly volcanoclastic composition (MacKinnon 1983, Roser et al. 1993) and the Torlesse with a dominantly quartzofeldspathic composition (MacKinnon 1983, Bradshaw 1989, Roser & Korsch 1999). The lithologic monotonous series of Caples and Torlesse rocks are intercalated by rare dm- to m-thick bands of greenschist and quartzite (Mortimer 1993b). Metamorphism increases from prehnite-pumpellyite facies in the nonschistose rocks on the flanks of the arch to greenschist facies in the schistose rocks near the centre (Mortimer 1993b, fig. 2.1b). Remnants of an earlier blueschist facies metamorphic event (Yardley 1982) in the central part of the Otago Schist show peak metamorphic temperatures and pressures of 350-400°C and 8-10kbar (Mortimer 2000). The peak of Otago Schist metamorphism might have occurred in the Early to Middle Jurassic (Adams & Robinson 1993, Little et al. 1999). Rocks of the northwestern part of the Otago Belt are overprinted by a Barrovian-type metamorphism, which increases towards the Alpine Fault (Adams & Gabites 1985, White 1996, Mortimer 2000, fig. 2.1b). According to the increase in metamorphic grade towards the central axis of the Otago Schist Belt, an increase in deformation occurs, described as textural zones (Bishop 1974, Norris & Bishop 1990, Turnbull et al. 2001; fig. 2.1c). The subdivision in textural zones is based on white mica grain size, foliation and segregations development (Turnbull et al. 2001). From textural zone I to IV the foliation strengthens, white mica grow and segregations evolve.

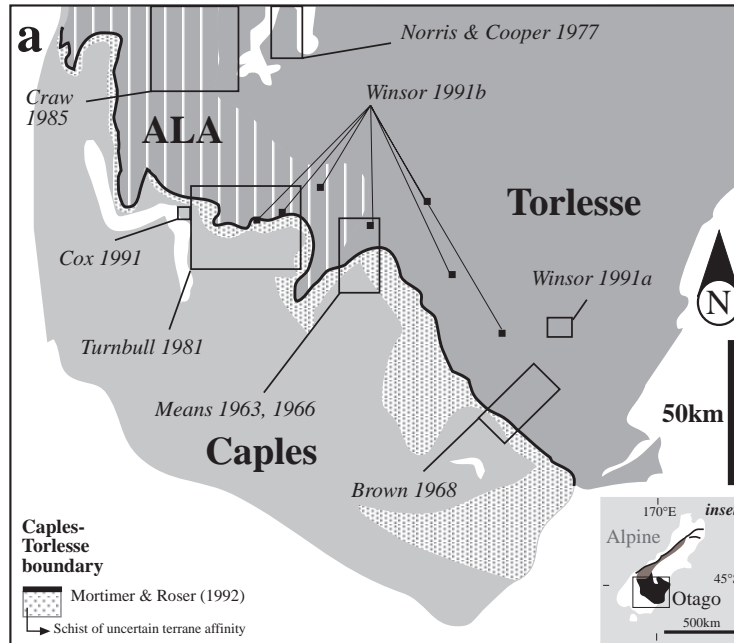


**Fig. 2.1: a)** Geological setting of the Otago Schist Belt (based on Mortimer & Roser (1992)); small inset shows the location of the Otago Schist Belt in relation to South Island, New Zealand). Boxes indicate locations studied by previous workers. See text for further information.

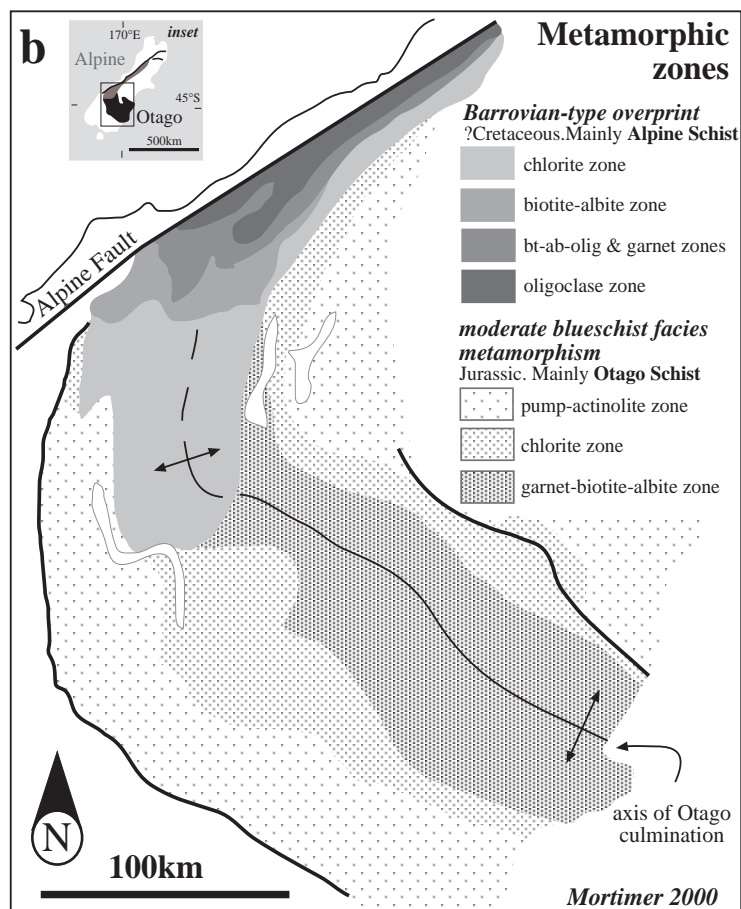


**Fig. 2.1: b)** (see caption next page)

**Fig. 2.1: b)** Metamorphic zones within the Otago and Alpine Schist Belt (map based on Mortimer (2000)). Metamorphism in the Otago Schist Belt increases from prehnite-pumpellyite facies in the nonschistose rocks on the flanks of the arch to greenschist facies in the schistose rocks near the centre (Mortimer 1993b, 2000). Remnants of a blueschist facies metamorphic event (Yardley 1982) in the central part of the Otago Schist show peak metamorphic temperatures and pressures of 350°- 400°C and 8-10kbar (Mortimer 2000). Towards the Alpine Fault a younger Barrovian-type metamorphism overprints the Jurassic metamorphism. The metamorphic overprint increases up to amphibolite facies metamorphism towards the Alpine Fault. The boundary between Alpine and Otago Schist Belt is defined by the incoming of the new-grown biotite (Mortimer 2000).

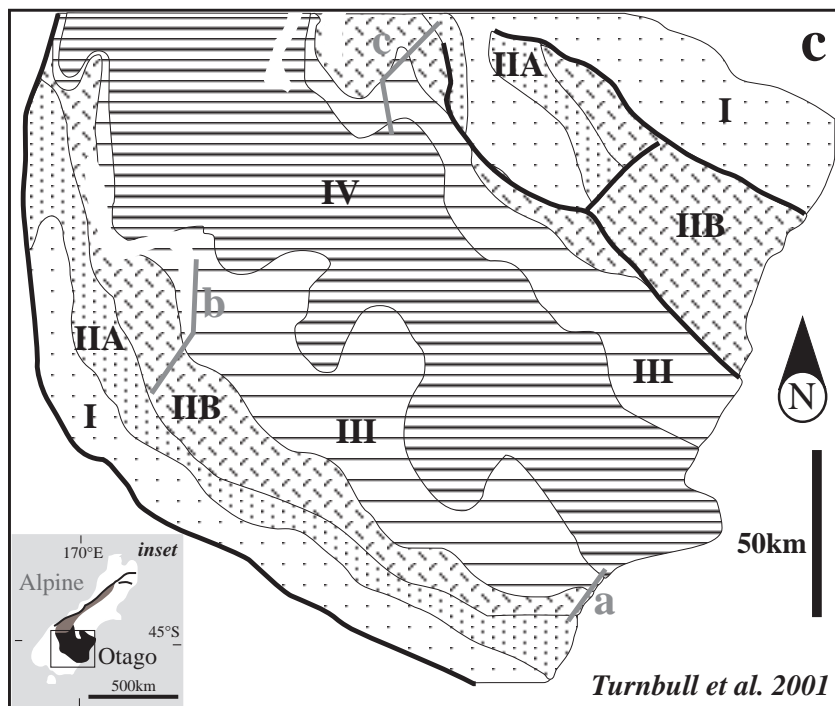


**Fig. 2.1: c)** Distribution of the textural zones I-IV in the Otago Schist Belt (based on Turnbull et al. 2001, inset shows the location of the Otago Belt in relation to South Island, New Zealand). Lines indicate the cross-sections chosen to describe the extent of the second and third fold generation ( $F_2/F_3$ ). See text for further information (section 2.1.1. and 2.4.5.).

### 2.1.2. Former concepts of regional folding in the Otago Belt

The pioneering investigation of the structure of the Otago Schist of Turner (1936-1942, see references in Wood (1978)) leads to the interpretation of macroscopic folds of one generation but the nature of them is obscure. During mapping of huge parts of the Otago Schist Belt, Wood (1963) and Grindley (1963) postulate a concept of recumbent regional folds in the schist. The principal basis for this interpretation is the observation that opposite limbs of a large fold bear small folds having opposite senses of asymmetry or vergence. Further investigations of Means

(1966) show that the axial planes of the mesofolds change gradually in orientation from gentle dips at the vergence boundary to dips in opposite direction on each side of the boundary (fig. 2.1a, 2.2a). Furthermore the enveloping surfaces dip gently towards the vergence boundary on either side of it and become subvertical in the zone of vergence change. Consequently Means (1966) adopts the model of large recumbent folds (Wood 1963) as a satisfactory working hypothesis, but he notices that there is a possible fanning of the axial planes, and as well different areas of different fold geometry and superposition's. Wood (1978) reaffirms later his model of regional folds and describes them as recumbent E verging folds, which are tilted at the flanks of the Otago Belt (fig. 2.2b).

The studies of Brown (1968) and Turnbull (1981) strengthen the interpretation of recumbent regional folds of one generation (fig. 2.1a, 2.3). But both workers remark that these regional folds ( $F_2$ , fig. 2.3) are locally overprinted by a resembling fold generation ( $F_3$ , fig. 2.3), an approach followed up in this study. Furthermore this study takes into account the observation of Brown (1968) that the orientation of the folds is constant over large areas but that locally parasitic hinge lines successively rotate towards each other becoming coaxial (*see section 2.4.3. and chapter 3*).

Winsor (1991b) tries to re-classify these resembling mesoscopic fold generations (fig. 2.1a, 2.3). He differentiates between fold axes oriented parallel or oblique to a former mineral elongation direction, a questionable classification because previous formed lineations tend to rotate towards a superposed fold axis within a hinge zone (Ramsay 1960, 1967, Ghosh & Chatterjee 1985, Ramsay & Huber 1987). Neither an interference pattern, nor a regional fold concept is described by Winsor (1991a,b).

Craw (1985) differentiates the observed Mesozoic fold structure in two regions, W and E of the Moonlight Fault (fig. 2.1a, 2.3). W of the Moonlight Fault the regional folds ( $D_2$ ) are vertical, locally overprinted by a younger fold generation, whereas E of the Moonlight Fault the regional folds ( $D_3$ ) are recumbent. Consequently Craw (1985) correlates his third generation of folds ( $D_3$ ; fig. 2.3) to the second fold generation ( $F_2$ ) of Means (1963, 1966). His correlation entices some workers to rename the first foliation as a second one (Winsor 1991a,b (fig. 2.3), Mortimer 1993b). Craw (1985) describes the recumbent regional folds as being formed as nappe-like folds with highly sheared lower limbs ("high strain zones"). He remarks that the mesofolds successively tighten toward the inferred lower limb showing a continuous transition into "high strain zones", where the fold hinges and lineations rotate towards a transport direction.

Cox (1991) adopts the model of Craw (1985) and compares the regional fold of the Remarkables Mountains (fig. 2.1a, 2.2c;  $D_2$ , fig. 2.3) with the Morcles Nappe, Switzerland (Ramsay et al. 1983, Ramsay & Huber 1987, p. 377). Ramsay et al. (1983) outline the structure of the Morcles Nappe as a development of minor folds in the hanging wall anticline of a propagating thrust fault. Because the maximum shear strain was concentrated along the base of the nappe, the minor folds maybe reverse their asymmetry due to the imposed simple shear (passive shear folding, Ramsay et al. 1983).

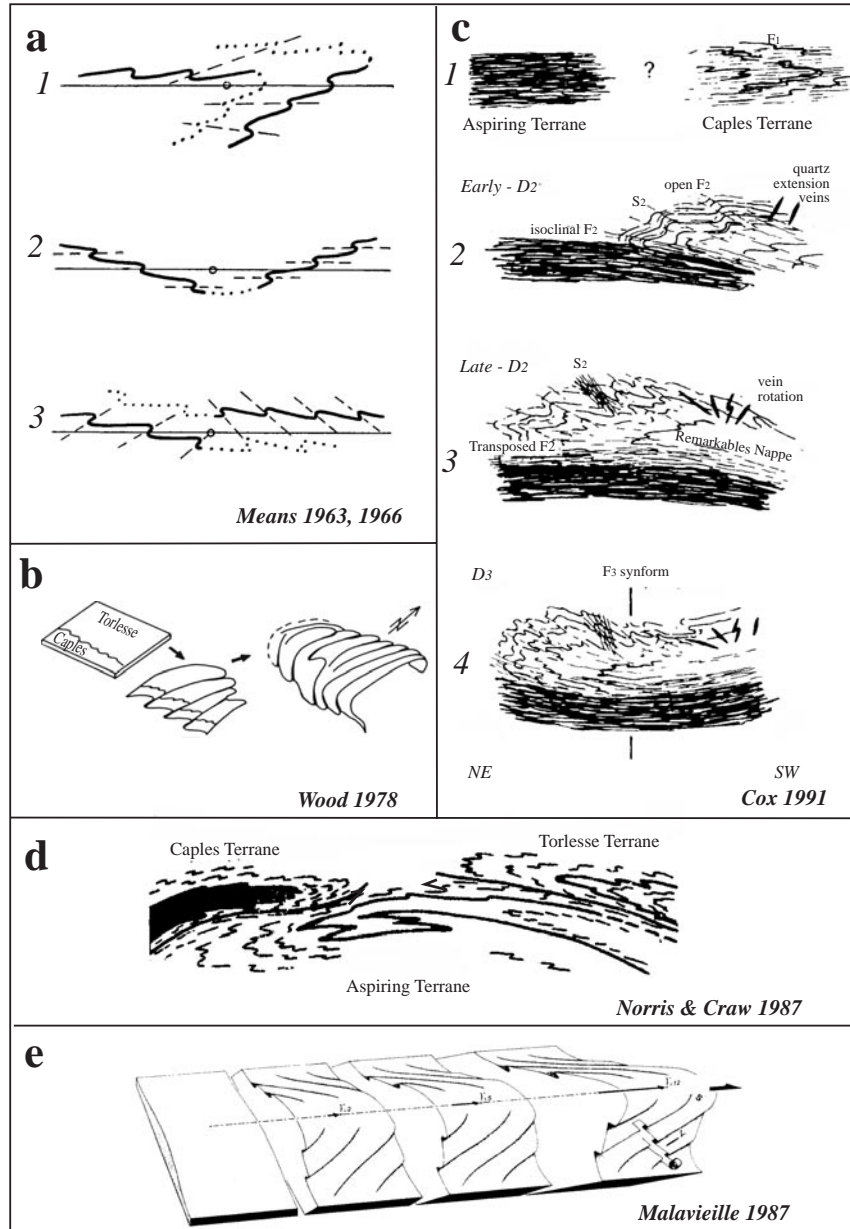


**Fig. 2.2:** Former models of regional folds in the Otago Schist Belt: **a)** Several interpretations of a vergence boundary after Means (1966, Figure 5), who defines the vergence boundary as (1) a trace of the axial plane of a recumbent fold, (2) a trace of the axial surface of an open flexure predating F<sub>2</sub> or (3) a centre of a conjugate fold system (after Johnson 1956). **b)** Wood (1978, Figure 4) describes regional recumbent E vergent folds, which are successively tilted at the flanks of the Otago Schist Belt. **c)** Cox (1991, Figure 11) considers that the regional folds develop as nappe folds at the example of the northern flank of the Remarkables Mountains assuming overall simple shear: (1) Caples terrane overthrusts onto Aspiring terrane, (2) open buckle folds at the nose of the nappe, (3) further tightening of the folds near to the thrust zone, (4) postmetamorphic overprinting. Note that Cox's F<sub>3</sub> is not the F<sub>3</sub> of my interpretation (see fig. 2.3.). **d)** Craw (1985, Figure 21) and Norris & Craw (1987) suggest that the recumbent nappe folds verge towards the internal part of the Otago Schist Belt. The Caples terrane overthrusts from the S, the Torlesse terrane from the N onto the Aspiring terrane, which is postulated as a basement nappe. **e)** A-type folds are caused by opposite overturning of folds due to uniform sense of shear (Malavieille 1987, Figure 16).



The formation of the nappe folds is linked to the assumption of the collision of three terranes, namely Torlesse, Caples and Aspiring terrane (fig. 2.1a). Norris & Craw (1987) propose an unusual model in which the nappes of the Torlesse and the Caples verge towards the internal part of the Otago Belt (fig. 2.2d). So the Caples overthrusts from S and the Torlesse from N/NE onto the Aspiring terrane as basement nappes (Craw & Norris 1991). The theory of nappe folds is also associated with an interpretation of the “high strain zones” as tectonic boundaries, which separate distinctly different lithologic assemblages (Craw 1985, Cox 1991, Craw et al. 1994). Observations of “high strain zones” show no lithologic change over these zones except as described for the footwall of the Remarkables fold nappe by Cox (1991). Moreover I have observed that greenschist bands, which strike oblique to the “high strain zones”, are folded in the hanging wall of the assumed recumbent fold and cross the “high strain zone” in the footwall without any remarkable displacement (for example Dunstan, fig. 2.4h and Gentle Annie, fig. 2.4q). The concordance of “high strain zones” and lithologic boundaries is more or less coincidental. Moreover investigations show that the Aspiring cannot be described as a “terrane” on its own but only as a more pelitic variation of the Torlesse (Mortimer & Roser 1992; fig. 2.1a).

Further observations of Mortimer (1993b) suggest that the concept of nappe folds itself is not particularly convincing. In some places upper limb folds do not consistently verge in one direction (Turnbull 1981, Mortimer 1993b) and in other places folds of the inferred lower limb have the identical vergence as the upper limb folds (Mortimer 1993b). The folds of the assumed lower limb are either absent or weakly developed or reappear out of a zone of complex foliation transposition in the hinge zone such that correlation with the phase of folding on the upper limb is suspect (Mortimer 1993b). Mortimer (1993b) considers that the regional recumbent folds appear to be half folds with lower limbs missing and represented by high strain zones of transposed foliation (“high strain zones” of Craw (1985), Cox (1991)). Furthermore Mortimer (1993b) assumes that most of the inferred major fold axes are subparallel to a stretching lineation indicating a fold axis-parallel shearing rather than fold axis-perpendicular shearing (Wood 1978, Craw 1985). Mortimer (1993b) bases one of his suggested models on the idea of a-type-folds (fig. 2.2e) by Malavieille (1987). It describes that folds obtain opposite vergences on both limbs, during uniform sense of simple shearing of layers with inverse obliquity relative to the shear plane. Because simple shear is imposed the fold hinges and lineations rotate towards a stretching lineation. This model may be applied to the folds in central part of the Otago Belt because main vergences are to NW or NE with a stretching lineation plunging mostly to N (Turnbull 1981). The main problem of this theory (Mortimer 1993b) is that different lineation types of different generations are grouped together in one single “stretching” lineation. For example, deformed long axes of conglomerate pebbles (Norris & Bishop 1990) are mainly developed during an older deformation phase ( $F_1$ ) and sometimes display an angle of about  $15^\circ$  with the younger fold axes (Norris & Bishop 1990). Quartz rods are formed here as a distinct crenulation lineation parallel to one particular fold axis (Wilson 1961, Ramsay & Huber 1987, p. 472) and not as a “stretching” lineation (*see section 2.2.2.*).

However, many questions arise from the examination of published literature on the fold structure of the Otago Schist Belt. Not only whether stretching occurs parallel or perpendicular to the fold axis, but what is the strain geometry of the fold structure? How do the mesofolds change in style or appearance in relation to a regional fold? Are these regional folds continuous in the whole Otago Schist Belt or do they vary in their extent? Is there really only one generation of fold, which develops regional folds as considered by many previous workers above? And how do these “high strain zones” generate?

	locations							
	NW ←							→ SE
	Hawea	Aspiring W of Moonlight Fault	Aspiring E of Moonlight Fault	Remarkables Mountains	Cromwell	Middle Otago	Alexandra, Manor- burn Dam	East Otago
<b>F1</b>		<b>D1</b> ↷		<b>D1</b>	<b>F1</b>	<b>D2</b>		<b>F1</b>
<b>F2</b>	<b>F1</b> ↷	<b>D2</b> ↷		<b>D2</b>	<b>F2</b> ↷	<b>D3A</b> ↕	<b>F1</b> ↕	<b>F2</b> ↷
<b>F3</b>	<b>F2</b> ↷	<b>D3</b> ↕	<b>D3</b> ↷		<b>F3</b> ↷	<b>D3B</b> ↕	<b>F2</b> ↕	<b>F3</b> ↷
<i>correlation (this study)</i>	<i>Norris &amp; Cooper (1977)</i>	<i>Craw (1985)</i>	<i>Craw (1985)</i>	<i>Cox (1991)</i>	<i>Turnbull (1981)</i>	<i>Winsor (1991 a, b)</i>	<i>Means (1963, 1966)</i>	<i>Brown (1968)</i>

**Fig. 2.3:** Correlation diagram for deformation phases in the Otago Schist Belt (see locations in fig. 2.1a). Arrow indicate that the deformation phase described by previous workers contains hints of a further deformation phase. The structural outline follows mainly the work of Brown (1968) and Turnbull (1981), who classify the Mesozoic fold structure of the eastern and central Otago Belt into three deformation phases ( $F_1$ - $F_3$ , fig. 2.3), a concept applicable on the whole Otago Belt.

## 2.2. Structural elements and sequence

### 2.2.1. $F_1$

In the Otago Schist Belt bedding is folded into similar tight to isoclinal folds ( $F_1$ ) and is extremely transposed (transposed bedding, Bishop 1972). Parallel aligned to the first fold axis ( $B_1$ ) is an object lineation ( $L_1$ , Turnbull 1981), which can be observed both as an aggregate and parallel-aligned grain lineation (definition of lineations by Piazzolo & Passchier 2002). Long axes of pebbles of intraformational quartzite conglomerates define an aggregate lineation (Norris & Bishop 1990). Metamorphic minerals grow along the pervasive axial plane surface ( $S_1$ ) forming a continuous grain lineation ( $L_1$ , Turnbull 1981). The transposed bedding is reinforced by quartz-albite and mica segregation (Cooper 1974), which is formed parallel to the axial planar foliation. The resulting “layering” is an irregular spaced, discontinuous alteration of mm-thin quartz-albite-rich and mica-rich layers in the metagreywacke (Turnbull et al. 2001).

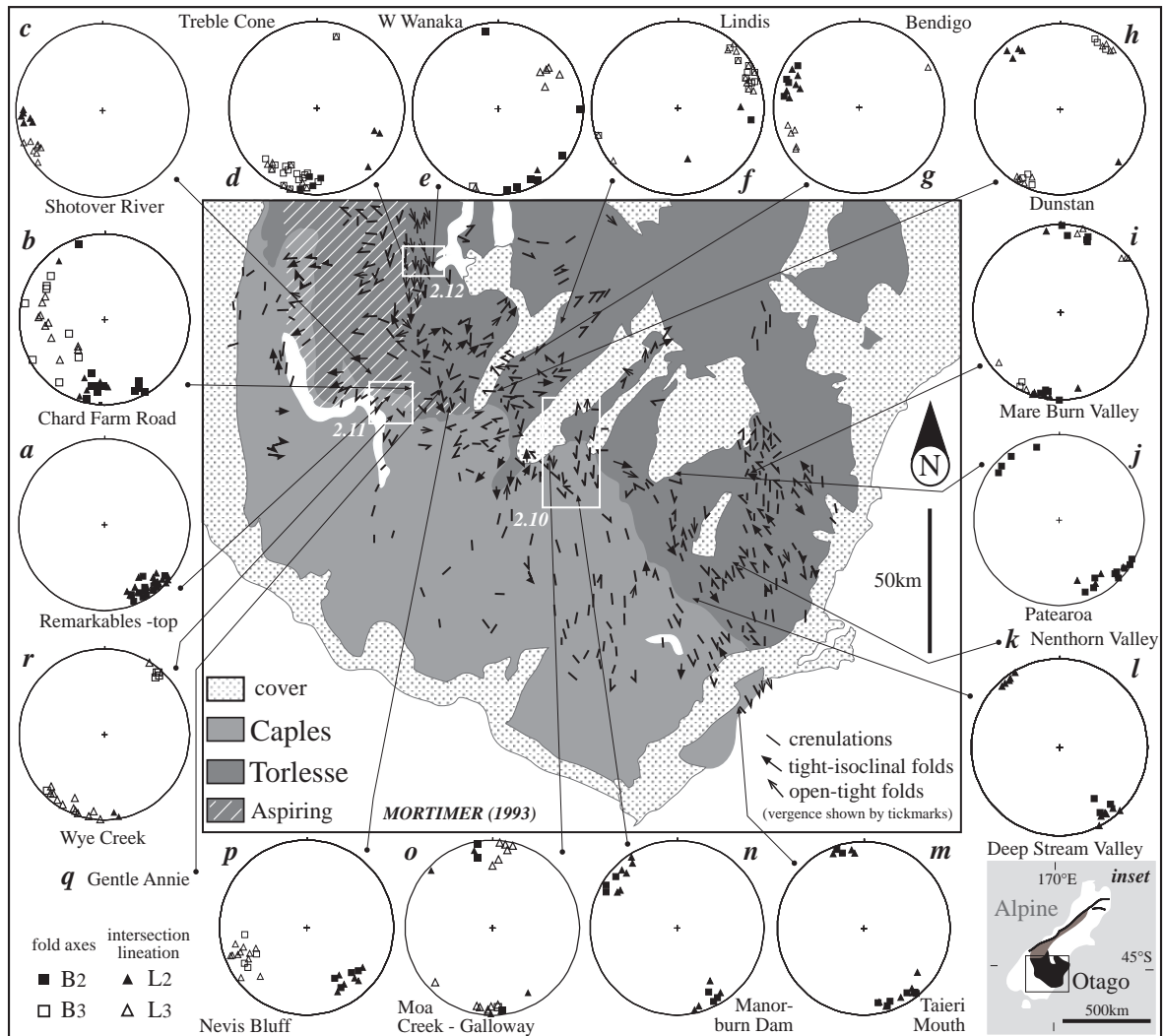


**Fig. 2.4:** Distribution and orientation of dominant fold axes and crenulation lineations in the Otago Schist Belt (based on Figure 4 of Mortimer (1993b); small inset shows the location of the Otago Schist Belt in relation to South Island, New Zealand). Stereograms (equal area, lower hemisphere projection) reflect the fold axes and intersection lineations of indicated locations. Boxes indicate the locations of fig. 2.10a (Manorburn area), fig. 2.11a (Remarkables area) and fig. 2.12a (Treble Cone area).

### 2.2.2. $F_2$

Folds of the second generation ( $F_2$ ) are the most common and conspicuous mesoscopic structures within the eastern and central Otago Schist Belt (Brown 1968, Wood 1978, Turnbull 1981, Cox 1991). Regional folds are related to this generation of folds by almost all previous workers (Means 1963, 1966, Norris & Cooper 1977, Wood 1978, Turnbull 1981, Craw 1985, Norris & Craw 1987, Cox 1991, Mortimer 1993b). The  $F_2$  mesofolds are cylindrically formed around the fold axis ( $B_2$ ) with  $S_1$  as form surface (Brown 1968, Turnbull 1981). The first object lineation ( $L_1$ ) is clearly folded around the second fold axis ( $B_2$ ). The fold axes plunge gently to

the SE or NW (fig. 2.4a, g, j, k, l, m, p), the axial planes of the second fold generation dip gently to the SW or NE (Brown 1968, Turnbull 1981). A weak and discontinuous crenulation cleavage ( $S_2$ ) is developed in the mica-dominated layers at the hinges of the mesofolds. The intersection of the first foliation ( $S_1$ ) and the crenulation cleavage ( $S_2$ ), which is parallel aligned to the fold axis ( $B_2$ ), leads to a lineation  $L_2$  mostly recognised as a lithologic striping of the rock's surface. These mesofolds with dm-scale wavelength and amplitude are thickened in the fold hinge zone and thinned on the fold limbs describing overall similar, tight to isoclinal folds (Turnbull 1981, Craw 1985). The more incompetent rock types (e.g. greenschist and metapelite) have highly thickened hinges and attenuated limbs (Craw 1985). An extensional quartz vein system develops during  $F_2$  folding crosscutting the layering (Cox 1991) and dipping gently to the NE or SW. The earlier formed veins are rotated to a higher intersecting angle with the layering and so they are stretched or folded. The vergence of these folds reflects the vergence pattern of the  $F_2$  folds.

### 2.2.3. $F_3$

Folds of the third generation ( $F_3$ ) closely resemble style of  $F_2$  folds (Turnbull 1981, Winsor 1991a). The  $F_3$  mesofolds are cylindrically formed around the fold axis ( $B_3$ ) with  $S_1$  as form surface (Brown 1968, Turnbull 1981). The axial planes dip gently to the SE and fold axes plunge gently to SW or NE (fig. 2.4d, f, h, p, and r). In contrast to the second crenulation cleavage, the third crenulation cleavage ( $S_3$ ) is strengthened in the mica-dominated layers at the hinges of the  $F_3$  mesofolds and thus continuously developed in  $F_3$  folded regions. Consequently the intersection of the first foliation ( $S_1$ ) and the crenulation cleavage ( $S_3$ ) leads to a penetrative crenulation lineation  $L_3$ , which is parallel aligned to the fold axis ( $B_3$ ). The first object lineation ( $L_1$ ) can be traced around the hinges of the  $F_3$  folds, although the angle between the first object lineation and the third superposed fold axis ( $B_3$ ) is small varying between 10 to 30°. The behaviour of the first object lineation in relation to the superposed folds ( $F_2$ ,  $F_3$ ) will be discussed in further investigations (*see chapter 4*). Small  $F_2$  folds and the lithologic striping lineation ( $L_2$ ) behave like passive markers and rotate around the third fold axis ( $B_3$ ). An extensional quartz vein system develops during  $F_3$  folding crosscutting the layering and dipping gently NW or SE (Brown 1968, Turnbull 1981, Winsor 1991b).

## 2.3. Strain geometry of the mesofolds of the second and third generation

Small folds are developed parasitically on the back of the mesofolds with a wavelength and amplitude on cm-scale (fig. 2.5). They are themselves folded by smaller folds with mm-scale wavelength and amplitude (fig. 2.5). Their hinge lines are all parallel aligned to the respective fold axis ( $B_2/B_3$ ) of the mesofolds. The consistent orientation of hinges of the small folds within one mesofold and again the consistent orientation of mesofolds at regional scale circumstantiates that the folds of both generations develop as cylindrical folds. The small structure can be described as a polyharmonic folding of mm-thin competent quartz-albite- and incompetent mica-dominated layers. The competent quartz-albite layers show parallel fold

structure, sometimes with slightly thinned limbs (class 1B – 1C, Ramsay & Huber 1987). The incompetent mica-dominated layers, which taper off into the hinge zones of the quartz-albite layers, can be described as class 3 folds (Ramsay & Huber 1987).

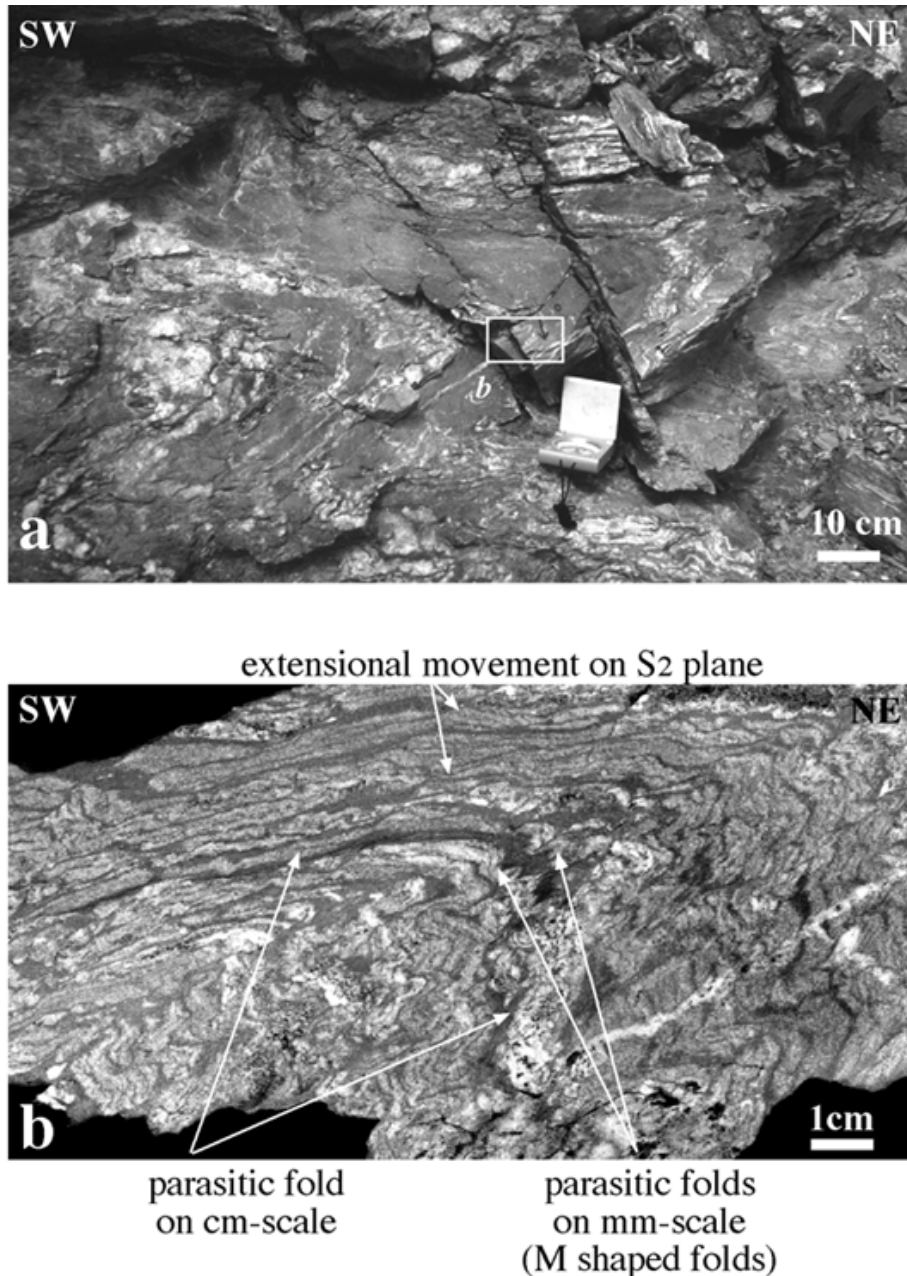


**Fig. 2.5:** *a)  $F_2$  mesofold at the top of the Remarkables Mountains (fig. 2.1a). b) Cut surface of sample R4 (Remarkables, top) viewed perpendicular to the fold axis  $B_2$  displaying small parasitic folds on cm- and mm-scale. The long limb of the parasitic fold on cm-scale is stretched by layer-parallel extension resulting in unfolding of the tiny parasitic folds and extensional movement on  $S_2$  planes.*

The crenulation folding of the thin quartz-albite- and mica-dominated layers causes a cusped-lobate fold structure at microscopic scale (Ramsay 1967, Cosgrove 1980, Ramsay & Huber 1987, p. 397, Hudleston & Lan 1993; fig. 2.6a, b). The cusped-lobate structure is enhanced especially on the interface between quartz veins and surrounding rock forming highly characteristic rippled and corrugated surfaces of the vein (fig. 2.6), mostly described as quartz rods (Wilson 1961, Ramsay & Huber 1987, p. 472). This strengthened crenulation lineation on quartz-rich surfaces is parallel aligned to the respective fold axis ( $B_2/B_3$ ; Mortimer 1993b) and thus classified as a b-lineation (Wood 1978). The orientation of the first object lineation ( $L_1$ ) almost subparallel to the orientation of the superposed fold axes ( $B_2/B_3$ ) misleads to the interpretation of the quartz rods as stretching or a- lineations (Mortimer 1993b). The behaviour of the first object lineation ( $L_1$ ) in relation to the superposed folds will be focused on in further investigations (*chapter 4*).

Due to the layer-parallel extension the crenulation is flattened on the limbs of the small folds. As the crenulation folds become asymmetric, the local cleavage ( $S_2/S_3$ ) rotates towards the first foliation  $S_1$  (fig. 2.6a). The cleavage ( $S_2/S_3$ ) acts as small normal faults, which cut through the competent quartz-rich layers forming small boudins with their axes ( $b_2/b_3$ ) parallel to the local fold axis ( $B_2/B_3$ ; fig. 2.5b, 2.6c). The sense of relative rotation of the boudins is opposed on the two limbs of any single fold domain ( $F_2/F_3$ ).

Extensional quartz veins pervade regions folded by  $F_2$  or  $F_3$  at all scales. At the scale of mesofolds, small quartz veins (width up to 5mm) are observed flatly on the limbs of the mesofolds whereas they are folded at the hinge. The layer- parallel extension leads to quartz fibre growth ( $L_{2\text{grain}}, L_{3\text{grain}}$ ) subparallel to the extension direction in the new-formed extensional veins (fig. 2.6a).

In the western part of the Otago Schist Belt, chlorite and albite overgrow syn- to post-tectonically the  $F_3$  folded microstructure in greenschist rocks (fig. 2.7b). Chlorite laths grow with their basal plane (001) parallel aligned to the overall extension direction of the third fold generation and overprint as a grain lineation ( $L_{3\text{grain}}$ ) the third crenulation lineation ( $L_3$ ; fig. 2.6b). This grain lineation ( $L_{3\text{grain}}$ ) has a constant ESE – WNW trending plunge. It is oriented perpendicular to the fold axis ( $B_3$ ) in pronounced folds of the third generation (Lindis, fig. 2.4f). But in the footwall of a regional hinge intersection, it is subparallel aligned to the fold axis (Chard Farm Road, fig. 2.4b, 2.7c), or any angle in between due to superposition ( $45^\circ$  to  $B_3$  orientation, Treble Cone, fig. 2.4d, 2.7d). The outlined sense of shear reflects mostly the vergence pattern of the  $F_3$  folds (fig. 2.7b, d). Fibrous growth of quartz, epidote and chlorite in  $F_3$  extensional veins displays the same orientation ( $L_{3\text{grain}}$ ) as the chlorite flakes in the greenschist (fig. 2.7a).

The described strain characteristics of the mesofolds of both generations outline a development as buckle folds, whose internal deformation reflect a combination of tangential-longitudinal strain and flexural flow pattern. The extension direction of both fold generation is not oriented parallel but perpendicular to the respective fold axis.

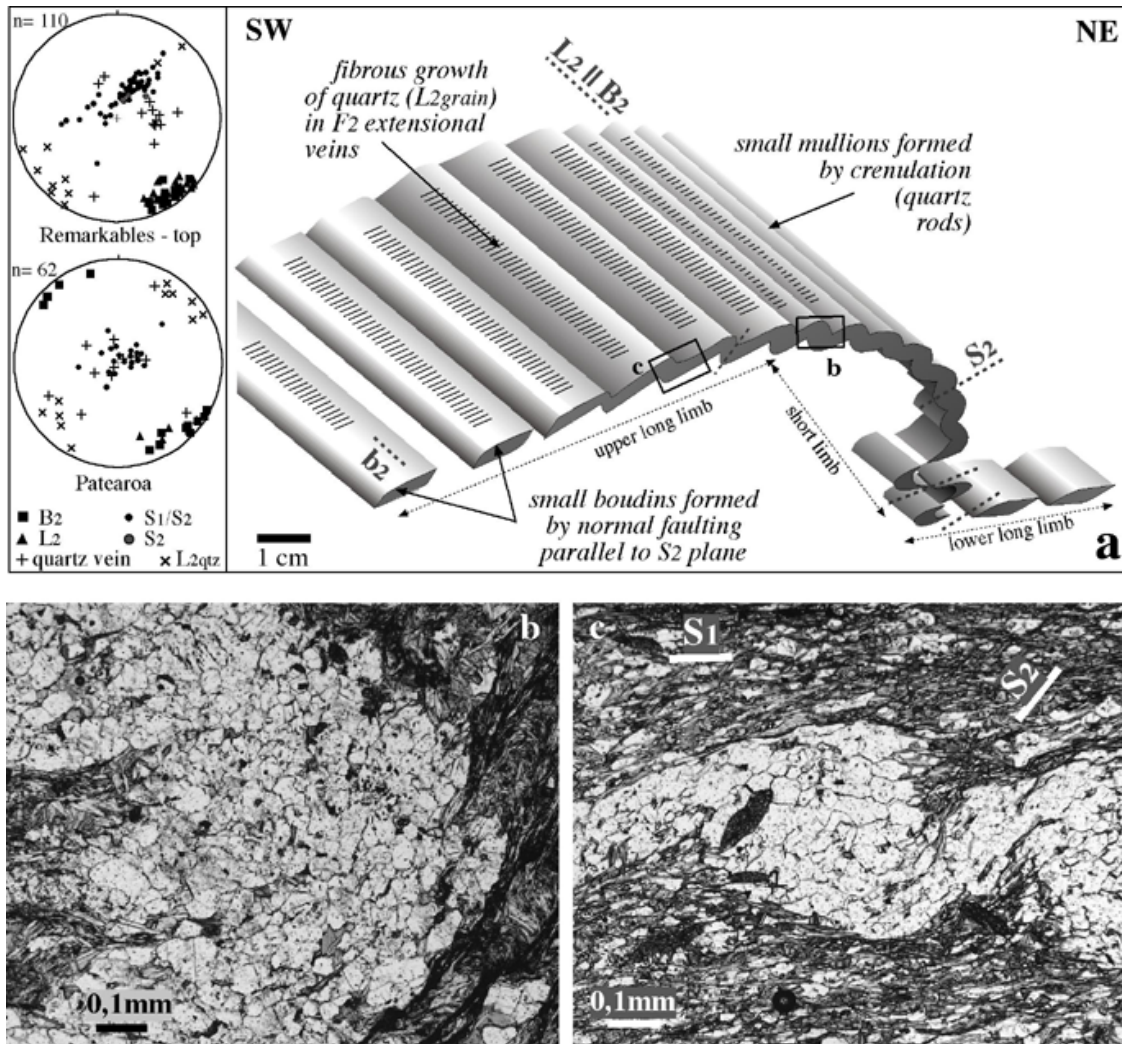


**Fig. 2.6:** *a)* Development and deformation of an extensional quartz vein sheet during  $F_2$ . Fibrous quartz grains ( $L_{2\text{grain}}$ ) grow perpendicular oriented to the second fold axis  $B_2$  in extensional veins (see stereograms (equal area, lower hemisphere projection) compiled at Remarkables (fig. 2.4a) and Patearoa (fig. 2.4j)). The quartz vein sheet is folded by small mullions on the short limb and disrupted by boudinage on the long limb because the vein displays a higher competence contrast than the surrounding host rock. *b)* Parallel fold of quartz vein (class 1B or 1C) and pinned folds of mica-rich layers (class 3) display a cusped-lobate structure (Remarkables, top;  $\perp B_2$  and  $S_2$ , plane polarised light). *c)* The second cleavage cuts through a folded quartz vein. The limbs of the small asymmetric folds are thinned parallel to the second cleavage outlining the starting influence of layer-parallel extension (boudinage; Remarkables, upper base;  $\perp B_2$  and  $S_2$ , plane polarised light)

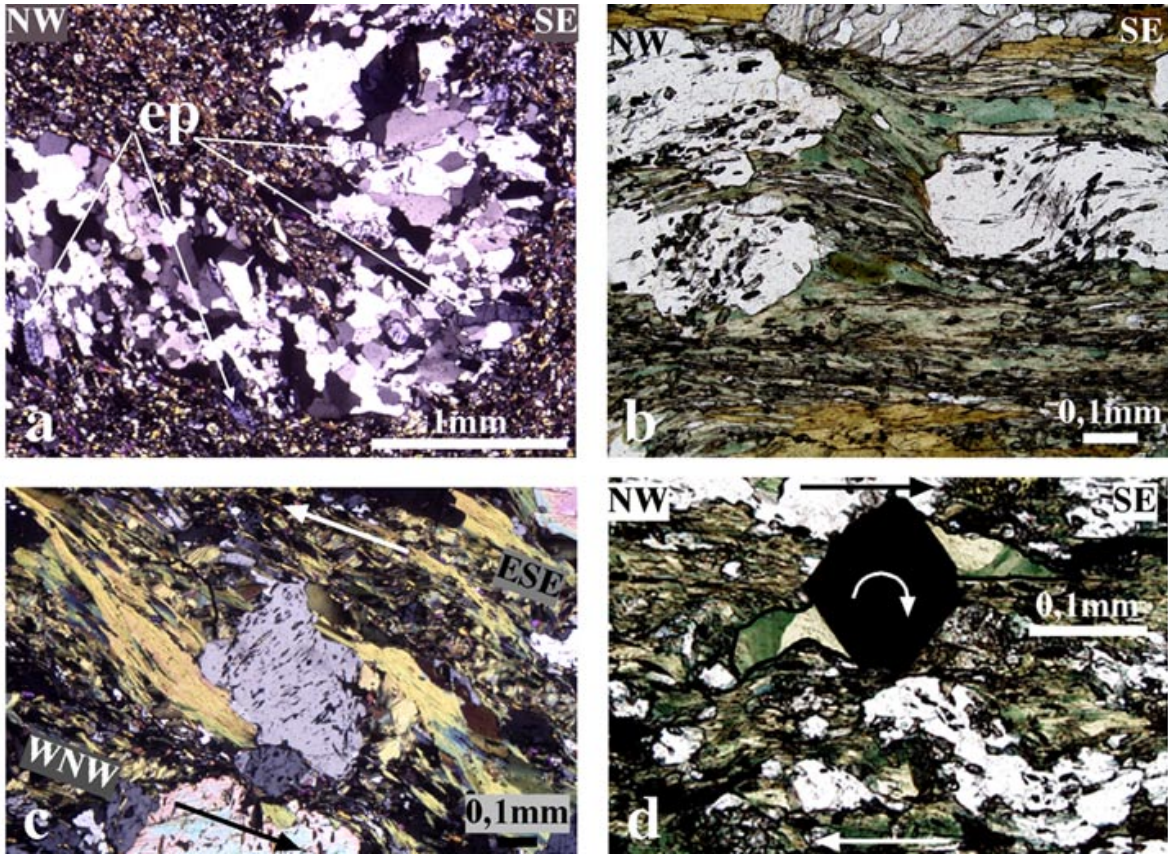


**Fig. 2.7:** **a)** Epidote grains grow almost perpendicular from the vein wall into the void during sealing of a small  $F_3$  tension gash, which is subsequently folded ( $F_3$ , Wye Creek;  $\perp B_3$  and  $S_3$ ,  $\parallel L_{3\text{grain}}$  crossed polarised light). **b)** Albite porphyroblasts overgrow  $F_3$  folded foliation (greenschist, Arrow River, N of Remarkables Mountains;  $\perp B_3$  and  $S_3$ , plane polarised light). **c)** Albite porphyroblasts are rotated top to the WNW during further fold evolution (greenschist, Chard Farm Road;  $\perp S_3$ ,  $\parallel B_3$  and  $L_{3\text{grain}}$  plane polarised light). Chlorite laths grow with their base (001) parallel to  $L_{3\text{grain}}$ . **d)** Chlorite fibres grow in fringes of pyrite porphyroclast. A rotation of pyrite and chlorite fringes during folding displays a shear sense top to the SE (rotation sense determination after Koehn et al. 2000; greenschist, Treble Cone;  $\perp S_3$ ,  $\parallel L_{3\text{grain}}$   $45^\circ$  oriented to  $B_3$ , plane polarised light).

## 2.4. Regional folds of the second and third generation

### 2.4.1. Relationship between mesoscopic and macroscopic folds of both generations

Regional folds are determined by the progressive change of style of the mesofolds: the asymmetry (vergence), the interlimb angle, amplitude, the orientation of the fold axes, lineations and axial planes as well as the interference pattern of the small parasitic folds. Although both fold generations extend over the entire Otago Belt, each fold generation is not penetrative on regional scale. In other words, the interference pattern of the regional folds is at km-scale, thus regional folds of both generation can be observed without a remarkable influence of the respective earlier or later fold generation.



In  $F_2$  folded regions the mesofolds grow from highly asymmetric, close to tight folds to recumbent tight to isoclinal folds displaying a vergence to NE (e.g. Remarkables (fig. 2.4a), Patearoa (2.4j), Deep Stream Valley (2.4l), Taieri Mouth (2.4m), Upper Manorburn Dam area (2.4n), Gentle Annie (2.4q); see fig. 2.8a). A vergence change to the SW of the mesofolds is only preserved in small areas (e.g. Gentle Annie/Roaring Meg (fig. 2.4q), northern part of Upper Manorburn Dam area (fig. 2.4n); see fig. 2.8a). The SW vergent mesofolds are only slightly asymmetric tight to isoclinal folds which are confined to the hanging wall and footwall by recumbent symmetric tight to isoclinal folds (M- shaped; fig. 2.8). The huge areas of NE vergent mesofolds and the small, sometimes-absent areas of SW vergent mesofolds describe asymmetric open to close regional folds verging to the NE. The mesofolds are mainly developed on the short limbs of the macroscopic folds (fig. 2.8a). The hinge zones extend for 1 to 2 km perpendicular to the  $F_2$  fold axis (see fig. 2.10- 2.12).

Towards a major  $F_3$  hinge zone, the small  $F_2$  folds continuously flatten, whereas the number of small  $F_3$  folds increase and mesofolds occur. At the major  $F_3$  hinge zone only rare and tiny  $F_2$  folds are preserved. The small  $F_2$  folds and the lithologic striping lineation ( $L_2$ ) behave like passive markers and rotate around the third fold axis ( $B_3$ ) describing a small circle in the stereographic projection (fig. 2.8b, 2.3). Just as the second fold generation ( $F_2$ ), the appearance of  $F_3$  mesofolds outlines asymmetric open to close regional  $F_3$  folds. NW vergent, tight to isoclinal  $F_3$  mesofolds are concentrated at the hinges and short limbs of the macroscopic folds displaying a vergence of the regional folds to the NW (e.g. Treble Cone (fig. 2.4d), Lindis (2.4f), Dunstan (2.4h)). On the upper long limb the mesofolds get more asymmetric and smaller in amplitude and larger in wavelength continuously dying out (fig. 2.8b). Inverse vergence of mesofolds is only observed in  $F_3$  folded areas in the northwestern part of the Otago Belt (e.g. Dunstan (fig. 2.4h), Treble Cone (2.4d)). The wavelength and amplitude of observed regional  $F_3$  folds are significantly smaller than the one of  $F_2$  in the eastern and central part of the Otago Belt (e.g. Mare Burn Valley (fig. 2.4i), Nenthorn Valley (2.4k), Moa Creek – Galloway (2.4o), Lindis (fig. 2.4f), Chard Farm Road (2.4b)). The short limb extends only for tens to hundreds of meters. In the northwestern part of the Otago Belt (e.g. Treble Cone (fig. 2.4d)),  $F_3$  folded regions expand and the amplitude of  $F_3$  regional folds grows up to the one of  $F_2$  regional folds at km-scale.

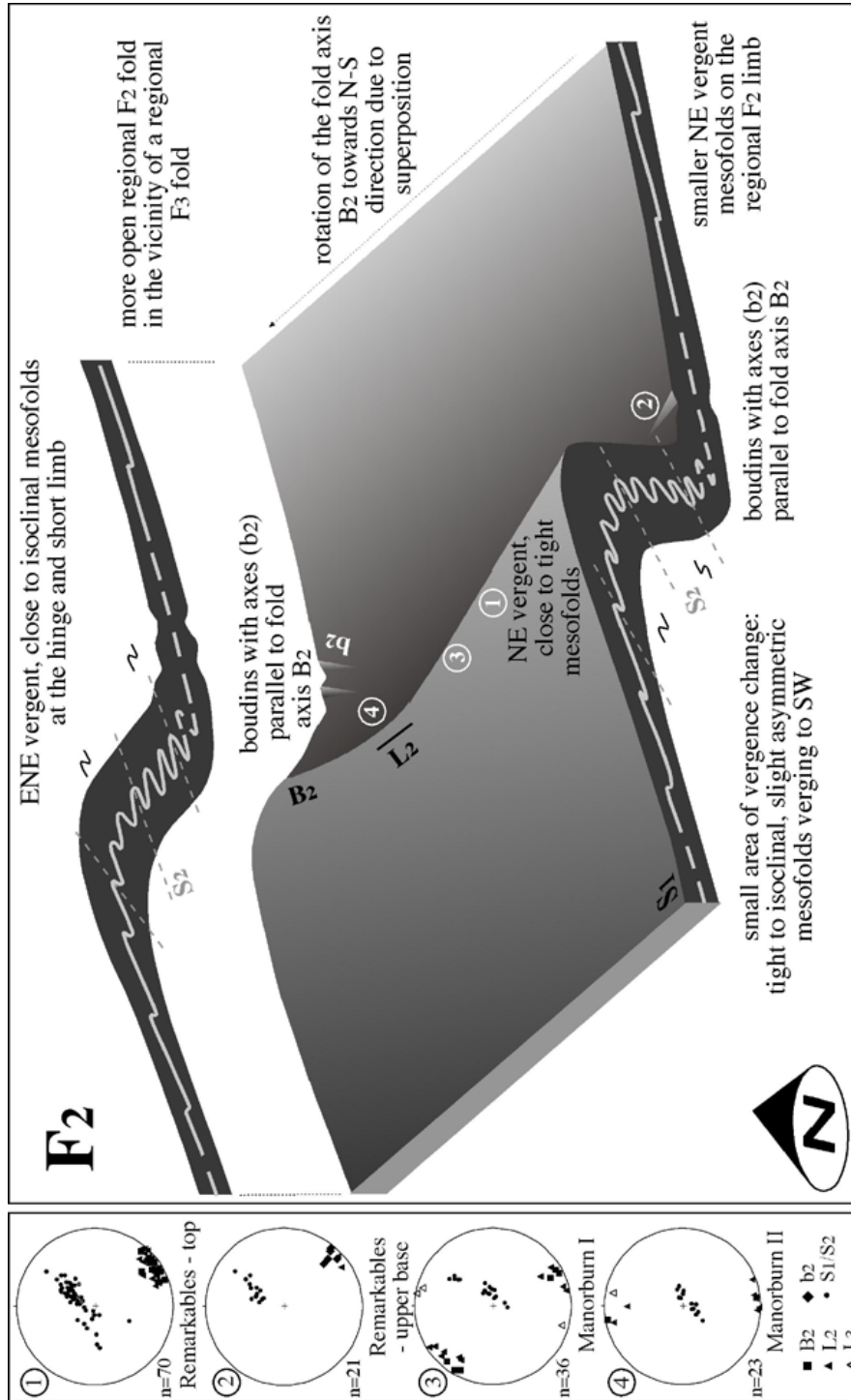


**Fig. 2.8:** Sketches of the regional folds ( $F_2$  and  $F_3$ ) outlining the continuous change of style, orientation, vergence and appearance of mesofolds. Note that the mesofolds are increased in scale relative to the macroscopic fold. In the foreground of the sketch, the regional folds are shown without the influence of superposition ( $F_2$  or  $F_3$  folded region), whereas in the background the regional folds attain a gentle amplitude due to the superposition ( $F_2/F_3$  folded region). Notice the rotation of the fold axes of both generations because of the superposition. Stereograms (equal area, lower hemisphere projection) reflect the structure at the indicated point. There is no geographical relationship between the locations and the sketch.

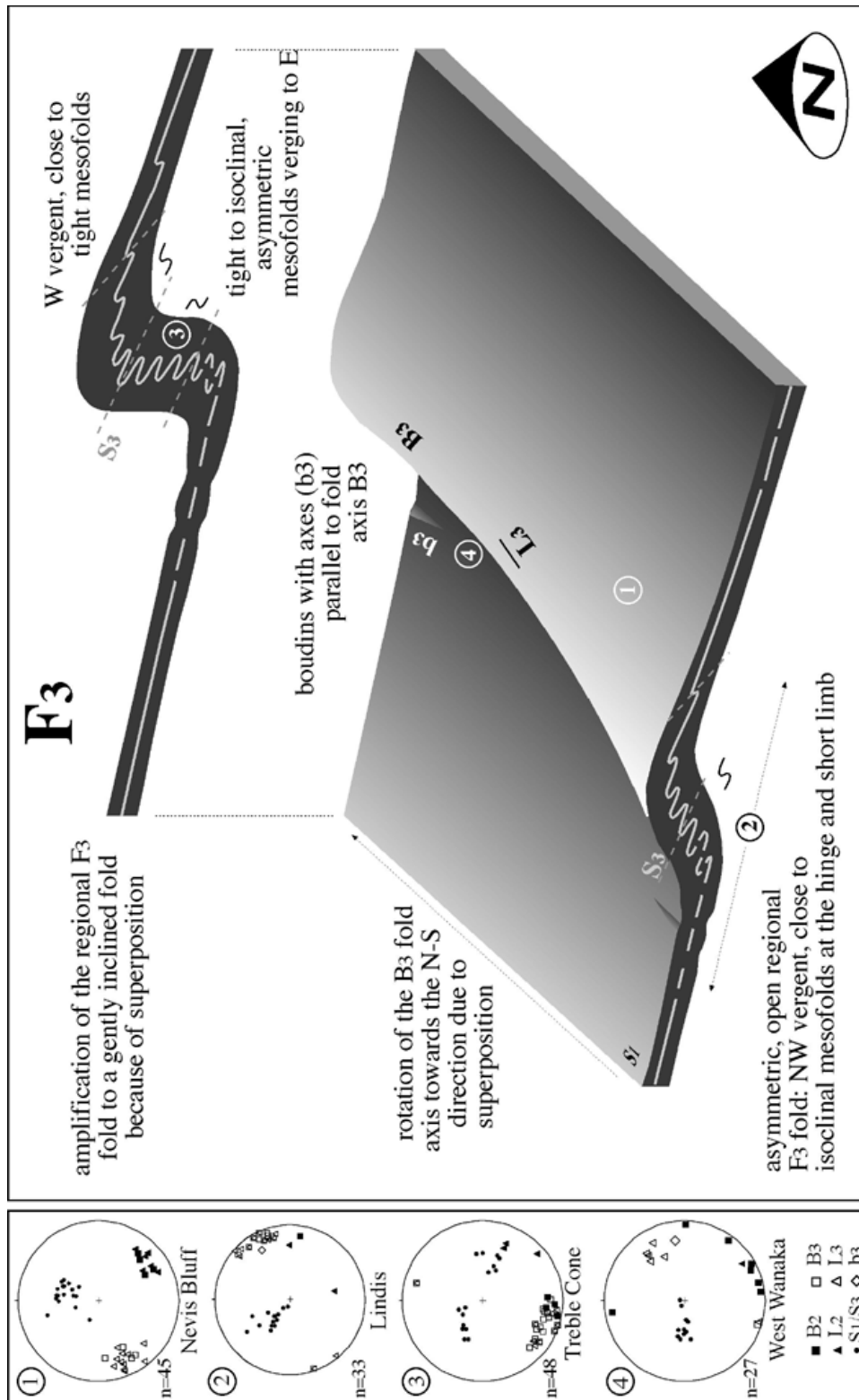
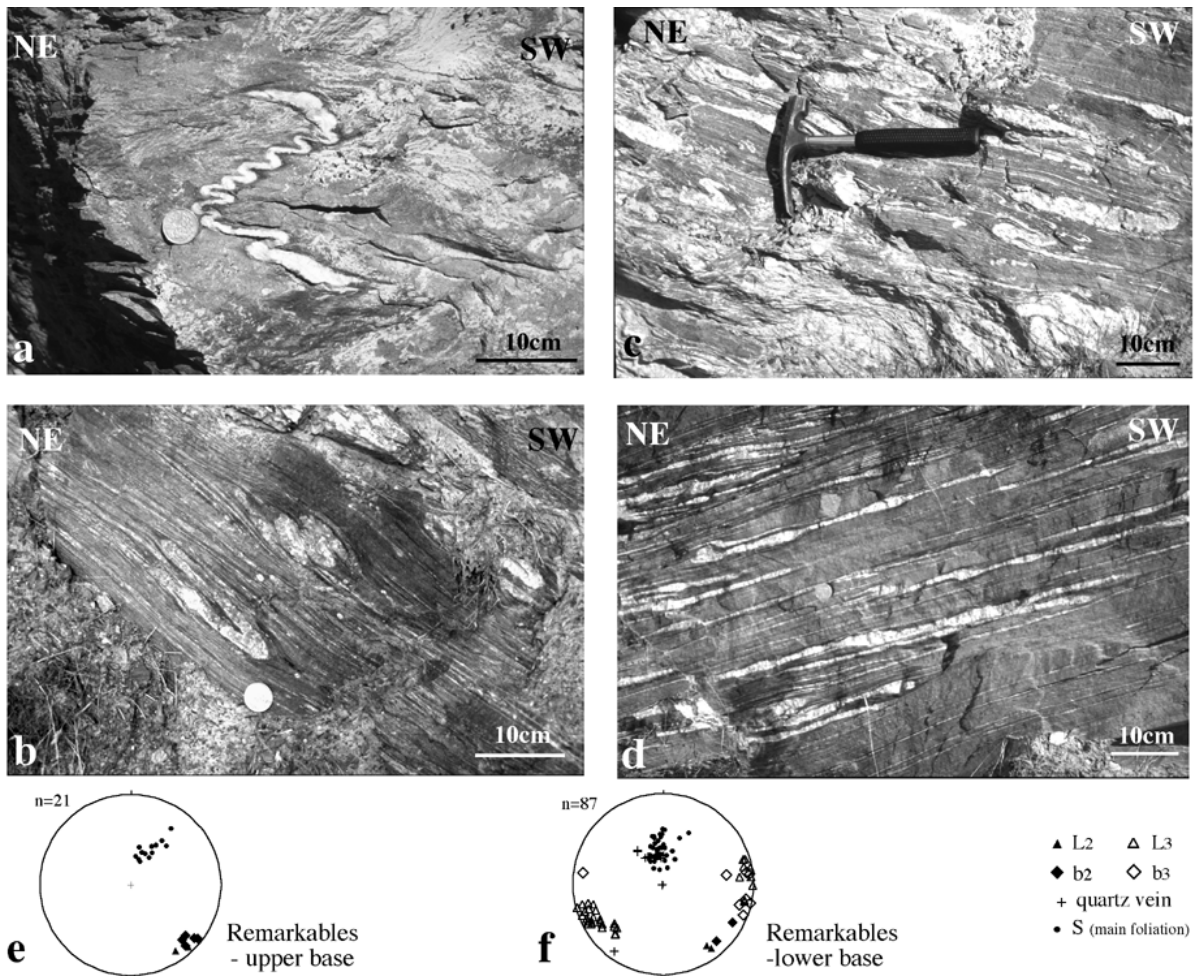


Fig. 2.8: Sketch of the F<sub>3</sub> regional fold (see caption of previous page)

### 2.4.2. Re-investigations into the “high strain zones”

A combined process of buckling and flattening leads to the development of consistent vergences of open to close regional folds of both generations. Asymmetry of buckle folds is generally considered to result from a stiff layer lying initially oblique to the maximum shortening direction in pure shear (Treagus 1973) or from the amplification of an initial asymmetric perturbation (Abbassi and Mancktelow 1990). The development of asymmetric parasitic folds on the back of larger folds (Ramberg 1964) is excluded here because folds of regional scale are considered. The asymmetry causes, as the regional buckle fold grows, that the two limbs make different angles to the principal directions of bulk strain and thus undergo different strain histories; one limb is continually shortened, whereas the other rotates to enter the field of extensional strain (Lan & Hudleston 1991). The style of the regional folds reflects a steeply plunging shortening direction to the NE ( $F_2$ ) or WNW - NW ( $F_3$ ) and a gently plunging extension direction to the SW ( $F_2$ ) or ESE - SE ( $F_3$ ). The tighter folding of the mesofolds at the hinge zone of both regional folds (fig. 2.8a, b) causes a rotation of the mesofolds' limbs normal to the overall shortening direction. Consequently quartz-albite rich layers are disrupted by boudinage as a result of the rheological contrast between adjacent layers (Ramberg 1955, Kidan & Cosgrove 1996). Planes of brittle failure, generally the second or third cleavage separate competent layers into pinch-and-swell structures or boudins. The axes of the boudins ( $b_2/b_3$ ) are aligned parallel to the respective fold axis ( $B_2/B_3$ ) reflecting the overall contraction and extension directions. Quartz veins with a higher competence than the surrounding mica-rich layers become preferentially stretched and thinned (fig. 2. 2.9a-d). Failure occurs on fractures near small fold hinges (fig. 2.9b) and further extension leads to boudins with separated fold hinges as cores (fig. 2.9c). Further thinning and flattening of the isoclinal intrafolial folds results in a pinch-and-swell structure (Ramsay & Huber 1987; fig. 2.9d).

This transition from the tight to isoclinal mesofolds of the short limb into intrafolial folds and boudins outlines the beginning of the lower limb of a regional fold. It is widely accepted that such boudinage never occurs at the hinge zones of folds even at a mature stage of folding (Ramsay 1967, Ghosh 1993). Small, highly asymmetric, NE ( $F_2$ ) or NW ( $F_3$ ) vergent, close to tight mesofolds growing at the footwall of the boudinage zone starting a new upper limb succession reinforce the notion (fig. 2.8a, b). In  $F_3$  folded regions, structures developed by layer-parallel extension - as boudinage and normal faulting along  $S_3$  foliation planes - are reinforced as it is disposed for superposed folds by Grujic (1993). Consequently the boudinage event is especially strengthened, where both major hinges of regional folds ( $F_2/F_3$ ) intersect.



**Fig. 2.9:** Fortified zone of boudinage on the succeeding lower limb of a regional hinge intersection, which is designated as a “high strain zone” by *Craw (1985), Norris & Craw (1987) and Cox (1991)* at the example of the lower northern flank of the Remarkables Mountains. **a)** Due to their higher competence, folds of the quartz veins are more accentuated forming ptygmatic folds (*Ramsay & Huber 1987*). The vergence of the folds reflects the vergence pattern of the  $F_2$  folds to the NE (Remarkables-top). **b)** Small folds of competent quartz veins are preserved in boudins, which are developed with their axes ( $b_2$ ) subparallel to second fold axis ( $B_2$ ; Remarkables – upper base). **c)** Stretching and thinning of the long limbs of the mesofolds causes intrafolial folds (Remarkables – lower base). **d)** Further thinning and flattening of the isoclinal intrafolial folds results in a disrupted pinch-and-swell structure (Remarkables – lower base). **e)** Stereogram (equal area, lower hemisphere projection) displays boudins of the second fold generations ( $b_2$ ) at the upper base of the Remarkables. **f)** Stereogram outlines the change from  $F_2$  boudins ( $b_2$ ) to  $F_3$  boudins ( $b_3$ ) at lower base of Remarkables.

### 2.4.3. What happens at the hinge zone of both interfering regional folds?

Looking at the stereograms of figure 2.4, it is visible that in these regions the mesofolds of both generations do not display an orthogonal pattern anymore. Hinge lines and intersection lineations rotate into N-S direction as observed at locations like Treble Cone (fig. 2.4d), Mare Burn Valley (2.4i), Moa Creek – Galloway (2.4o) and Wye Creek (2.4r). The hinge lines of both fold generations become almost coaxial as previously mentioned by Brown (1968) for the Nenthorn Valley (fig. 2.4k). The rotation of the hinge lines is outlined by the change of the interference pattern of both fold generations. Commonly the parasitic folds of both generations display a type 2 interference pattern (Thiessen & Means 1980, Ramsay & Huber 1987), where both fold axes are almost orthogonal oriented and the  $F_2$  axial fold plane is folded by  $F_3$  folds. Changing to an almost coaxial orientation of both fold axes leads to a type 3 interference pattern (Ramsay & Huber 1987), where the  $F_2$  axial plane is almost coaxially refolded by  $F_3$  folds. In this zone,  $F_3$  mesofolds are dominant displaying a main vergence to W, subordinate to E, whereas only small  $F_2$  folds are preserved disturbing the  $F_3$  fold structure. The rotation of the  $F_2$  and  $F_3$  hinge lines and the herewith-implied change of the interference pattern will be considered in further investigations (*chapter 3*). It should be noted that the rotation of the hinge lines towards each other does not imply any tectonic transport direction as considered by Norris & Craw (1987) because the plunge of the hinge lines is almost perpendicular to the overall superimposed third extension direction (section 2.3.) and not parallel to it.

### 2.4.4. Examples from the SE to the NW of the Otago Belt

It is beyond the scope of this thesis to generate a map of the Otago Belt with all the regional folds, their hinge lines and vergences. So three examples are chosen to describe the regional fold structure and the changing effect of the growing third fold generation ( $F_3$ ) on the prior developed second folds ( $F_2$ ). The repetition of these interference patterns of regional folds can be an instruction for following workers.

In the eastern part of the Otago Belt (Mare Burn Valley, Manorburn Dam; fig. 2.4i,m, fig. 2.10), macroscopic  $F_3$  folds only appear when meeting a regional  $F_2$  fold hinge. In the Manorburn Dam – Alexandra- Ophir area (fig. 2.10) the hinge zone of a regional  $F_2$  fold extends from Alexandra towards Manorburn Dam.  $F_2$  mesofolds display a vergence change from NE to SW across the previously mapped vergence boundary (Means 1963, 1966). The major  $F_3$  hinge zone spans between Ophir and Alexandra. The  $F_3$  hinge lines plunge to the SW in the northern area, whereas they rotate into N-S direction towards the hinge intersection, plunging southwards. The  $F_3$  mesofolds are distributed in a small area showing no vergence change (only W vergent) and less pronounced M-shaped mesofolds. On the succeeding major lower limb the M-shaped folds are attenuated and flattened but only a pinch-and-swell structure is developed in a small area. The lesser-evolved regional fold of the third generation implies the diminished boudinage (fig. 2.10).

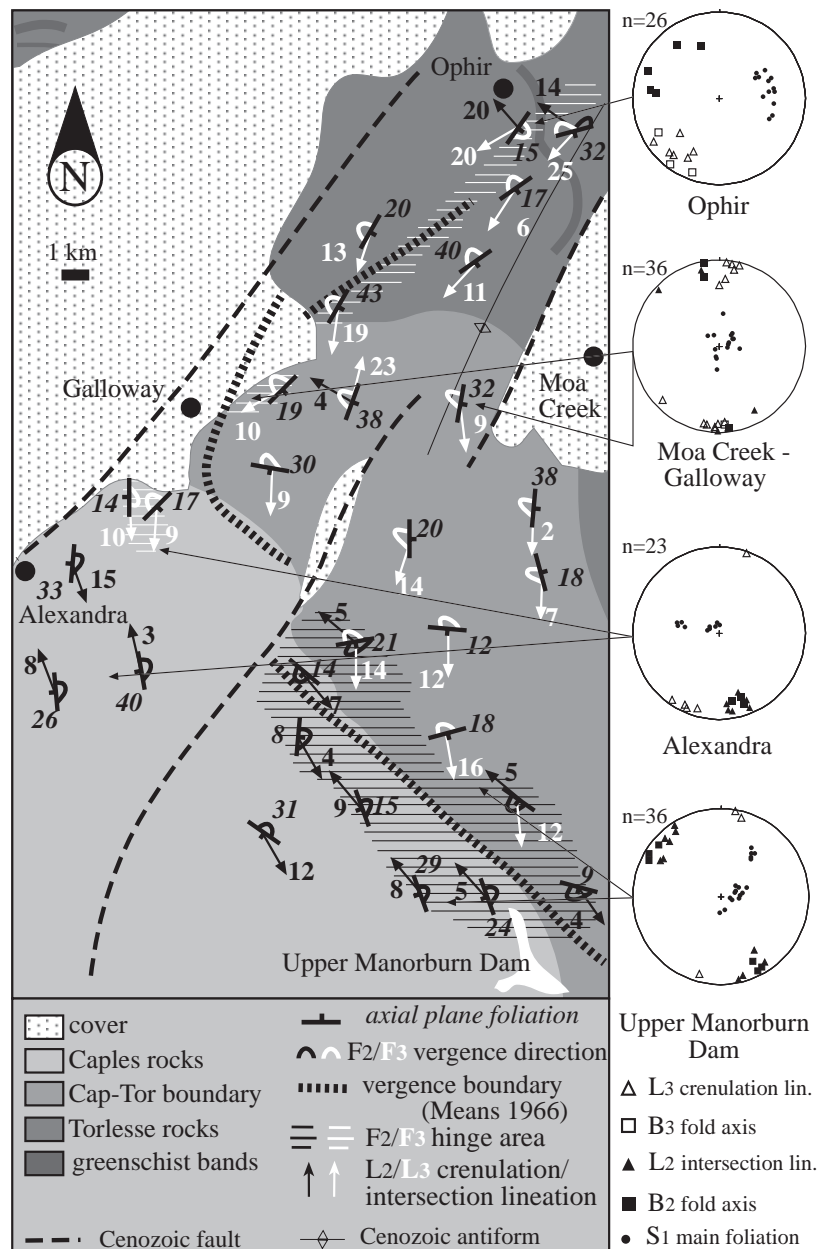


**Fig 2.10: a)** Map of the area between Alexandra, Upper Manorburn Dam and Ophir (see fig. 2.4): the depicted fold axes, axial foliation planes and vergences display a model of intersecting regional folds for the eastern part of the Otago Schist Belt (fig. 2.10 b). The vergence boundary mapped by Means (1966) outlines almost the hinge area of both intersecting regional folds. The vergence boundary or regional hinge zone parallel to Galloway – Upper Manorburn Dam line display a close regional F<sub>2</sub> fold, where the vergence of the mesofolds change from the NE (S of the line) to the SW (N of the line). The regional hinge zone parallel to Galloway – Ophir line outlines an open F<sub>3</sub> fold, where the F<sub>3</sub> mesofolds verge mainly to the W. A vergence change to the E is restricted to a very small area. In the vicinity of the regional fold intersection of both generations, the fold axes and crenulations of the F<sub>3</sub> parasitic folds (B<sub>3</sub> // L<sub>3</sub>) rotate into N-S direction.

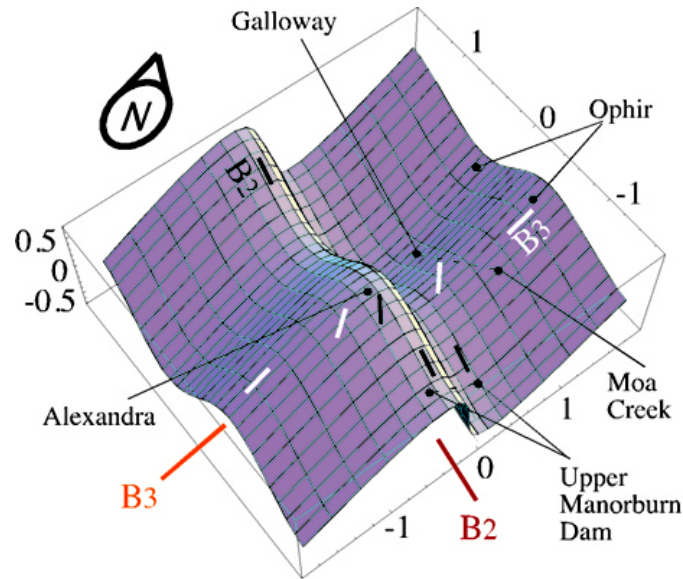


**Fig 2.10: b)** A model, depicted here as an enveloping surface of the  $F_2$  and  $F_3$  mesofolds, outlines the regional fold structure: an open regional fold of the third generation ( $F_3$ ) of a lesser extent (NE-trending) rides over a close NW trending regional fold of the second fold generation.  $F_3$  mesofolds only grow in the vicinity of the  $F_2$  major hinges. Apart from the  $F_2$  major hinge,  $F_3$  mesofolds deamplify and continuously disappear. c) Stereograms (equal area, lower hemisphere projection) reflect the structure at the indicated locations (fig. 2.10 b).

Towards the western part of the Otago Belt the regional folds of the third generation become a more pronounced folding phase. In the Remarkables Mountains, for example (fig. 2.4a, b, r, fig. 2.11), the major  $F_2$  hinge zone extends from WNW to ESE at the northern flank and the major  $F_3$  hinge zones from NNE to SSW on the western flank of the Remarkables. The  $F_2$  mesofolds of a major  $F_2$  hinge zone display no vergence change anymore and the area of M-shaped recumbent folds is less pronounced as well as the structures of boudinage are fortified on the lower limb (fig. 2.8a). Consequently the regional  $F_2$  fold deamplifies in the vicinity of a major  $F_3$  fold attaining an open fold style (fig. 2.8a). Just as the  $F_2$  regional fold flattens, it appears that the macroscopic  $F_3$  fold grows in amplitude while riding over a major  $F_2$  hinge zone (fig. 2.8b). The  $F_3$  folded area widens towards the regional hinge intersection. Macroscopic  $F_3$  folds in this area beside a hinge intersection with a major  $F_2$  hinge zone display a distinctly smaller amplitude (e.g. Chard Farm Road, fig. 2.4b, 2.11). Below this major hinge intersection, the boudin axes ( $b_3$ ) rotate into the E-W direction (fig. 2.9e,f, 2.11). Further along the lower long limb new parasitic  $F_3$  folds grow with their hinge lines oriented in E-W direction (Chard Farm, fig. 2.11). Similarly, the second lineation  $L_2$  and fold axis ( $B_2$ ) of the new developing folds rotate into the E-W direction (Shotover River, fig. 2.4c). The superposition of regional folds at the same size causes the rotation of the parasitic hinge lines and intersection lineations of the major lower long limbs of both generations in E-W direction. It seems that the parasitic folds side step the regional hinge intersection.



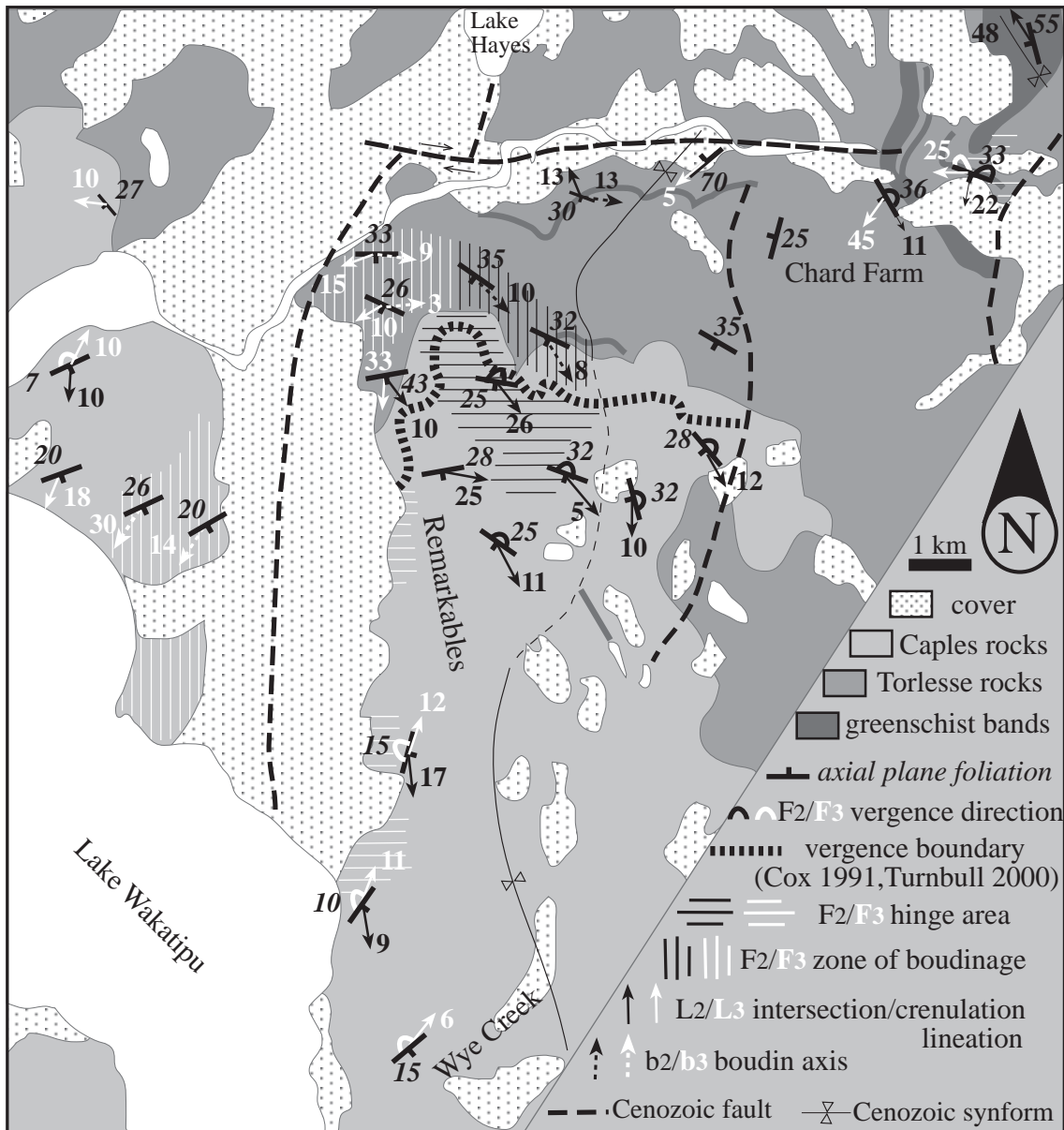


**Fig. 2.11: a)** Map of the Remarkables Mountains from Wye Creek in the south to Chard Farm Road in the west: the depicted fold and boudin axes, axial foliation planes and vergences display the assumed model (fig. 15b). The vergence boundary mapped by Cox (1991) coincides at the northern flank of the Remarkables Mountains with the hinge area of NW trending regional  $F_2$  fold. The western NE trending part of the vergence boundary can be extended on the western flank of the Remarkables Mountains to the S joining into the hinge area of a NE trending regional  $F_3$  fold (Wye Creek). The intersection of both commensurate regional folds causes an extended zone of boudinage on the succeeding major lower long limb of both fold generations.

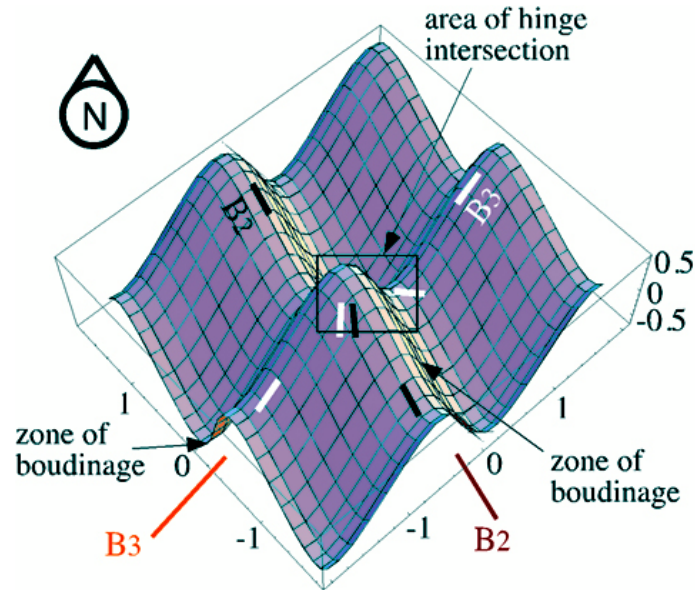


**Fig. 2.11:b)** A model, depicted as an enveloping surface of the  $F_2$  and  $F_3$  mesofolds, outlines the regional fold structure of the Remarkables area: an open NE verging regional fold of the second generation ( $F_2$ ) intersects with a close NW verging regional fold of the third generation ( $F_3$ ). The regional interference pattern displays an intermediate type 2 / type 1 geometry (Box represents the map area of fig. 2.11a). Note that the regional fold structure is cut and dextrally displaced along Cenozoic fault planes.

In the north-western part of the Otago Belt, adjacent to the Alpine Belt, the third fold generation is the dominant folding phase. Regional  $F_3$  folds attain the km-scale amplitude of the macroscopic  $F_2$  folds. The  $F_3$  mesofolds display here a clear vergence change from the W to the E (Treble Cone; see fig. 4d, h, fig. 2.12). Walking along the chosen cross-section (fig. 2.12) from Treble Cone (A) towards Glendhu Bay (B), the cross-section starts in an area of boudinaged layers with boudin axes subparallel to the local  $F_3$  fold axis. This area changes in a zone of E verging mesofolds with fold axes plunging to the S-SE, a major lower  $F_3$  hinge zone (fig. 2.12b). The deviating hinge lines display noncylindrical folds, previously interpreted as sheath folds by (Craw 1985). The noncylindrical folds evolve from a type 3 interference pattern of almost coaxial aligned folds of the second and third generation. The major  $F_3$  hinge zone extends towards N (fig. 2.12). The  $F_3$  fold axes display a rotation to a more easterly plunge in the northern area showing the decreasing influence of the regional  $F_2$  fold apart from the major hinge intersection zone. Crossing a Cenozoic fault, a major upper  $F_3$  hinge zone occurs, where the mesofolds verge to the NW. Parasitic folds and intersection lineations of the second fold generation ( $F_2$ ) are folded around the third fold axis  $B_3$  as passive linear markers. The refolding of the parasitic  $F_2$  folds displays the diminished influence of a regional  $F_2$  fold. Further E a regional  $F_2$  hinge zone occurs trending from the NNW to the SSW. The  $F_2$  mesofolds show no vergence change anymore, a hint that the macroscopic  $F_2$  fold is deamplified displaying an open fold style. W of Glendhu Bay the  $F_3$  hinge lines plunge eastwards on the major lower long  $F_2$  limb, a rotation caused by the major hinge intersection.

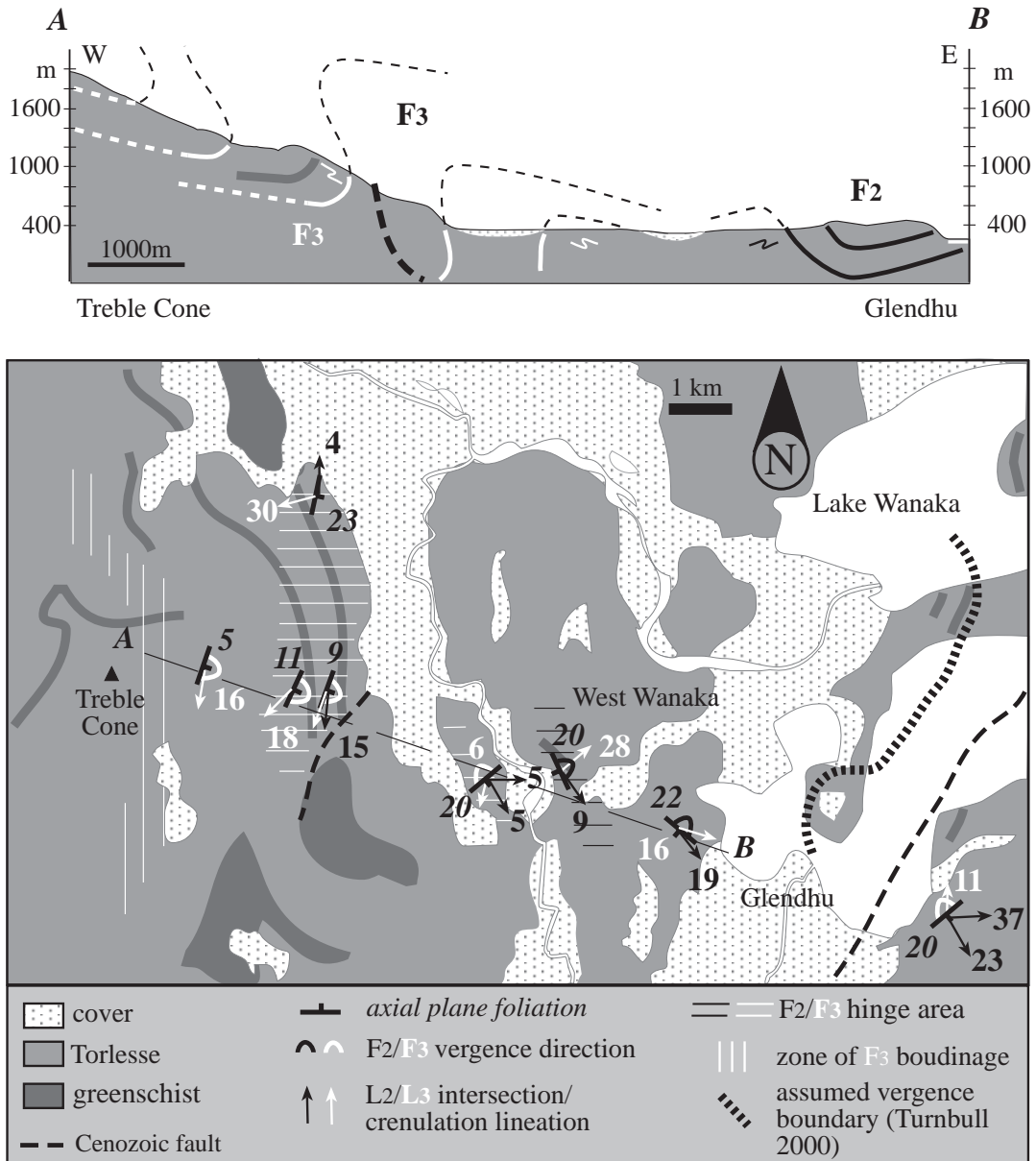


**Fig. 2.12: a)** Map of the Matukituki Valley with a cross-section from the Treble Cone in the west to the Lake Wanaka (Glendhu) in the east perpendicular oriented to the third fold axis. In the northwestern Otago Belt, enlarged regional folds of the third generation with a wavelength and amplitude at km-scale superpose  $F_2$  regional folds, which get flattened in the vicinity of the regional hinge intersection. Note that in the cross section only the regional fold characteristics of the second (black lines) and third generation (white line) are depicted but not the intersection itself. Cenozoic uplift in the western part of the cross-section causes the unusual feature that the  $F_3$  synform (Treble Cone) is exposed at a higher level than the  $F_3$  antiform (W of West Wanaka). The vergence boundary mapped by Turnbull (2000) may be a further regional fold of the third generation to the E

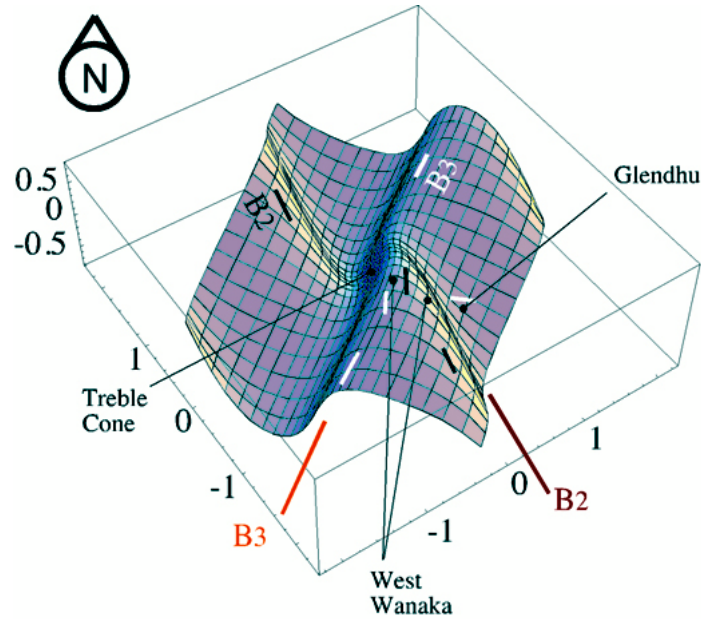


**Fig. 2.12: b)** Model of a dominant  $F_3$  macroscopic fold riding over a smaller deamplified  $F_2$  regional fold. Points indicate locations of the cross-section (fig. 2.12a). Note that the location Treble Cone is on the  $F_3$  short limb, lower  $F_3$  hinge zone.

#### 2.4.5. Extent of the second and third fold generation

In the eastern part of the Otago Belt, regions folded by the third generation folds ( $F_3$ ) are restricted to small areas (e.g. Mareburn Valley, fig. 2.4i, Moa Creek, fig. 2.4n), whereas in the north-western part of the Otago Belt the third fold generation is the dominant folding phase (e.g. Treble Cone, fig. 2.4d). This observation coincides with the set of data (crenulation lineation and fold axes) given by Mortimer (1993b; fig. 2.4). In the southeastern part of the Otago Belt the second generation of folds ( $F_2$ ) predominates. In the northwestern part the more diversely orientated lineations can be explained by growing regional  $F_3$  folds and the resulting interference pattern.

Regional folds are mostly described in the central part of the Otago Belt (Means 1963, 1966, Brown 1968, Turnbull 1981, Craw 1985, Cox 1991, Mortimer 1993a, Turnbull 2000, this study (see section 2.4.4.)), an area designated as textural zone IV (Turnbull et al. 2001, fig. 2.1c). Connected with this classification in textural zones is a description only of the development of  $F_2$  folds. Turnbull et al. (2001) describe that in textural zone IIb  $F_2$  folds may develop locally, whereas in textural zone III they can start to dominate. However, the effect of a lower textural grade on the Mesozoic fold structure is observed in three cross-sections (fig. 2.1c): two in the textural zones II-III of the Caples (Taieri Mouth – Brighton and Parawa – Garston – Kingston – Wye Creek) and one in the textural zone II-III of the Torlesse (SW of Omarama – Lindis).

Between textural zone IV and III, the subdivision depends more or less on the segregation's width; the first foliation occurs pervasively in both zones. The amplitude and wavelength of the mesofolds of both generations remains, but the style of the mesofolds changes due to the lesser-developed segregations. The underdeveloped "pseudo-layering" leads to fewer orders of small parasitic folds than in textural zone IV. Getting into the textural zone IIb, where the first foliation is still penetrative, the superposed folds have a smaller amplitude, almost no small parasitic folds are developed and only a weak superposed crenulation cleavage of both generations occur locally. In textural zone IIa, where the first foliation is developed as a slaty cleavage and only a weak object lineation ( $L_1$ ) is observed, only rare mesofolds occur. Generally it can be concluded that the development of the folds of the second and third generation depends on the pervasiveness of the first foliation ( $S_1$ ).

## 2.5. Discussion

### 2.5.1. *Timing of the development and superposition of both fold generations*

The moderate high pressure metamorphism of the Otago Schist (Yardley 1982, Mortimer 2000) is related to the formation of a penetrative first foliation ( $S_1$ ) with an object lineation ( $L_1$ ; Brown 1968, Turnbull 1981, Yardley 1982, Turnbull et al. 2001). This first deformation phase and the herewith related regional metamorphic peak (Rangitata I orogeny, Bradshaw 1989) must be younger than the Late –Middle Traissic depositional age of the Torlesse sediments (Harland et al. 1982, Kamp et al. 1989, Mortimer 1995). Geochronological studies (K-Ar, Rb-Sr, Ar-Ar on mica, fission track on zircon) reveal timing of start of this Rangitata I exhumation in the Early to Middle Jurassic (e.g. Adams et al. 1985, Kamp et al. 1989, Adams & Robinson 1993, Little et al. 1999).

In opposite to the timing of  $F_1$ , an exact timing of the onset of the second fold generation ( $F_2$ ) is not available from known geochronological studies. The second fold generation ( $F_2$ ) clearly overprints the first deformation phase. Micas aligned parallel to the first object lineation ( $L_1$ ) are folded around the second fold axis but no new minerals grow parallel to  $S_2$  (Mortimer 2000). This lack of overgrowth shows that the rocks of the Otago Schist Belt are shortened under lower metamorphic or drier conditions (Passchier & Trouw 1996, p.84) during  $F_2$  shortening. Instead of an assumed long-continued phase of cooling extending from Early Jurassic until Early Cretaceous (Adams et al. 1985, Graham & Mortimer 1992, Adams & Robinson 1993), several episodes of cooling are considered (Kamp et al. 1989, Little et al. 1999). Following the model of Little et al. (1999), the schist of the Otago Belt have been held at depth until ~ 135Ma and then rapidly unroofed during ongoing crustal shortening. Apatite fission track data (134 – 141 Ma) may represent cooling ages giving the time since the schist passed through the closure temperature of c. 110°C for apatite (Kamp et al. 1989). The same time span, late Jurassic, in several studies (Kamp et al. 1989, Little et al. 1999, Mortimer 2000) may be correlated to the cooling generated by the shortening during the second deformation phase ( $F_2$ ).

Albite and chlorite overgrowth in greenschist and the growth of epidote and chlorite in extensional veins during the third folding phase ( $F_3$ ) in the western part of the Otago Belt can be related to branches of the Alpine Barrovian-type metamorphic overprint (Mortimer 2000). Moreover the foam structure of quartz in metapsammitic layers, indicative of static recrystallisation (Passchier & Trouw 1996), corroborate this metamorphic influence. In the Alpine Schist (see fig. 2.1b) the Barrovian-type metamorphic overprint is clearly related to the third fold generation (Cooper 1974, Craw et al. 1994, Little et al. 2002a, b). The timing of the Alpine metamorphism is discussed by Mortimer (2000). Geochronologic studies (K-Ar, Rb-Sr, Ar-Ar on mica, fission track on apatite/zircon) reveal two periods of reheating, one between <119-124Ma and the other between <75-94Ma (Little et al. 1999, see Kamp et al. 1989, Graham & Mortimer 1992, Adams & Robinson 1993, Adams & Graham 1997). The younger ages (<75-94Ma) are related to pegmatite intrusions in the Alpine Schist (Kamp et al. 1989, Batt et al. 2000), which may be better related to a transtensional regime overprinting the Rangitata II orogeny (Bradshaw 1989, Bishop 1992, Chamberlain et al. 1995). Thus the older ages could be referred to the Alpine Barrovian-type metamorphism overprint and thus could be the age of thickening and unroofing caused by the development of the third fold generation ( $F_3$ ). Moreover, these ages fit to the biostratigraphically dated Middle – Late Cretaceous breccias composed of Otago Schist, which unconformably overlay the Otago Schist in half-graben systems (e.g. Fleming 1970, Turnbull et al. 1993). It is conspicuous that these dating (130-110Ma) are in areas, where pronounced deformation of the third fold generation ( $F_3$ ) exists (for example Brighton, see Adams & Robinson (1993); Nenthorn Valley ( $F_3$  of Brown 1968), see Adams & Graham (1997); Nevis Bluff and Cardrona Valley, see Graham & Mortimer (1992)).

### 2.5.2. Mesozoic fold structure versus Caples – Torlesse boundary

Terranes have been defined as “fault-bounded geologic entities of regional extent, each characterised by a geological history that is different from the history of contiguous terranes” (Jones et al. 1982). Following this definition Norris & Craw (1987), Craw & Norris (1991) and Craw (1998) establish a terrane concept for the South Island of New Zealand. Collision of the three terranes during the Rangitata I orogeny (Coombs et al. 1976, Wood 1978, Bradshaw et al. 1981) shall result in overthrusting of both Caples (from the south) and Torlesse Terrane (from the north or northeast) onto the Aspiring Terrane (fig. 2.2d). It is considered that the margins of the terranes, which separate distinctly different lithologic assemblages (Craw 1985, Cox 1991, Craw et al. 1994), are complex but presently dominated by large, nappe-like folds and shear zones (Norris & Craw 1987). The formation of these large, nappe-like folds is referred to  $D_2/D_3$  phase of deformation (Norris & Craw 1987) which is correlated to the second and third generation of folds ( $F_2, F_3$ ) of my work (fig. 2.3). The theory of nappe tectonism is rejected, because the regional and mesoscopic folds of both generations develop by a combined process of buckling and flattening. The asymmetry of the regional folds causes a boudinage at the transition from the lower regional hinge zone to the major lower long limb. Consequently those inferred “high strain zones” of Norris & Craw (1987) and Cox (1991), which have been out-

lined as the margin of terranes, are developed by the formation of the regional folds, no thrust is neither needed nor developed. Certainly one can observe reverse faults propagating within these boudinaged zones as “easy-slip horizons” but the reverse faults are not evolved during Mesozoic times but later during Cenozoic shortening (*see chapter 5*).

Investigations into the development of both Mesozoic fold generations ( $F_2$ ,  $F_3$ ) show that there is no structural break at the Caples-Torlesse boundary (fig. 2.1a, 2.4) that means both units have the same deformation history as previously noted by Mortimer (1993b) and Little et al. (1999). Although Craw (1998) outlines that these “structural continuity across the boundary arises because ductile strain, which caused juxtaposition of the rock bodies, results in development of new foliation (or foliations) in both terranes”. The development of the respective folds causes only a subordinate foliation, which is only locally developed at the major hinge zones of the regional folds, and even there the new-formed foliation can be discontinuous. The first foliation remains the dominant or main foliation over large areas (Mortimer 1993b, Turnbull et al. 2001) which occurs irregular or wavy due to the subordinate new-developed foliations ( $S_2$  or  $S_3$ ). Furthermore, Norris & Craw (1987) relates the moderate high-pressure metamorphism of the Otago Belt (Yardley 1982, Mortimer 2000) to their nappe emplacement history ( $D_2$ ,  $D_3$ ). It should be stressed that the Otago peak metamorphism is distinctly before folding ( $F_2$ ,  $F_3$ , Turnbull 1981, Yardley 1982, Mortimer 1993b, 2000). Consequently the assumed accretion of the sedimentary pile (e.g. Coombs et al. 1976, Korsch & Wellman 1988, Bradshaw 1989) and the attended Otago peak metamorphism cannot be related to the second and third fold generation but to the first deformation phase in the Otago Belt (*see chapter 4*). Moreover Craw (1998) notes that the biotite + garnet zone of the Otago peak metamorphism is confined to the Torlesse with the Caples-Torlesse boundary as its southern limit. He suggests that either the Caples had not the bulk composition to evolve this mineral assemblage or that the Caples was metamorphosed to a lesser grade than the Torlesse. Mortimer (2000), however, shows that the biotite + garnet zone is as well found in the Caples. Both units of the Otago Belt have undergone a blueschist facies metamorphic peak at the same time and the same degree (Mortimer 2000). Thus there is no metamorphic hiatus at the Caples- Torlesse boundary.

Following the definition of terranes (Jones et al. 1982, *see above*) the Caples and Torlesse cannot be defined as terranes because they are not fault-bounded geologic entities with a different geologic history. However, the word terrane could here only be construed as an informal stratigraphic designation, a prior meaning which has been long used in the geological literature (Sengör & Dewey 1991), because the only differentiation between the Caples and the Torlesse is their sedimentary composition (MacKinnon 1983, Bradshaw 1989, Mortimer & Roser 1992, Roser et al. 1993). Thus the Caples-Torlesse boundary is thought to be a broad zone of lithologic transition (lithologic mixing, Mortimer & Roser 1992), maybe both sediment sources were contiguous as proved for the Marlborough Schist, NW South Island, by Vitaliano (1968).

## 2.6. Conclusions

The description of both fold generations show that the folds are developed by some early layer-parallel shortening, which causes the development of buckles of differing wavelength as a result of thickness and competence variations between the layers. However, once initiated, any differential shear takes place on the limbs of a large wavelength, which modifies the initial symmetric fold geometric in asymmetric S and Z forms (Ramsay & Huber 1987). The absence of this shear component at the hinge zone leads to parasitic folds retaining their M form (Ramberg 1964, Ramsay & Huber 1987, p. 454). This flexural flow component leads to extensional features on the fold limbs of both generations at all scales:

- An extensional quartz vein system is developed during regional folding forming vein arrays consistent in attitude over distances of 1- 10km.
- Within these veins a grain lineations of quartz ( $L_{2\text{grain}}$ ,  $L_{3\text{grain}}$ ) is generated perpendicular oriented to the respective fold axis.
- In the north-western part of the Otago Belt, chlorite grows with its long axis (001) subparallel to  $L_{3\text{grain}}$  in greenschist rocks during the Barrovian-type metamorphic overprint.
- Small scale normal faulting and boudinage occur along the second or third cleavage on parasitic long fold limbs within a regional hinge zone ( $F_2/F_3$ ).

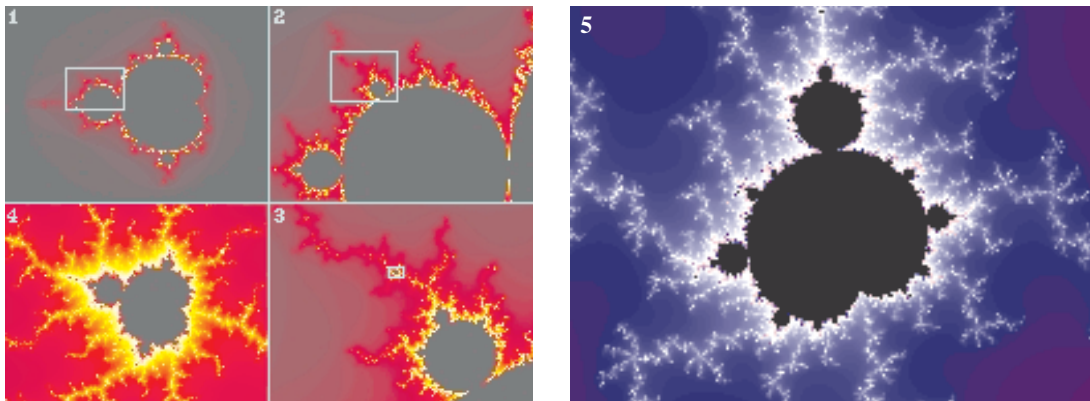
The listing of extensional features shows that the overall extension direction, and also the shortening axis, is almost perpendicular oriented to the respective fold axis. Consequently no “stretching” lineation parallel to any fold axis of both fold generations is developed contrary to Mortimer’s (1993b) interpretation.

One long discussed problem of regional folds is that boudinage occurs at the transition from lower regional hinge zone to major long limb overprinting the small and mesoscopic fold structure, the so-called “high strain zone” (Craw 1985). This succession leads Mortimer (1993b) to his interpretation of “half folds”, regional folds cut by a transposition zone, or Craw (1985), Norris & Craw (1987) and Cox (1991) to their interpretation of nappe folds, regional folds cut by a thrust zone. However, many authors (see Ramsay & Huber 1984, pp. 224-226, Ghosh 1993, Ramsay & Lisle 2001, pp.1025-1026) describe that the boudinage on fold limbs is connected with a precedent folding phase as this study does. The re-orientation of the lower long regional limb normal to the shortening direction results in boudinage at a later stage (Ramberg 1955, Ramsay 1967). Thus the theory of nappe tectonism and with it the related tectonic evolution of the Otago Schist Belt is rejected. The juxtaposition of the Caples and Torlesse rocks and the attended moderate high pressure metamorphism cannot be related to the described regional folds of the second and third generation ( $F_2$ ,  $F_3$ ) but maybe due to the first deformation phase in the Otago Belt.

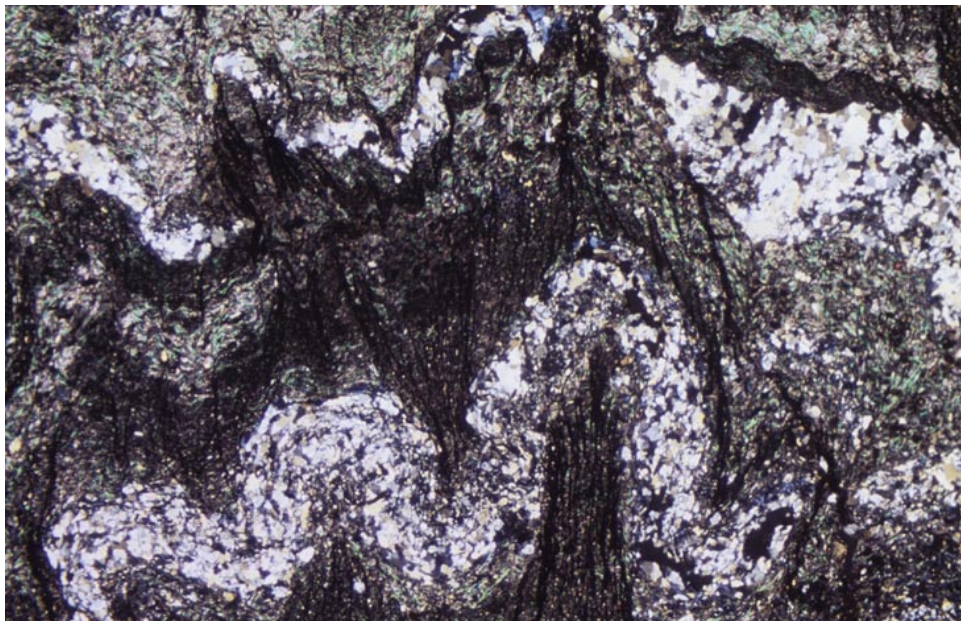


# Chapter 3

A fractal is a rough or fragmented geometric shape that can be subdivided in parts, each of which is (at least approximately) a reduced-size copy of the whole. Fractals are generally self-similar and independent of scale (see stepwise enlargement of one „Apfelmännchen“ below (1-4)). In other words, fractals are infinitely complicated: the closer you look the more detail you see. Most fractals are generated by relatively simple equations where the results are fed back into the equations again and again. The recursiveness of this procedure is why one sees structure at one scale in a fractal repeated, perhaps shrunk, rotated, and slightly distorted, on another smaller scale (see distorted „Apfelmännchen“ below (5)). The mathematician Benoit Mandelbrot, long a student of unusual statistical processes, coined the name "fractal" in the mid-1970s for this class of self-similar complicated objects that emerge out of simple recursive rules. (taken from <http://www.exploratorium.edu/complexity/CompLexicon>)



The theory of fractals can be compared to the relationship between parasitic and macroscopic folds. The refolding of the smaller structure by a larger fold causes flattening and unfolding on the major limbs, whereas the small fold structure is tightened at the major hinge zone. The relationship of small to larger folds is repeated at different scales: crenulation to tiny folds (mm-scale, see picture below) to small folds (cm-scale) to mesofolds (dm-scale) to regional folds (km-scale).



## Do parasitic folds always predict the orientation of a larger fold?

### Abstract

Investigations into the parasitic fold structure of two regional fold generations, which intersect at km-scale, reveal that the orientation of the parasitic folds of all scales varies. Where one regional fold generation dominates, all the parasitic hinge lines of this fold generation plunge in the same direction following Pumpelly's law. Interfering major upper long limbs of both asymmetric regional folds cause a variable type 2 interference pattern of the parasitic folds. Variations from type 1 to type 2 geometry result from the alternating tightness of the parasitic folds but the orientation of the parasitic hinge lines reflects the orientation of the regional fold axes of both generations. However, where both regional hinge zones intersect, strain localisation causes the parasitic hinge lines of both generations to rotate towards each other and the interference pattern changes from type 2 to type 3. The orientation of the resulting conical noncylindrical parasitic folds does not stringently imply the orientation of the regional fold axes anymore. But the change from orthogonal to almost coaxial orientation of the interfering parasitic folds infers that the superposed shortening direction is not subparallel but almost enclosing an angle of 30° to the second fold axis to the E.

### 3.1. Introduction

Polyharmonic folding of multilayers generates parasitic small folds on the back of a larger fold (Pumpelly et al. 1894, Turner & Weiss 1963, Ramberg 1964, Cosgrove 1980, Ramsay & Huber 1987, p.320 and 454). The parasitic folds change their vergence, interlimb angle, amplitude and frequency in relation to the larger fold (Ramberg 1964, Ramsay & Huber 1987, p. 454, Alsop & Holdsworth 1999). One of the most important geometric characteristics of parasitic folds is that their hinge lines are aligned parallel to the hinge lines of the larger scale folds as long as cylindrical folds are considered (Pumpelly's law). In very intensely folded rocks, the parasitic folds are generally particularly strongly developed near the hinges of major folds and less developed on the fold limbs. The relative intensity of the parasitic folds can therefore be a valuable field guide to help to locate the traces of major folds (Ramsay & Huber 1987, p. 454-456). But what will happen to the parasitic small folds of larger folds if two different oriented regional cylindrical folds intersect?

The behaviour of the small parasitic folds in relation to regional folds is examined in the Otago Schist Belt, New Zealand. Two main sets of regional folds are observed, the first set trending NW-SE, the second superposed set trending NE-SW. However, where both regional folds intersect, only one set of parasitic fold appears, which trends midway between both defined trends.

### 3.2. Fold structure of the Otago Schist Belt – the second and third fold generation

#### 3.2.1. $F_2$ and $F_3$ in areas, where one fold generation dominates over the respective other fold generation

Re-examination of the fold structure in the Otago Schist Belt reveals two successive, resembling fold generations with a wavelength and amplitude at km-scale, the second fold generation ( $F_2$ ) verges to the NE and the third one ( $F_3$ ) to the NW (*chapter 2*). Both regional folds have an open to close, asymmetric style, with long upper limbs of NE ( $F_2$ ) or NW ( $F_3$ ) vergent parasitic mesofolds growing to M-shaped, recumbent mesofolds in the hinge areas. These mesofolds with dm-scale wavelength and amplitude are thickened in the fold hinge zone and thinned on the fold limbs describing overall similar, tight to isoclinal folds (Turnbull 1981, Craw 1985). Inverse vergence, typical for a lower hinge zone, is observed locally. The asymmetric fold style and the boudinage of the long limbs of the parasitic folds reflect that the shortening direction has a steep plunge either to the NE ( $F_2$ ) or to the NW ( $F_3$ ). This almost subvertical shortening direction results in that the short major limb of a regional fold with its tight to isoclinal parasitic mesofolds succeeds into the lower long major limb, where the mesofolds get subsequently boudined until an apparent flat foliation appears. Further along the lower long major limb, a new succession of parasitic folds develops and grows in amplitude. Both generations have the first foliation  $S_1$  as form surface. The first object lineation ( $L_1$ ) is clearly folded around the respective fold axis ( $B_2/B_3$ ). The fold axes of  $F_2$  parasitic mesofolds plunge gently to the SE or the NW (fig. 3.1a, g, j, k, l, m, p) and of  $F_3$  folds to the NE or the SW (fig. 3.1d, f, h, p, and r; Brown 1968, Turnbull 1981). The axial planes of  $F_2$  dip gently to the SW or the NE and of  $F_3$  gently to the SE or NW (Brown 1968, Turnbull 1981). Almost perpendicular to the second fold axis, a grain lineation ( $L_{2\text{grain}}$ ) develops subparallel to the extension direction, preferably in new-formed extensional quartz veins (*chapter 2*). During the superposition of the third fold generation, a third grain lineation ( $L_{3\text{grain}}$ ) develops parallel to the overall extension direction, which trends ESE-WNW, but with varying enclosing angles to the third fold axis (*chapter 2*).

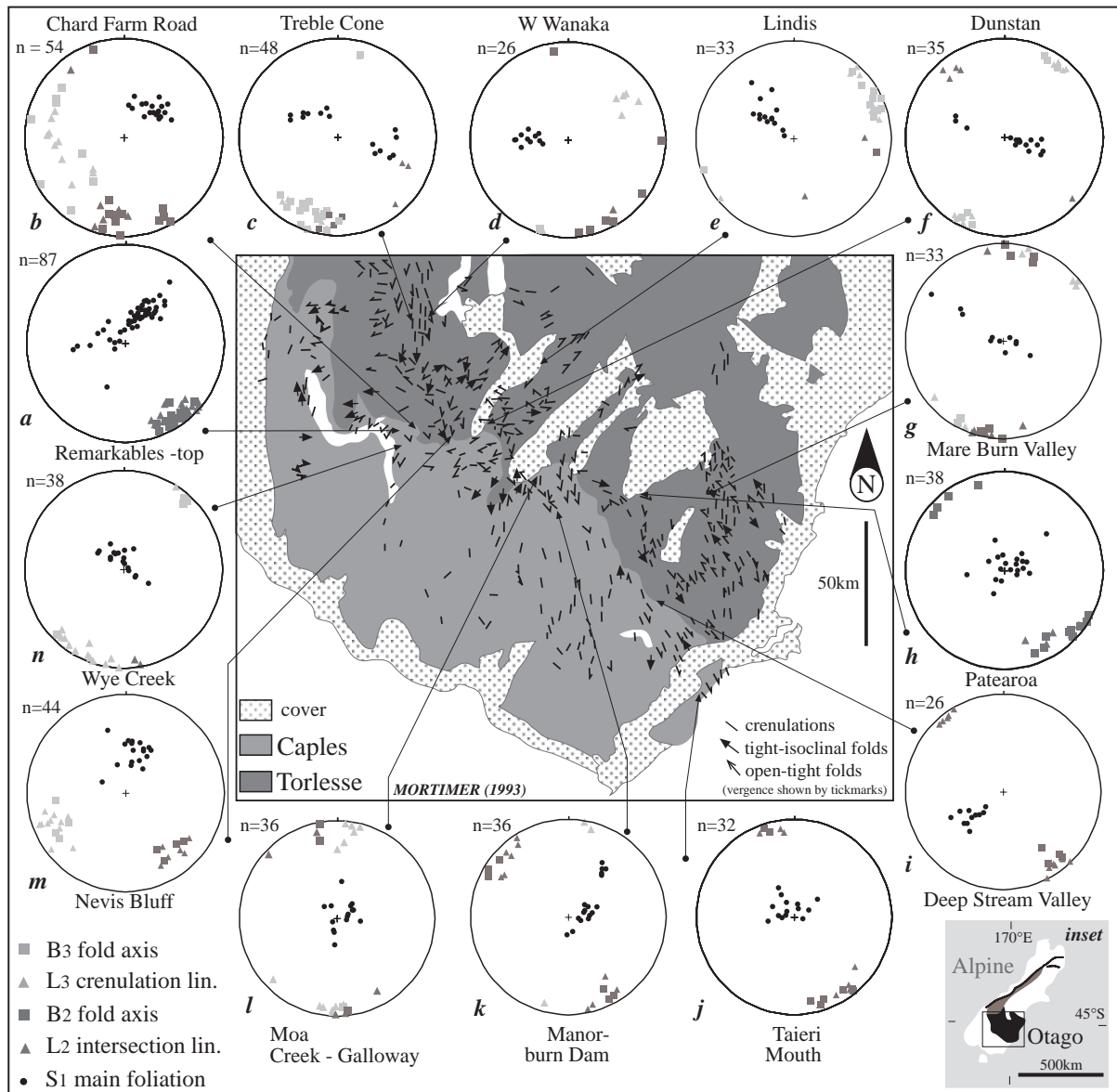


**Fig. 3.1:** Geological setting of the Otago Schist Belt (based on Figure 4 of Mortimer 1993b; small inset shows the location of the Otago Schist Belt in relation to South Island, New Zealand): Stereograms (equal area, lower hemisphere) reflect the fold axes and intersection lineations of indicated locations (fig. 3.1a-n).

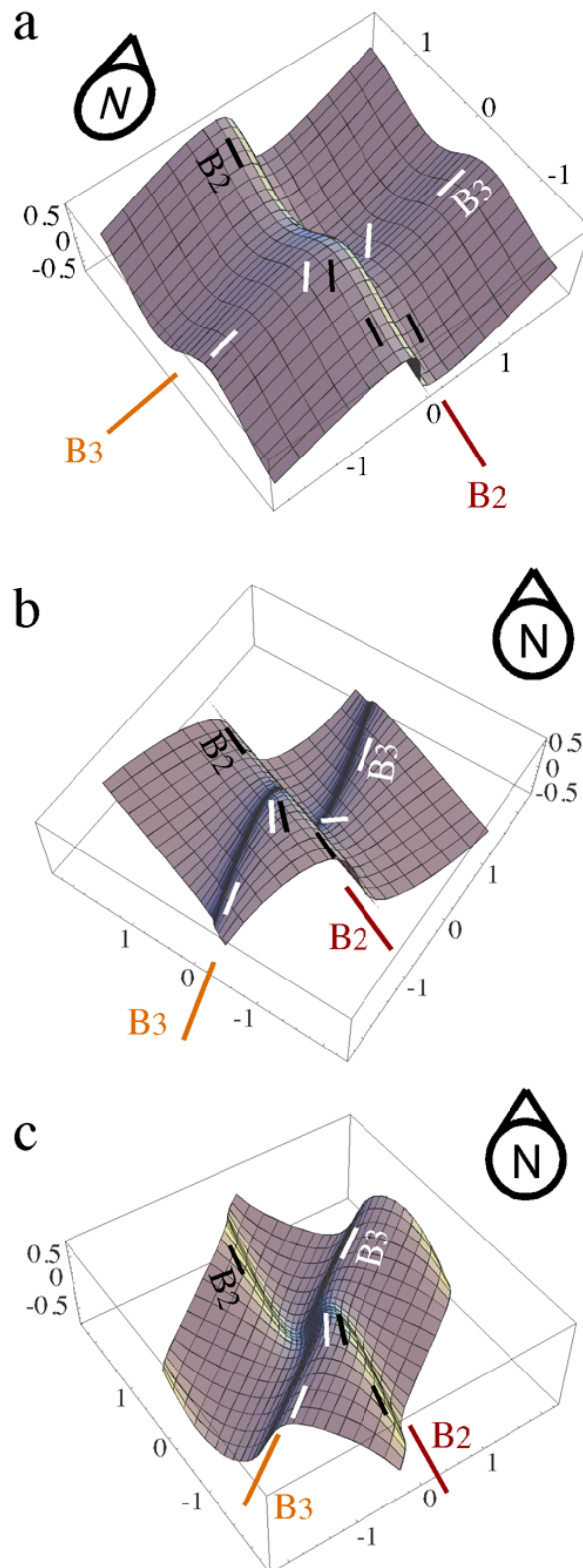


**Fig. 3.2:** The growth in amplitude of the regional folds of the third generation from the E to the W of the Otago Belt causes an alternating type 2 regional interference pattern. **a)** In the eastern Otago Belt, the regional interference pattern outlines that an open  $F_3$  regional folds of small extent rides over a dominant, close  $F_2$  regional fold. **b)** In the central Otago Belt, the regional folds of both generations ( $F_2$ ,  $F_3$ ) have an amplitude and wavelength of the same size. **c)** In the northwestern Otago Belt, the  $F_3$  regional fold amplifies and tightens, whereas the  $F_2$  regional fold flattens attaining an open fold style.

### 3.2.2. Regional interference pattern of $F_2$ and $F_3$

The regional interference pattern of both fold generations depends on the growth of the superposed  $F_3$  regional folds (*chapter 2*). Usually the second folds are more continuous than the superposed third folds, a general rule established by Skjernaa (1975). The  $F_3$  regional folds are only locally developed in the eastern Otago Belt, commonly occurring at the regional hinge intersection with a  $F_2$  regional fold (fig. 3.2a). Towards the W, the  $F_3$  regional folds grow in amplitude attaining km-scale comparable to the amplitude of the  $F_2$  regional folds (fig. 3.2b). In the northwestern Otago Belt, the third fold generation dominates over the second one (fig. 3.2c). The superposition of the third fold generation on the second one causes a change in amplitude of the second fold generation. In the eastern Otago Belt,  $F_2$  is the dominant fold generation (fig. 3.2a), which gets successively flattened attaining an open regional fold style towards the W (fig. 3.2c). The flattening of the  $F_2$  regional folds results from the extensive layer-parallel extension of the third fold generation, which is almost perpendicular to the third fold axis ( $B_3$ ) oriented.

The intersection of the almost orthogonal oriented regional folds of both generations causes an intermediate type 1/type 2 interference pattern (fig. 3.2a-c; Thiessen & Means 1980, Ghosh 1993). This “open” type 2 or deformed type 1 interference pattern is developed by the constant asymmetry of the regional folds and the open fold style of the early ( $F_2$ ) and the superposed ( $F_3$ ) fold generation (*chapter 2*).

### 3.3. Interference pattern of the small parasitic folds of both generations ( $F_2$ , $F_3$ )

Small folds are developed parasitically on the back of the mesofolds with a wavelength and amplitude on the cm-scale. They are themselves folded by smaller folds with mm-scale wavelength and amplitude. Their hinge lines are all parallel aligned to the respective fold axis ( $B_2$ / $B_3$ ) of the mesofolds. The consistent orientation of small fold’s hinges within one mesofold and again the consistent orientation of mesofolds at regional scale circumstantiates that the folds of both generations develop as cylindrical folds.

The small fold structure can be described as a polyharmonic folding of mm-thin competent quartz-albite- and incompetent mica-dominated layers. The competent quartz-albite layers show parallel fold structure, sometimes with slightly thinned limbs (class 1B – 1C, Ramsay & Huber 1987). The incompetent mica-dominated layers, which taper off into the hinge zones of the quartz-albite layers, can be described as class 3 folds (Ramsay & Huber 1987). The interlimb angle of  $F_2$  small folds displays close (interlimb angle  $30^\circ$ - $70^\circ$ ) to isoclinal folds. The dip of the axial planes of the  $F_2$  small folds outline inclined to recumbent folds. Small  $F_3$  parasitic folds have a greater variety in style than the  $F_2$  small folds. Small folds on the long limb are upright to inclined, open (interlimb angle  $120^\circ$ - $70^\circ$ ) to close whereas on the short limb they are inclined to recumbent, tight (interlimb angle  $30^\circ$ - $0^\circ$ ) to isoclinal.

Small parasitic folds of both generations ( $F_2$ / $F_3$ ) display an interference pattern, which is determined by the change of the asymmetry (vergence), the interlimb angle and the intersection angle between the trend of both fold axes. The second folds influence the development and

shape of the superposed third folds as well as themselves being deformed by superposition (Skjernaa 1975, Thiessen & Means 1980, Watkinson 1981, Grujic et al. 2002). It is assumed that the tightness of the initial folds (here  $F_2$ ) has a strong influence, while the hinge curvature has less influence on the interference pattern (Grujic 1993, Hudleston & Lan 1993, Grujic et al. 2002). The superposition of the small folds is reconstructed with the help of a Mathematica subprogram written by Moore & Johnson (2000).

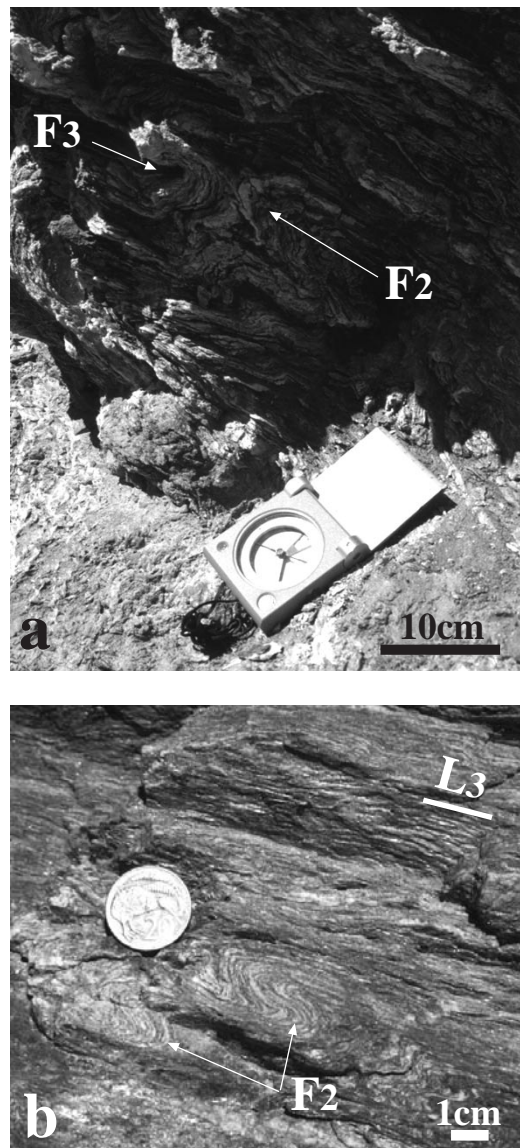


**Fig. 3.3:** **a)** Outcrop face oblique to both right-angled fold axes: NW vergent recumbent isoclinal  $F_2$  fold with tiny parasitic folds refolded by recumbent isoclinal  $F_3$  fold (Chard Farm road, Kawarau Gorge). **b)** Outcrop face viewed in direction of the second fold axis ( $B_2$ ): Right angle between the fold axis of the NE vergent small  $F_2$  fold and the crenulation lineation ( $L_3$ ), which is subparallel aligned to third fold axis (Nevis Bluff, Kawarau Gorge).

*3.3.1. Type 2 to 1 geometry of the parasitic folds on the major long limbs of both regional folds*

On the major long limb of both regional folds the gently to subhorizontally plunging fold axes of both fold generations enclose a large angle ( $70^{\circ}$ - $90^{\circ}$ ) displaying a type 2 interference pattern (Ramsay 1967, Thiessen & Means 1980, Ramsay & Huber 1987; fig. 3.3a,b). The moderately steep to gently dipping axial plane of tight to isoclinal, recumbent  $F_2$  small folds are refolded by small  $F_3$  folds. The small  $F_3$  folds have variable fold shapes ranging from upright folds (fig. 3.4) with a subvertical axial plane to gently inclined folds to isoclinal recumbent folds with a gently dipping axial plane (fig. 3.4). The refolded  $F_2$  folds have a nonplanar, cylindrically curved axial surface. The resulting type 2 interference pattern (Ramsay 1967, p. 531; Ghosh 1993) delineates circular or crescent-shaped outcrops when each of the  $F_2$  and  $F_3$  fold hinges meets a more or less planar outcrop face at more than one point. If the outcrop pattern is viewed parallel to the  $F_3$  hinge and meets the  $F_2$  hinge at more than one point a mirror-like pattern will be observed.

In case when the small  $F_2$  folds change their dip of the axial plane from recumbent to inclined and the interlimb angle displays open to close folds as the small  $F_3$  folds, the asymmetry of the folds determines the interference pattern. The resulting interference pattern is between type 2 and type 1, but never a true type 1 interference pattern is observed because the small  $F_2$  folds are always asymmetric. This observation coincides with the model of succession from an open type 2 to a type 1 interference pattern (fig. 3.5): the asymmetry of one fold generation results in a deformed dome and basin structure. If the outcrop pattern is viewed parallel to one of the fold axes ( $B_2/B_3$ ) respectively the other generation of folds will be observed. An outcrop face cut oblique to both fold axes, displays a “double vergence” pattern (Alsop & Holdsworth 1999) because of the opposite dipping axial planes of both fold generations (fig. 3.5). The “double vergence” can be misconceived as evidence of sheath folds, which Gray et al. (1995) assumes for the folds of the Otago Schist Belt.



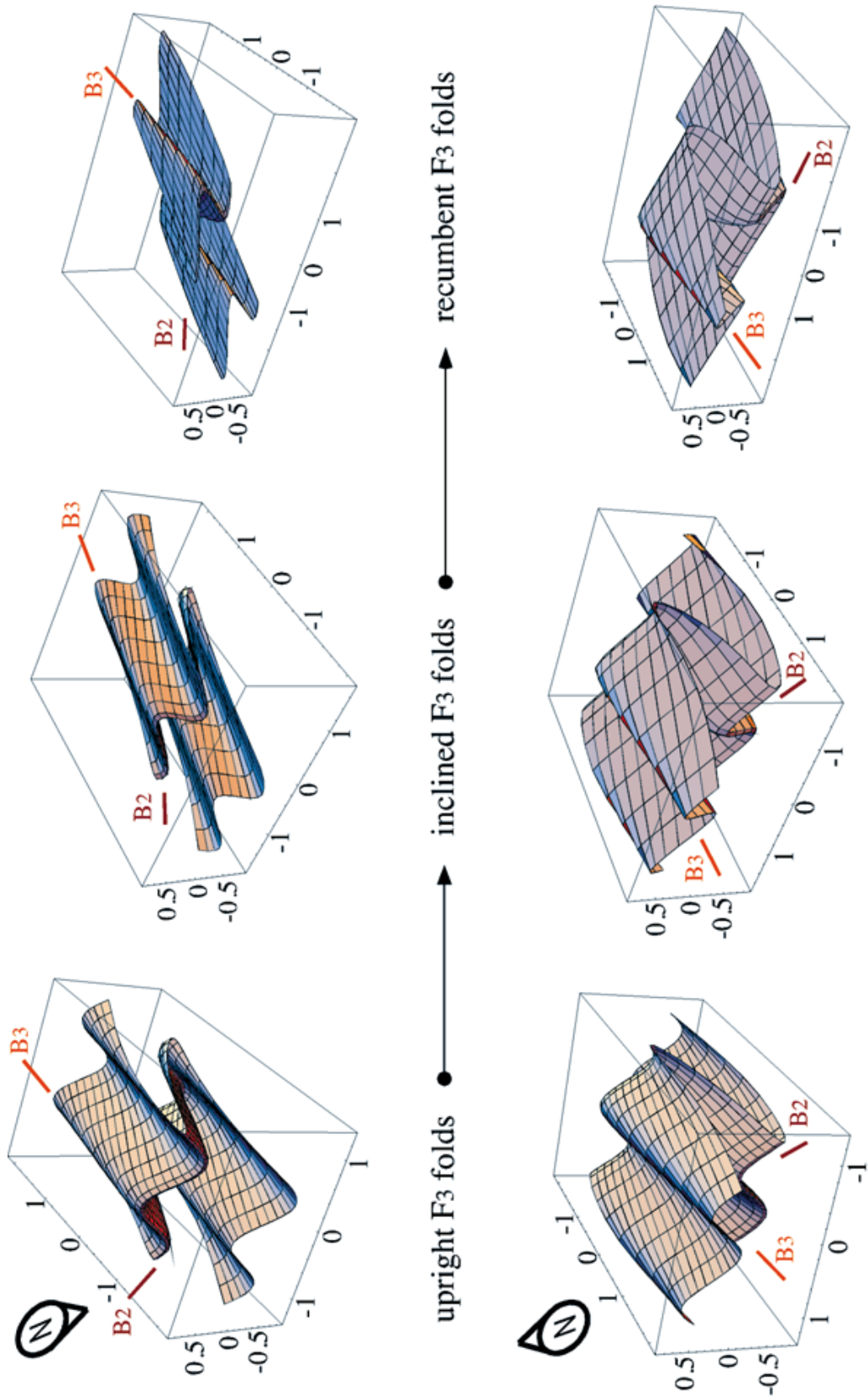


Fig. 3.4: Succession from upright to recumbent tight to isoclinal  $F_3$  folds superposed on recumbent tight to isoclinal  $F_2$  folds (second row displays the same succession from another viewpoint)

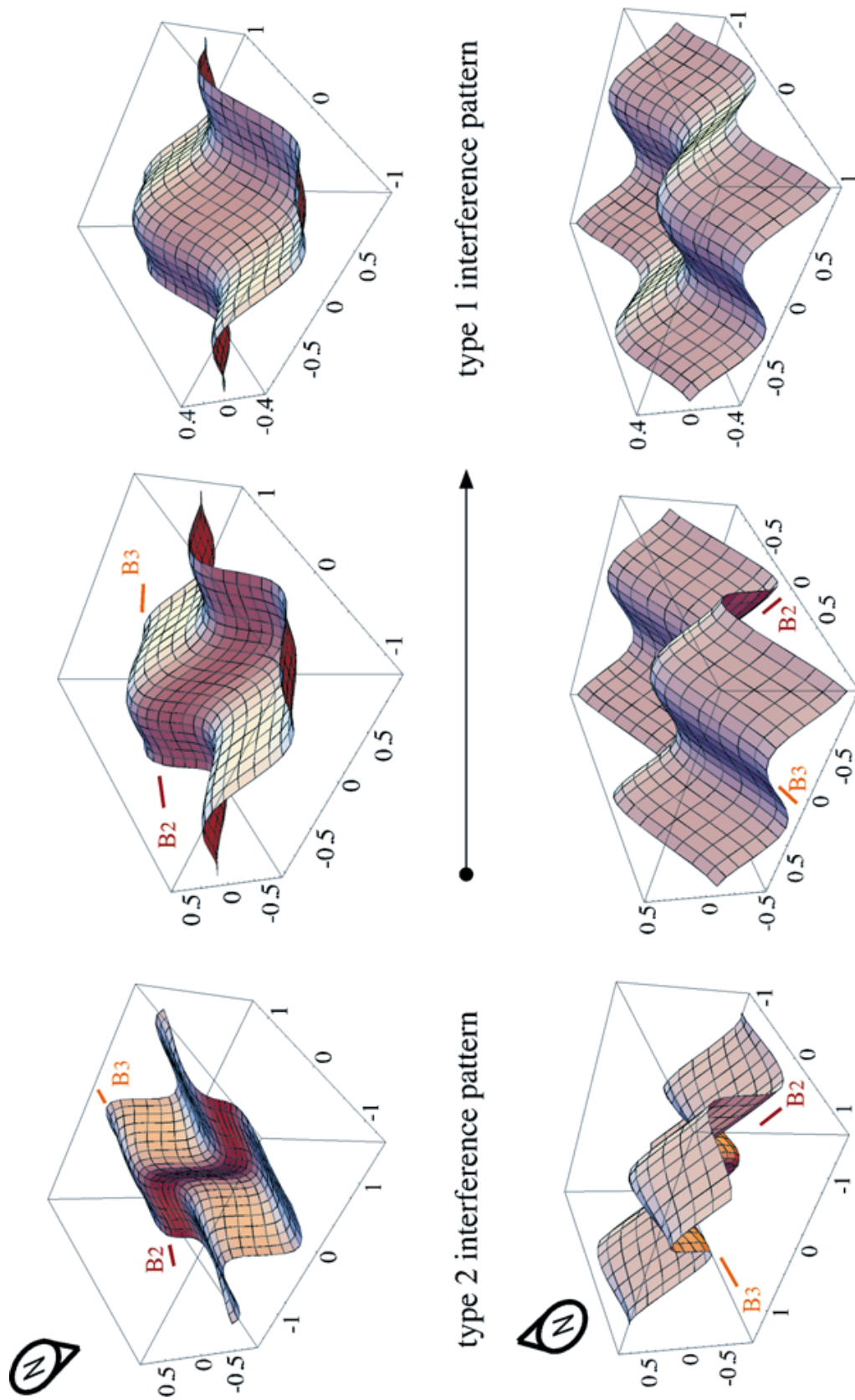
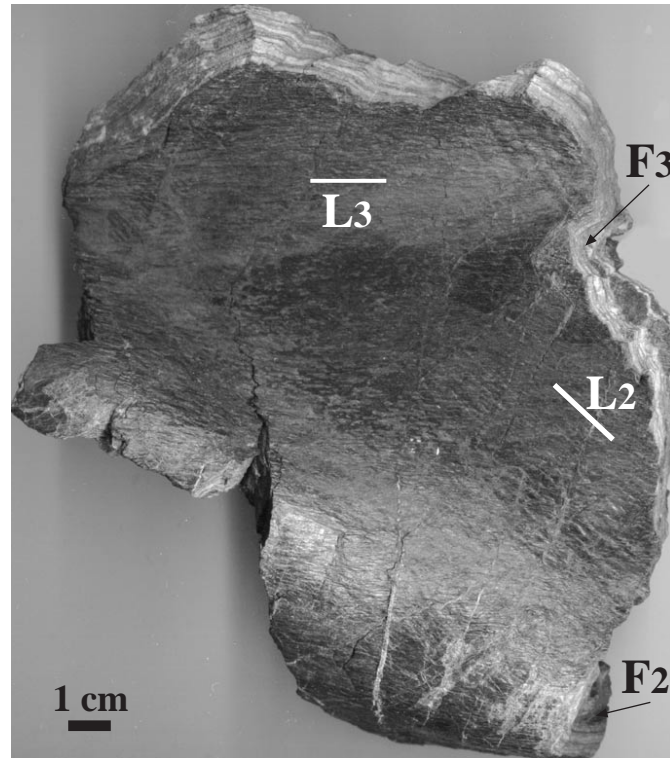


Fig. 3.5: Succession from type 2 to type 1 interference patterns (second row displays the same succession from another viewpoint)



**Fig. 3.6: a)** Open type 2 interference pattern: The second intersection/crenulation lineation ( $L_2$ ) is overprinted by the crenulation lineation of the third generation ( $L_3$ ). The intersection angle between the trends of both lineations amounts to  $50^\circ$ . The resulting interference pattern of open folds can be misinterpreted as noncylindrical folds of one fold generation ( $S$  of Lake Hawea Neck). **b)** Crenulation lineation of the third fold generation ( $L_3$ ) outlined here as quartz rods overprints quartz rods of the second fold generation ( $L_2$ ; Shotover River).

### 3.3.2 Type 3/0 geometry of the parasitic folds at the regional hinge intersection of both generations

Where both regional folds intersect, the parasitic hinge lines of both generations rotate towards each other resulting in a smaller intersection angle between both trends. Consequently the interference pattern change from a type 2 to almost type 3 (fig. 3.6, 3.7). The axial plane of small  $F_2$  folds is folded almost coaxial by the third fold generation. The small  $F_2$  folds flatten and tend to unfold during rotation and finally show no distinct vergence pattern anymore (fig. 3.7). The progressive unfolding of the second generation of folds results from the orientation of their axial planes perpendicular to the principal extension direction of the superposed strain ellipsoid (Grujic 1993, Grujic et al. 2002). Because of this flattening the typical type 3 interference pattern (Ramsay 1967, p. 531; Thiessen & Means 1980, Ghosh 1993) outlining hook shaped outcrops, when each of the  $F_2$  and  $F_3$  fold hinges meet a planar outcrop face at more

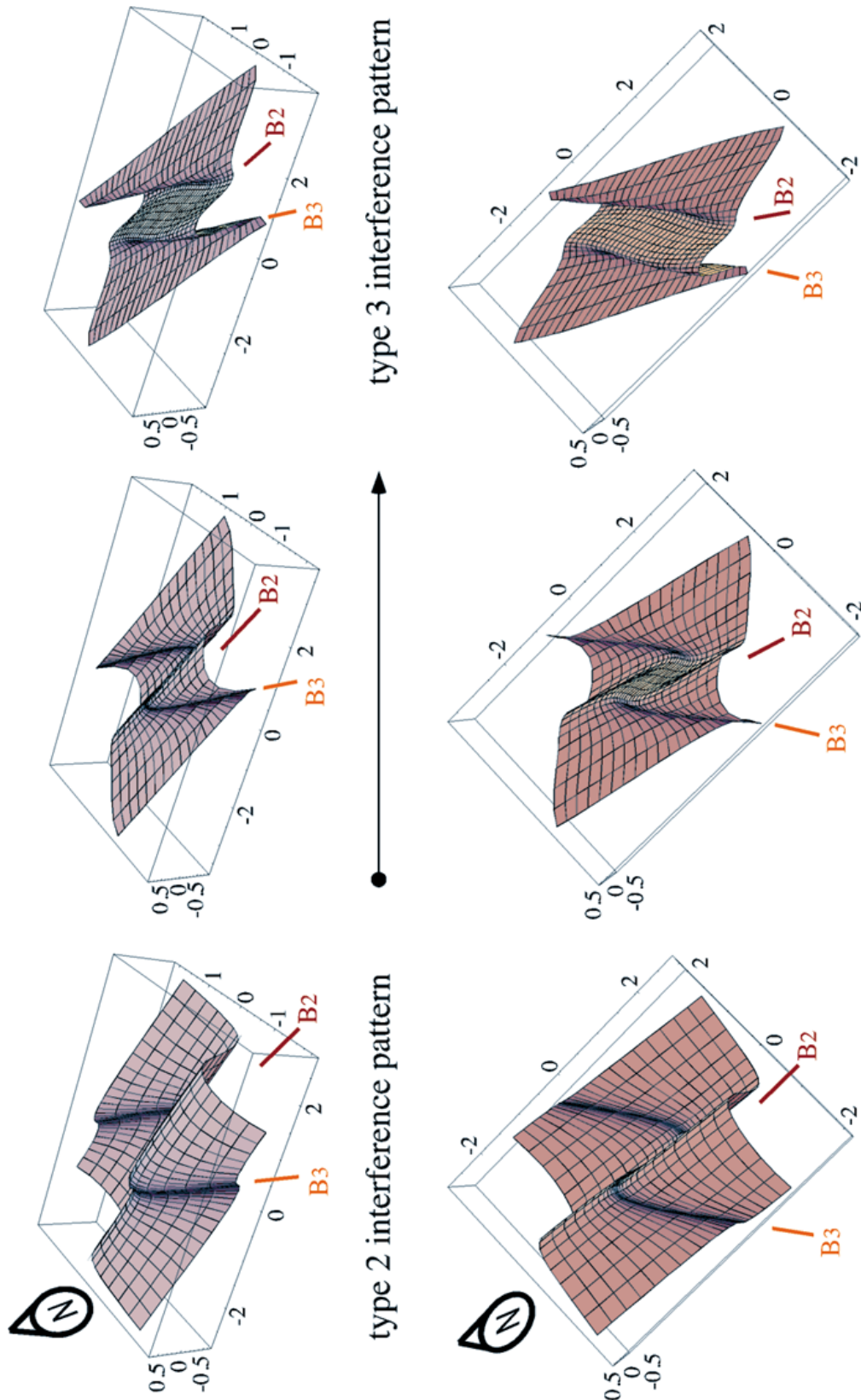


**Fig. 3.7:** Succession from type 2 to type 3 interference patterns (second row displays the same succession from another viewpoint). Note that the folds of the second generation ( $F_2$ ) are flattened during further rotation due to superposition of the third generation ( $F_3$ ).

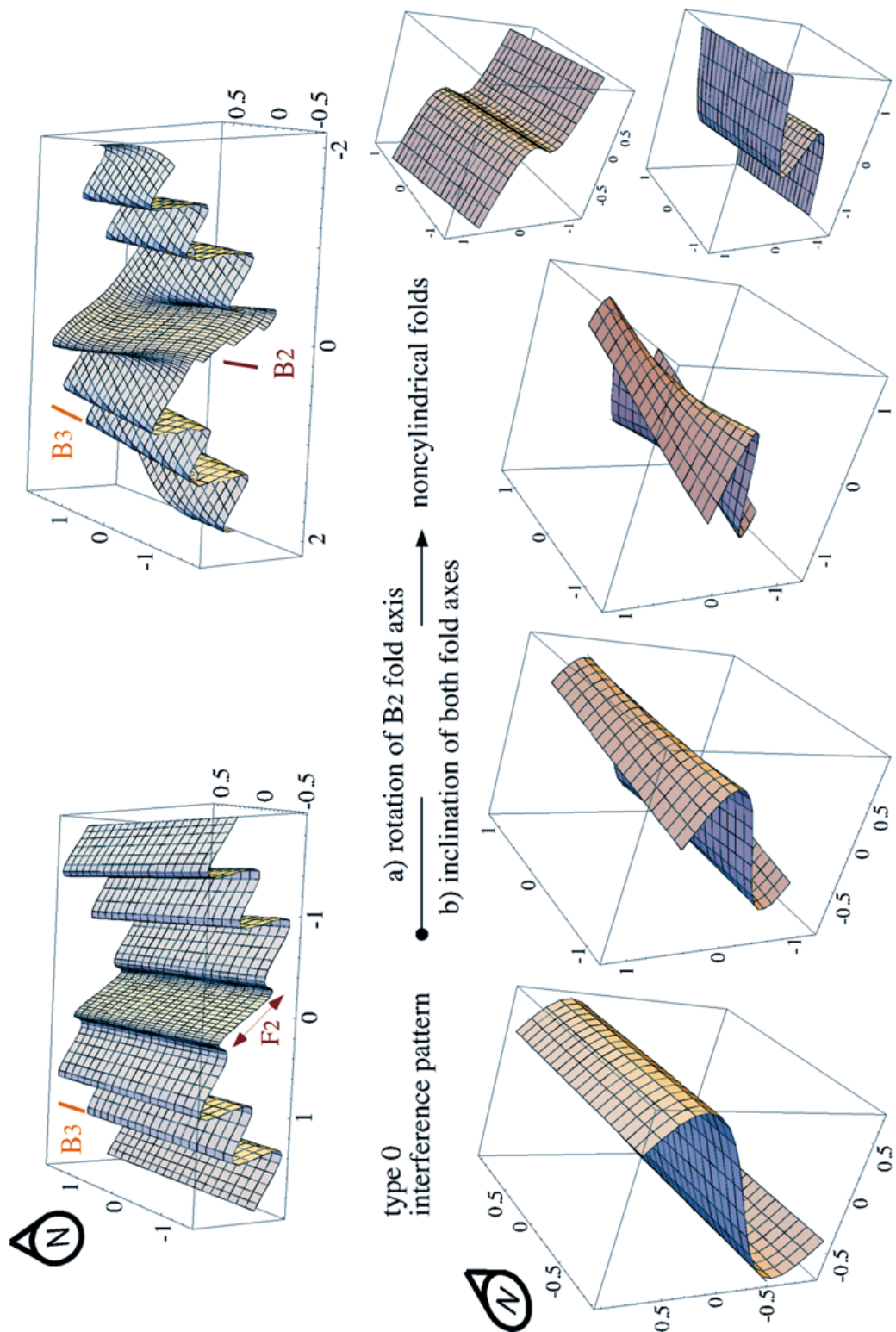


**Fig. 3.8:** **a)** First row shows the succession from flattened  $F_2$  folds in a dominant  $F_3$  folding (type 0 geometry) to the development of noncylindrical folds by rotation of trend of  $F_2$  fold axis. **b)** Second row displays the succession from type 0 interference pattern to noncylindrical folds by inclination of the fold axes ( $B_2/B_3$ ) of inverse vergent folds. Both opposite vergent folds with their inclined fold axes are separately shown on the right side.

than one point, is hard to see. If the outcrop pattern is viewed parallel to the  $F_2$  and  $F_3$  hinge a planar, transposed layering will be observed. The interference with the more open second folds maybe outlines rather a type 0 interference pattern (Thiessen & Means 1980, Ramsay & Huber 1987, Ghosh 1993), where the  $F_3$  folds are reinforced or diminished due to the appearance and orientation of the  $F_2$  folds. Moreover the opposite vergence of the small  $F_2$  folds causes an irregular fold pattern of the  $F_3$  small folds. Especially, where both fold axes are not subparallel aligned, conical noncylindrical folds are observed. The development of noncylindrical folds is reconstructed on the one hand by the rotation of strike of one fold axis ( $B_2$ ) leading to a smaller intersection angle ( $10^\circ$ ; fig. 3.8a) and on the other hand by different inclination of the fold axes of both opposite vergent folds (fig. 3.8b). The observed individual fold axes display plunge culminations and depressions which result in a sinusoidal wave-like pattern in the axial direction. The strike of the noncylindrical fold axes varies up to  $20^\circ$  (fig. 3.9). The dip of the axial surface adopts between the dip of the third and the flattened second axial plane outlining a noncylindrical curvilinear axial plane.

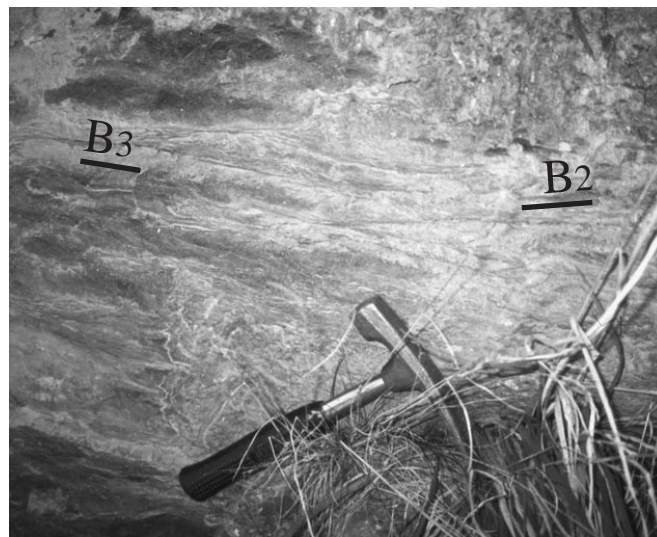


**Fig. 3.9:** Outcrop surface parallel to third fold axis ( $B_3$ ): noncylindrical folds result from type 3 interference pattern. The trend of noncylindrical folds varies up to  $20^\circ$  (Treble Cone).

### 3.4. Discussion - Conformity of the interference pattern with physical models of superposition

#### 3.4.1. Change from type 2 to type 1 interference pattern

The change from type 2 to type 1 interference pattern is outlined in many experimental models. Johns and Mosher (1996) indicate that the competence contrast strongly controls the style of the fold interference. Multilayers with significant competence contrast are characterised by a type 2 interference pattern, whereas low competence contrast results in a type 1 interference pattern. The high competence contrast – indicated here by the cusped-lobate structure – influences certainly the pronounced interference pattern of the small folds. As the alternating layering is only mm-thick, the influence of the rheological contrast diminishes on larger scale, maybe indicated by the fact that mesofolds display overall similar folds, a fold style characteristic of lower competence contrast (Ramsay 1967, p.422; Thiessen & Means 1980, Thiessen & Haviland 1986). However, although a significant competence contrast between the narrow-spaced quartz- and mica-rich layers exists, different interference patterns of the small fold structure are generated. The major factor whether type 1 or 2 develops, is the initial fold geometry and not the kinematics of the third deformation as Grujic (1993, see Ghosh & Ramberg 1968, Skjernaa 1975, Watkinson 1981, Ghosh et al. 1993) outlines. Similarly, it is shown here that close to tight  $F_2$  folds re-fold into type 2 interference pattern, which become even more pronounced as the tightness of the second generation folds increases. Open  $F_2$  folds produce type 1 interference pattern, which is always slightly distorted due to the inclination of the  $F_2$  fold axial plane (vergence).

#### 3.4.2. Change from type 2 to type 3 interference pattern

The intersection of small parasitic folds of both generations display the change from orthogonal to almost coaxial interference pattern (*see section 3.3.2*), also prementioned by Brown (1968) for the eastern part of the Otago Schist Belt. The unusual change in the geometry of fold superposition is compared to physical models in the following section.

The behaviour of the  $F_2$  small folds during the superposition depends on the position on the interfering regional folds of both generations. At a  $F_3$  regional hinge zone developed on the major upper long  $F_2$  limb, the second folds behave as passive linear markers (Lindis (fig. 3.1f), West Wanaka (fig. 3.1e)), because the second folds ( $F_2$ ) are sufficiently small relative to the superposed ones ( $F_3$ ). Where both major hinges intersect, the hinge lines of both parasitic folds ( $F_2$ ,  $F_3$ ) rotate towards each other in N-S direction. A rotation of the hinge lines of two successive generations is shown in the experimental studies of Ghosh & Ramberg (1968) and Odonne & Vialon (1987). Odonne & Vialon (1987) show that for a small angle between both experimental compression directions ( $15^\circ$ - $45^\circ$ ) the new-formed folds have a tendency to align with the initial folds. The initial folds are reused and reinforced (Odonne & Vialon 1987) forming an almost type 0 interference pattern (Thiessen & Means 1980, Ramsay & Huber 1987, Ghosh 1993). Odonne & Vialon (1987) suggest that in case of an angle of  $60^\circ$  between both compression directions some classical features of type 1 interference pattern are present at the same

time as features of type 0 one (see Figure 8 of Odonne & Vialon 1987). Gentle to open initial folds are refolded in an orthogonal type 1 pattern, whereas open to close initial folds are reused and strengthened forming a type 0 pattern. The transition from type 1 to 0 seems to be a progressive changeover as Odonne & Vialon (1987) note. Ghosh et al. (1996) state that this phenomenon of rotation resulting from interference of two oblique fold waves is quite distinct from the concept of hinge migration as defined for a single generation of cylindrical folds.

In these experimental studies superposed folding is only processed with a single layer, but a multilayer influence the type of superposition. Especially, where different competent layers are folded together, various interference types between major and parasitic folds develop as Ghosh (1970, 1974), Thiessen & Means (1980) and Ghosh et al. (1993) notes. In multilayers the variation in orientation of the small fold hinges is mostly greater than that of the major fold hinges (Ghosh et al. 1993). Ghosh (1974) notes that if different orders of parasitic folds of one generation are shortened parallel to their fold axis, different orders of superposed parasitic folds will successively develop resulting in noncylindrical nonplanar fold shapes. Consequently the unrolling of a larger superposed fold will not restore the hinges of the smaller folds to their original straight shape. This large variation of fold hinges is as well reinforced in multilayers where the compression directions enclose an angle smaller than  $90^\circ$  (Ghosh et al. 1993). Johns & Mosher (1996) only indicate that in some of their multilayer models the axial traces appear to be coaxially refolded although the whole experiment is formed in a non-coaxial geometry.

The pronounced asymmetry of both fold generations influences the development of interference patterns as well (fig. 3.4, 3.5, 3.7, 3.8). Although Thiessen & Means (1980) note that the superposition on asymmetrical early folds (here  $F_2$ ) does not change the interference geometry and thus the angular criteria's between both fold generations maintain. Especially the extension direction of every fold generation, which is oriented perpendicular to the respective fold axis and subparallel to the axial plane of the respective fold, may play a role. The overall extension direction of the superposed fold generation ( $F_3$ ), which trends in ESE-WNW direction (*chapter 2*), encloses a small angle to the second fold axis ( $B_2$ ). Consequently the second folds ( $F_2$ ) tend to unfold and flatten on every scale in the vicinity of the regional  $F_3$  folds. Thus when the superposed folds are smaller than the second folds, the superposed third folds show a pronounced tendency to develop at right angles to the second folds rather than at right angles to the shortening or extension direction (Skjernaa 1975). But the weakened influence of the second folds in the vicinity of dominant superposed third folds may result in the orientation of the third fold axis perpendicular to the overall third extension direction rather than perpendicular to the second fold axis. This result is strengthened by stereograms of locations with pronounced superposed third folding (fig. 4.1. Treble Cone (c), Dunstan (f) and Wye Creek (n)), which show a more southerly trend of the third fold axis than locations with interference of commensurate fold generations (fig. 4.1. Nevis Bluff (m)). Thus it may be concluded that the shortening direction of the superposed third fold generation is not parallel but encloses an angle of  $20-30^\circ$  to the second fold axis. Instead of SE-NW direction for an orthogonal pattern the shortening direction trends in ESE-WNW direction subparallel to the overall extension



direction of the third fold generation (*chapter 2*). The small angle of almost  $30^\circ$  of the shortening direction of the superposed folds ( $F_3$ ) to the trend of the second folds axes causes the change from an orthogonal to an almost coaxial interference pattern as experimentally modelled by Odonne & Vialon (1987). But the experimental models of Odonne & Vialon (1987) only outline a change from a type 1 to type 0 interference pattern. The vergence of the folds and the gentle plunge of the fold axes of both generations in the Otago Schist Belt cause a type 2 interference pattern resulting in an almost type 3 geometry at a regional hinge intersection. It is suggested that the vergence affects the interference pattern (*section 3.3.2*) but both may not directly influence the rotation of the fold axes. Following the model of Odonne & Vialon (1987), it may be concluded that in areas with a relative lesser contraction a type 2 or 1 interference pattern evolves, whereas in areas with a relative higher contraction type 3 or 0 geometry develops. Thus the rotation of the parasitic hinge lines of both generations results also from a larger shortening within a regional hinge intersection.

### 3.5. Conclusion

The observation of the parasitic fold structure within regional folds shows that the orientation of the parasitic folds of all scales varies. Plunges of parasitic fold hinges remain constant and thus reflect the orientation of a larger fold, when only one generation of the regional folds dominates ( $F_2$  or  $F_3$ ; fig. 3.10a, b). On the major long limbs of both regional folds, just in the vicinity of the regional hinge intersection, parasitic folds of both generations intersect. The resulting interference pattern of the cm-scale small parasitic folds change from a deformed dome and basin structure (almost type 1, fig. 3.10d) to recumbent refolded folds (type 2, fig. 3.10c) from the long limb to the hinge zone of intersecting mesofolds, which have a wavelength and amplitude at dm-scale. The observed plunge of both parasitic folds reflects as well the orientation of the regional folds of both generations ( $F_2/F_3$ ).

Within a regional hinge intersection, strain localisation results in a rotation of hinge lines of both previously almost orthogonal oriented parasitic folds ( $B_2/B_3$ ) towards each other and therewith in a change of interference pattern from type 2 to type 3 (fig. 3.10e). The inverse dipping axial planes and gently plunges of both fold axes ( $B_2/B_3$ ) as well as the small intersection angle between both trends of fold axes ( $B_2/B_3$ ) mislead to the interpretation of noncylindrical folds of one generation. However, the orientation of these noncylindrical folds does not stringently imply the orientation of regional folds anymore. The re-orientation of the parasitic folds within a regional hinge intersection does not result in a complete re-orientation of the regional folds themselves in the Otago Belt. Except in the northwestern Otago Belt, where the noncylindrical folds display almost the orientation of the superposed dominant third fold generation ( $F_3$ ; see Treble Cone, fig. 3.1c and fig. 3.2c).

However, the change from orthogonal to almost coaxial fold pattern infers that the superposed shortening direction of the third generation is not initially oriented subparallel to the early fold axis ( $F_2$ ), but encloses an angle of almost  $30^\circ$  towards the E.

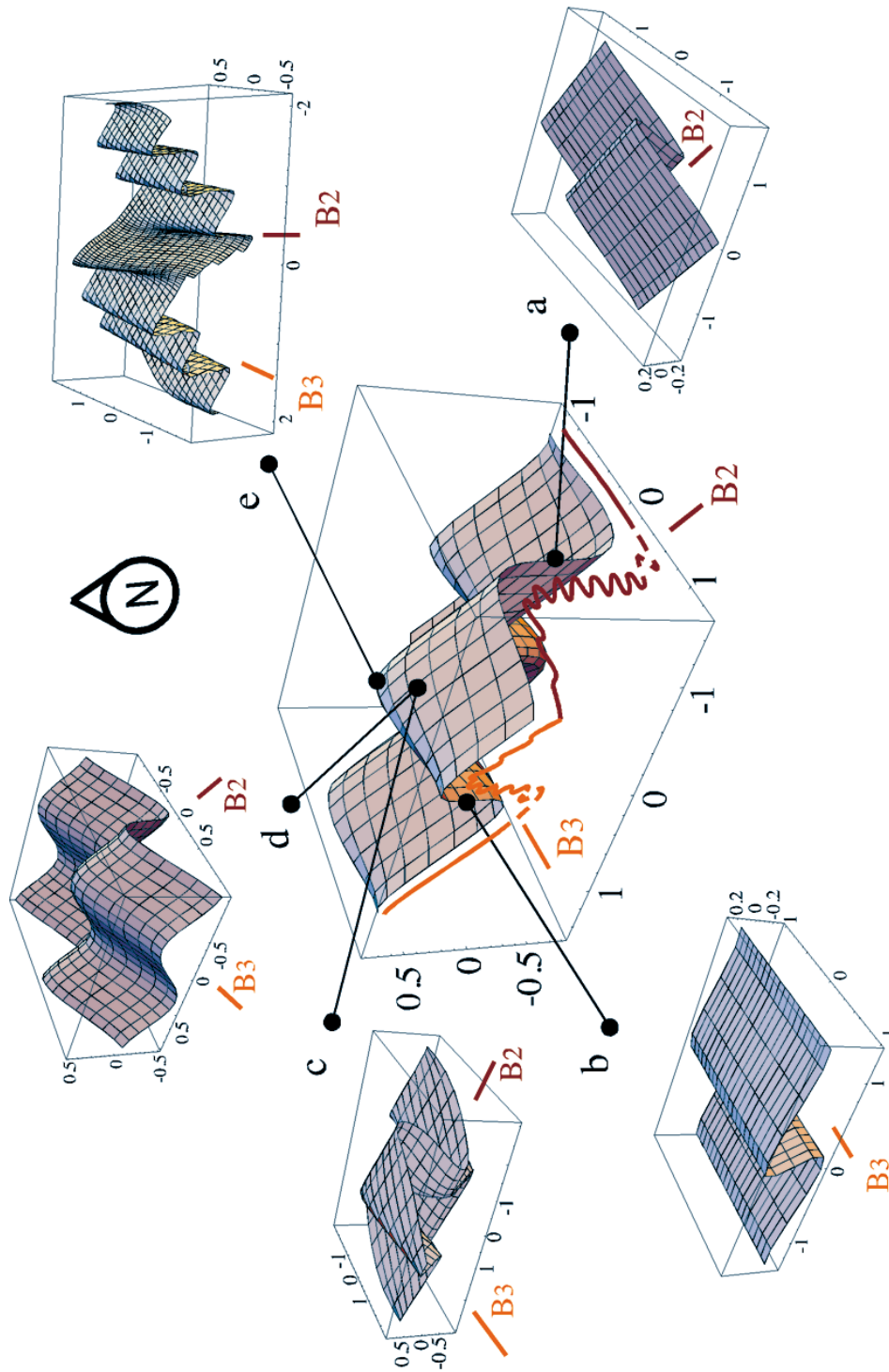


**Fig. 3.10:** Mesozoic fold structure outlining two successive fold generations, which are almost orthogonal oriented at regional scale (centre of the figure). Folded lines display the change in asymmetry and tightness of the mesofolds from the upper limb to the hinge of the regional fold (mesofolds are not to scale). The mesofolds get subsequently boudinaged at the transition from the short to the long limb. Small boxes (fig. 3.3 a-e) display the change of interference pattern of the parasitic folds in relation to the regional folds. **a)** dominant NE vergent  $F_2$ , **b)** dominant NW vergent  $F_3$ , **c)** type 2 interference pattern, **d)** intermediate type 1/type 2 interference pattern, **e)** type 3 interference pattern as observed on the limbs of intersecting mesofolds (modelled with the help of a Mathematica subprogram written by Moore & Johnson (2000)).

# *Chapter 4*

*Alles in der Welt geht in der Wellenlinie. Jede Landstraße und so weiter.  
Wehe dem, der überall ein Lineal anlegt!  
(Wilhelm Raabe)*



*Bent twig*

## Superposed folding of an early lineation

### - is it possible to reconstruct the initial rectilinear orientation?

#### Abstract

The refolded pattern of the first object lineation  $L_1$  due to the superposition of both Mesozoic fold generations ( $F_2/F_3$ ) is discussed.  $L_1$  is preserved on the main foliation plane ( $S_1$ ), which is folded by both Mesozoic fold generations ( $F_2/F_3$ ) but never completely transposed by new foliations ( $S_2/S_3$ ). The linear structure  $L_1$  rotates within the short limbs of the parasitic folds towards the respective fold axis ( $B_2/B_3$ ), whereas it comes to lie at a higher angle to the fold axis on the parasitic fold limbs (type 2 geometry of Ghosh & Chatterjee (1985)).  $L_1$  is generally strengthened on the short limbs displaying an N-S to NE-SW trend. However, reconstruction of these refolded lineation patterns reveals that the initial rectilinear  $L_1$  trends in ENE-WSW direction on the main foliation  $S_1$ .

#### 4.1. Introduction

A dominant structural feature of many orogenic belts is the complex outcrop pattern produced by several phases of folding. In regions showing such a pattern, linear structures of many types are common, and several sets of lineation occur together. The linear patterns that arise from polyphase deformation are geometrically complex because the lineations related to early folds vary as a result of deformation by the new folds (Ramsay 1960, Ramberg & Ghosh 1977, Ghosh & Chatterjee 1985). The pattern of a deformed early lineation ( $L_1$ ) over a superposed fold ( $F_2$ ) is controlled essentially by (1) the competence contrast of the associated rocks, (2) the initial orientation of the planar segment of  $F_1$  on which  $L_1$  lies, (3) the initial angle between  $L_1$  and  $F_2$  and (4) the nature and intensity of bulk deformation (Gosh & Chatterjee 1985). In the Otago Schist Belt, folds of superposed generations are formed as buckle folds (*see chapter 2*), which show an internal deformation by a combination of flexural flow and tangential longitudinal strain (Ramsay 1967). Ramsay (1967) describes that the tangential longitudinal strain changes the angle between the early lineation and the superposed fold axis within a buckle fold. On the outer arc of the finite neutral surface, the layers are subjected to a tangential extension, which reaches a maximum value around the hinge zone. On these surfaces the angle between the deformed lineation and the fold axis is increased by an amount which depends on the amount of the extension (type 3 geometry of Ghosh & Chatterjee (1985)). On the inner arc, layers undergo tangential contraction. For these surfaces the angle between the deformed lineation and the fold axis is decreased by an amount which depends on the amount of contraction (type 2 geometry of Ghosh & Chatterjee (1985)). The finite neutral surface is unstrained. On these surfaces, lineations will be deformed in exactly the same way as with the flexural flow model, where the strain is plane at all points in the fold. Consequently the angle between the early lineation and the superposed fold axis remains at all points of the fold (Ramsay 1960, 1967; type 1 geometry of Ghosh & Chatterjee (1985)). In this paper the refolded pattern of an early lineation (fig. 4.1a), which is superposed by two fold generations, is discussed. The com-

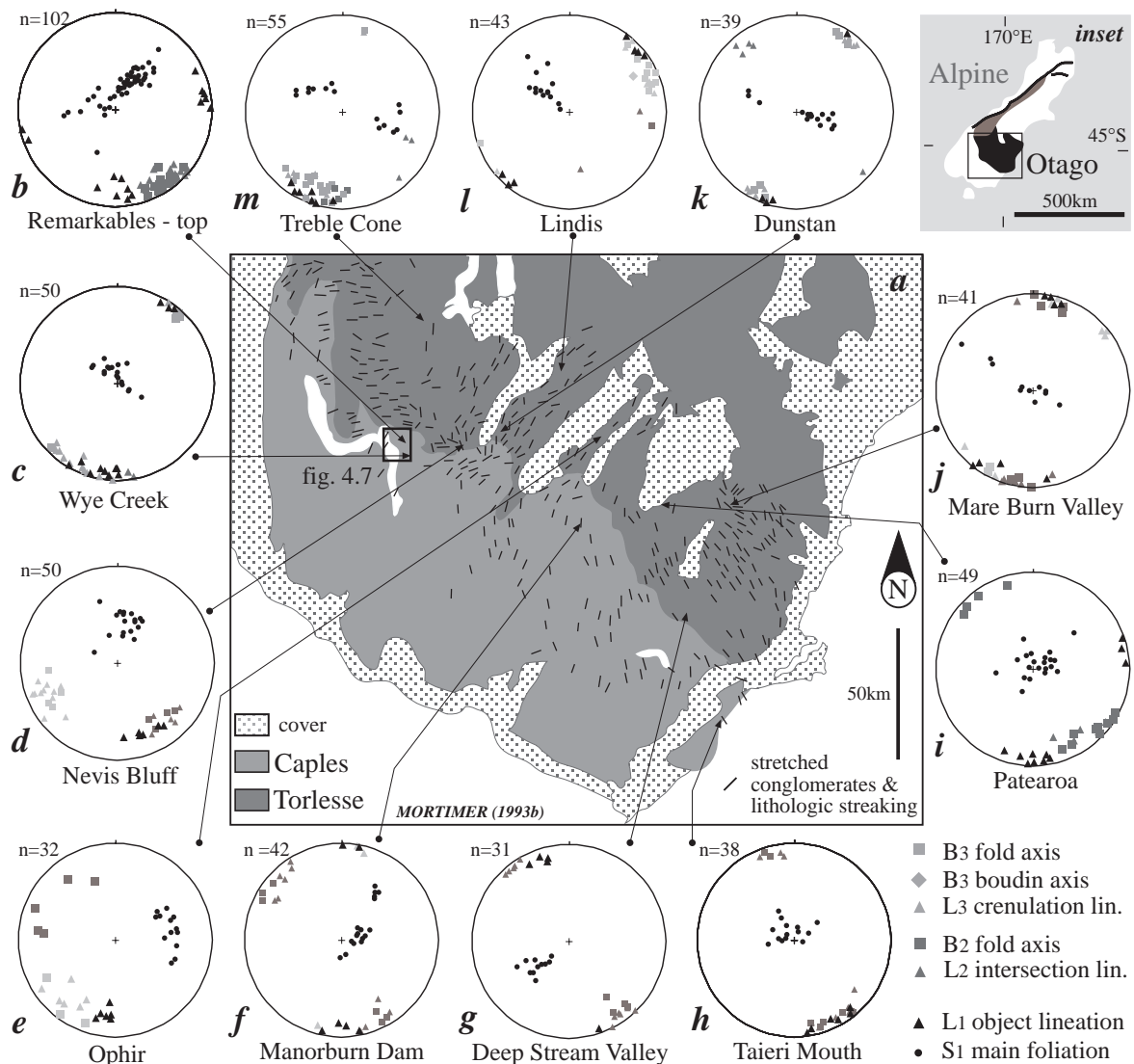


**Fig. 4.1:** **a)** Geological setting of the Otago Schist Belt (Based on Figure 4 of Mortimer 1993b. Small inset shows the location of the Otago Schist Belt in relation to South Island, New Zealand. Box indicates the location of fig. 4.7.): The refolded pattern of the early lineation  $L_1$  is diversely oriented as recorded for the eastern and central part of the Otago Belt by Mortimer (1993b). The mapped E-W direction in the westernmost Otago Belt shall be excluded because in this area a later developed grain lineation occurs ( $L_{3\text{grain}}$  mainly perpendicular to the third fold axis  $B_3$ ).

**b - m)** Stereograms (equal area, lower hemisphere projection) reflect the relationship between the early lineation  $L_1$  and the fold axes ( $B_2/B_3$ ) and intersection lineations ( $L_2/L_3$ ) of the superposed fold generations ( $F_2/F_3$ ) at the indicated locations.

bined folding process of buckling and flattening causes a simpler refolded lineation pattern than described before. Shortening is concentrated at the fold hinge leading to a rotation of the early lineation towards the superposed fold axis. At the fold limbs, extension exceeds and the early lineation comes to lie at a higher angle to the later fold axis. Some questions arise from the investigations into this refolded lineation pattern: how does the early lineation develop? Does any shear occur subparallel to this lineation as proposed by previous studies (Norris & Bishop 1990, Mortimer 1993b)? Why is the first foliation preserved as the main one? Is it possible to reconstruct the initial orientation of a once rectilinear lineation? Does the shear associated with the early lineation influence the reorientation?

## 4.2. The first deformation phase $F_1$ of the Otago Schist Belt

### 4.2.1. The first foliation $S_1$

$S_1$  develops by tight to isoclinal folding of the bedding. Layer-parallel extension disrupts the once continuous bedding (transposed bedding, Bishop 1974). Small intrafolial  $F_1$  folds are sometimes preserved, generally in the eastern part of the Otago Belt (Brown 1968, Turnbull 1981). The axial plane foliation  $S_1$  is parallel aligned to  $S_0$  on the limbs and normal to the enveloping surface ( $S_0$ ) on the hinges (Turnbull 1981). Commonly a continuous new foliation ( $S_1$ ) evolves parallel to the axial planes of the  $F_1$  folds (Bishop 1974, Turnbull 1981).  $S_1$  is strengthened by quartz-albite and mica-rich segregation (Cooper 1974) caused mainly by rotated and disrupted early quartz-albite veins (Norris & Bishop 1990). The resulting “layering” is an irregular spaced, discontinuous alteration of mm-thin quartz-albite-rich and mica-rich layers in the metagreywacke (Turnbull et al. 2001).  $S_1$  parallel grown white mica grains reflect a moderate high pressure metamorphism showing peak metamorphic temperatures and pressures of 350°-400°C and 8-10 kbar (Mortimer 2000). The orientation of the mainly gently dipping first foliation displays the superposition of both fold generations ( $F_2/F_3$ ; fig. 4.1b-e).

### 4.2.1. The first object lineation $L_1$

The layer-parallel extension causes the development of an object lineation ( $L_1$ ) subparallel to the first fold axis ( $B_1$ , Turnbull 1981; definition of lineations by Piazzolo & Passchier 2002).  $L_1$  occurs both as an aggregate lineation, which is defined by long axes of pebbles in intraformational quartzite conglomerates (Norris & Bishop 1990, fig. 4.2) and a parallel-aligned grain lineation, which is defined by the oriented growth of metamorphic minerals along the pervasive axial plane surface ( $S_1$ , Turnbull 1981). Commonly  $L_1$  plunges gently enclosing a small angle to one superimposed fold axis ( $B_2/B_3$ ), respectively the one of the dominant fold generation (fig. 4.1b-e).

Some previous workers infer a certain amount of shear subparallel to the grain lineation  $L_1$  (Turnbull 1981, Norris & Bishop 1990, Winsor 1991a, Mortimer 1993b, Little et al. 1999), others describe  $L_1$  only as an intersection lineation (Means 1966, Cox 1991). To clarify this feature, amphibole-rich rocks, which occur in the Caples Group at the Remarkables and Wye Creek (fig. 4.1b-c), are examined. The amphiboles consist of equigranular cores of hornblende

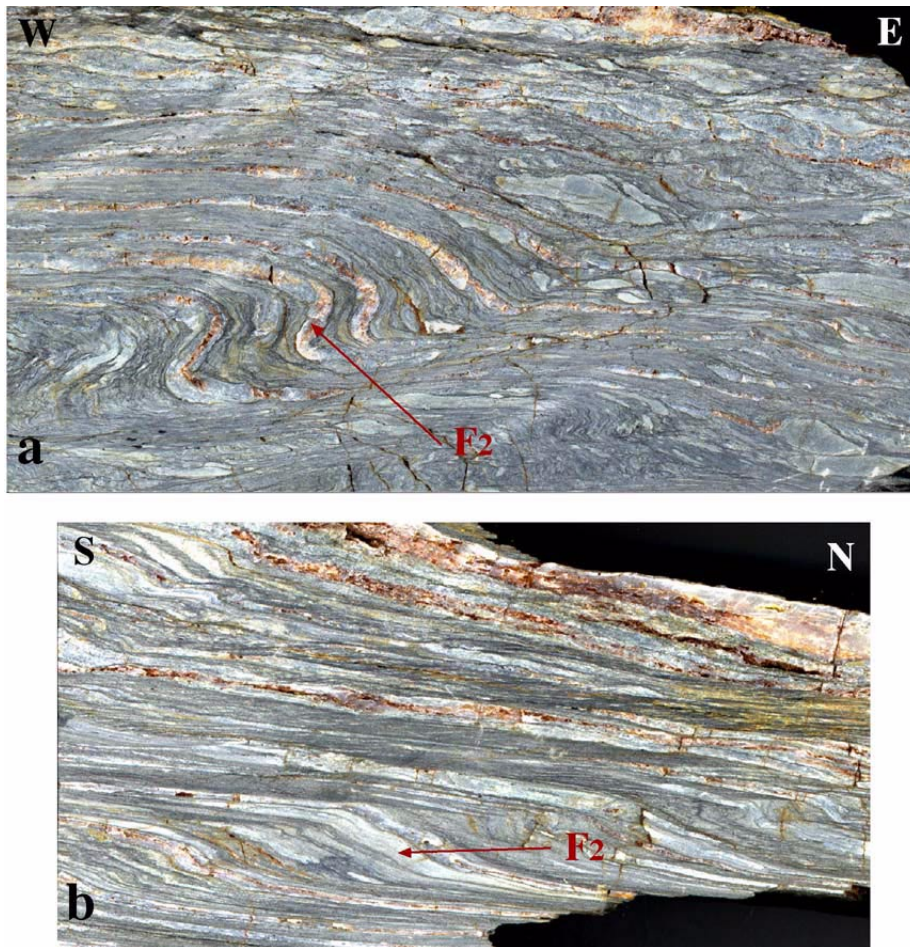


**Fig. 4.2:** The first object lineation  $L_1$  developed as an aggregate lineation in a matrix-supported intraformational quartzite conglomerate of the Torlesse Group, Mare Burn Valley (fig. 4.1j): **a**) perpendicular to  $L_1$  and  $B_2$  showing that the conglomerate is discontinuously folded; **b**)  $L_1$  almost subparallel to  $B_2$  – the apparent angle between both lineations varies between  $10^\circ$  and  $30^\circ$  (Because the sample is taken near a regional hinge intersection of both fold generations).

and elongated rims of actinolite, which overgrow the hornblende cores epitaxially (fig. 4.3a, b). The actinolite-rims extend with their long axes (c-axis) parallel to the first mineral lineation  $L_1$  on the main foliation  $S_1$  (fig. 4.3b, d). Basis plates of both amphibole grains (normal to the c-axis,  $\{011\}$ ) are visible in thin section perpendicular to  $S_1$  and  $L_1$  (fig. 4.3a, c). The orientation of the amphibole grains defines more than a grain lineation. Thin sections parallel to  $L_1$  (and normal to  $S_1$ ) show that the actinolite grains are not only grown but as well stretched parallel to  $L_1$ . Once continuous actinolite grains are disrupted by boudinage (fig. 4.3b) or extremely lengthened (fig. 4.3d). Commonly there is no fibre growth of quartz and mica preserved between disrupted, stretched amphiboles because of the pervasive recrystallisation under low-grade conditions (Mortimer 2000), which accompanies the first deformation phase.

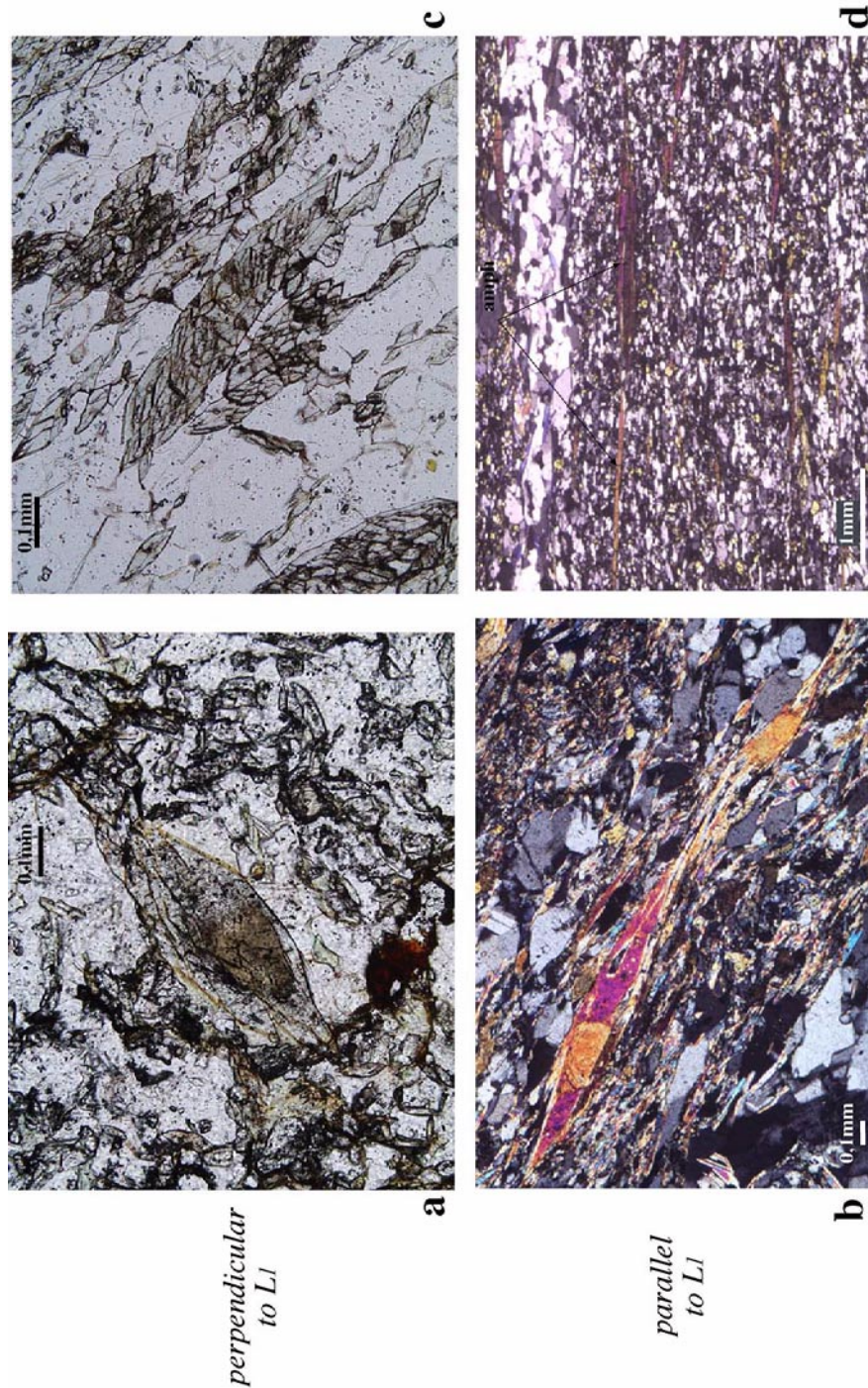


**Fig. 4.3 a)** Hornblende core with its rhombic cleavage and typical pleochroism (light brown, olive green, greenish brown) shows a slightly higher refraction than its overgrown rim of actinolite with a pallid pleochroism (achromatic, yellowish, greenish) as observed perpendicular to  $L_1$  ( $\perp S_1$  and  $B_3$ , plane polarised light; Wye Creek). **b)** A rectilinear cleavage of the hornblende and actinolite and an elongated rim of actinolite occurs subparallel to  $L_1$  ( $\perp S_1$  and  $\parallel B_3$ , crossed polarised light; Wye Creek). **c)** Basis cut (normal to the  $c$ -axis,  $\{011\}$ ) of an actinolite which is broken along its rhombic cleavage achieving an elongated form maybe due to the superposed layer-parallel extension perpendicular to the second fold axis  $B_2$  ( $\perp S_1$  and  $L_1$ , plane polarised light; Remarkables). **d)** Stretched and disrupted actinolite laths aligned subparallel to  $L_1$  ( $\perp S_1$  and  $\parallel B_2$ , crossed polarised light; Remarkables).



Indicators of any shear sense, which are developed subparallel to  $L_1$ , are rarely observed. Quartz and mica filled pressure shadows around epidote grains commonly display a symmetric or a slightly sigmoidal shape. Considering the observed stretch of the amphibole grains parallel to  $L_1$ , the less sigmoidal pressure shadows are possibly generated by a synthetic rotation due to buckling counterbalanced by an antithetic flexural flow (Bell & Forde 1995) during the superimposed fold development of both generations ( $F_2/F_3$ ). Consequently a certain amount of shear is associated with  $L_1$  but a distinctive shear sense direction cannot be determined.

### 4.3. Folding of the main foliation $S_1$ or the development of superposed cleavages ( $S_2/S_3$ )

#### 4.3.1. The second crenulation cleavage ( $S_2$ )

In the Otago Schist the second cleavage ( $S_2$ ) is commonly developed as a crenulation cleavage (Turnbull 1988, Mortimer 1993b, Bishop 1994 in Turnbull et al. 2001), so the first disjunctive foliation  $S_1$  is folded and reoriented. The second crenulation cleavage is always developed with a gradational transition between cleavage domains and microlithons (Passchier & Trouw 1996; fig. 4.4a, 4.5a). A discrete generated crenulation cleavage with a typical sharply defined new foliation is only developed at the hinge of parasitic folds (fig. 4.4b, 4.5b). Commonly  $S_2$  is spaced and highly asymmetric at the limbs of parasitic folds, whereas it is zonal and symmetric only at the hinge zone of the parasitic folds. The high layer-parallel extension on the limbs and the gradational character of  $S_2$  results in a weak and discontinuous second crenulation cleavage ( $S_2$ ).

The development of a crenulation cleavage is generally influenced by the presence and activity of a fluid phase, the presence of soluble minerals and the growth of new minerals (Cosgrove 1976, Gray & Durney 1979a, Gray 1979, Wright & Platt 1982, Passchier & Trouw 1996). Quartz and less intense albite grains in the Otago Schist rocks are dissolved at preferred boundaries of mica (001) forming flattened grains in cleavage domains. The  $S_1$  parallel-aligned mica grains are folded and re-oriented but they are neither overgrown, nor replaced by new micas (Mortimer 2000). The solution is hampered in mica-rich layers, which are accompanied by a high portion of finely distributed epidote (fig. 4.5e). Epidote as a less soluble mineral prevents the combined process of microfolding and dissolution.

The weak and less penetrative development as well as the lack of recrystallisation and overgrowth indicates that the second crenulation cleavage generates under lower metamorphic or drier circumstances (Passchier & Trouw 1996, p.84) than the first disjunctive synmetamorphic foliation  $S_1$ . During progressive metamorphism, water is generally released by mineral reactions favouring complete recrystallisation during  $S_1$  development. After the peak of metamorphism, under retrograde circumstances when the rock has lost most of its water, recrystallisation is difficult and deformation results mainly in folding and boudinage of  $S_1$ .

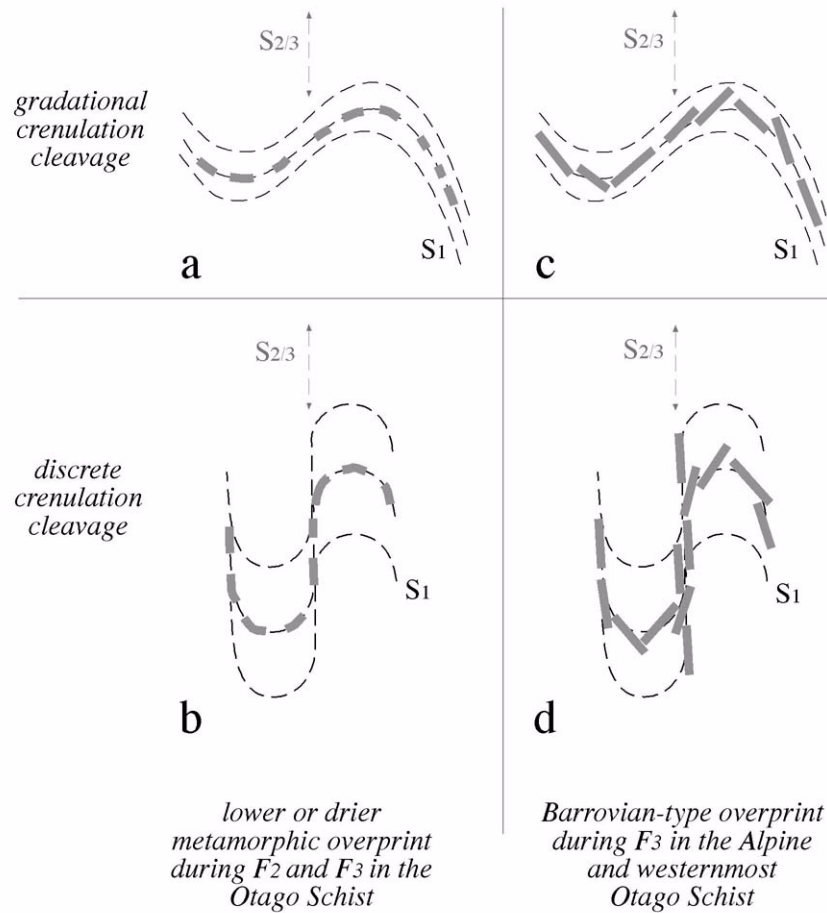


**Fig. 4.4:** **a**) A pre-existing foliation ( $S_1$ ) can be followed from microlithons through the crenulations displaying a gradational crenulation cleavage (Passchier & Trouw 1996). The spaced gradational crenulation cleavage prevents that a new foliation plane ( $S_2$ ) is developed. **b**) A crenulation cleavage is described as discrete, where the pre-existing foliation truncates against the crenulations. A new foliation plane is generated ( $S_2/S_3$ ), whereas the early lineation is only preserved in the microlithons. A discrete crenulation cleavage is only developed at the hinge of parasitic folds of both generations ( $F_2/F_3$ ). **c**) The gradational crenulation cleavage is overgrown by mica grains parallel to their basis (001) resulting in a herringbone structure. **d**) Polygonal arcs (Passchier & Trouw 1996) are evolved by overgrowth of a discrete crenulation cleavage by mica grains (001).

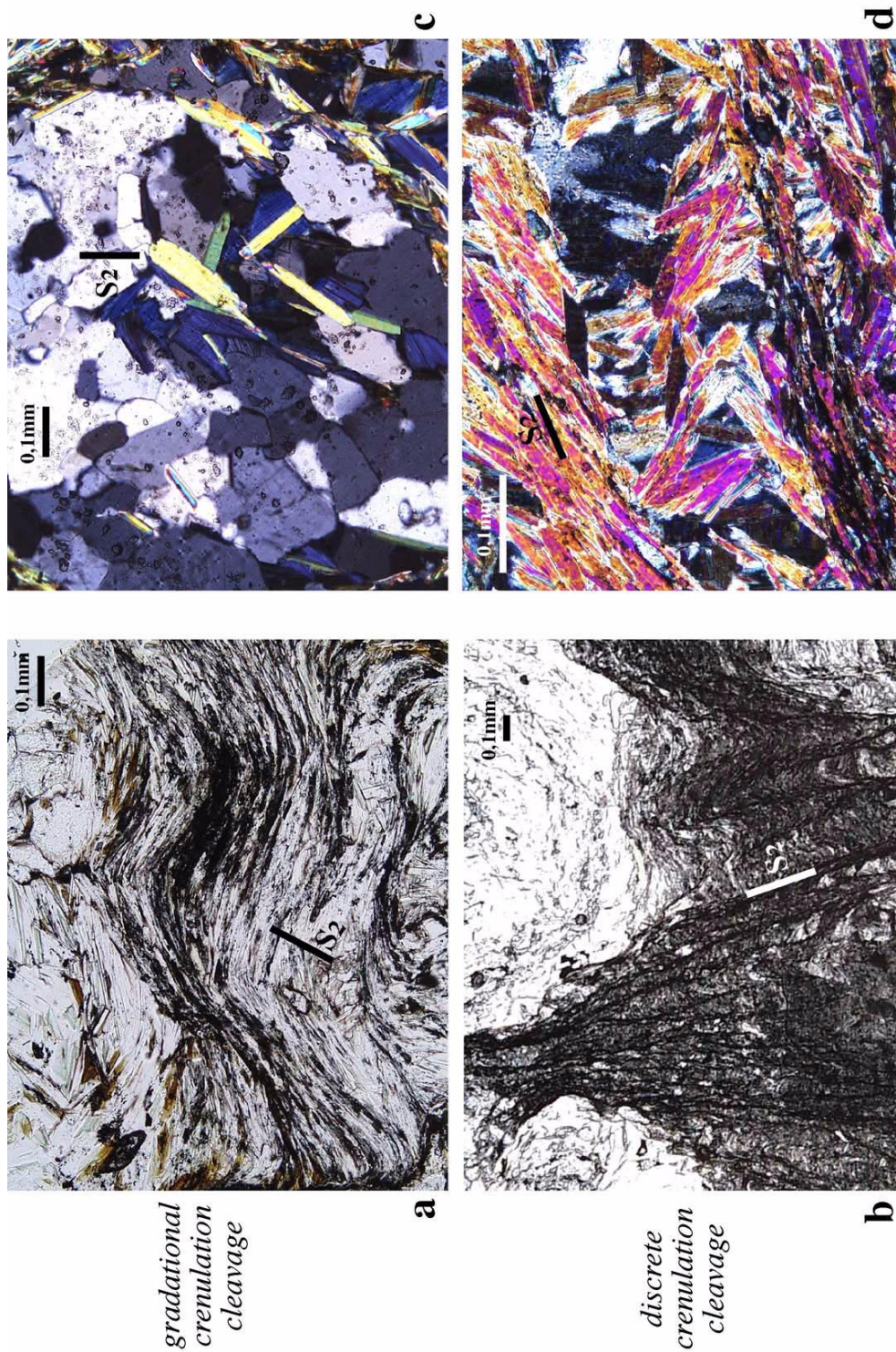


**Fig. 4.5:** **a)** Gradational crenulation cleavage without the development of a second foliation plane  $S_2$  ( $\perp B_2$  and  $S_1$ , plane polarised light; Chard Farm, Remarkables area). **b)** Discrete crenulation cleavage with a continuous second cleavage plane  $S_2$  ( $\perp B_2$  and  $S_1$ , plane polarised light; Mare Burn Valley). **c)** Herringbone structure developed by overgrowth of  $S_2$  gradational crenulation cleavage ( $\perp B_2$  and  $S_1$ , crossed polarised light; Remarkables – top) **d)** Overgrown discrete crenulation cleavage  $S_2$  forming polygonal arcs ( $\perp B_2$  and  $S_1$ , crossed polarised light; Remarkables – top).

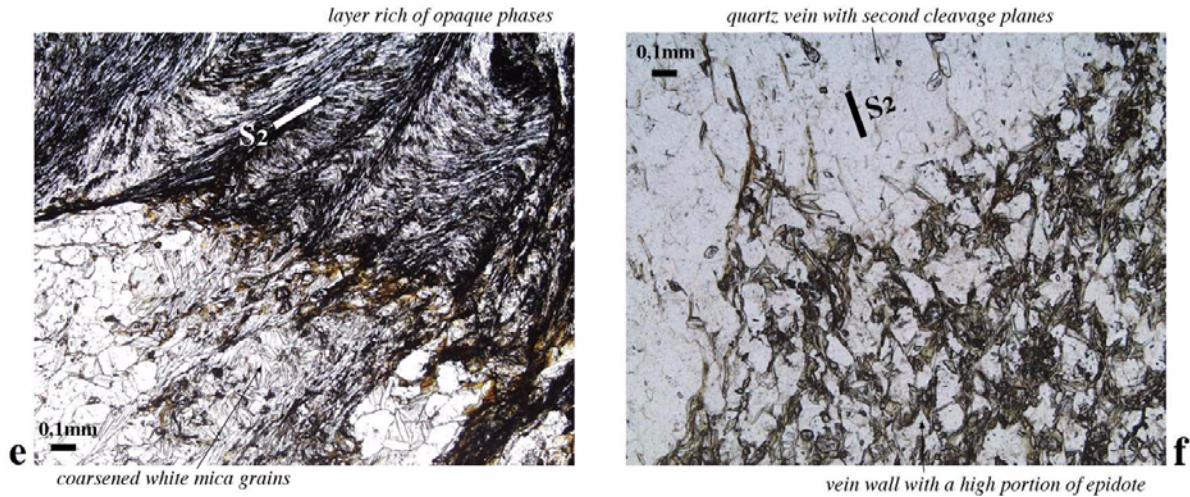


**Fig. 4.5:** *e*) Influence of opaque phases on the grain growth of mica: grain growth is hampered in layers rich of opaque phases (upper half of the picture) in opposite to a quartz-rich layer (lower half;  $\perp B_2$  and  $S_1$ , plane polarised light; Remarkables - top). *f*) A high portion of epidote finely distributed in a mica-rich layer (lower half of the picture) prevents a development of a cleavage in opposite to a present cleavage in the quartz vein (upper half;  $\perp B_2$  and  $S_1$ , plane polarised light; Remarkables - top).

#### 4.3.1. The third crenulation cleavage ( $S_3$ )

In the eastern and central part of the Otago Schist Belt, the third crenulation cleavage ( $S_3$ ) occurs locally at the hinge zone of  $F_3$  regional folds resembling in its style and development the second crenulation cleavage ( $S_2$ ).

In the northwestern part of the Otago Belt, the third crenulation cleavage is strengthened by amplified regional folding of the third generation (*chapter 2*). Consequently the third crenulation cleavage  $S_3$  is discrete and planar at the hinge zones of large  $F_3$  folds (fig. 4.4d, 4.5d), whereas  $S_3$  displays also a gradational transition between the cleavage domains and the micro-lithons on the  $F_3$  limbs (fig. 4.4c, 4.5c). The development of the third fold generation synchronous to the Alpine Barrovian-type metamorphic overprint (Cooper 1974, *chapter 2*) results in recrystallisation and grain growth of quartz and mica. The epitaxial overgrowth of mica grains preserves the orientation of the folded foliation  $S_1$ . Commonly the overgrowth causes polygonal arcs at parasitic  $F_3$  hinge zones (fig. 4.4d, 4.5d), whereas the spaced and highly asymmetric crenulation cleavage at parasitic  $F_3$  limbs is observed as a herringbone structure (fig. 4.4c, 4.5c). In layers rich of mica and opaque phases, the overgrowth of mica grains is hampered, possibly by the opaque phases (fig. 4.5f; Passchier & Trouw 1996). The overgrowth is strengthened at the vein wall - host rock transition. Intercalated chlorite-white mica grain growth mimics the crenulation taking mica grains of the vein wall as nucleus. In phyllites and greenschist rocks, the growth of mica grains is generally oriented subparallel to the overall third extension direction causing a ESE-WNW oriented grain lineation  $L_{3\text{grain}}$  (fig. 4.1a, *chapter 2*).

No matter what overprints the first foliation  $S_1$ , it persists as the main foliation in the Otago Schist Belt as previously noted by Norris & Bishop (1990). The weak and discontinuous development of  $S_2$  and  $S_3$  causes only undulations in the main foliation surface due to the crenulations deforming the smooth and planar  $S_1$  surfaces (Turnbull et al. 2001).

#### 4.4. Folding of the first object lineation $L_1$ by the second and third fold generation ( $F_2/F_3$ )

$L_1$  can be traced around the hinges of both superposed folds ( $F_2/F_3$ ; fig. 4.6a, b). The angle between the first object lineation ( $L_1$ ) and the hinge lines of the superposed folds is variable. The deformed lineations near the hinge of the fold come to lie closer to the fold axis, while those situated on the fold limb generally come to lie at a higher angle to the fold axis ( $B_2/B_3$ ). The sense of curvature of  $L_1$  is opposite on both long limbs, which are connected by a short limb (type 2 geometry of Ghosh & Chatterjee 1985; fig. 4.6a, b). On  $F_2$  parasitic folds,  $L_1$  plunges gently to the E or W on the long limbs and gently to the S or N on the short limb (fig. 4.7d). The high curvature of  $L_1$  on the long limbs reflect that  $L_1$  may enclose a large initial angle to the second fold axis  $B_2$  (fig. 4.7a). However, tracing  $L_1$  around  $F_3$  hinges, a less distinct deviation of the trend is observed because  $L_1$  encloses only a small angle to  $B_3$  (fig. 4.7b). On  $F_3$  parasitic folds,  $L_1$  plunges gently more SW or NE than the third fold axis  $B_3$  on the long limbs and more to the S or N than  $B_3$  on the short limbs (fig. 4.7b).

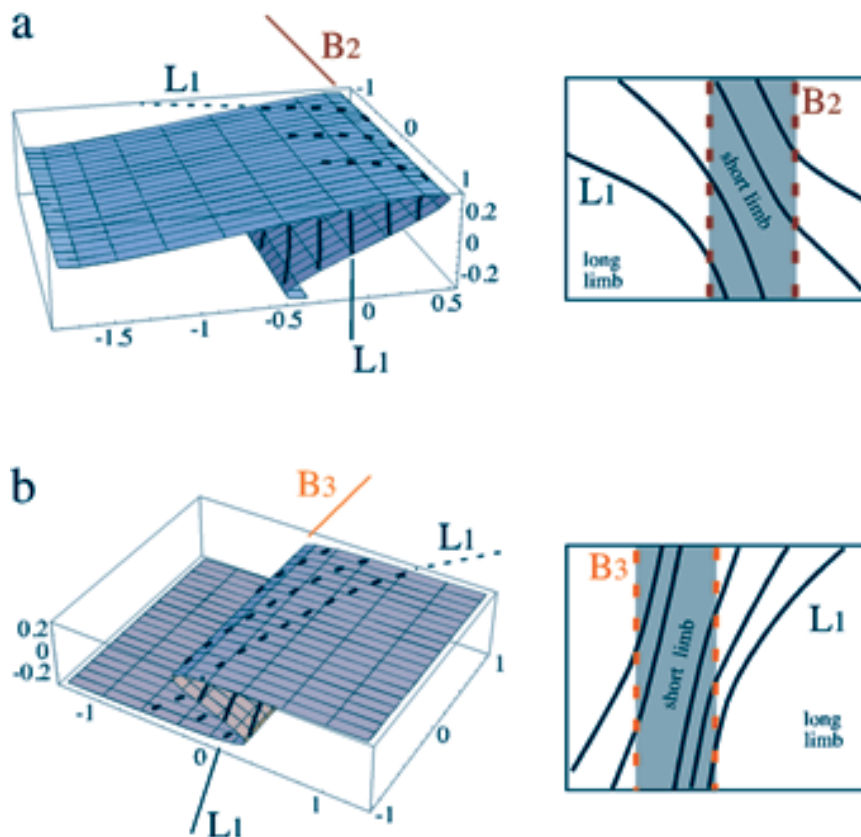
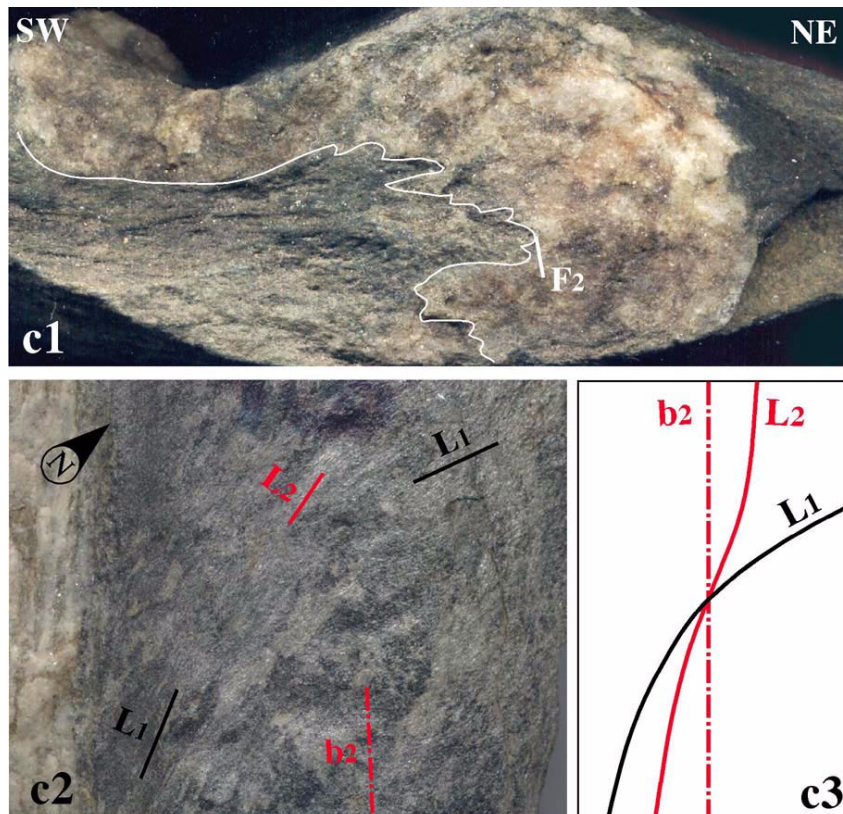


Fig. 4.6a and b (see caption next page)

**Fig. 4.6:** **a)** Trace of the first object lineation  $L_1$  around a superposed NE vergent second fold ( $F_2$ ) and **b)** around a superposed NW vergent third fold ( $F_3$ ) as observed at different locations in the Otago Schist Belt. The first object lineation  $L_1$  displays a greater deviation from its initial trend or a higher curvature at a  $F_2$  hinge than at a  $F_3$  hinge. Taking the technique of Ghosh & Chatterjee (1985) the lineation pattern can be unrolled by placing a transparent overlay on the parasitic folds and drawing the lineation on it. The unrolled lineation pattern of both fold generations shows that the first object lineation  $L_1$  rotates toward the respective fold axis ( $B_2/B_3$ ) at the short limb, whereas on the long limb it comes to lie at higher angle to the respective fold axis ( $B_2/B_3$ ). Ghosh & Chatterjee (1985) call this lineation pattern a type 2 geometry.



**Fig. 4.6:c** (1) Extensional quartz vein folded during  $F_2$  and then subsequently stretched parallel to the second grain lineation ( $L_{2\text{grain}}$ ) leading to a boudin axis ( $b_2$ ) almost parallel to the second fold axis ( $B_2$ ; see orientations in the stereogram of the Remarkables – base, fig. 7c). (2) Extension on the major lower long limb of a regional fold leads to a “stretched” first object lineation traced around the boudins. (3)  $L_1$  shows the same curvature on both sides of the boudin displaying a type 3 geometry described by Ghosh & Chatterjee (1985). The angle between  $L_1$  and the boudin axis ( $b_2$ ) increases on the NE limb of the boudin.

A change in vergence of the parasitic folds causes an inverse curvature of the  $L_1$  lineation pattern but the overall orientation of  $L_1$  on the short and long limb remains as observed in the Remarkables area (fig. 4.7). Commonly  $L_1$  is strengthened on the short limbs of the parasitic folds, whereas it is weakened on the long limbs (fig. 4.8, 4.9). Consequently this strengthened  $L_1$  of the short limbs is mostly recorded deceiving only one orientation of  $L_1$  (see lineation pattern in the eastern and central Otago Belt recorded by Mortimer 1993b, fig. 4.1a and fig. 4.1 c, d, e, f, g, h, j, k and l, as well as fig. 4.7a, e).

The refolded lineation pattern of  $L_1$  changes on the transition of the major short limb to the major lower long limb of a regional fold of both generations, where the extension perpendicular to the respective fold axis results in disrupted layers by boudinage (e.g. Remarkables – base, fig. 4.7c). Folded quartz veins as the cores of boudins reflect that first  $L_1$  is folded and then subsequently stretched (fig. 4.6c). The deformed linear structure traced around the boudins displays neither a double curvature nor a rotation towards the former fold hinge anymore (fig. 4.6c). The first object lineation  $L_1$  is straightened showing the same curvature on both sides of the boudins limbs (type 3 geometry of Ghosh & Chatterjee 1985). The enclosed angle between  $L_1$  and a respective hinge line can increase on one boudins limb (fig. 4.6c).

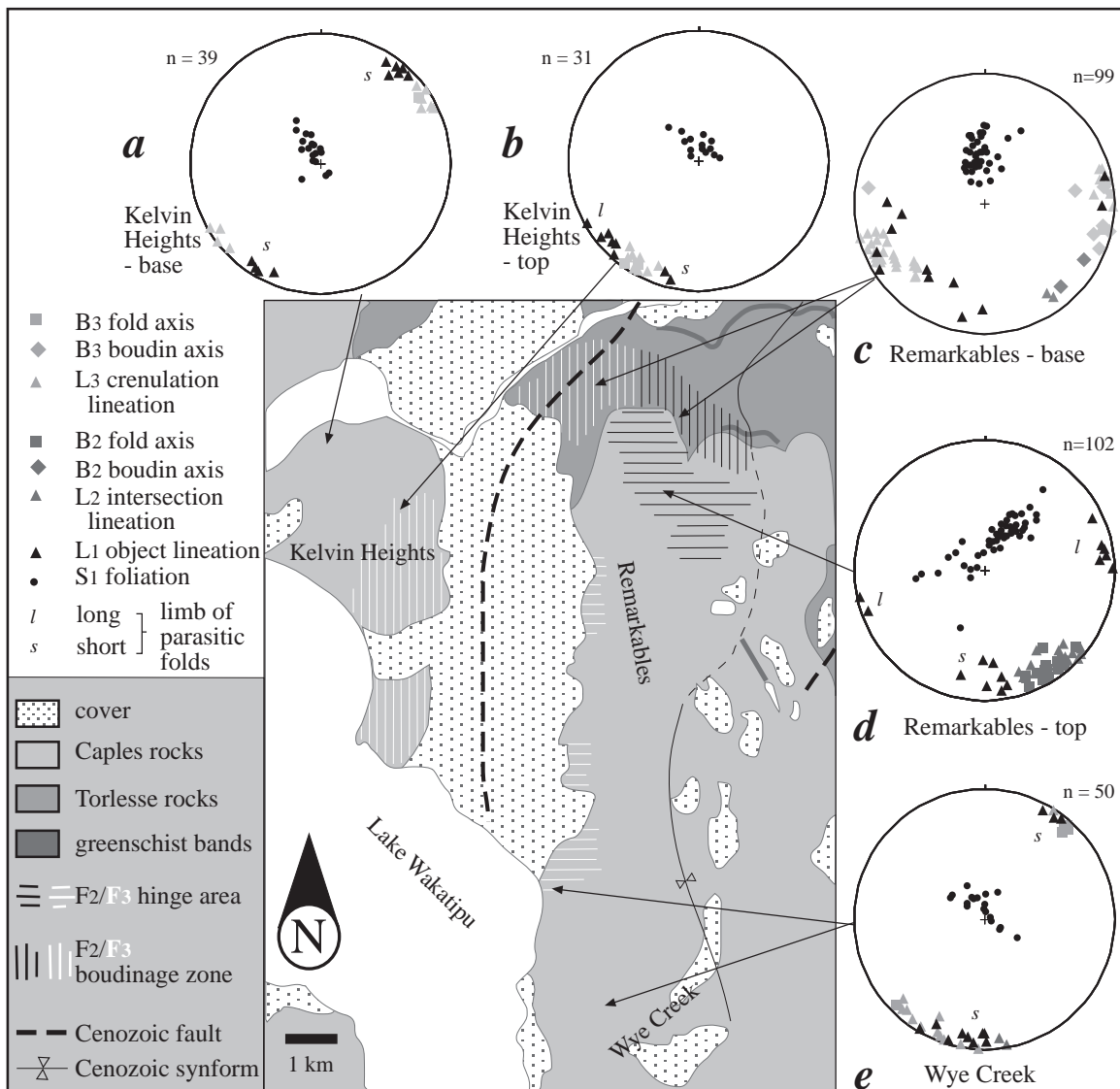


**Fig. 4.7:** The orientation of the first object lineation in relation to the superposed folds of both generations ( $F_2/F_3$ ) at the example of the Remarkables area (see fig. 4.1a). Stereograms (a-e; equal area, lower hemisphere projection) reflect the different orientation of  $L_1$  on the long and short limbs of parasitic folds of both generations: a) Kelvin Heights – base: upper long  $F_3$  regional limb, b) Kelvin Heights – top: lower long  $F_3$  regional limb, c) Remarkables – base: lower long  $F_2$  regional limb, d) Remarkables – top: short  $F_2$  regional limb, e) Wye Creek: short  $F_3$  regional limb.

## 4.5. Discussion

### 4.5.1. Reconstruction of $L_1$ as a crenulation lineation

The refolded  $L_1$  pattern is reconstructed with the help of a Mathematica subprogram written by Moore & Johnson (2000). Both superposed fold generations ( $F_2/F_3$ ) are modelled as buckle folds with subhorizontal fold axes. The sometimes-gentle plunge of the superposed fold axes does not influence the reconstruction and is therewith neglected. The tightness of the folds is alterable. A variable shear perpendicular to the fold axis generates both the vergences of the folds and the extension on the fold limbs.  $L_1$  is firstly taken as a crenulation lineation because the lineation is subparallel aligned to the first fold axis  $B_1$ . The reconstruction as an intersection lineation neglects a possible shear parallel to  $L_1$ , which is later taken into account. Variation within this chosen simple model reflects the observed refolded  $L_1$  pattern of the Otago Schist. Changing the vergence of the superposed folds causes the observed inverse bending of  $L_1$  towards  $B_2/B_3$ . Tight to isoclinal parasitic folds show a higher curvature of the  $L_1$  lineation than open to close folds (fig. 4.8, 4.9).

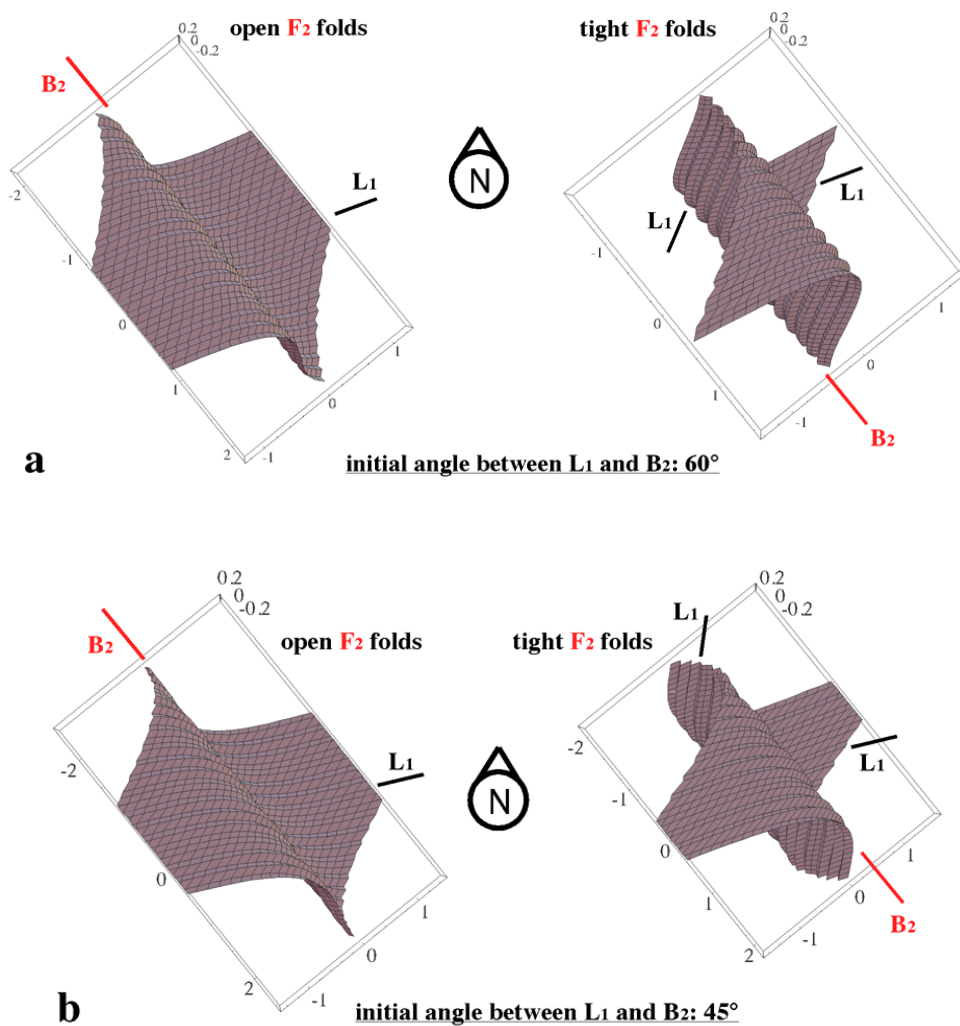


**Fig. 4.8:** **a)** Reconstruction of  $L_1$  lineation pattern folded by various tight, NW vergent folds of the second generation with an initial angle of  $60^\circ$  between  $L_1$  and  $B_2$ , **b)** and with an initial angle of  $45^\circ$  (with the help of a Mathematica subprogram written by Moore & Johnson (2000)).



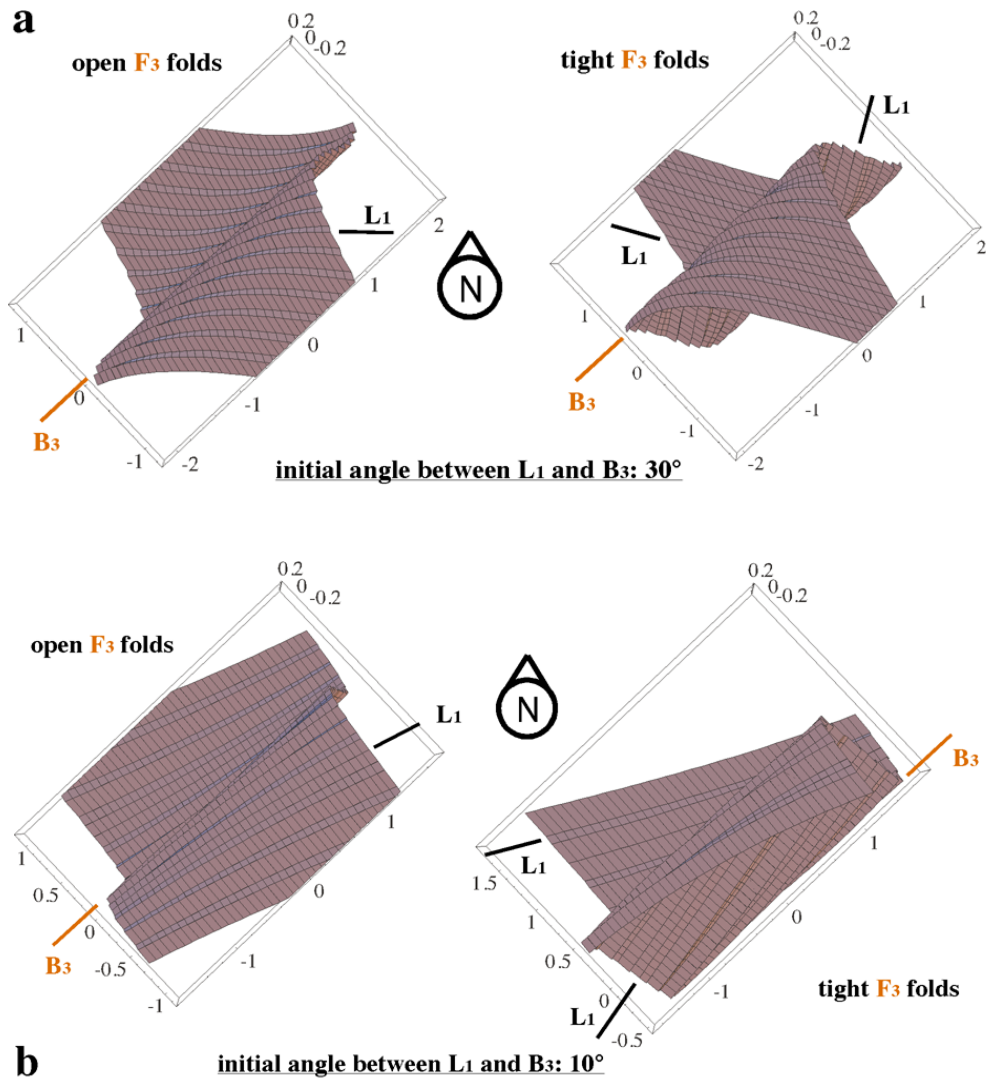


**Fig. 4.9:** **a)** Reconstruction of  $L_1$  lineation pattern folded by various tight, NW vergent folds of the third generation with an initial angle of  $30^\circ$  between  $L_1$  and  $B_3$ , **b)** and with an initial angle of  $10^\circ$  (with the help of a Mathematica subprogram written by Moore & Johnson (2000)).

To reconstruct the refolded  $L_1$  pattern in relation to the superposed folds, different initial angles between  $L_1$  and the respective fold axis ( $B_2/B_3$ ) are chosen. A large initial angle ( $45^\circ$ - $60^\circ$ ) between  $L_1$  and the second fold axis  $B_2$  (fig. 4.8a, b) reflect the observed patterns within a regional  $F_2$  fold (e.g. in the Remarkables area, fig. 4.1b, 6d or in the Patearoa area, fig. 4.1i). Between  $L_1$  and the third fold axis  $B_3$  (fig. 4.9a, b) a small initial angle ( $10^\circ$  -  $30^\circ$ ) coincides with the observed patterns (e.g. Treble Cone, fig. 4.1m or Kelvin Heights – top, fig. 4.7b). The respective smaller initial angle between  $L_1$  and  $B_2/B_3$  and thus the less curved lineation pattern is observed, where intensified parasitic folds of all scales occur. Thus in highly refolded regions  $L_1$  shows a smaller rotation and therewith deceives a smaller initial angle between  $L_1$

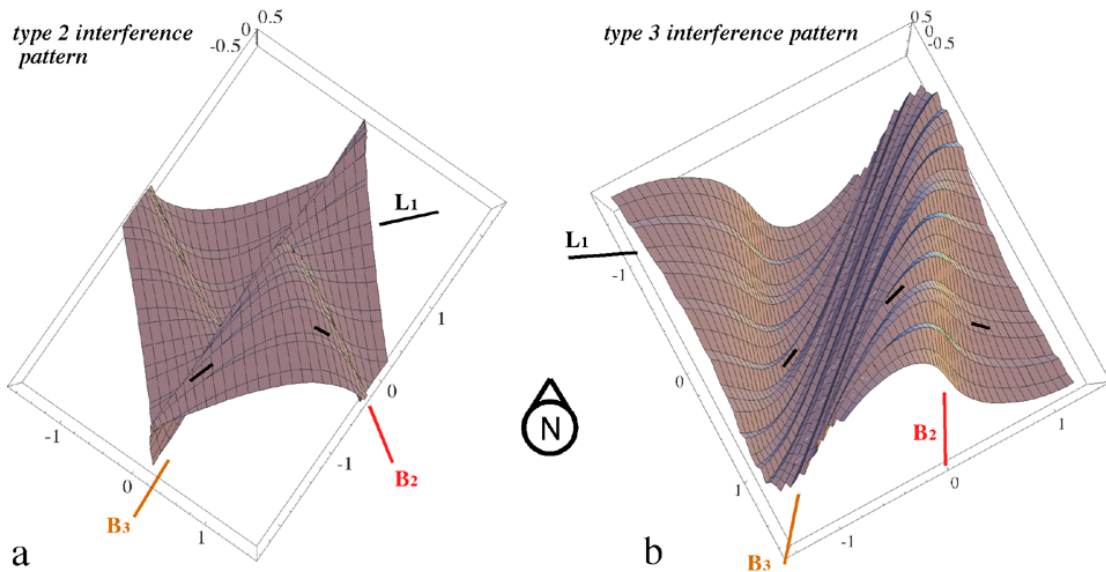


**Fig. 4.10:** Behaviour of the first object lineation  $L_1$  in relation to the superposed folds of both generations ( $F_2/F_3$ ) **a)** in a type 2 interference pattern ( $L_1 \wedge B_2 = 60^\circ$ ,  $L_1 \wedge B_3 = 30^\circ$ ,  $B_2 \wedge B_3 = 90^\circ$ ) and **b)** in an almost type 3 interference pattern ( $L_1 \wedge B_3 = 30^\circ$ ,  $B_2 \wedge B_3 = 45^\circ$ ,  $L_1 \wedge B_2 = 75^\circ$ ; modelled with the help of a Mathematica subprogram written by Moore & Johnson (2000)).

and  $B_2/B_3$ . Moreover, more competent quartz-rich layers show a less rotated early lineation pattern and therewith a higher initial angle between  $L_1$  and  $B_2/B_3$  than the more incompetent mica-rich layers. The reorientation in more competent layers depends on the external rotation and the associated tangential longitudinal strain during buckling (Ghosh 1974) resulting in a slightly curved refolded pattern of  $L_1$ . The reorientation of an early lineation by late stage strain is mostly confined to the more incompetent layers (Ghosh 1974) leading to a highly curved refolded pattern of  $L_1$ .

Taking the higher initial angle of  $60^\circ$  between  $L_1$  and  $B_2$  (fig. 4.8a) as well as  $30^\circ$  between  $L_1$  and  $B_3$  (fig. 4.9a), a rectilinear initial orientation of  $L_1$  can be generated. Applying this initial orientation of  $L_1$  on both superposed folds ( $F_2/F_3$ ) in one reconstruction, the lineation swings around the nose created by the intersecting folds in a type 2 interference pattern (fig. 4.10a).  $L_1$  is strengthened on the short limbs of the respective dominant fold generation, for example parallel to the second fold axis  $B_2$  at location Nevis Bluff (fig. 4.1d) or parallel to  $B_3$  at location Ophir (fig. 4.1e). The superposition of both fold generations on  $L_1$  rotates the once orthogonal oriented fold axes ( $B_2/B_3$ ) to a smaller intersection angle (c.  $70^\circ$ , fig. 4.10a). Thus the small change in the intersection angle between both fold generations is not only caused by an oblique shortening during the superposition of the third fold generation ( $F_3$ ) as discussed in *chapter 3* but also by the superposition of both fold generations ( $F_2/F_3$ ) on  $L_1$ .

The oblique  $F_3$  shortening deforms the regional folds of the second generation ( $F_2$ ) when intersecting with regional  $F_3$  folds. The parasitic  $F_2$  folds tend to deamplify and to rotate into the orientation of the superposed  $F_3$  folds (*chapter 3*), whose hinge lines also rotate into N-S direction (fig. 4.1. e, i, l). Consequently a small intersection angle between both fold hinges results in an almost type 3 interference pattern.  $L_1$  is parallel aligned to the towards each other rotated parasitic hinge lines of both fold generations as observed at different locations throughout the Otago Belt (e.g. Manorburn Dam, fig. 4.1e, Mare Burn Valley, fig. 4.1i, or Treble Cone, fig. 4.1l). Reconstructing  $L_1$  enclosing an initial angle of  $30^\circ$  with  $B_3$  and a decreasing intersection angle between  $B_2$  and  $B_3$  (fig. 4.10b) shows a weakening of the second parasitic folds and a strengthening of  $L_1$ , which is almost subparallel aligned to the third fold axis  $B_3$  in the  $F_3$  hinge zone. The small initial angle between  $L_1$  and  $B_3$  strengthens the rotation of the second parasitic folds. Although the reconstructed intersection angle between  $B_2$  and  $B_3$  is high, the rotated  $F_2$  hinge line displays a greater rotation angle and therewith a smaller intersection angle.

#### 4.5.2 Initial plunge of $L_1$

But what is about the initial plunge of  $L_1$ ? Modelling  $L_1$  with an increasing plunge and here-with with an increasing dip of the main foliation  $S_1$  shows that a steep plunge of  $L_1$  on  $S_1$  results in a steeply plunging fold (fig. 4.11). The result reflects the conclusion of previous studies (Ghosh & Ramberg 1968, Skjernaa 1975, Watkinson 1981, Grujic 1993) that an early lineation influences later folding. Neither a steeply dipping  $S_1$  (Mortimer 1993b) or a steeply plunging superposed fold ( $F_2/F_3$ ) is developed during Mesozoic times in the Otago Schist Belt. Consequently a subhorizontal to gentle initial plunge of  $L_1$  is considered.

#### 4.5.3. Reconstruction of $L_1$ as a “stretching” lineation

Not taken into account till now is any stretching inherited parallel to the first object lineation  $L_1$ . Investigations into the  $L_1$  pattern reveals that a certain amount of shear is associated with  $L_1$  but that a distinctive shear sense is hardly to determine (*see section 4.2.1.*). Reconstructing  $L_1$  as crenulations with a stretch parallel to the crenulations fold axis reveals that there is no change in the orientation or curvature of the refolded lineation pattern (fig. 4.12a and b). The stretch parallel to  $L_1$  leads to a strengthening or weakening of the lineation pattern.

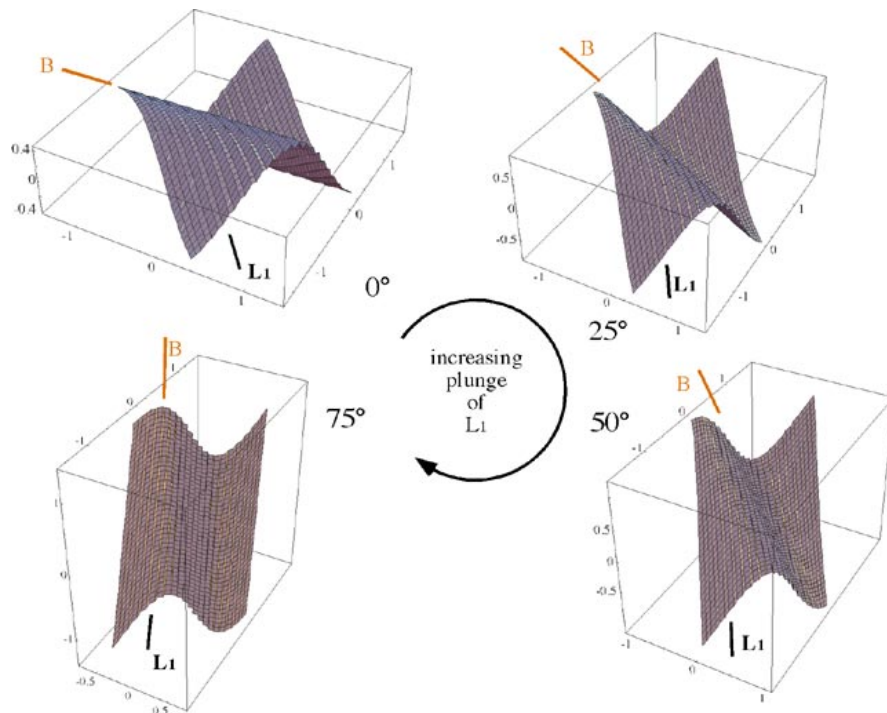


**Fig. 4.11:** A successively increasing plunge of  $L_1$  and therewith an increasing dip of the main foliation  $S_1$  is modelled (with the help of a Mathematica subprogram written by Moore & Johnson (2000)) showing that the plunge of  $L_1$  influences the superposed fold.

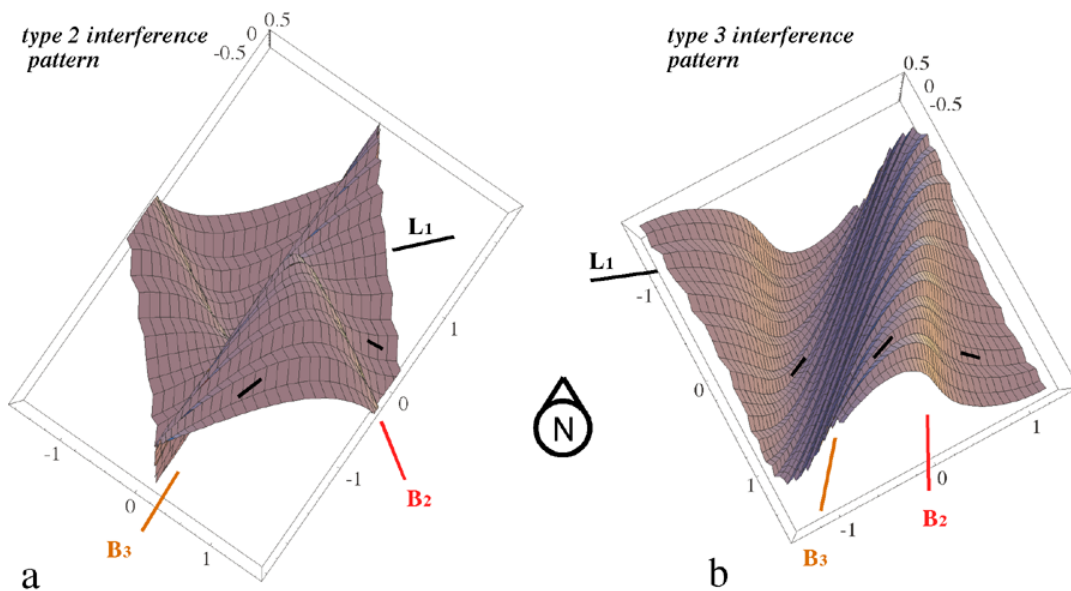


**Fig. 4.12:** Influence of a shear subparallel to  $L_1$  and normal to  $S_1$  in relation to the superposed folds of both generations ( $F_2/F_3$ ) **a**) in a type 2 interference pattern ( $L_1 \wedge B_2 = 60^\circ$ ,  $L_1 \wedge B_3 = 30^\circ$ ,  $B_2 \wedge B_3 = 90^\circ$ ) and **b**) in an almost type 3 interference pattern ( $L_1 \wedge B_3 = 30^\circ$ ,  $B_2 \wedge B_3 = 45^\circ$ ,  $L_1 \wedge B_2 = 75^\circ$ ; modelled with the help of a Mathematica subprogram written by Moore & Johnson (2000)). No change in the orientation or curvature of the refolded lineation pattern is reconstructed.

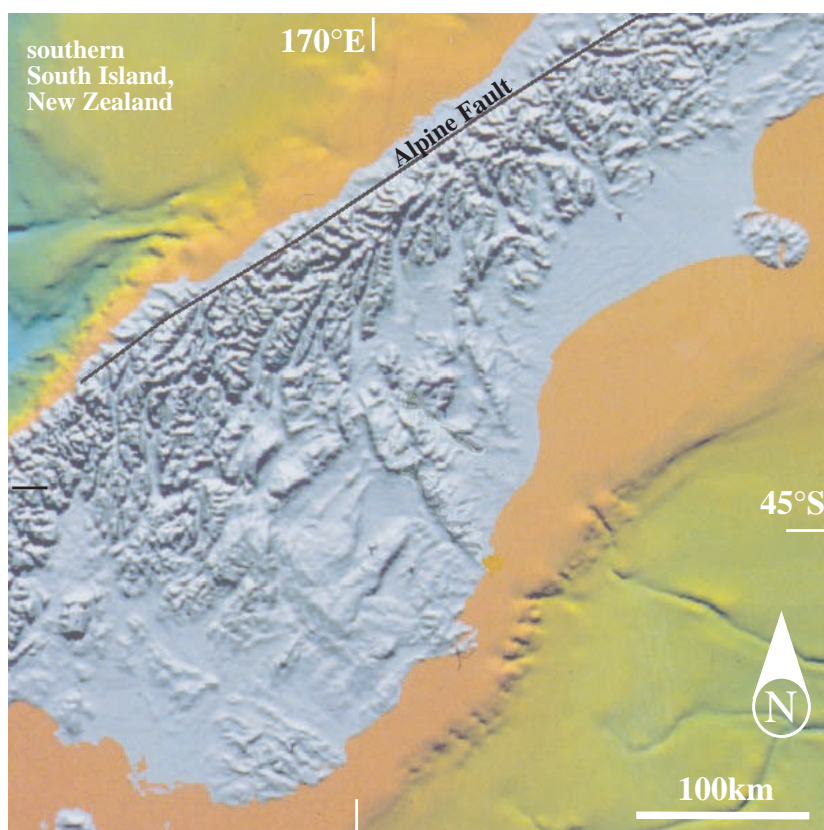
#### 4.6. Conclusion

The first object lineation  $L_1$  is preserved on the main foliation plane ( $S_1$ ), which is folded by both Mesozoic fold generations ( $F_2/F_3$ ) but never completely transposed by new foliations ( $S_2/S_3$ ). The linear structure  $L_1$  rotates within the short limbs of the parasitic folds towards the respective fold axis ( $B_2/B_3$ ), whereas it comes to lie at a higher angle to the fold axis on the parasitic fold limbs (type 2 geometry of Ghosh & Chatterjee (1985)). The initial orientation of  $L_1$  influences the superposition of both fold generations ( $F_2/F_3$ ) resulting in an apparent smaller intersection angle between the hinge lines of both fold generations. The strengthened  $L_1$  on the short limbs of the parasitic folds of both respective Mesozoic fold generations ( $F_2/F_3$ ) may mislead to the interpretation that the initial  $L_1$  trends midway between  $B_2$  and  $B_3$ , almost in NNE-SSW to NE-SW. However, reconstruction of the refolded lineation pattern reveals that the initial rectilinear  $L_1$  trends in ENE-WSW direction on the main foliation  $S_1$ . The certain amount of shear associated with  $L_1$ , as reflected by stretched pebbles of intercalated quartzite conglomerates, causes no change in the reorientation and curvature of  $L_1$  during buckling.

## Chapter 5



*The view shows Lake Hawea, 350m above sea level. The Maori name “Hawea” means doubt. Apparently a Maori party were in doubt as to which route to take. Well, when I arrived at Lake Hawea, I could easily integrate the observed structures found at the eastern flank of Lake Hawea (shown here) but structures of the western flank of Lake Hawea really rack my brain.*



*The Alpine Fault, a major transcurrent plate boundary exposed along the west coast of South Island, New Zealand, separates continental crust of the Australian and Pacific plates (Wellman 1955, Suggate 1963, Walcott 1978, Walcott & Cresswell 1979)*

## **Tilting of regional folds in a superposed fold and thrust belt - a continuous tectonic concept for the Otago and Alpine Schist Belt**

### **Abstract**

The superposition of a Cenozoic two-sided fold and thrust belt on the Mesozoic fold structure within the transpressional Alpine Fault System is described. The Mesozoic fold structure ( $F_2/F_3$ ) is folded in Cenozoic N-NE trending long wavelength syn- and antiforms. The propagation of reverse faults subparallel to the Mesozoic main foliation and the reactivation of previously formed faults causes a complex fault pattern, especially in the western Otago Belt, where the Mesozoic fold structure ( $F_2/F_3$ ) changes due to superposition of the amplifying third fold generation ( $F_3$ ). At the tip line of the reverse faults, the Mesozoic structure is steepened and shortened orthogonal to the previous main foliation resulting in strongly foliated rocks without a new-formed lineation. The former inclined to recumbent Mesozoic mesofolds are rotated to upright folds ( $F_3$ ), where the fold axis ( $B_3$ ) is subparallel to the Cenozoic fold axis, or to vertical folds ( $F_2$ ), where the fold axis ( $B_2$ ) is oblique to the Cenozoic fold axis. In the Otago Belt, the fold and thrust belt is widely spaced, where the foliation remains flat and only rotates to a steeper dip in the vicinity of a reverse fault. Towards the Alpine Fault the fold and thrust belt gets continuously more narrowly spaced. In the Alpine Belt the upright Cenozoic fold structure can be subdivided in extensive zones of steeply dipping foliation, respectively the limbs and synforms of the steepened folds adjacent to the reverse faults, and antiforms, where the Mesozoic foliation remains flat. Consequently the Cenozoic structure of the Otago and Alpine Belt reflects an asymmetric large scale flower structure with an uplifted and tilted western wing in the vicinity of the Alpine Fault.

### **5.1. Introduction**

Transpression results in combinations of wrenching and thrusting structures (Sanderson & Marchini 1984, Dewey et al. 1998). It can be related to particular boundary conditions at the regional scale, such as an obliquity between the imposed shear motion and pre-existing major faults or oblique convergence at plate boundaries (Tikoff & Teyssier 1994). At the scale of plate tectonics, transpressive motion caused by oblique convergence can be expressed by a single fault zone or it can be partitioned (Karig et al. 1980, Koons 1990, 1994, Cobbold et al. 1991, Tikoff & Teyssier 1994, Jones & Tanner 1995, Koons & Henderson 1995, Fossen & Tikoff 1998). Oblique convergent plate boundaries are commonly characterised by wide orogenic zones, bounded or cut by major strike-slip faults oriented subparallel to the plate boundary (Teyssier et al. 1995). These orogen-parallel strike-slip faults are assumed to take up a percentage of the transcurrent component of plate motion (Teyssier et al. 1995; fig. 5.1a). In contrast to this “parallel partitioning” Norris & Cooper (1997) observe a “serial partitioning” in the Alpine Fault Zone, New Zealand, where the strike-slip faults are not aligned parallel to the plate boundary but trending in the direction of the overall plate motion vector. The movement along the transcurrent Alpine Fault is partitioned into orogen parallel fold and thrust systems linked by en echelon strike-slip faults (Norris & Cooper 1997, 2001; fig. 5.1b).

The angle of  $29^\circ$  between the trend of the Alpine Fault ( $055^\circ$ ; Norris et al. 1990) and relative plate motion direction ( $084^\circ$ ; DeMets et al. 1990) as well as the thrust-dominated deformation

(Spörl 1979, Norris et al. 1990) is indicative of a bulk pure-shear dominated transpression system (Teyssier et al. 1995, Casas et al. 2001). Casas et al. (2001) model in their experiments an asymmetric flower structure (Harding 1985, Sylvester 1988) with a steep retro-wedge, the Alpine Fault, and a flat lying pro-wedge. The different dip of the main foliation reflects this asymmetric flower structure. In the vicinity of the Alpine Fault, outlined as Alpine Belt (fig. 5.2), the main foliation displays a steep dip (Grindley 1963, Findlay 1987, Holcombe & Little 2001, Little et al. 2002 a, b), whereas towards the E, in the Otago Belt, the main foliation remains almost flat-lying (Mortimer 1993b). The asymmetry of flower structure is increased and deformation is concentrated within the main frontal fault zone, because erosion occurs during deformation (Casas et al. 2001).

Folds developed during a transpressive regime are usually described as wrench folds (e.g. Jamison 1991, Tikoff & Peterson 1998). Wrench folds are initiated at c. 45° to the transcurrent fault independent of the convergence angle in a simple-shear model (Tikoff & Peterson 1998; fig. 5.1a). The fold axes rotate during further strike-slip movement into parallelism to the trans-

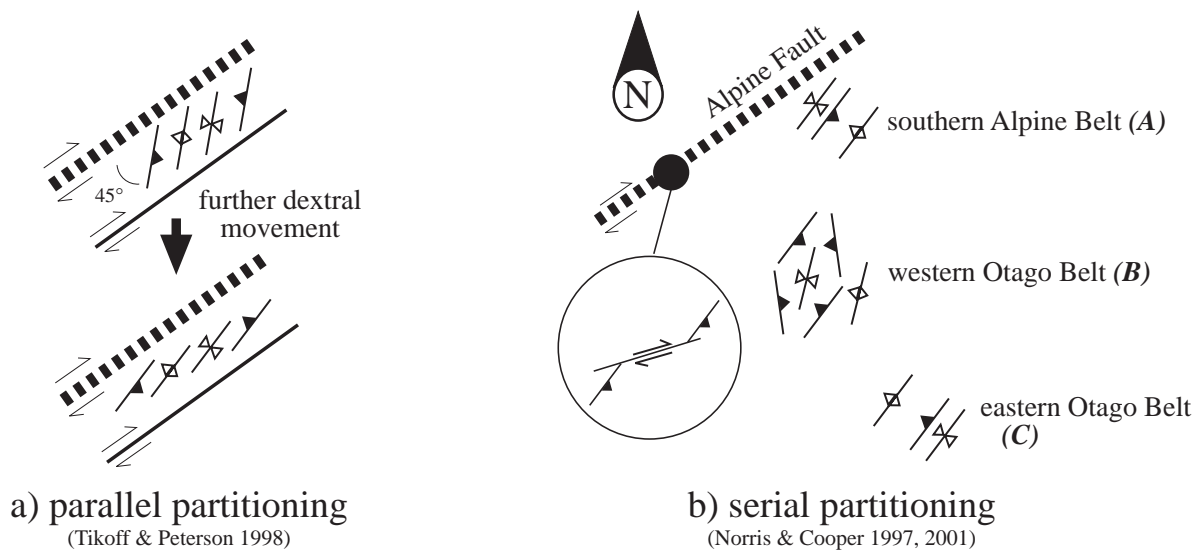


**Fig. 5.1:** **a)** If movement on the fault are predominantly those of simple shear (strike-slip dominated) the initially formed fold traces and thrust strike directions will be oriented at 40-45° to the main fault trace independent of the convergence angle (Tikoff & Peterson 1998). The displacement vector on the thrust surface may show components of strike-slip as reversed dip-slip. With further dextral movement the initially right-stepping folds may rotate towards the main fault trace. As rotation proceeds, stretching is likely to occur subparallel to the fold axes (Tikoff & Peterson 1998). **b)** Contrary to the model presented in fig. 5.1a, the strike-slip movement of the main fault trace, here the Alpine Fault, is not partitioned onto parallel aligned strike-slip faults (“parallel partitioning”) but onto orogen-parallel fold and thrust systems linked by en echelon strike-slip faults (“serial partitioning”, Norris & Cooper (1997, 2001)). The fold traces and thrust strike directions trend with 15° northerly than the trend of the Alpine Fault in the southern Alpine Belt (A) and eastern Otago Belt (C). In the western Otago Belt (B) the fold traces trend in a NNE direction, whereas the thrust strike directions split into NW- and NE- trending reverse faults (see locations in fig. 5.2).



current fault (Tikoff & Peterson 1998; fig. 5.1a) as described for the Alpine Fault zone by Jamison (1991) and Little & Mortimer (2001). The rotation of fault-related folds may take place about a vertical axis as proposed by Norris (1979) and Little & Mortimer (2001). However, the range and basin pattern of the southern South Island, New Zealand, developed as a fold and thrust belt during the transcurrent movement of the Alpine Fault, displays an unusual feature. Towards the foreland, in the eastern Otago Belt, the ranges strike almost c. 15° towards N from the trend of the Alpine Fault (fig. 5.1b). In the central to western part of the Otago Belt, the fold traces rotate further N-NNE subdivided on branching NW- and NE-trending faults. But in the vicinity of the Alpine Fault the ranges trends again almost subparallel to the Alpine Fault (Norris & Cooper 2001) enclosing only an angle of c. 15° towards N from the trend of the Alpine Fault as observed also in the eastern Otago Belt. Although the changing trend towards N of the Cenozoic folds may display a right stepping geometry in a dextral transpressive system (Sylvester 1988; fig. 5.1b) and therewith implied a vertical axis rotation between the trends of the central Otago and Alpine Belt, another development of the fold and thrust belt will be considered in this study.

Previous studies focus on the late Cenozoic deformation neglecting the Mesozoic and Early Cenozoic development, especially of the Alpine Belt. I consider that previously formed structures control the development of the transpressional Alpine Fault system since Miocene. For this purpose the known Mesozoic structure of the Otago Belt is compared to the structure of the Alpine Belt to reveal the extent of Cenozoic deformation evoked by the initiation and development of the Alpine Fault zone.

## 5.2. Tectonic continuity between the Otago and the Alpine Schist Belt

Some previous workers outline that the Mesozoic structural style of the Alpine Schist is distinct from that of the schist of Otago Belt (Lillie et al. 1957, Gunn 1960, Grindley 1963, Wood 1978, Findlay & Spörli 1984, Findlay 1987). However, a continuous deformation from the Otago to the Alpine Schist is circumstantiated following Andrews et al. (1974, 1976), Ward & Spörli 1979, Craw (1985), Holm et al. (1989), Grapes & Watanabe (1992), Craw et al. (1994) and Little et al. (2002a, b). Ductile structures in the greenschist facies rocks at the margin of the Alpine Schist are formed during Mesozoic deformation similar to those in the Otago Schist to the south (Craw et al. 1994). Craw et al. (1994) describe that the same fold generations form a ductile deformation continuum in the Otago Belt as well as in the Alpine Belt. They assume that the progressive development of recumbent nappe-like folds with regional high strain zones is characteristic of tectonic boundaries between distinctly different lithologic associations in the Otago Belt (Craw 1985, Cox 1991) and Alpine Belt (Craw et al. 1994). Their theory of Mesozoic nappe folds is rejected in favour of superposed folding as proposed by Holcombe & Little (2001) for the Alpine Belt and as described for the Otago Belt in this study (*chapter 2*). The latter studies call for regional strongly asymmetric Mesozoic folds with structurally inverted short limbs (Holcombe & Little 2001, Tünker & Ring 2001).

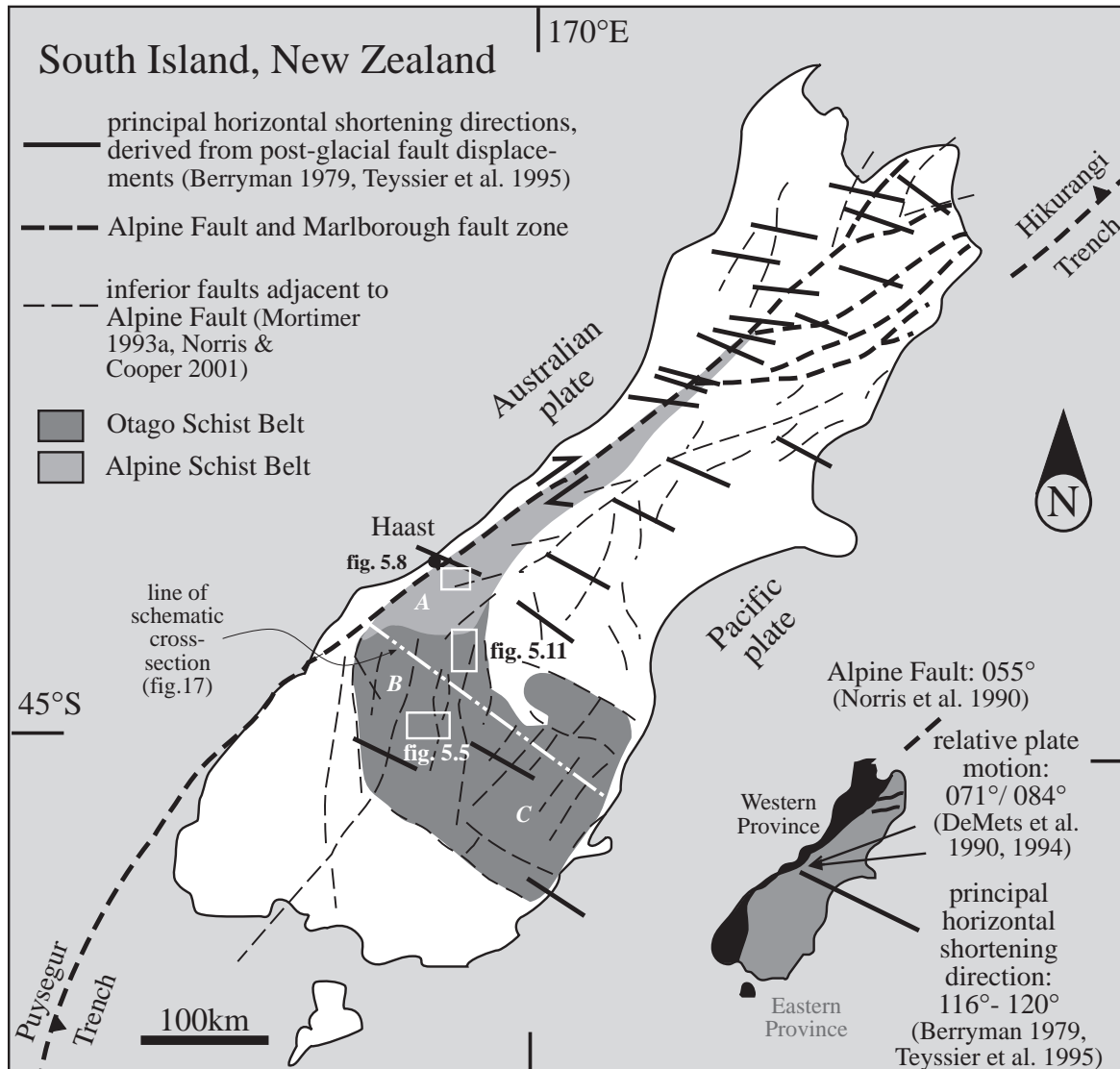


**Fig. 5.2:** Geological setting of the Alpine Fault Zone, the Alpine and Otago Schist Belt. Cenozoic shortening directions measured by Berryman (1979) show a uniform ESE-WNW direction over the whole South Island. Small inset shows the differentiation of the rocks of the South Island in Eastern and Western Province. Arrows indicate the directions of plate motion calculated by De Mets (1990, 1994). Two angles are given in recently published literature.

In this paper the Mesozoic main fold generation of the Alpine Belt ( $F_3$ ), which is related to the Alpine metamorphism (Cooper 1974, Craw et al. 1994, Holcombe & Little 2001), is separated from the Late Cenozoic overprint as Craw et al. (1994) proposed. This approach is contrary to the studies of Findlay & Spörl (1984), Findlay (1987) and Little et al. (2002a, b).

### 5.3. Otago Schist Belt

#### 5.3.1. Mesozoic deformation

A new model of regional folds (fig. 5.3) for the Otago Belt is developed by the analysis of orientation and superposition's criteria, described in detail in *chapter 2* and *3*. Just to remember the fold model a summarising figure (fig. 5.3) is given.

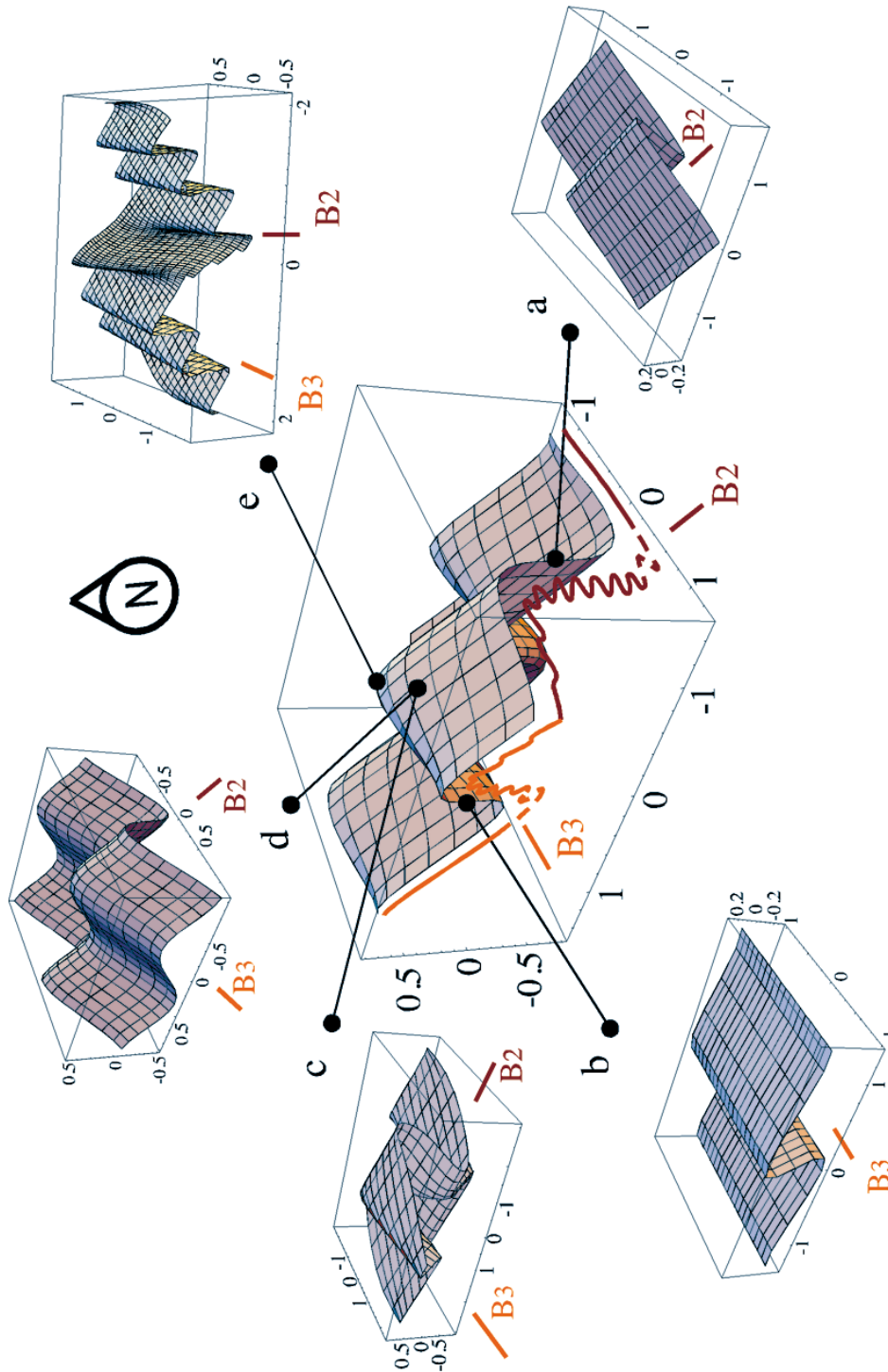


**Fig. 5.3:** Mesozoic fold structure outlining two successive fold generations, which are almost orthogonal oriented at regional scale (centre of the figure). Folded lines display the change in asymmetry and tightness of the mesofolds from the upper limb to the hinge of the regional fold (mesofolds are not to scale). The mesofolds get subsequently boudinaged at the transition from the short to the long limb. Small boxes (fig. 5.3 a-e) display the change of interference pattern of the parasitic folds in relation to the regional folds. **a)** Dominant NE vergent  $F_2$ , **b)** dominant NW vergent  $F_3$ , **c)** type 2 interference pattern, **d)** intermediate type 1/ type 2 interference pattern, **e)** type 3 interference pattern as observed on the limbs of intersecting mesofolds (modelled with the help of a Mathematica subprogram written by Moore & Johnson (2000)).

### 5.3.2. Cenozoic deformation

Associated with the movement on the Alpine Fault in the Late Cenozoic, a set of large NNE to NE trending reverse faults evolves a fold and thrust belt throughout the Otago Schist (Beanland & Barrow-Hurlbert 1988, Beanland & Berryman 1989). At the tip line of the thrust the main foliation is tilted towards the fault plane (fig. 5.4). Movement on a major W-dipping fault leads to a long wavelength antiform at the western step and synform at the eastern step. Branching steep reverse faults cause box-shaped antiforms in some parts of the eastern Otago Belt, maybe developed due to a small transcurrent component on the reverse faults (Markley & Norris 1999). Markley & Norris (1999) note that the reverse faults do not always surface at the inflection line of the regional Cenozoic folds (blind thrusts, Butler 1982). In the central part of the Otago Schist Belt, antithetic E-dipping faults are developed as back thrusts leading to pop-up structures (Elliott 1981, Butler 1982, Beanland & Berryman 1989). Movement on an antithetic fault leads to a km-scale antiform at the eastern step and synform at the western step. Adjacent to major reverse faults, small branching splay-faults are developed as forelimb thrusts (Butler 1982), mostly with a shallower dip. Beanland & Berryman (1989) suggest that in the Otago Belt the individual listric splay-faults root into a regional crustal decollement zone within the basement rocks forming a piggy-back sequence (Butler 1982) as proposed for the Moine Thrust Zone, NW Scotland, by Boyer & Elliot (1982). Horizontal layering within the schist, which is evident at the surface as a subhorizontal foliation (Mortimer 1993a,b), is likely to extend to the depth and would facilitate regional decollement thrusting. In the western part of the Otago Belt (fig. 5.5) a set of E-W to ESE-WNW trending moderate to steep faults (e.g. Kawarau Gorge) with a dextral strike-slip movement is observed (Turnbull et al. 1993), which is evolved as tear faults conjugate to the NNE trending reverse faults.



**Fig. 5.4:** Warping of the main foliation towards a Cenozoic fault plane (standpoint on the fault zone; Cardrona Valley; see location in fig. 5.5c).

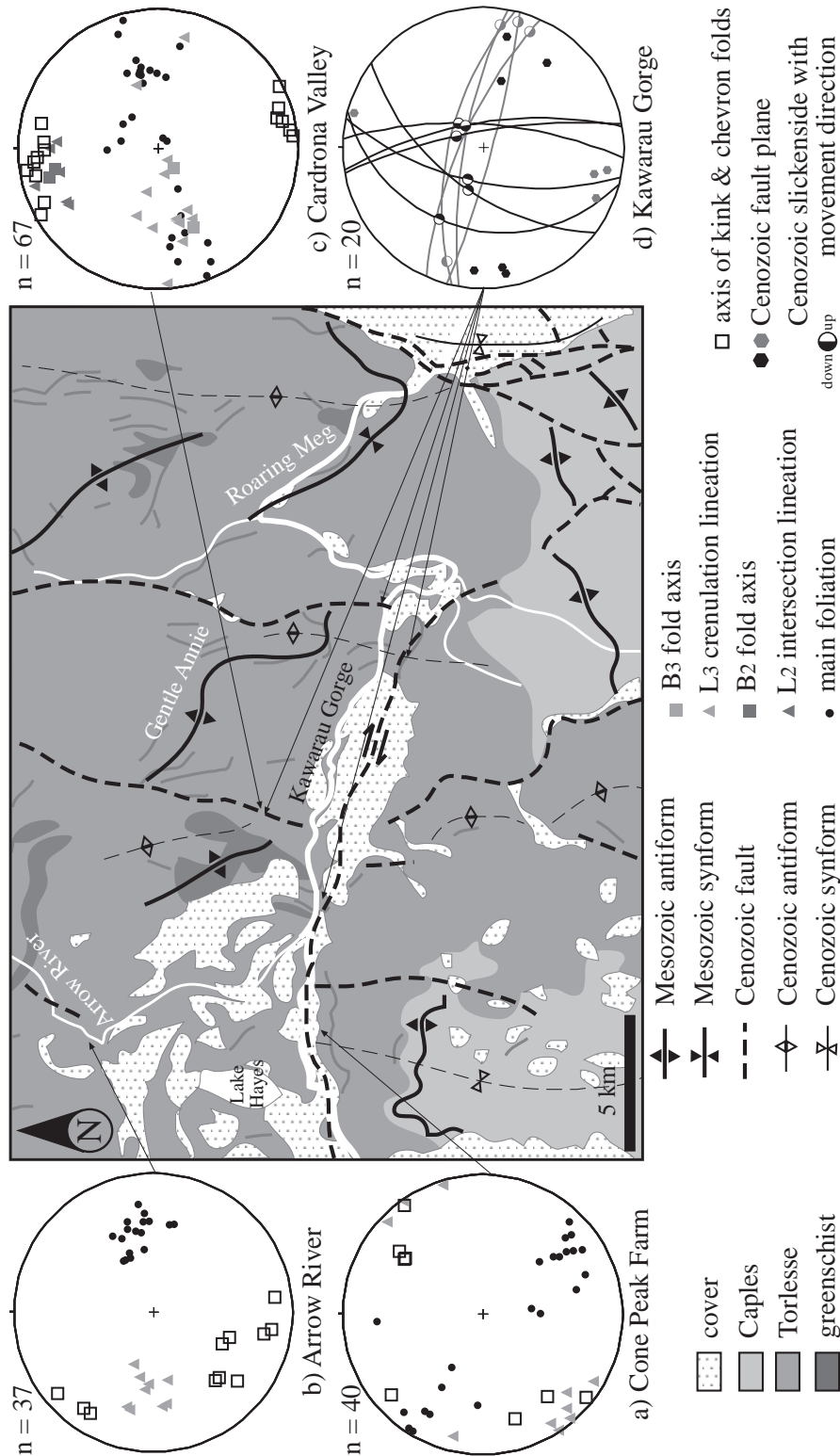


**Fig. 5.5:** Map of the Cenozoic range and basin structure, which folds Mesozoic regional syn- and antiforms ( $F_2/F_3$ ), as observed in the Kawarau region, Otago Belt (based on of Turnbull (2000) and this study; see location on map, fig. 5.2). Stereograms (equal area, lower hemisphere projection) outline structures found in a Cenozoic synform (Cone Peak Farm, **a**), almost orthogonal oriented kinking of the main foliation (Arrow River, **b**) and structures in an antiformal hinge zone (Cardrona Valley, **c**). **d**) Cenozoic minor fault planes (depicted as great circles and poles) and slickensides comprised at different locations along the Kowarau Gorge. The steep dextral strike – slip faults (grey) are distinguished from the almost flat reverse faults (black).

Subordinate to the NE-trending faults, there are WNW-NW-trending reverse faults with NE dips in the eastern part of the Otago Belt (fig. 5.2), which predate the NE-trending ones. Reactivation of Cretaceous WNW-NW-trending normal faults during the development of the NE-trending fold and thrust belt misleads to the interpretation that the two sets of faults appear to have been active simultaneously (Bishop 1974, Madin 1988). However, most of the evidence for late Quaternary displacement has been reported on NE-trending faults (Makgill & Norris 1983, Beanland & Barrow-Hurlbert 1988, Norris & Cooper 2001).

The brittle deformation is concentrated along the fault plane resulting in a several hundred metre wide zone of steeply dipping strongly foliated schist with abundant gouge seams parallel to foliation (Turnbull 1981). Shortening and flattening in the vicinity of the fault is mainly orthogonal to the previously existing foliation leading to an S-shape fabric of the rocks. Antiforms are characterised by an open mesoscopic warping in foliation (Turnbull 1981), mostly in thin laminated schist, with one set or two sets of parasitic open kink folds (fig. 5.5, 5.6a). The area of synforms is penetrated by a conjugate set of parasitic close to tight kink or chevron folds with planar limbs and non-penetrative axial plane fractures (Turnbull 1981; fig. 5.5, 5.6b). The fold axes of the kink and chevron folds are developed subparallel to one of the Mesozoic fold axis ( $B_2$  or  $B_3$ ; fig. 5.5). The north-eastern trend is more dominant than the NW one showing an overall ESE-WNW trending shortening direction. It roughly coincides with the principal horizontal shortening direction for Cenozoic deformation given by Berryman (1979, Teyssier et al. 1995, fig. 5.2).

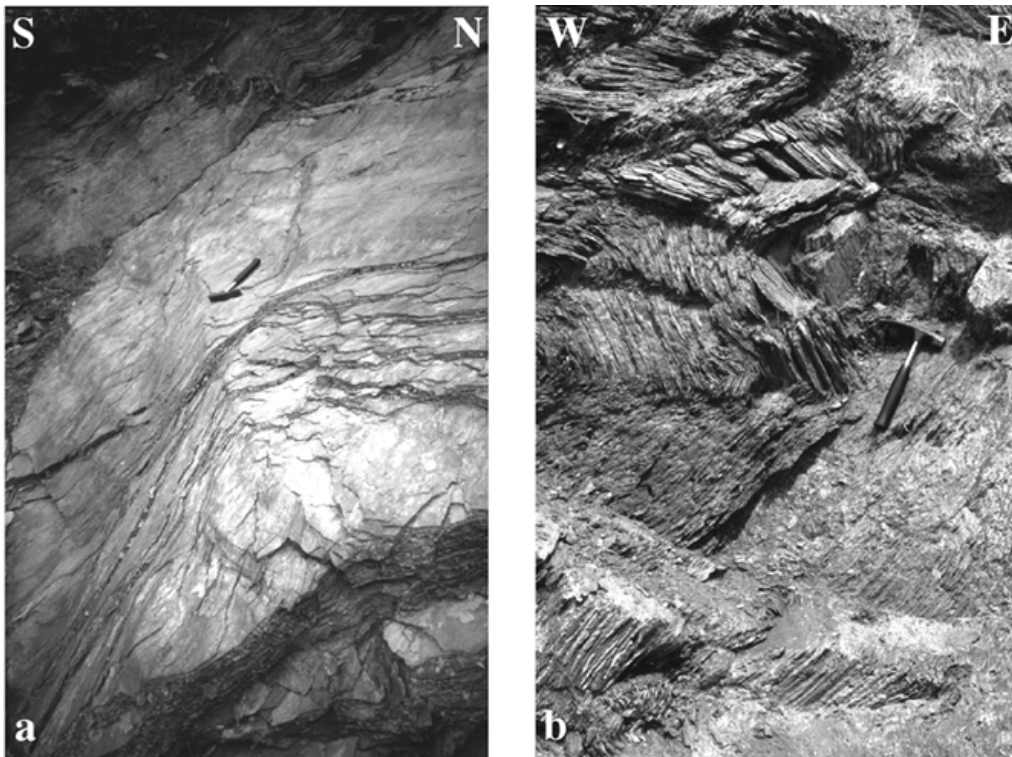


**Fig. 5.6:** **a)** Conjugate kink folds near a Cenozoic antiform (Arrow River; see location in fig. 5.5b). **b)** Conjugate chevron folds in a Cenozoic synform (Cone Peak Farm; see location in fig. 5.5a).

Between the wide-spaced reverse faults, the main foliation remains almost subhorizontal (Mortimer 1993a, b) and the orientation of the Mesozoic second and third fold generations ( $F_2/F_3$ ) is preserved. In the vicinity of major faults the main foliation as well as the Mesozoic regional folds of the second and third generation are steepened (fig. 5.4). The Mesozoic regional anti- and synforms ( $F_2/F_3$ ) are folded in Cenozoic anti- and synforms (Turnbull 1981), for example in the Kawarau region (fig. 5.5; Gentle Annie, Roaring Meg). Mesofolds of both generations are shortened orthogonal to foliation and successively attenuated and flattened in the vicinity of the fault plane. Only small folds of more competent quartz veins are preserved rotating either to upright folds ( $F_2/F_3$ ), if former fold axis is parallel to kink axis or vertical folds ( $F_2/F_3$ ), if former fold axis is oblique to kink axis (fig. 5.7). These observations strengthen the interpretation of Ward & Spörli (1979) who describe that NNE facing recumbent folds (here  $F_2$ ) are rotated “sideways” about a horizontal axis oriented almost perpendicular to the recumbent fold axes (model C, Figure 2 of Ward & Spörli 1979).

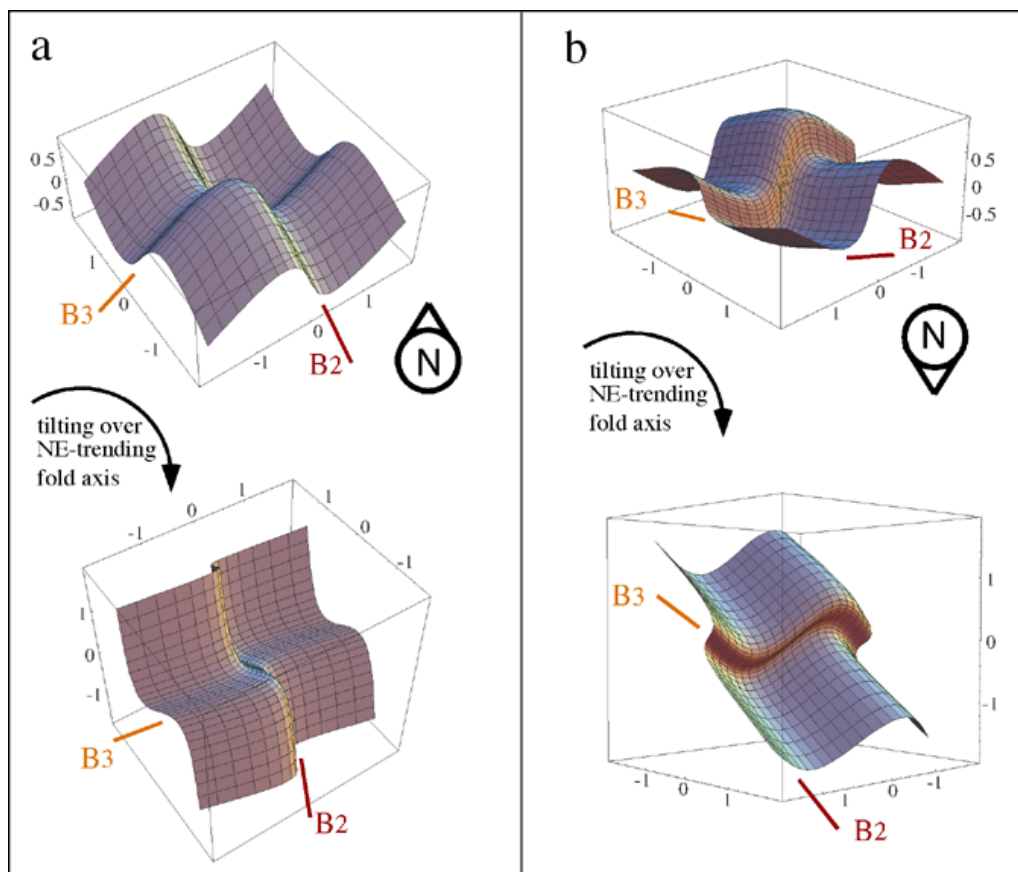


**Fig. 5.7:** Tilting of the Mesozoic folds about a NE trending Cenozoic fold axis leading to upright  $F_3$  folds and almost vertical  $F_2$  folds **a)** on the short limb of a SE verging antiform (as observed in the eastern Otago Belt); **b)** on the short limb of a NW verging antiform (as observed in the southern Alpine Belt; modelled with the help of a Mathematica subprogram written by Moore & Johnson (2000)). The rotation of the Mesozoic fold structure over subordinate NW-trending Cenozoic fold axis in the western Otago Belt leads to opposite tilted folds, almost vertical  $F_3$  folds and upright  $F_2$  folds.

## 5.4. Alpine Schist Belt

### 5.4.1. Haast area

Mesozoic pervasive foliation ( $S_1$ ) is deformed into upright, open to close kilometre-scale folds in Cenozoic times (Grindley 1963, Cooper et al. 1987, Craw et al. 1994, Little et al. 2002a,b). The NNE- to NE-trending folds axes plunge gently north-eastwards (fig. 5.8a). Abundant parasitic kink bands and chevron folds occur (fig. 5.9), especially in the synforms. The Mesozoic regional folds ( $F_2/F_3$ ) are bent around the NNE-NE trending Cenozoic fold axis. In the anti-forms the Mesozoic structures are preserved and only slightly rotated due to the Cenozoic folding. The fold axes of the Mesozoic parasitic folds as well as the penetrative crenulation lineation plunge gently either to the NE or to the SW outlining the dominance of the third generation of folds ( $F_3$ ). The  $F_3$  mesofolds grow from asymmetric W verging, close to tight folds on the long limb to symmetric tight to isoclinal folds (M-shaped) in the  $F_3$  antiformal hinge area of the regional folds. Inverse vergence is observed at the  $F_3$  synforms, where the mesofolds verge to the E (fig. 5.8b). Due to the asymmetry of the  $F_3$  regional folds the synform is less evolved than the  $F_3$  antiformal hinge zone. Just as in the Otago Belt, the transition from the short major limb to the lower major limb of a regional fold is marked by disrupted layers by boudinage (*see section 5.3.1. of this chapter or chapter 2*). The boudin axes trend subparallel to the fold axis of the dominant fold generation. In the Haast area the boudin axes plunge moderately to SW subparallel aligned to the dominant  $B_3$  fold axis (fig. 5.8a, b). Only small parasitic  $F_2$  folds are preserved during superposition of the third fold generation in the Haast area (fig. 5.8a). They are either folded around the third fold axis in a type 2 geometry or the  $B_2$  fold axis is rotated towards the superposed third fold axis displaying a type 3 interference pattern (fig. 5.3). In the Haast antiform (fig. 5.8a) the  $B_2$  fold axis plunges moderately to the S enclosing only a small angle to the SW plunging  $B_3$  fold axis. The orientation of both fold axes could be a hint for a major intersection of both regional-scale fold generations (fig. 5.3e, *see section 5.3.1. of this chapter or chapter 2*).

On the Cenozoic limbs and synforms the main foliation steepens displaying a steep dip to the E-SE. The Mesozoic former gently SE plunging  $B_2$  fold axis and subparallel aligned lithologic striping lineation  $L_2$  steepens, whereas the NE plunging  $B_3$  fold axis and crenulation lineation  $L_3$  get only slightly inclined. The crenulation lineation ( $L_3$ ) of the third fold generation ( $F_3$ ) is folded at a very low angle over the Cenozoic kink axis. Consequently the steeply plunging  $B_2$  fold axis results in nearly vertical folds (fig. 5.7b). The small  $F_2$  folds are mostly Z-shaped on the long limb and S-shaped on the short limb of a  $F_3$  mesofold. On the short limb of the regional  $F_3$  fold the relationship of mesofolds and vergence of small  $F_2$  folds is vice versa. The inclination of the main foliation changes the asymmetric recumbent  $F_3$  mesofolds with a gently dipping axial plane to almost upright folds (fig. 5.7b). On a regional  $F_3$  fold (fig. 5.8b) the mesofolds change their vergence from upward W verging on the long limb to downward E verging on the short limb.



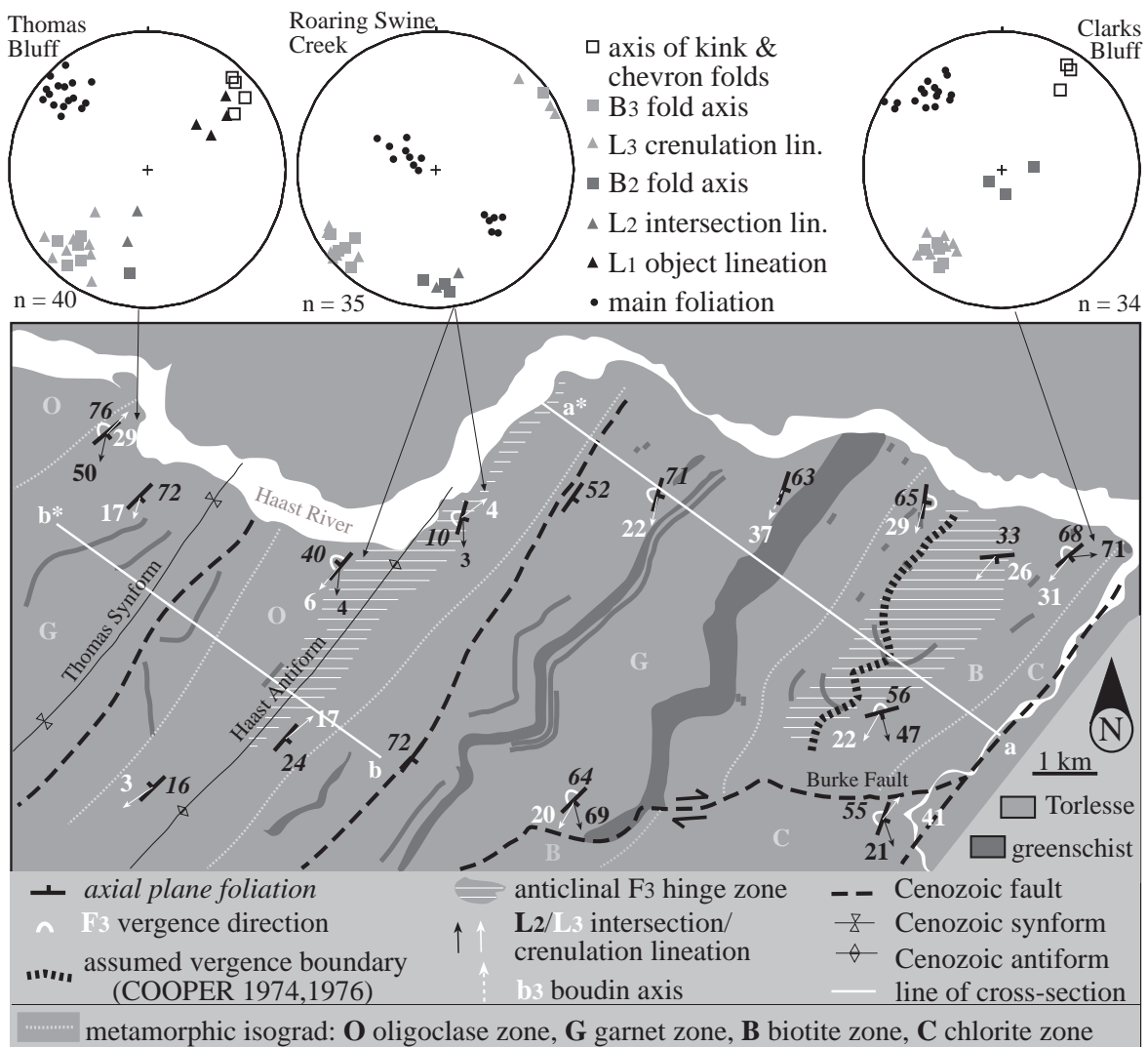


**Fig. 5.8: a)** Map of the Haast area (based on Cooper (1974, 1976); see location in fig. 5.2). The Mesozoic fold structure is folded in NE trending Cenozoic syn- and antiforms. Note that the Alpine Barrovian-type metamorphic zones (Cooper 1976, Mortimer 2000) are folded around the Cenozoic fold axis as well. The metamorphic isograds trend subparallel to the Cenozoic syn- and antiforms. Stereograms (equal area, lower hemisphere projection) of the structure at Clarks and Thomas Bluff reflect the folded Mesozoic structure in Cenozoic synforms, where the foliation dips steeply to the SE. The tilting of the whole structure results in vertical second folds ( $F_2$ ) at Clarks Bluff. The lesser inclined  $F_2$  folds in the western part of the Haast region (Thomas Bluff) can be explained that the second fold axis ( $B_2$ ) rotates towards the superposed third one ( $B_3$ ) due to a Mesozoic regional hinge intersection. The stereogram (equal area, lower hemisphere projection) of location Roaring Swine Creek reflects the structure observed in a Cenozoic antiform, where the main foliation is flat lying. The almost unrotated Mesozoic fold structure displays a dominant  $F_3$  generation comparable to locations somewhere in the northwestern Otago Belt.

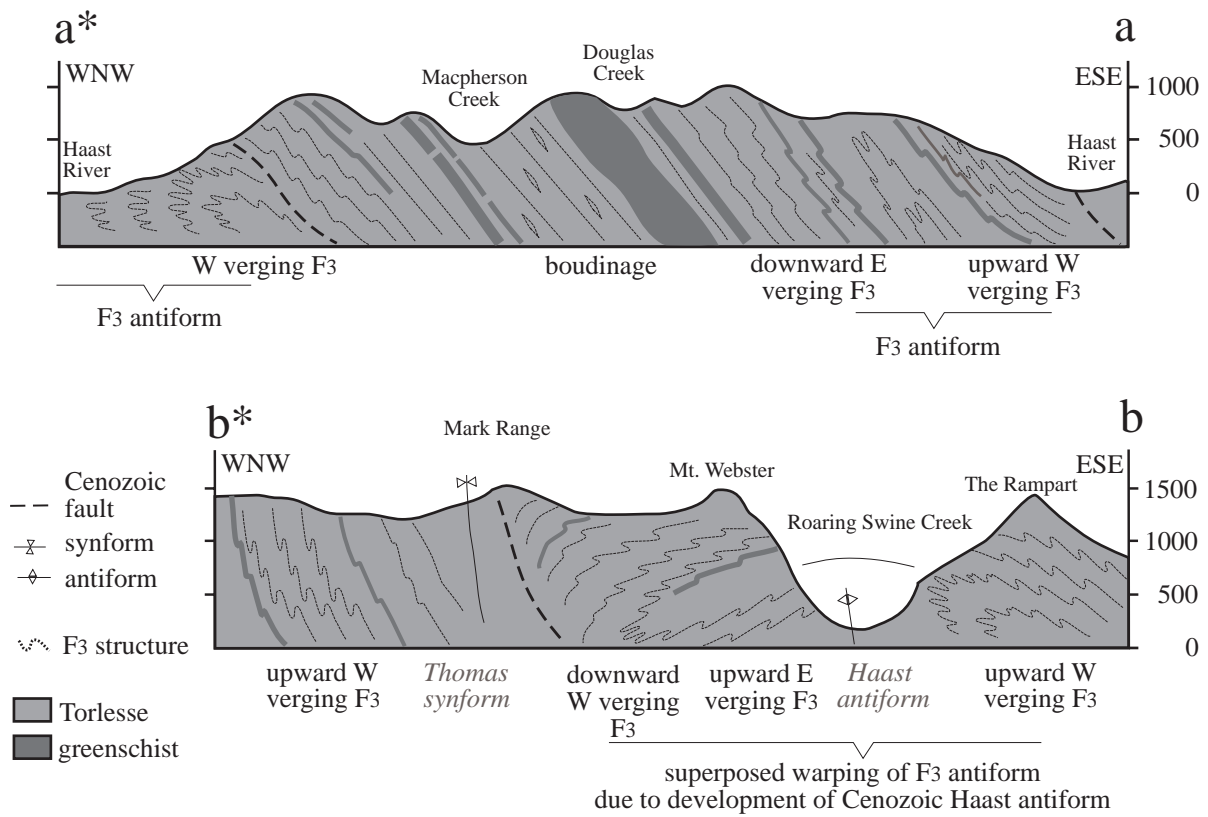


**Fig. 5.8:b)** Two schematic cross-sections are parallel aligned through the Haast area as shown on map, fig. 5.8a. The cross-section a- a\* outlines an upright  $F_3$  anticlinal hinge zone, which succeeds to the WNW into a zone of boudinage, the lower  $F_3$  limb. The cross-section b-b\* shows a  $F_3$  anticlinal hinge zone, which is folded around the Haast antiform leading to a different vergence appearance on both limbs of the antiform.



**Fig. 5.9:** Parasitic kink folds in Cenozoic synforms, Haast area, Alpine Belt.

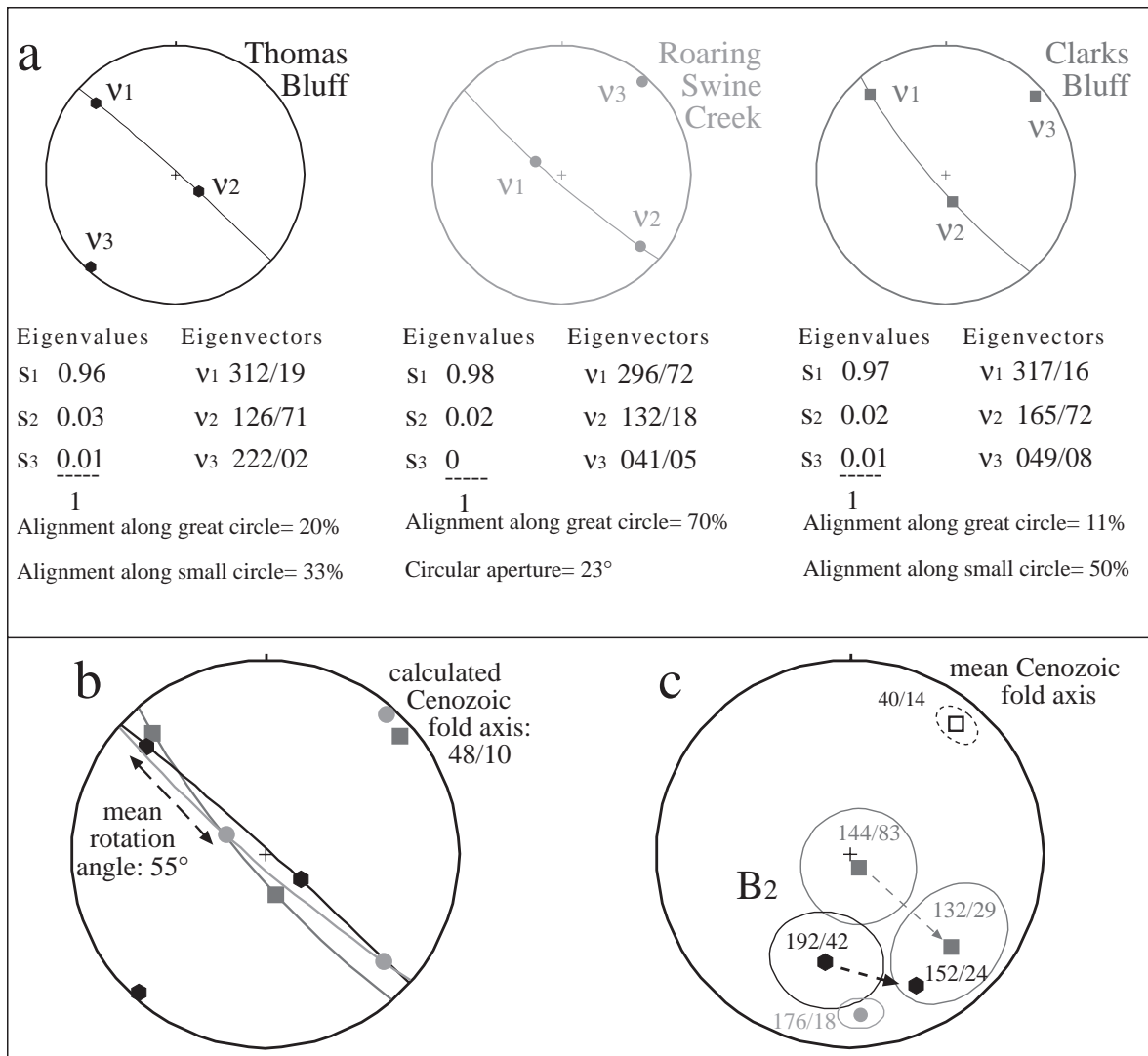


**Fig. 5.10: a)** The  $F_3$  axial planes are analysed by the calculation of eigenvector and eigenvalue, a method described by Woodcock (1977) and Lisle (1999). The calculated eigenvector and -value define the average structural trends ( $v_1$ ), including the best-fit fold axis ( $v_3$ ), for each subarea. **b)** Calculations of the Haast area's structure show that the  $F_3$  axial fold planes ( $v_1$ ) of the Cenozoic synforms (Clarks and Thomas Bluff) are rotated c. 55° to steeper dip around the mean Cenozoic axis oriented 48°/10°. The high eigenvalue ( $s_1$ ) of the average eigenvector ( $v_1$ ) displays that the  $F_3$  axial planes are cylindrically folded around the Cenozoic axis. **c)** Related to the measured  $B_2$  fold axes, the rotation around the Cenozoic fold axis display various orientations of the second fold axis. At Clarks Bluff the re-orientation of  $B_2$  leads to a typical SE plunge as observed in the Otago Belt. At Thomas Bluff and Roaring Swine Creek the second fold axis  $B_2$  is rotated to a northerly trend due to the Mesozoic regional hinge intersection.

Figure 5.10 shows the results of rotation calculations to bring the Mesozoic fold structure of the Haast antiform into coincidence with the one of the adjacent Cenozoic synforms, near Thomas Bluff and Clarks Bluff (fig. 5.8a). The reconstructed rotation axis in the Haast area outlines a NNE-NE trend with a subhorizontal to gentle plunge to the NE (fig. 5.10). The eigenvector calculation (Woodcock 1977, Lisle 1999) reveals that the Mesozoic  $F_3$  axial planes are cylindrically folded around an almost subhorizontal Cenozoic fold axis. The high eigenvalue ( $s_1$ ) of the average eigenvector  $v_1$  leads to the interpretation that no shear occurs parallel to the Cenozoic fold axis.

#### 5.4.2. Transition to the Otago Belt: Lake Hawea – Lake Wanaka area

Whereas in the Haast area the Mesozoic third fold generation is dominant over the second one as described before (see section 5.4.1.), both fold generations are about the same size on the rim of the Otago Belt, for example in the Lake Hawea – Lake Wanaka area (fig. 5.11a). Being on a Cenozoic limb, the main foliation ( $S_1$ ) is steepened, dipping to the E (fig. 5.11a). Abundant Cenozoic kink folds with fold axes trending in NNE, subordinately in NNW direction, display a conjugate set parallel to the Mesozoic fold axes (fig. 5.11a). This conjugate set outlines a horizontal shortening in ESE-WNW direction as described before in the western Otago Belt (fig. 5.5). Walking along the western shore of Lake *Hawea* over the *neck* to the northeastern shore of Lake *Wanaka* the mesofolds display a vergence change from downward ENE to upward WNW vergent mesofolds, a vergence boundary mapped by Turnbull (2000; fig. 5.11a). On first sight the change of vergence may be misinterpreted as a major synform of a regional  $F_3$  fold. But the Mesozoic fold structure is more complex in the Lake *Hawea* - Lake *Wanaka* area.

In the *Wanaka* section the axial planar foliations of mesofolds dip to the ESE - SE. Fold axes and subparallel aligned penetrative crenulation lineations plunge gently to the NNE. Walking from the neck westwards along the north-eastern shore of Lake *Wanaka*, upward WNW vergent mesofolds change to symmetric (M-shaped) than to an area of downward SE vergent mesofolds. The appearance and orientation of the mesofolds outline a  $F_3$  regional antiform (fig. 5.12), which is steeply tilted to the E.



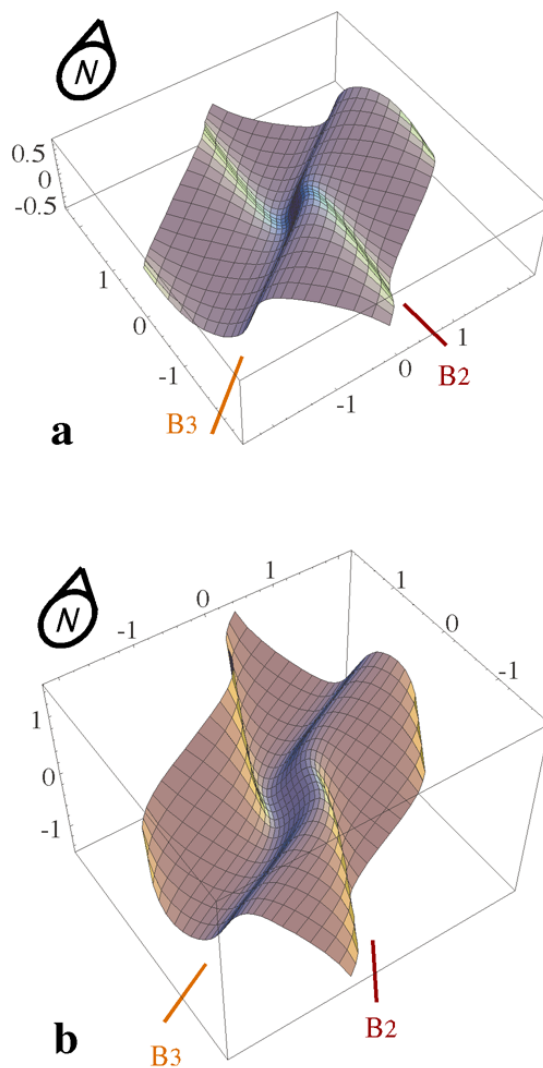


**Fig. 5.12:** On the basis of the model for the regional folds in the western Otago Belt (**a**; chapter 2), a model for the Lake Hawea- Lake Wanaka region (**b**) is developed. The Cenozoic tilting towards the E results in a moderately plunging second fold axis ( $B_2$ ), whereas the third fold axis ( $B_3$ ) remains with a gentle plunge. The regional  $F_3$  fold is rotated to an upright W vergent fold, whereas the NE vergent regional  $F_2$  fold is tilted to a steeply plunging fold. Near a major hinge intersection, both fold axes of mesofolds rotate towards each other. In the area of hinge intersection, the third fold generation ( $F_3$ ) is dominant and the influence of the second fold generation is diminished. The vergence boundary of the third fold generation remains almost straight throughout the area of hinge intersection (modelled with the help of a Mathematica subprogram written by Moore & Johnson (2000)).

In the *Hawea* section, the ENE-vergent mesofolds have developed abundant small parasitic folds on their back. A lithologic striping lineation is aligned parallel to the fold axis, both plunging moderately to the SSE. The axial planar foliation of the mesofolds dips to the E. Walking along the southern shore of the western inlet of the Lake Hawea mesofolds grow in amplitude from close, inclined (fig. 5.13a) to tight to isoclinal folds (fig. 5.13b), which verge downwards to the NE. The isoclinal mesofolds are successively boudined forming highly asymmetric, intrafolial, downward NE vergent folds (fig. 5.13c). The described succession dis-

plays an open regional  $F_2$  fold (fig. 5.12), where the  $F_2$  mesofolds only occur on the short major limb. Macroscopic  $F_2$  folds are flattened to open folds in the vicinity of a superposed  $F_3$  regional fold as described for comparable regional folds in the Otago Belt (*chapter 2*). The orientation and appearance of the  $F_2$  mesofolds reflects that the regional  $F_2$  fold is tilted to the E in the Hawea section. The major hinge intersection of both commensurate regional folds ( $F_2/F_3$ ) is marked by the rotation of both fold axes towards a northerly trend. The immediate area of hinge intersection E of the neck between Lake Wanaka and Lake Hawea (fig. 5.11a, b) outlines upright noncylindrical folds with gently either to NNE or to SSE dipping fold axes. Towards the E, the influence of the third fold generation decreases and successively  $F_2$  mesofolds grow (fig. 5.11b).

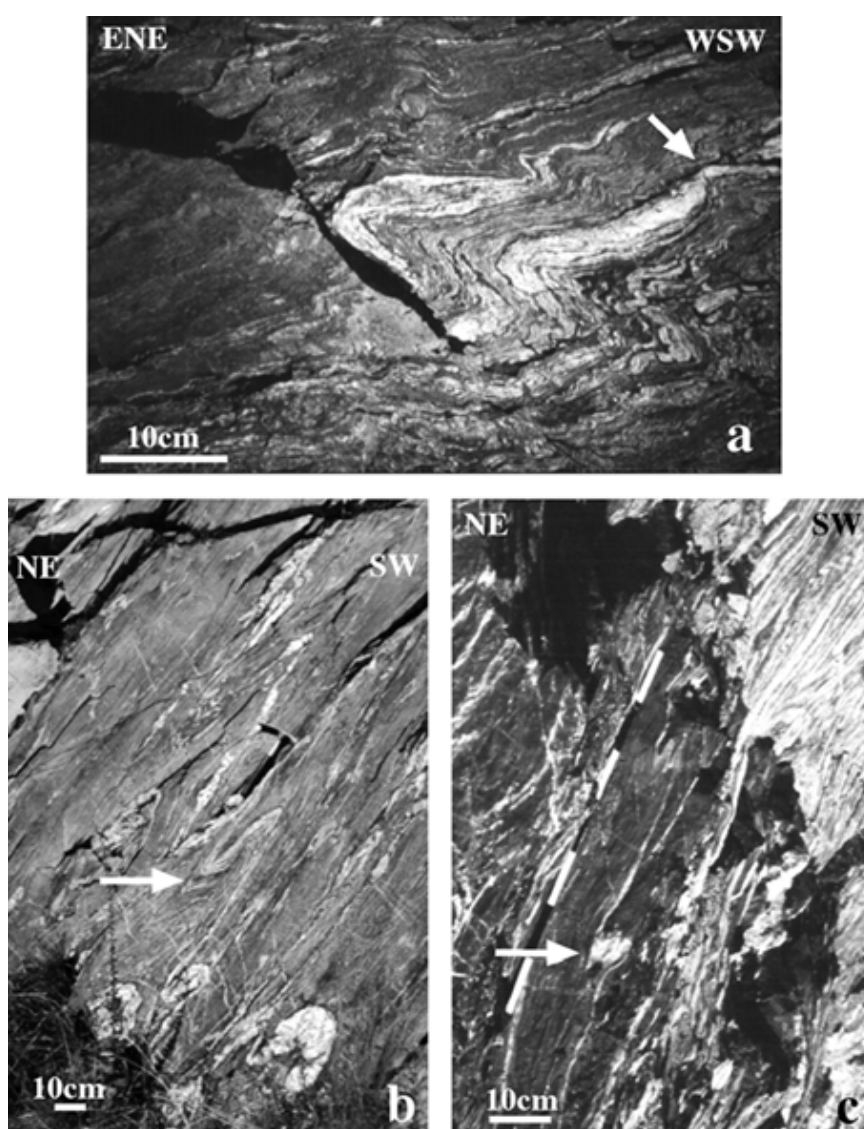


**Fig. 5.13:** Outcrops of the southern shore of the western inlet of Lake Hawea from the W to the E show a succession from close (a) to isoclinal  $F_2$  mesofolds (b, see arrow), which verge downward to the NE, to boudinaged  $F_2$  folds (c, see arrow). Note that the long limb of the  $F_2$  mesofold in fig. 5.13a is gently folded over an N-plunging  $B_3$  fold axis (see arrow) forming an asymmetric box-shaped fold.

Both regional folds ( $F_2$  and  $F_3$ ) are rotated over a NNE-NE trending Cenozoic fold axis (fig. 5.12). Due to the superposition of the third fold generation the  $B_2$  fold axes have a northerly trend, and so the  $B_2$  fold axes are less rotated to a steep plunge in the *Hawea* section than in the Haast area (fig. 5.12b).

The geochronological study of Kamp et al. (1989, their figure 2) reflects the described Mesozoic fold structure. Areas dominated by the second fold generation as the *Hawea* section yield Late Jurassic ages, whereas the *Wanaka* section, which is dominated by the third fold generation, show Early Cretaceous ages (*see as well chapter 2*).

#### 5.4.3. Shortening of the Mesozoic structure

Mesozoic mesofolds in Cenozoic antiforms (e.g. Haast antiform, fig. 8a, b) display a type 1B/1C fold geometry (Ramsay & Huber 1987) for quartz-rich layers and a type 3 geometry for mica-rich layers like the mesofolds in the core of the Otago Belt (e.g. Treble Cone/ Matukituki Valley, Remarkables, see locations in fig. 5.18). The cm-scale parasitic folds as well as the mesofolds themselves outline rounded hinges.

In the Cenozoic synforms the Mesozoic folds are shortened orthogonal to the foliation plane. The flattened mesofolds outline round hinges of the cm-scale parasitic folds in the inner arc and tapered hinges at the outer arc of the mesofold hinge (fig. 5.14). Compared to the Mesozoic mesofolds observed in the Cenozoic antiforms, these flattened folds in the synforms are

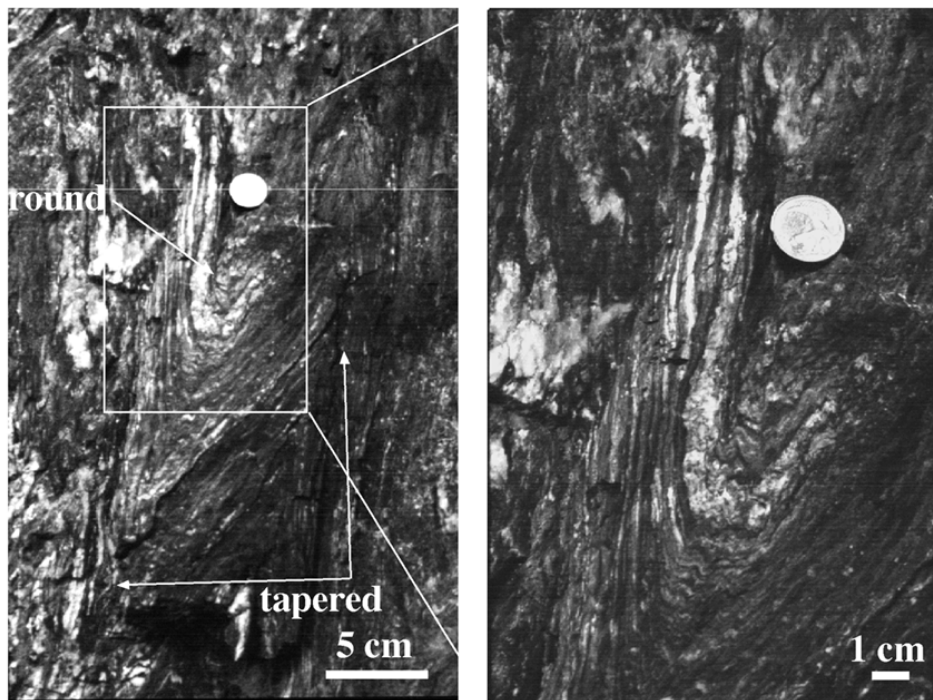


**Fig. 5.14:** Shortening of the Mesozoic  $F_3$  mesofolds orthogonal to the foliation results in a tapered outer arc at the hinge zone, whereas the cm-scale parasitic folds remain rounded at the inner arc (neck between *Lake Wanaka* and *Lake Hawea*). Box in fig. 5.14a indicates the enlarged view of fig. 5.14b.



shortened between 50-75% perpendicular to the foliation plane (fig. 5.15). The shortening increases the amplitude and decreases the wavelength. Small parasitic folds are unfolded and stretched in the foliation plane. The calculated shortening rate (50-75%) is in the same range as that of Holm et al. (1989) for the Alpine Schist. They document quartz-rich veins, which form part of a regionally sequence of structures ranging from brittle displacements of deglaciated surfaces through structures exhibiting brittle-ductile transitional to ductile behaviour. The minimum shortening estimates are averaging between 50% and 75% perpendicular to foliation (Holm et al. 1989). Also Holcombe & Little (2001) suggest on the base of microstructural observations that the rocks may undergo oblate flattening of up to 75% maximum shortening. The flattening strain results in strongly foliated rocks without a lineation (S-fabrics; Holcombe & Little 2001, Little et al. 2002a,b). No new stretching lineation is observed, only a Mesozoic object lineation plunging gently to moderate steeply either almost subparallel to the second ( $B_2$ ) or third fold axis ( $B_3$ ) occurs (fig. 5.8a, 5.11). This object lineation ( $L_1$ ), which is folded at a small angle around the second and third fold axis, can be classified to the first deformation phase ( $F_1$ ) from investigations in the Otago Belt (*chapter 4*). The preservation of the relative orientation of both Mesozoic fold axes and the resulting interference pattern during Cenozoic overprint indicates pure-shear-dominated deformation, also noted on microstructural evidence by Holcombe & Little (2001).

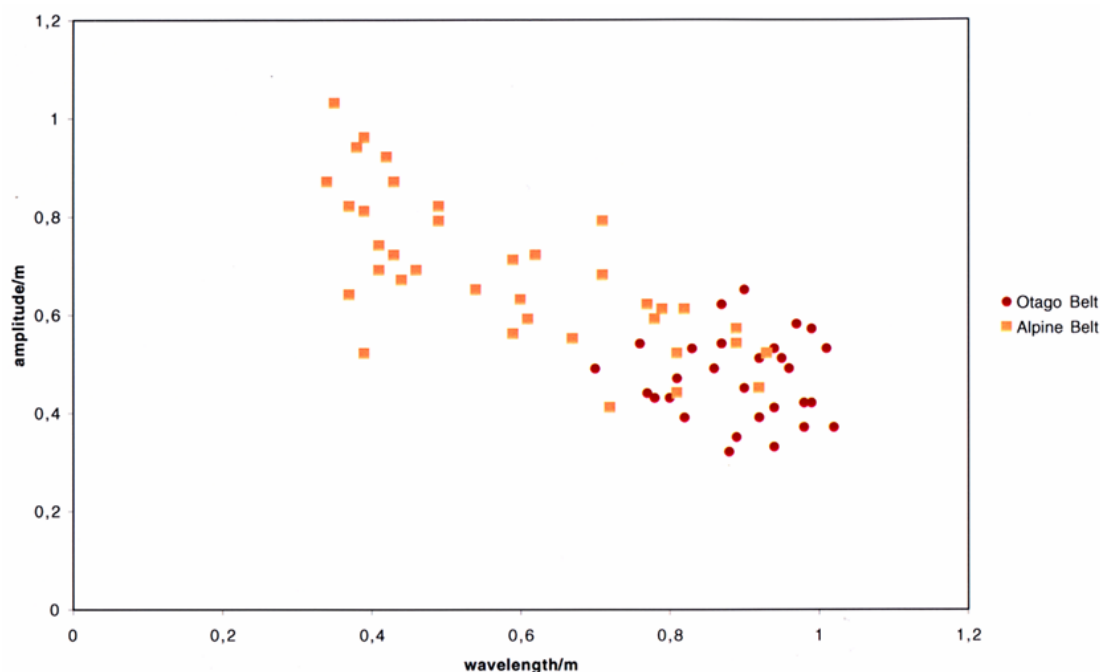
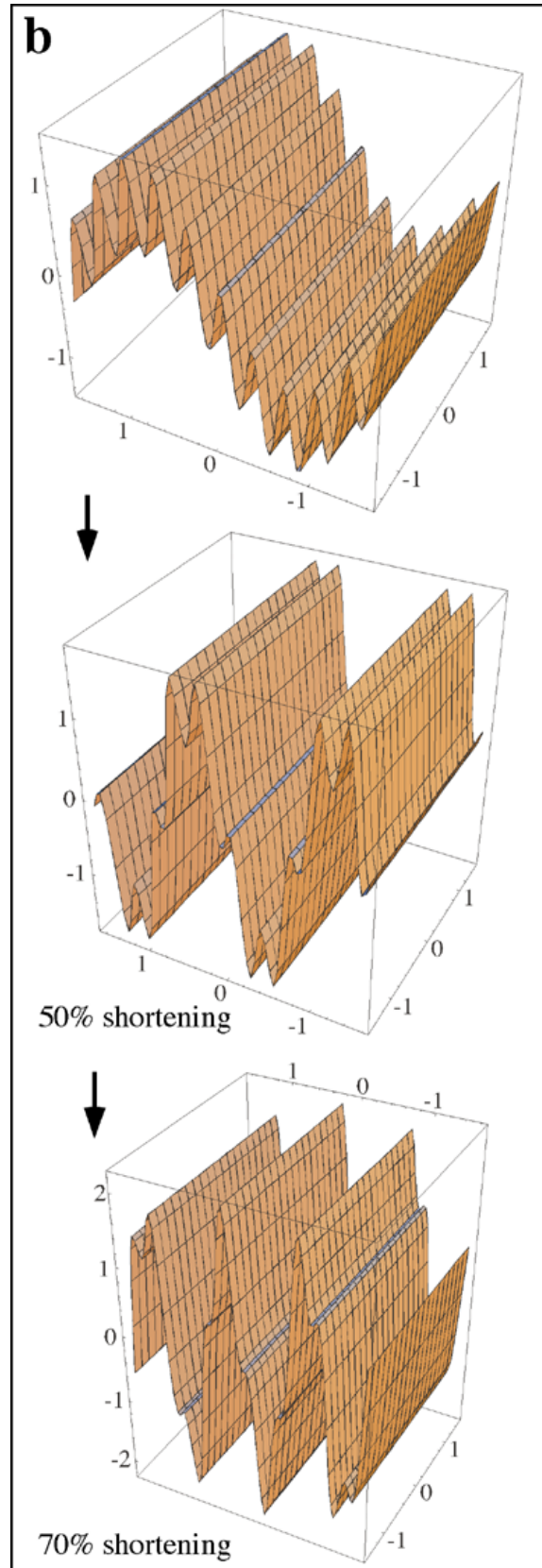


**Fig. 5.15: a)** Amplitude and wavelength of  $F_2/F_3$  mesofolds measured in the Otago Belt compared to Mesozoic  $F_2/F_3$  mesofolds observed in the southern Alpine Belt. Only the mesofolds within the regional fold hinge zones are taken into account. Alpine mesofolds with the same amplitude/wavelength ratio than Otago mesofolds occur in the Cenozoic antiforms. Shortening orthogonal to the main foliation leads to a decreased wavelength and increased amplitude of the mesofolds in the Alpine Belt. Shortening up to 75% is calculated in the Cenozoic synforms.



*b) Fold models displaying the observed shortening of the  $F_2/F_3$  mesofolds in the Cenozoic synforms (modelled with the help of a Mathematica subprogram written by Moore & Johnson (2000)). Parasitic folds are successively stretched on the limbs of the mesofolds.*

#### 5.4.4. Cenozoic fault pattern

Investigations into the fault pattern reveal that reverse faults propagate parallel to the main foliation (compare fig. 5.16 to fig. 5.11 and 5.8a). Slickensides on small reverse splay-faults plunge steeply to the E (reverse dip-slip component, fig. 5.16). Branching reverse fault zones occur in the hanging wall of the Cenozoic synforms and at the footwall of the Cenozoic anti-forms (fig. 5.8b). In general, reverse splay-faults pervade the whole Cenozoic synform. Thus the Cenozoic folds are developed by parallel to the main foliation propagating forelimb thrusts. Movement on the E to SE steeply dipping reverse faults leads to km-scale antiforms at the eastern step and small synforms at the western step (see fig. 5.8b).

E-W trending gently dipping strike-slip faults with dextral-slip lineations cut the reverse faults (see Burke Fault, Cooper 1974, 1976, fig. 5.8a, 5.16). The strike-slip faults occur like the reverse faults on all scales. The subdivision of the minor fault pattern in reverse and strike-slip faults reflects the movement of the Alpine Fault. Norris & Cooper (1995, 1997, 2001) describe the movement of the Alpine Fault with the term “serial partitioning”: en echelon strike-slip faults, which trend in the direction of the overall plate motion vector, displace an orogen-parallel fold and thrust belt.

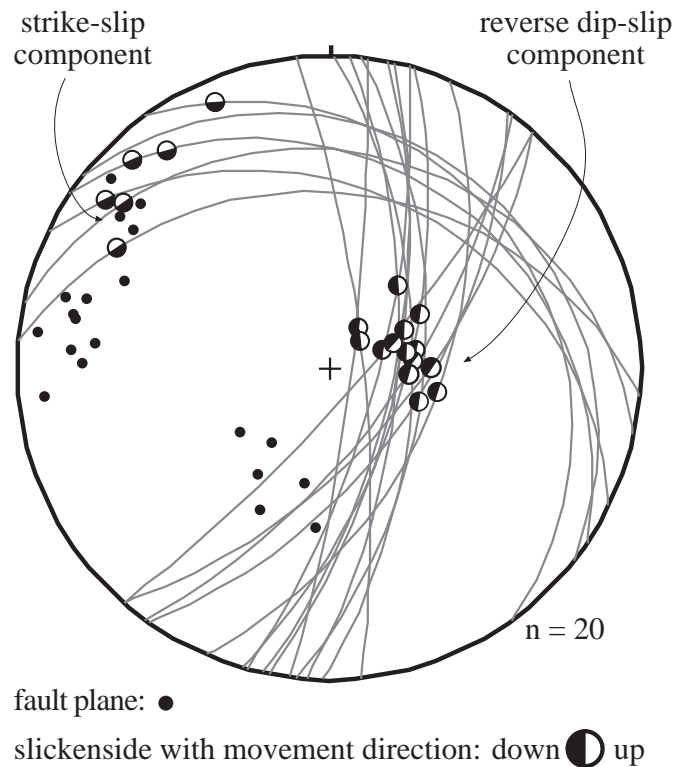


**Fig. 5.16:** Stereogram (equal area, lower hemisphere projection) of fault planes (depicted a great circles and poles) and slickensides comprised from the Haast area to the Lake Hawea- Lake Wanaka area (including Haast and Makarora River Valley), reflecting the strike-slip and reversed dip-slip component on minor faults.

## 5.5. Discussion and Conclusion

### 5.5.1. Tilting of the fold and thrust belt

The Cenozoic folds of the Alpine and Otago Belt develop at the tip line of parallel to the main foliation propagating forelimb thrusts. A two-sided fold and thrust belt is proposed because the asymmetric Cenozoic folds evolved by the movement on reverse faults display two opponent movement directions. In the eastern part of the Otago Belt the asymmetric Cenozoic folds outline a movement of the reverse faults to the SE, whereas in the central and western part of the Otago Belt opposite dipping reverse faults lead to pop-up structures (Beanland & Berryman 1989; fig. 5.17). Towards the Alpine Fault, in the north-western Otago and Alpine Belt, the reverse faults dip steeply to the E-SE. The asymmetric Cenozoic folds reflect a movement to the W-NW on the reverse faults (fig. 5.17). The development of this two-sided fold and thrust belt is continuous in the whole Otago and Alpine Belt. It arises subhorizontally, almost orthogonal to the principal shortening direction measured by Berryman (1979, Teyssier et al. 1995, fig. 5.2). In the eastern part of the Otago Belt the initial orientation of the flat-lying fold and thrust belt remains. Further oblique convergence and attended continuous erosion within the Alpine Fault System (Casas et al. 2001) causes shortening and tilting of the western wing of the fold and thrust belt. The deformation is bounded on faults leading to a further reverse movement. The Mesozoic structure within the thrust sheets is tilted about horizontal axes as a whole. The former structure is shortened orthogonal to the main foliation plane and the pre-existing main foliation is reinforced (Little et al. 2002a,b) on the limbs and synforms of the long wavelength Cenozoic folds (S-shape fabric). As the reverse faults are steepened in the vicinity of the Alpine Fault, the strike-slip faults change their dip from moderate steep in western Otago Belt to flat-lying in the Alpine Belt. Consequently the Alpine strike-slip faults are initiated as steeply dipping faults in the initial flat-lying fold and thrust belt structure. The steepening of the western wing of the fold and thrust belt is accompanied by the formation of backthrusts (like the Main Divide Fault Zone, Cox & Findlay 1995) off the Alpine Fault plate boundary (fig. 5.17; Norris et al. 1990, Koons 1990, 1994, Cox & Findlay 1995).

### 5.5.2. Rotation of the fold and thrust belt to a northerly trend in the western Otago Belt?

In map-view (fig. 5.2) it seems that the ranges of the western Otago Belt are rotated c. 25° anticlockwise to the ones of the eastern Otago Belt. Or they are rotated c. 25° clockwise to the ranges in the Alpine Belt as proposed by Jamison (1991). A process suggested on the North Island (Lamb 1988), in the northern branching part of the Alpine Fault system (Marlborough Fault System, fig. 5.2) and in the Otago/Alpine Belt is that the rotation takes place about a vertical axis (Norris 1979, Reilly 1986, Little & Roberts 1997, Little & Mortimer 2001). Vertical axis rotation of rigid blocks within shear zones depends on the motion of the boundaries, on the attitude of the blocks within the zone, and also on the mechanism by which rotation is imparted on the blocks (Jackson & Molnar 1990, Little & Roberts 1997). Independent of these boundary conditions, all models imply a rotation of the rigid block itself. When every thrust sheet of the western Otago Belt is rotated as a rigid block, the Mesozoic structure within this

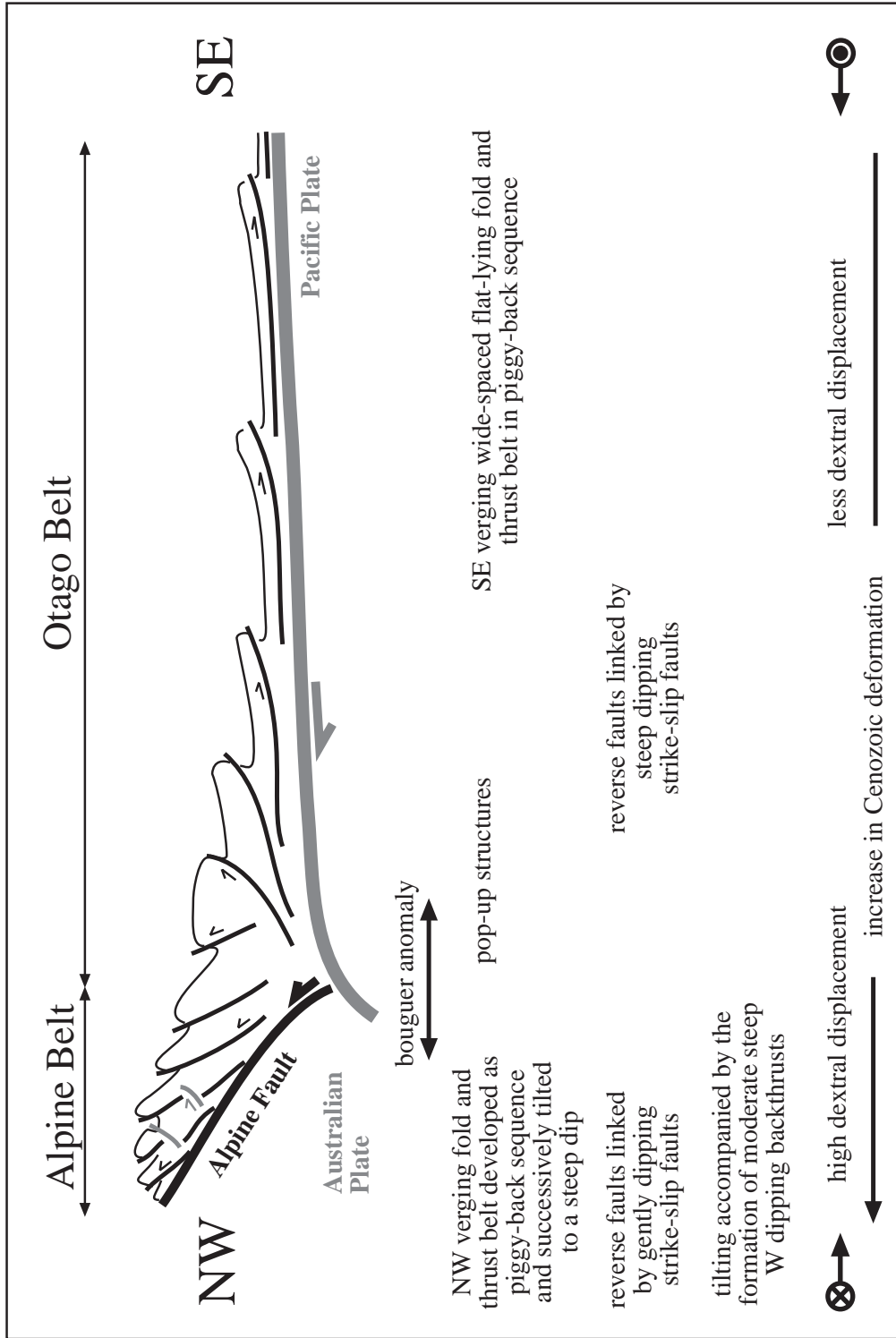


**Fig. 5.17:** Schematic cross-section of a positive flower or palm-tree structure through the Alpine and Otago Belt (see location of cross-section in fig. 5.2, based on geophysical data by Davey et al. 1995, 1998, Beavan et al. 1999). The presence of a large negative Bouguer gravity anomaly, east of the main divide, implies a thickened crust due to the development of a root (Woodward 1979, Allis 1986, Norris et al. 1990). See text for further details.

thrust sheet shall as well display a rotation compared to an unrotated thrust sheet in the eastern part of the Otago Belt. But no anticlockwise or clockwise rotation of the Mesozoic structure within the thrust sheets is observed (fig. 5.18). Furthermore Bradshaw et al. (1996) shows that Early Cretaceous structures occurring in the Western Province (see fig. 5.2, inset), which have almost the same age as the  $F_3$  development, do also not rotate in the vicinity of the Alpine Fault.

In a fold and thrust belt, the propagation of the thrusts depends on the orientation of the main foliation. In the eastern Otago Belt the main foliation remains subhorizontal (Mortimer 1993b) although it is folded tightly to isoclinally around a subhorizontal Mesozoic fold axis ( $F_2$ ). The overprinting third fold generation occurs only locally. Variations in main foliation's dips causes a change in the extent and appearance of the Cenozoic antiforms as described by Markley & Norris (1999) but the Cenozoic regional antiform axis is developed perpendicular to the overall shortening direction. Towards the western Otago Belt the Mesozoic second fold generation ( $F_2$ ) is overprinted by a growing third generation of folds ( $F_3$ ). The intersection of both Mesozoic regional folds ( $F_2/F_3$ ) results in various dips of the main foliation. The propagation of the Cenozoic fold and thrust belt is maintained by different oriented gently dipping foliations. Consequently a conjugate set of NW- and NE-trending folds and faults subparallel to the Mesozoic fold axes is evolved leading to a major Cenozoic fold axis trending almost N-S (fig. 5.5). Dextral strike-slip faults accomplish the hinge migration of the major Cenozoic folds. This propagation on diversely oriented "easy-slip horizons" is accompanied by re-activation of Cretaceous to Early Cenozoic extensional fault zones (Spörli 1979, Madin 1988, Norris et al. 1990, Turnbull 2000).

In the Alpine Belt the Mesozoic third fold generation ( $F_3$ ) is dominant over the second fold generation ( $F_2$ ) leading to a general NE trending Cenozoic fold axis (fig. 5.8a). It should be stressed that the parasitic kink axes show a constant NE-trend in the whole Otago and Alpine Belt (see fig. 5.5 and 5.8a), which is only supported by a conjugate NW-trend mainly in the western Otago Belt.

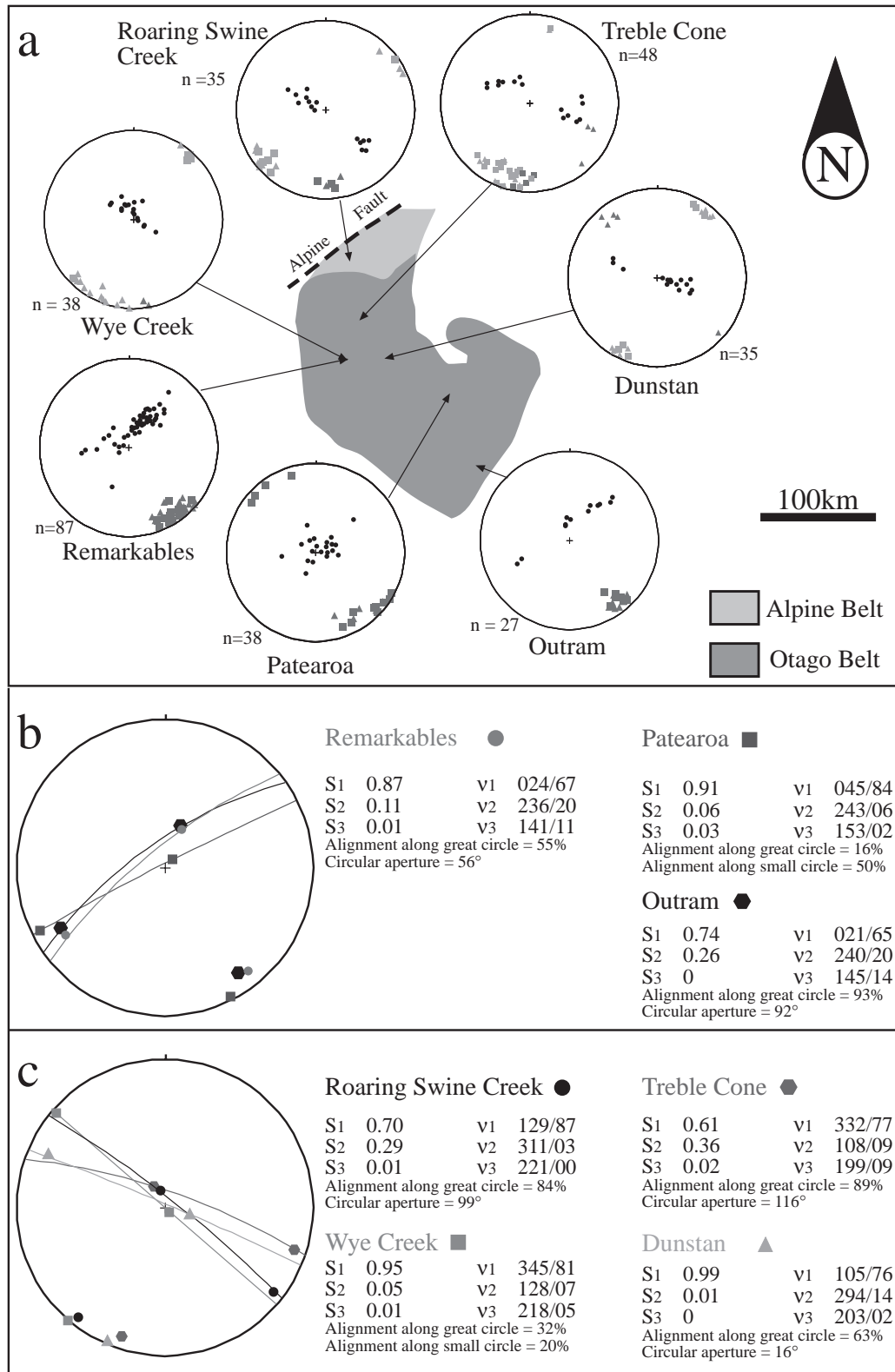


**Fig. 5.18:** Comparison of locations of resembling Mesozoic fold structure, dominant  $F_2$  generation in the eastern to western part of the Otago Belt and dominant  $F_3$  generation from the western Otago Belt to the southern Alpine Belt (a). The eigenvector calculation of the main foliation ( $S_1$ ) after Woodcock (1977) and Lisle (1999) shows that no vertical axis rotation of the Mesozoic fold structure occurs due to the Cenozoic overprint (b, c). In fig. 5.18c) the trend of the eigenvector  $v_3$  deviates because of the superposition of the third fold generation ( $F_3$ ) on the second fold generation ( $F_2$ ).

### 5.5.3. *Bending of the Otago and Alpine Belt – during Mesozoic or Cenozoic times?*

A long-discussed problem is the bent orogenic trend of the Otago and Alpine Belt (see fig. 5.2). Some workers interpret the curved arc as a gigantic drag fold developed by the dextral movement of the Alpine Fault in the Late Cenozoic (Hunt 1978, Korsch & Wellman 1988, Sutherland 1999). The interpretation of the development of such a structure, which implies large scale non-coaxial deformation, is rejected. Investigations into the Mesozoic fold structure show that this structure is cylindrically refolded and that shear is restricted on the reverse fault zones during the Late Cenozoic. Also the fragmented Mesozoic fold structure reveals no vertical axis rotation in the studied parts of the Otago or Alpine Belt.

Many workers previously propose that the oroclinal bending takes place during the Mesozoic (Grindley 1963, Cooper 1974, Wood 1978, Kamp 1987, Bradshaw 1989, Bradshaw et al. 1996). Bradshaw et al. (1996) consider that the bending of the arc occurs just prior to the inception of the mid-Cretaceous extensional stage in opposite to Kamp (1987), who suggests a Late Triassic – Early Jurassic age and therewith a bending during the Rangitata I orogeny. I follow Bradshaw's (1989) interpretation who notes that the orogenic trend has been bent to some degree before Cenozoic but that there is a significant increment of late Cenozoic bending. Investigations into the Mesozoic fold structure show that the recurved orogenic trend of the Otago and Alpine Belt (see fig. 5.2) is partly developed by superposition of the Mesozoic fold generations ( $F_2/F_3$ ). The formation and successive uplift of growing regional folds of the second generation ( $F_2$ ) in the centre of the eastern part of the Otago Belt causes a NW-SE oriented orogenic trend. The third fold generation ( $F_3$ ), which is superimposed on the second fold generation ( $F_2$ ), occurs only locally in the eastern Otago Belt and amplifies westwards being the dominant fold generation in the Alpine Belt. The development of the third fold generation bends the orogenic trend in the Alpine Belt to a NNE direction in the Early Cretaceous.

Combined movement on reverse and dextral strike-slip faults rotates the Alpine Fault successively to the E ( $055^\circ$ , Norris et al. 1990) as described by Norris & Cooper (1987, 2001), whereas the fold and thrust belt retains his NNE trend. The bending of the Otago and Alpine Belt is intensified by dextral strike-slip movement localised on re-activated Cenozoic steepened thrust faults. Because the dextral strike-slip movement increases on faults adjacent to the Alpine Fault (Turnbull 2000) the bending is strengthened in the Alpine Belt and western part of the Otago Belt. The localised movement on N to NE trending faults, which are almost aligned subparallel to the Alpine Fault, can be described as a parallel partitioning (Teyssier et al. 1995) but no strain is distributed within the fault bounded blocks and thus no vertical axis rotation occurs.



## *Chapter 6*

*On first examining a new district, nothing can appear more hopeless than the chaos of rocks;  
but by recording the stratification and nature of the rocks and fossils at many points,  
always reasoning and predicting what will be found elsewhere,  
light soon begins to dawn on the district,  
and the structure of the whole becomes more or less intelligible.  
(Charles Darwin)*



*Two Silvereye - birds hidden in the greenery*

## **Late Paleozoic to Cenozoic tectonic development of South Island, New Zealand**

### **Abstract**

The results of this thesis are presented in relation to the regional geology of the South Island, New Zealand. The reconstruction of the tectonic evolution of South Island starts with the Early Permian to explain the continuous sedimentation area of Caples and Rakaia Groups at the eastern flank of a Permian mid-ocean ridge – the later obducted Dun Mountain Group. In the Early to Middle Jurassic, underplating of Caples and Rakaia Groups thickens the accretionary wedge, which is developed at the eastern margin of Gondwana. ENE directed nappe stacking ( $F_1$ ) takes place at lower levels of the accretionary wedge under moderate high pressure metamorphism. In the Late Jurassic the accretionary wedge is successively shortened under retrograde metamorphic conditions resulting in NE or foreland verging regional folds ( $F_2$ ) within the present Otago Belt. The resulting steepening of the subduction zone causes the formation of a new NW-SE trending accretionary wedge to the NE, the Pahau Group. In the Early Cretaceous the Eastern and Western Province as well as the intermediate occurring Median Batholith are shortened due to the Pacific/Phoenix ridge collision. NW or hinterland verging regional folds ( $F_3$ ) are formed during Barrovian-type metamorphic overprint within the present Alpine Belt – an overprint on the Jurassic Otago Belt. The westward migrating rift system causes the opening of the Tasman Sea and the separation of New Zealand from Gondwana in the Late Cretaceous. The extensional or rifting stage is not previously and will not further considered within the scope of this thesis. In the Late Cenozoic further shortening results in the inception of the transpressional system of the Alpine Fault. A NNE trending fold and thrust belt is evolved building up a regional flower structure, whose western wing – the Alpine Belt – is uplifted by continuous shortening and erosion.

### **6.1. Introduction**

Changing theories and advanced techniques result in different views of the tectonic evolution of the South Island, New Zealand, over the last decades. Geosynclinal interpretations (Landis & Coombs 1967, Fleming 1970) are replaced by plate tectonic interpretations (Landis & Bishop 1972). Roughly two main plate tectonic interpretations can be distinguished, which all show the growth of New Zealand by progressive addition of material by plutonic and accretionary processes (Mortimer 1995): models of a conditional fixed subduction zone (Coombs et al. 1976, Korsch & Wellman 1988, Mortimer 1995) and models emphasising strike-slip motions (Howell 1980, Spörli & Ballance 1988, Sutherland & Hollis 2001).

Most previous workers (Coombs et al. 1976, Spörli 1978, Howell 1980, Spörli & Ballance 1988) consider that the Mesozoic Paleopacific offshore Gondwana margin has not been a simple mid-ocean ridge ocean floor but has been interrupted by terranes of various origin. Coombs et al. (1976) show the accretion of these terranes at a fixed subduction zone. The questionable sedimentary source and the formation of such terranes lead Spörli (1978) to the interpretation that some of the terranes might be juxtaposed later by strike-slip movement. But the question

remains how far apart these terranes have been spaced and how many convergent margins and spreading ridges intervened between them. Up to five different subduction systems with varying polarity postulates Howell (1980) for the Mesozoic. Spörli & Ballance (1988) stress that different sedimentation areas indicate that the terranes have arrived at Gondwana margin by strike slip motion rather than by rifting and drifting. A concept taken up by Sutherland & Hollis (2001), who stress the appearance of large scale strike slip motions along Gondwana margin.

In contrast to these models, Korsch & Wellman (1988) show that the whole accretionary wedge is built up at one single subduction zone by the accretion of once continuous sedimentation areas. Mortimer (1995) takes up this interpretation noting that the sedimentation areas change continuously along the axis of the subduction zone. The discussion shows that the regional geology of New Zealand and especially of the South Island results not from a simple case of a single subduction-arc complex that has been preserved along a continental margin (Mortimer et al. *subm.*).

In this paper the results of my thesis work are presented in relation to the geologic framework of the South Island, New Zealand. Of necessity, such model must remain speculative and fairly generalised and may prove inadequate in detail.

## **6.2. Short introduction into all rock types of the South Island**

This more detailed introduction has not been given in *chapter 1* because it was not necessary for the main themes of this thesis but it is relevant here to understand the tectonic evolution of South Island and the herewith presented reconstruction.

### *6.2.1. Western Province*

Rocks of the Western Province (fig. 6.1, 6.2), which comprise the oldest part of the South Island, are related to the margin of Gondwana (Mortimer 1995, Mortimer et al. 1999b). Early Paleozoic metasedimentary and metavolcanic rocks of the Takaka Group are amalgamated with Ordovician metasediments of the Buller Group during the Early Devonian Tuhua orogeny prior to the intrusion of the Devonian granites of the Karamea Suite (Rattenbury et al. 1998). Volumetrically trivial amounts of igneous and sedimentary rocks are recorded during Early Mesozoic times. The Topfer Formation comprises Triassic, volcanic and volcanoclastic sequences, which are a proof for a passive margin of Gondwana during Mesozoic times (Mortimer 1995). During Jurassic, tholeiitic sills (the Kirwan Dolerite) intrude into the Topfer Formation (Mortimer 1995).

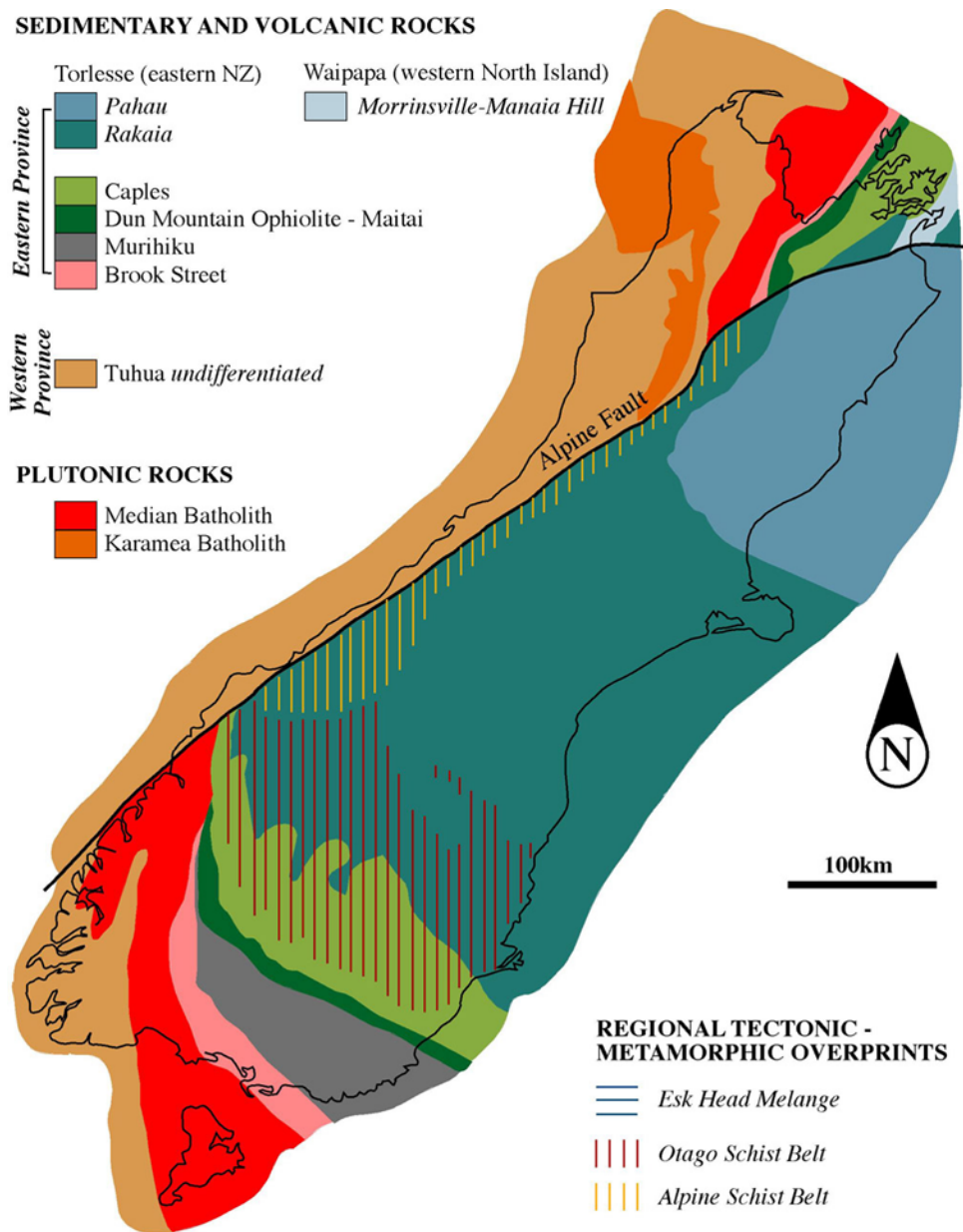


Fig. 6.1: Tectonostratigraphy of the South Island, New Zealand (based on Turnbull 2000, Figure 3)

### 6.2.2. Median Batholith

The Median Batholith (fig. 6.1, 6.2) forms in a long-lived and evolving subduction zone along the Carboniferous to Cretaceous margin of Gondwana, where dominantly calc-alkaline magmatism changes with time to dominantly adakitic (Tulloch & Rabone 1993, Kimbrough et al. 1994, Muir et al. 1998, Wandres et al. 1998, Waight et al. 1999, Mortimer et al. 1999b). The age and average composition of rocks changes across the batholith axis: Permian gabbroids dominate the NE edge, Triassic-Early Cretaceous diorites the central part and late Early Cretaceous granitoids the SW margin of the batholith (Mortimer et al. 1999b). Plutonism is not con-

tinuous during the whole time span; a larger gap of magmatism is recorded from 195-157Ma (Mortimer 1995). The contacts to the adjacent rocks, the Western Province and the Brook Street Group, are intrusive (Mortimer et al. 1999a). Both rock types form enclaves within the Median Batholith plutons in the west and east of the batholith respectively. Associated Triassic to Cretaceous volcanism and sedimentation is represented by Mesozoic volcanogenic units, which are commonly intruded by younger plutons of the batholith.

### *6.2.3. Eastern Province*

#### *6.2.3.1. Brook Street Group*

The Brook Street Group comprises interbedded subaerial and submarine lavas and volcanoclastic rocks as well as plutons of Permian age (fig. 6.1, 6.2). Volcanoclastic rocks dominate and lavas are mainly of basaltic composition (Houghton & Landis 1989). The oldest plutonic body is recorded with c. 265 Ma age (Greenhills mafic-ultramafic complex) and the oldest fossiliferous strata with c. 275Ma (Kimbrough et al. 1992). The rocks are altered to prehnite-pumpellyite and pumpellyite-actinolite facies assemblage (Turnbull 2000).

The Brook Street Group is interpreted as a low latitude intra-oceanic island arc and basin complex (Coombs et al. 1976, Haston et al. 1989). The basaltic melt is possibly derived from oceanic crust of the type generated at spreading ridges (Coombs et al. 1976).

#### *6.2.3.2. Dun Mountain – Maitai Group*

The Dun Mountain-Maitai Group is a distinctive feature of South Island geology, which can be traced from SE of South Island into the northwest Otago, where it is truncated by the Alpine Fault. It reappears NW of the fault in Nelson (NW South Island), an offset by some 480km (fig. 6.1). The ultramafic nature of these rocks causes a strong positive magnetic anomaly, the so-called Stokes Anomaly (Woodward & Hatherton 1975, Hunt 1978). The group consists of two lithologic associations (Coombs et al. 1976, Bishop & Turnbull 1996): the Early Permian Dun Mountain-Livingstone Volcanics Group and the stratigraphically overlying Permian to Early Triassic Maitai Group (fig. 6.2).

The Dun Mountain-Livingstone Volcanics Group comprises several, commonly partly exhumed ophiolite sequences, which are crosscut by a dike complex (Coombs et al. 1976). The rocks are interpreted to be tectonically disrupted remnants of a 275-285Ma (Permian) ultramafic igneous complex that develop near an oceanic arc (Coombs et al. 1976, Kimbrough et al. 1992). Geochemical studies show that these rocks may be generated at a mid-ocean ridge (Coombs et al. 1976, Davis et al. 1980). The rocks have a complex metamorphic history char-

acterised by early sea-floor amphibolitisation followed by regional metamorphism to greenschist, pumpellyite-actinolite, and locally, lawsonite-albite-chlorite or prehnite-pumpellyite facies (Coombs et al. 1976, Turnbull 2000).

Greywacke and argillite of the Maitai Group overlay stratigraphically the Dun Mountain-Livingstone Volcanics Group. It consists of Middle Permian to Early Triassic volcanoderived siltstone, turbidite and conglomerate. The metamorphic grade ranges from weakly altered to zeolite facies to prehnite-pumpellyite facies up to lawsonite-albite-chlorite assemblages (Paull et al. 1996, Turnbull 2000). On the South Island the Maitai Group forms a regional syncline with steep dipping limbs.

Coombs et al. (1976) consider that these rocks derive from the erosion of the inactive Brook Street volcanic arc deposited in a forearc basin. New investigations show that the Maitai Group is better related to the Dun Mountain - Livingstone Volcanics Group (Kimbrough et al. 1992). The depositional settings range from fault-bounded basin with reworked shell banks to complex submarine fans in a large elongated basin (Landis 1980). The submarine fan deposition is accompanied by sporadic explosive volcanism (Aitchison & Landis 1990, Turnbull 2000).

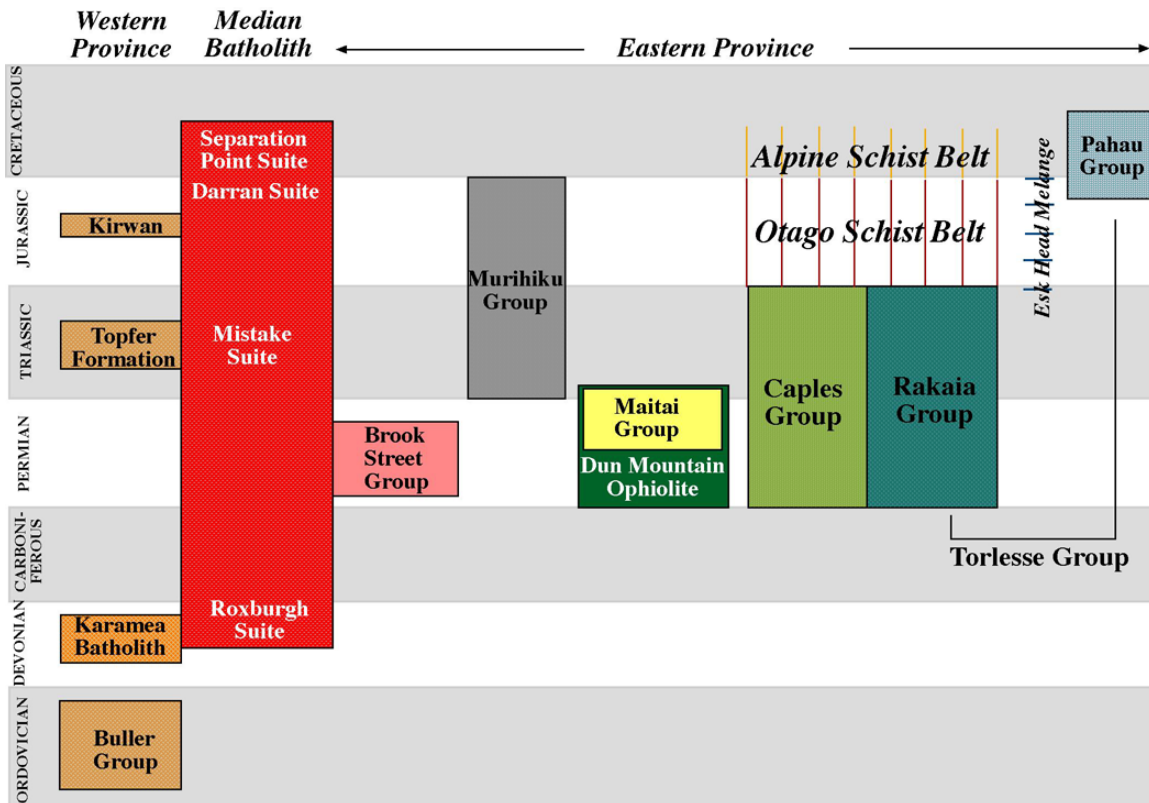


**Fig. 6.2:** Schematic summary of units comprising the Western and Eastern Province and the Median Batholith (time axis not to scale, based on Mortimer 1995, Figure 2 and Turnbull 2000, Figure 10)

### 6.2.3.3. *Murihiku Group*

The Murihiku Group (fig. 6.1, 6.2) consists of a thick sequence of essentially conformable volcanoclastic marine and non-marine Triassic to Jurassic basin fills (Campbell & Coombs 1966, Ballance & Campbell 1993). The volcanoclastic sediments with abundant ash beds but no flow rocks derive from a relative mature, active volcanic arc, the Median Batholith (Coombs et al. 1976, Mortimer 1995). The sedimentary stratigraphy reflects the changing character of the volcanic arc: a change from andesitic to acidic in Middle Triassic and back to an andesitic character in Late Triassic (Coombs et al. 1976). The volcanoclastic sediments are altered to zeolite facies assemblage (Coombs et al. 1976, Ballance & Campbell 1993).

On the South Island the Murihiku Group forms a long wavelength asymmetric fold – the Southland Syncline – with a subvertical north limb and a subhorizontal to gently dipping south limb that bears parasitic folds (Mortimer et al. *subm.*).

### 6.2.3.4. *Caples and Rakaia Group*

The Otago Schist Belt on the South Island consists of Rakaia rocks (older Torlesse) in the northern and Caples rocks in the southern part forming an approximately 150km-wide two-sided arch (fig. 6.1). Both rock types comprise Permian to Triassic greywacke and argillite (fig. 6.2), the Caples with a dominantly volcanoclastic composition (MacKinnon 1983, Roser et al. 1993) and the Rakaia with a dominantly quartzofeldspathic composition (MacKinnon 1983, Bradshaw 1989, Roser & Korsch 1999). The lithologic monotonous series of Caples and Rakaia rocks are intercalated by rare dm- to m-thick bands of greenschist and quartzite (Mortimer 1993a, b). Metamorphism increases from prehnite-pumpellyite facies in the nonschistose rocks on the flanks of the arch to greenschist facies in the schistose rocks near the centre (Mortimer 1993b). Remnants of an earlier blueschist facies metamorphic event (Yardley 1982) in the central part of the Otago Schist show peak metamorphic temperatures and pressures of 350-400°C and 8-10kbar (Mortimer 2000). The peak of Otago Schist metamorphism may occur in the Early to Middle Jurassic (Adams & Robinson 1993, Little et al. 1999). Rocks of the Alpine Belt experience the same deformation and metamorphism history as the Otago Schist. But the Alpine Schist are overprinted by a Barrovian-type metamorphism, which increases towards the Alpine Fault, during Early Cretaceous (Mortimer 2000).

The depositional setting of the Caples Group is considered to range from trench slope, to trench-slope basins, and possibly trench floor (Turnbull 1979a,b, Roser et al. 1993). The granitic provenance of the Rakaia Group is distinctive from the volcanogenic provenance of the Caples. The deepwater marine sedimentation (Retallak 1979, Campbell & Force 1972) with a

huge mass of felsic, plutonic detritus from Antarctica or Australia (Mortimer 1995) may be deposited as a submarine fan (Bradshaw et al. 1981). Although the Rakaia sediments show a more distal deposition than the Caples Group does, a continuous transition from Caples to Rakaia sedimentation area is considered. Vitaliano (1968) proves a continuous sedimentation area of both for the Marlborough schist (north South Island). Mayer (1969) and Skinner (1972) show that sequences of the Waipapa Group (North Island) have affinities of Caples and Rakaia.

### 6.3. Tectonic evolution

Commonly reconstruction of the regional geology of the South Island starts in Permian times (Coombs et al. 1976, Spörli 1978, Howell 1980, Bradshaw et al. 1981, Korsch & Wellman 1988), a time span, in which the deposition of most Eastern Province rocks begins. Consequently Coombs et al. (1976) and Korsch & Wellman (1988) consider that subduction of the Pacific Plate under the Indian Plate has commenced in the Early Permian. However, new investigations into the formation of the Median Batholith reveal that in situ plutonism exists since Carboniferous (Mortimer et al. 1999b). As plutons commonly intrude into a volcanic arc setting, a continuous subduction zone may exist on Gondwana Pacific margin since Carboniferous (Mortimer et al. 1999b). Most previous workers (Coombs et al. 1976, Carter et al. 1978, Spörli 1978, Howell 1980, Bradshaw et al. 1981, Korsch & Wellman 1988, Mortimer 1995) assume a westward dipping subduction zone – an interpretation taken up in this study.

#### 6.3.1. Early Permian (290-260 Ma)

Coombs et al. (1976) and Wood (1978) consider the Dun Mountain-Livingstone Volcanics Group as remnants of a mid-ocean ridge, the Maitai as a forearc basin and the Caples as well as the Rakaia Group as terranes of various origin distributed on the Carboniferous – Permian seafloor off Gondwana. Taken into account a continuous sedimentation area of the Caples and Rakaia Group (Vitaliano 1968, Mayer 1969, Skinner 1972), the volcanoclastic provenance of the Caples Group leads to the interpretation that this one is deposited in a trench-related setting (Turnbull 1979a,b, Korsch & Wellman 1988, Roser et al. 1993). However, the strong relationship between the Dun Mountain and Maitai Group (Kimbrough et al. 1992) and the large sedimentary volume of the Caples Group may lead to another conclusion. A flat mid-ocean ridge, the later obducted Dun Mountain -Livingstone Volcanics Group (fig. 6.3a) is considered near to felsic sedimentary source, maybe to the SE (Antarctica, Mortimer 1995, Roser & Korsch 1999, fig. 6.4a). At a proximal position, high felsic sedimentary detritus intercalated with deep-



water marine deposits thickens the sedimentary pile building up the Rakaia Group (fig. 6.4a). Towards the W, at a more distal position, the felsic detritus is intercalated with volcanogenic sediments derived from the mid-ocean ridge building up the Caples Group on the eastern flank of the flat ridge, and the Maitai Group on the western flank (fig. 6.4a). Furthermore, felsic sedimentary detritus from the nearby Gondwana margin maybe also feeds the Maitai Group (fig. 6.4a). The lack of Early Permian Maitai sediments may be interpreted that the older sediments are consumed at the subduction zone, whereas the Late Permian to Early Triassic sediments are coupled with the downgoing ridge and therewith accreted as a whole to Gondwana margin. A long-discussed problem is the formation of basaltic layers, which occur as greenschist bands abundantly in the Permian sediments of the Rakaia Group, less intense in the Caples Group. The oceanic significance of the basaltic layers (MOR; Grapes & Palmer 1984) and their appearance as pillow lavas (Coombs et al. 1976) lead to the interpretation that these layers are offscraped of the upper oceanic crust during accretion (Coombs et al. 1976, Spörli 1978, Korsch & Wellman 1988). Coombs et al. (1976) consider them to be formed as intrasedimentary flows. The lack of feeder dikes to generate these flows leads to a preference of the first interpretation by previous workers over the last decades. However, the basaltic layers mainly occur in Permian rocks and their oceanic significance can be related to the Permian mid-ocean ridge (Dun Mountain Group). Sporadic volcanism is recorded within volcanoclastic sediments of the Maitai and Caples Group, why should there not be generated pillow lavas? I suggest that the Permian mid-ocean ridge provides the feeder of sporadic basaltic flows, maybe flood basalt, which are interrupted by thick submarine fans. The high sedimentary detritus intercalated by basaltic flows on the eastern flank of the Permian ridge system thickens the sedimentary pile in the extent of an oceanic plateau (fig. 6.3a).

Geochronological studies reveal that the formation of the Dun Mountain – Livingstone Volcanics Group is just before the onset of volcanism and sedimentation within the Brook Street Group (Kimbrough et al. 1992). Consequently I consider that the spreading of the Permian ridge ceases during the Early Permian while approaching the subduction zone but that volcanism occurs sporadically throughout the whole Permian (Maitai, Caples and Rakaia Groups). The cessation of spreading activity but the constant high heat flow causes an intensified volcanism and plutonism on the margin (Müller et al. 2001). Consequently the approach of the Permian mid-ocean ridge at the subduction zone results in the extensive formation of the Brook Street Group as an island arc and basin complex.

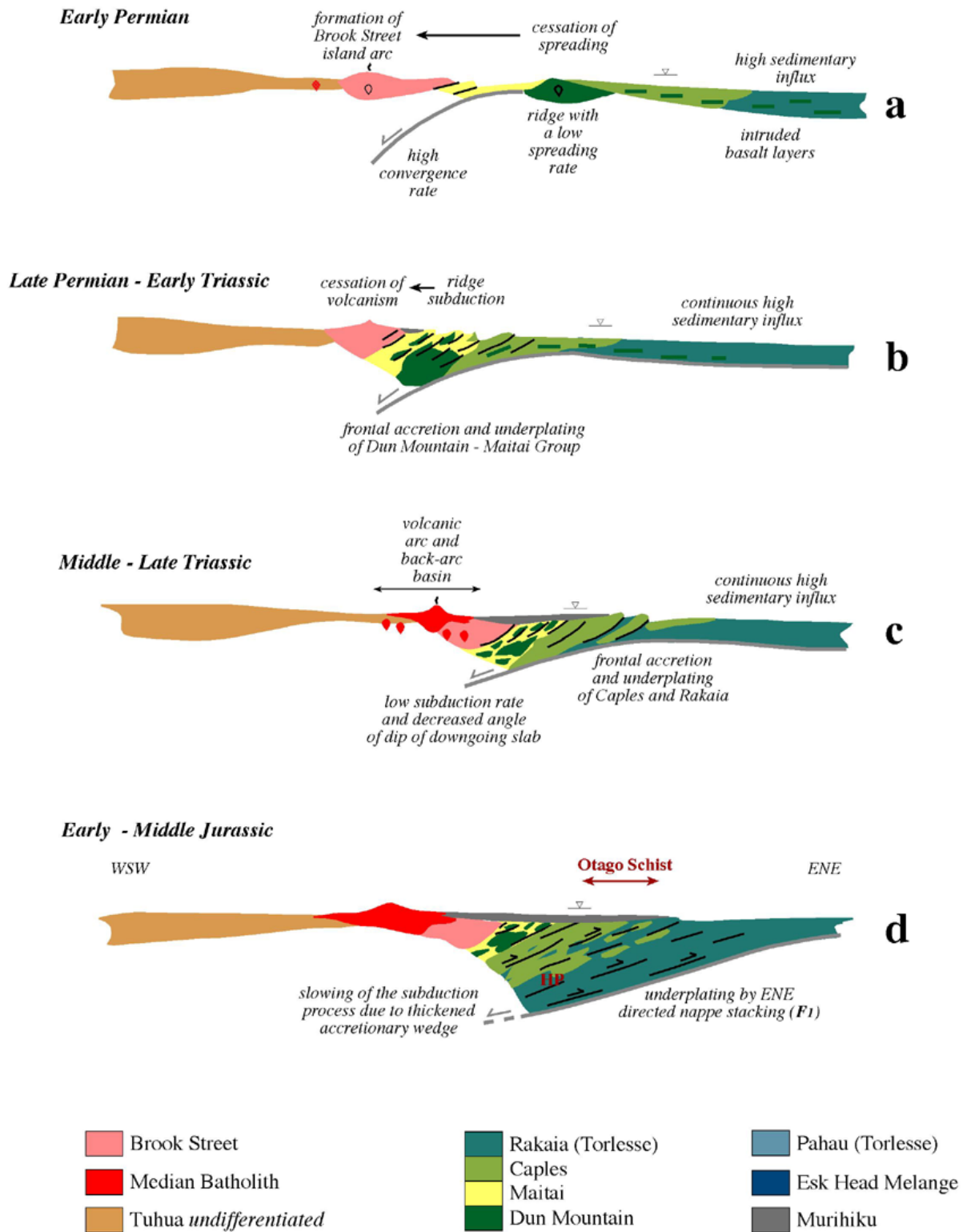


**Fig. 6.3a-d:** Cross-sectional sketches of the tectonic evolution of the South Island from the Early Permian to the mid-Jurassic (not to scale, see text for further information)

### 6.3.2. Late Permian to Early Triassic (260-240 Ma)

Investigation into the Brook Street Group reveal that the volcanism ceases during the Late Permian (Coombs et al. 1976, Mortimer et al. 1999b). The cessation may arise from the accretion of the Permian mid-ocean ridge as an ophiolitic melange – the Dun Mountain – Livingstone Volcanics Group – and its sedimentary overlay – the Maitai Group - at Gondwana margin (fig. 6.3b). Caples sediments deposited directly on the eastern flanks of the subducted Permian ridge are accreted with parts of originally oceanic crust in thrust slices (Croiselles, Patuki Melange, Coombs et al. 1976, Korsch & Wellman 1988).

Further accretion of the Caples and Rakaia sediments infer a continuous subduction process. A very low spreading rate of the ridge and a high convergence rate at the subduction zone result in a continuous but reduced subduction rate after ridge collision (Bradshaw 1989). The slowed subduction process and the approaching thick sedimentary pile decrease the angle of dip of the downgoing slab. The ridge collision changes the curvature of the active subduction zone in a NNW trend (fig. 6.4b).

Upper levels of the accretionary system are characterised by offscraping and frontal accretion (Davis et al. 1983, Kimura & Ludden 1995), whereas lower levels reflect the processes of underplating. Underplating is considered not to occur by duplex accretion involving footwall collapse and propagation of the basal detachment into the subducted sediment of the downgoing slab (Platt et al. 1985, Sample & Fisher 1986, Platt 1986, Sample & Moore 1987). It rather takes place by imbricate stacking of thrust nappes (Needham & MacKenzie 1988, Fisher & Byrne 1987, 1992, Miller & Gray 1996). The sediments of the Caples and Rakaia Group are underplated by ENE directed nappe stacking at the eastern side of the NNW trending active margin of Gondwana (*chapter 4*; fig. 6.3c, 6.4b).

### 6.3.3. Middle to Late Triassic (240-205 Ma)

Although some Carboniferous to Permian plutons are related to the Median Batholith, in the mid-Triassic extensive calc-alkaline plutons start to intrude into the Brook Street Group as well as into rocks of the Western Province (Mortimer et al. 1999b). Consequently the in situ plutonism shows that the Median Batholith develops between the Eastern and Western Province within a back-arc basin (Mortimer et al. 1999b; fig. 6.3c). But not only plutonic rocks are recorded within the Median Batholith, as well volcanic rocks and volcanoclastic sediments occur (Bradshaw 1993, Mortimer et al. 1999b) displaying that the Median Batholith sequences comprise the volcanic arc and the back-arc basin from at least Middle Triassic onwards. On the eastern side of the Median Batholith a forearc basin forms, where volcanogenic sediments

derived from the active volcanic arc are deposited as basin fill, the Murihiku Group (fig. 6.3c, 6.4b).

#### 6.3.4. Early to Middle Jurassic (205-150Ma)

Shortening at lower levels of the thickened accretionary wedge results in further ENE directed thrust movement under moderate high pressure metamorphism (Yardley 1982, Mortimer 2000) - the first deformation phase ( $F_1$ ) of the Otago Schist (*see chapter 3*; fig. 6.3d, 6.4b). The thickening of the accretionary wedge results in a decreased angle of dip of the downgoing slab slowing the subduction process while the convergence rate remains high. The interpretation of a flat subduction is strengthened by the simultaneous gap of magmatism within the Median Batholith (195-157Ma, Mortimer 1995). Similarly the Murihiku sequences reflect the cessation of volcanism in the S in the Early Jurassic, whereas towards the N the volcanism feeds continuously the Murihiku basin until latest Jurassic (Ballance et al. 1981).

This time span is inferred as the onset of the Rangitata orogeny (Suggate 1978). In opposite to the introduced model, which is partly based on Korsch & Wellman (1988) and Mortimer et al. (1999b), some workers consider a collisional stage between Gondwana margin and the Eastern Province rocks (Coombs et al. 1976, Wood 1978, Spörli & Balance 1988).

#### 6.3.5. Late Jurassic (150-135Ma)

Continuous convergence results in further shortening – the second deformation phase of the Otago Schist ( $F_2$ ). Rocks of the Caples and Rakaia Group are folded into NE or foreland verging  $F_2$  regional folds with a wavelength at km-scale (*chapter 2*; fig. 6.3e). The  $F_2$  regional folds are amplified at the lower levels of the accretionary wedge under dry retrograde conditions (*chapter 2*).  $F_2$  regional folds occur with abundant parasitic folds of different scales mainly on the major short limb. Almost subvertical shortening results in disrupted long limbs of parasitic folds by boudinage. An extensive zone of boudinage can occur at the transition from a major short limb to a lower long limb of  $F_2$  regional folds (*chapter 2*).

The age of the folding and therewith implied exhumation of the present Otago Schist is hardly to determine with geochronological investigations. Interpretations of a continuous slow cooling of the Otago Schist (Adams et al. 1985, Graham & Mortimer 1992) are rejected in favour of several cooling stages. Results of geochronological studies (Kamp 1987, Kamp et al. 1989, Graham & Mortimer 1992, Adams & Robinson 1993) can be interpreted that the Otago Schist experiences  $F_2$  shortening and exhumation within the time span of the Late Jurassic. The total amount of exhumation is less in the Rakaia sequence N of the Otago Belt than within the

Otago Belt (Kamp et al. 1989), which can be regarded to the amplified  $F_2$  regional folds in the central part of the Otago Belt.

The southwestern part of the accretionary wedge, the Murihiku forearc basin overlying the Dun Mountain–Maitai Group and the Brook Street Group, are folded into upright to hinterland verging regional folds with a wavelength and amplitude at km-scale (fig. 6.3e). Consequently the tectonic contacts within the Eastern Province are steepened. The intensified shortening of the Eastern Province rocks in the southern part of South Island results in a bending of the accretionary wedge axis, which is outlined by the Dun Mountain-Maitai Group and the associated Stokes Magnetic Anomaly. The southern part of the accretionary wedge axis is bent to a SW course – the  $F_2$  orogenic trend (fig. 6.4c, *see chapter 5*).

The shortening of the accretionary wedge causes an increased angle of dip of the downgoing slab. The resulting acceleration of the subduction process is reflected by the occurrence of the Esk Head Melange (fig. 6.3e), which is mainly derived from reworking of the Rakaia sediments (older Torlesse). The same high sedimentary detritus of felsic provenance that built up the Rakaia Group/older Torlesse is now deposited on the downgoing slab called Pahau Group/younger Torlesse (fig. 6.3e). The building of the NW-SE trending Pahau accretionary prism is driven by oblique subduction of the Phoenix plate, which is generated by spreading at the Pacific/Phoenix ridge situated a small distance to the NE (Bradshaw 1989; (fig. 6.4c). The subduction of relatively young oceanic crust causes adakitic magmatism in the Median Batholith (Tulloch & Rabone 1993, Mortimer et al. 1999b).

#### 6.3.6. *Early Cretaceous (135-105Ma)*

The approach and collision of the spreading ridge between Phoenix and Pacific plates at Gondwana margin is marked by the cessation of both spreading and subduction (Bradshaw 1989, Luyendyk 1995) – the so-called Rangitata II orogeny (Bradshaw 1989). The ridge collision causes not only shortening of the Pahau accretionary system with foreland verging folds and thrusts (fig. 6.3f) but also of the Permian to Jurassic Eastern Province rocks (Bradshaw 1989). NW or hinterland verging  $F_3$  regional folds with wavelength at km-scale shorten the hinterland or the retrowedge of the collisional zone (fig. 6.3f). The  $F_3$  regional folds are amplified at the lower levels of the former accretionary system under Barrovian-type metamorphism (*chapter 2 and 5*) – the setting of the Alpine Schist.  $F_3$  regional folds resemble the fold style of  $F_2$  regional folds with abundant parasitic folds at the short major limb and stretched long major limbs. The amount of uplift, maybe 5-6km in the Alpine Belt, reduces towards the E (Kamp et al. 1989) as the amplitude of  $F_3$  regional folds decreases continuously throughout the Otago

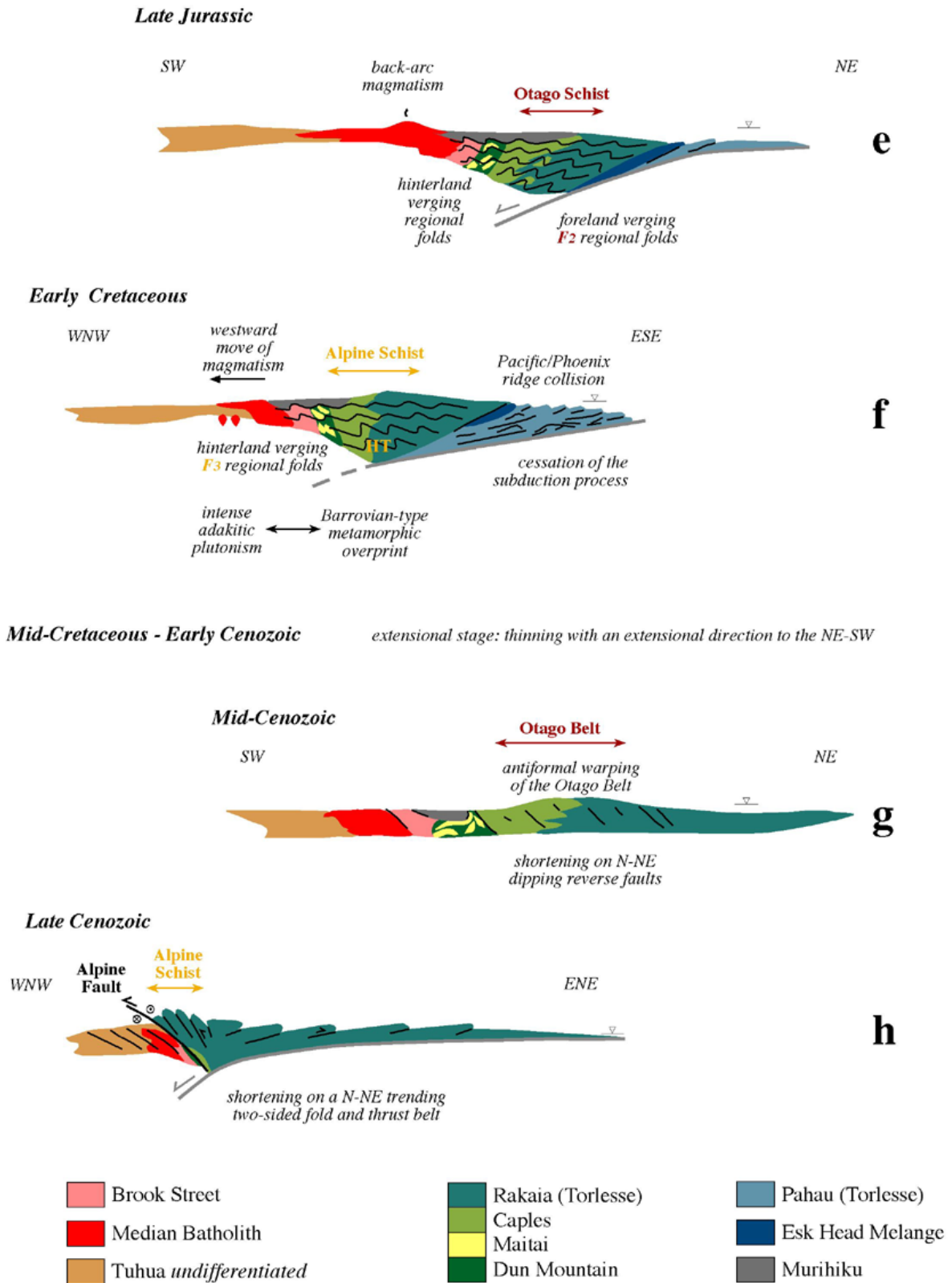


Fig. 6.3e-h: Cross-sectional sketches of the tectonic evolution of the South Island from the Late Jurassic to the Late Cenozoic (not to scale, see text for further information)

Belt to the E. In the eastern Otago Belt the  $F_3$  regional folds occur only locally, where they intersect with regional folds of the second generation ( $F_2$ ). The metamorphic overprint results from the cessation of the subduction process and the high heat flow of the subducted oceanic ridge, which as well leads to the intense adakitic plutonism in the Median Batholith. The shortening of the Eastern Province rocks and coupled parts of the Median Batholith causes a westward migration of the main axis of Mesozoic magmatism (Mortimer et al. 1999b).

Bradshaw (1989) considers that a further subduction zone to the W closes the back-arc region, which is presently comprised by the Median Batholith (Mortimer et al. 1999b), and therewith amalgamates the Eastern and Western Province. But close affinities between New Zealand and Gondwana Mesozoic floras (Retallak 1985) and the continuous intrusion of Median Batholith plutons in rocks of the Eastern and Western Province (Mortimer et al. 1999b) show that Gondwana and New Zealand have always been close. The collisional stage results in shortening even of the Median Batholith and the Western Province.

The overall  $F_3$  shortening bends the northwestern part of the whole accretionary system (the Permian to Early Jurassic as well as the Late Jurassic to Early Cretaceous accretionary prisms) to a northeastern course – the  $F_3$  orogenic trend (fig. 6.4d). The Late Jurassic to Early Cretaceous folding of both generations ( $F_2/F_3$ ) causes a recurved or Z-bent arc structure, which is most clearly expressed by the outcrop pattern and the associated geophysical signature of the Permian Dun Mountain – Maitai Group (fig. 6.4d). The result strengthens the hypothesis of Mesozoic oroclinal bending by previous workers (Grindley 1963, Cooper 1974, Wood 1978, Kamp 1987, Bradshaw 1989). Kamp (1987) and Bradshaw (1989) show a more N-NW trending central part and therewith a less curved arc than this reconstruction, which is based on the Mesozoic fold structure.

### 6.3.7. *Mid-Cretaceous - Mid-Cenozoic (105-23Ma)*

The short period of collision succeeds in a sudden change in the tectonic regime from subduction to extension in Mid-Cretaceous time (105+5 Ma; Bradshaw 1989) – a time span that is not previously dealt with in this thesis. The former active Pahau accretionary system is converted into a passively subsiding dormant margin (Bradshaw 1989). Maybe the active rift system, the former Pacific/Phoenix ridge, migrates westward to form a graben system within the Gondwana plate (Bradshaw, Müller et al. 2001). The renewed rifting within the Gondwana plate causes the opening of the Tasman Sea and therewith the separation of New Zealand from Gondwana (Howell 1980, Bradshaw 1989, Müller et al. 2001). The rifting stage arise only sparse plutonism within the Median Batholith (Waight et al. 1999, Mortimer et al. 1999b),

maybe a sign that the Median Batholith and the Pacific margin of Gondwana, the Western Province, are too thick to be intensively intruded by the migrating rift system.

The extension, which may be oriented NE-SW as indicated by the Cretaceous extension lineations in rocks of the Western Province (Bradshaw et al. 1996 and references therein), causes normal faulting and extensional basin formation (Spörli 1978, Korsch & Wellman 1988, Bradshaw 1989). Maybe low-angle faults (Bradshaw 1989) are formed at lower levels of the accretionary pile.

The seismic profile oriented N-S across the Otago Schist Belt by Mortimer et al. (subm.) reveals that the whole thickened accretionary pile is thinned maybe during Late Cretaceous crustal stretching and extension resulting in an abnormal thinned crust. High velocity zones, which have been previously interpreted as remnants of an oceanic crust subducted beneath the Rakaia accretionary prism (Smith et al. 1995) are now related to igneous intrusions and/or amphibolite-granulite facies recrystallisation due to the New Zealand -wide Late Cretaceous extensional stage (Mortimer et al. subm.).

The latest Cretaceous – early Eocene is probably a time of tectonic quiescence because there is no basis for a plate boundary through New Zealand at this time (Kamp 1986b, Spörli & Balance 1988). A transgressive sequence, which generally progresses from coastal paralic coal measures at the base into shallow-marine sediments, reflects a subsidence phase (Spörli & Balance 1988). Kamp (1986b) considers that in the Eocene – Oligocene the spreading of the Tasman ridge ceases and successively the Southeast Indian ridge, whose remnants occur S of the Puysegur trench, propagates as an active intercontinental rift zone through the western South Island. The ceased spreading of the Southeast Indian ridge causes the propagation of the Indian – Pacific plate boundary as a dextral transform fault through New Zealand – the inception of the Alpine Fault (Kamp 1986b, 1987). Norris et al. (1978) infer instead that it is a transtensional zone of pull-apart basins along the precursor Indian – Pacific oblique-slip plate boundary.



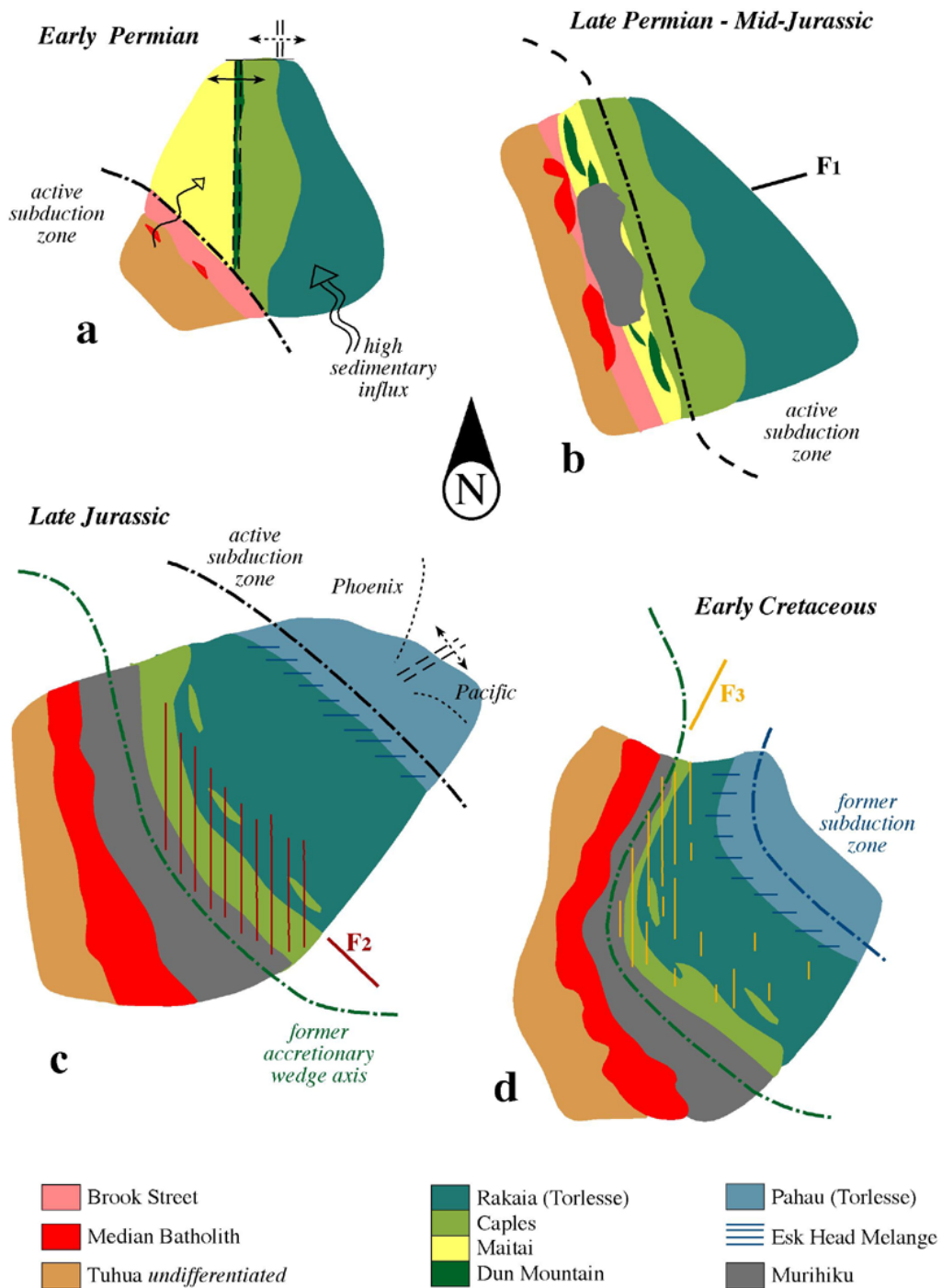


**Fig. 6.4:** Sketches of the tectonic evolution of the South Island from the Early Permian to the Late Cenozoic in map-view (see text for further information)

6.3.8. Since Mid-Cenozoic (23Ma)

Kamp (1986b, 1987) suggests earliest Miocene age for the start of the dextral movement on the Alpine Fault on the basis of biostratigraphic ages, which reflect a major change in sedimentation patterns in the former rift basins now adjacent to the Alpine Fault. The age is strengthened

by further geological observations by Carter & Norris (1976) and Cooper et al. (1987) in accord with plate tectonic predictions by Molnar et al. (1975) and Stock & Molnar (1987). Thus the Alpine Fault is initiated as a transcurrent boundary in the middle to late Oligocene (~ 30-23Ma) and continued through to the late Miocene (~ 10 Ma; Walcott 1979, Holm et al. 1989). A NE-SW oriented plate motion direction in the early Miocene (Stock & Molnar 1987) leads to shortening on N-NE dipping faults (fig. 6.3g), maybe re-activated Cretaceous extensional faults. The shortening causes the warping of the Otago Schist and the tightening of the Mesozoic regional folds in the adjacent Eastern Province rocks in the Miocene –especially in the Murihiku Group and Dun Mountain – Maitai Group (fig. 6.3g).

In the Pliocene the previously transform plate boundary changes to a broad zone of oblique continental collision (Wellman 1979, Cooper 1980, Holm et al. 1989, Grapes & Watanabe 1992, Walcott 1998) - the Kaikoura orogeny (Suggate 1978). The increase in the component of strike-slip movement on the Alpine Fault results in a greater component of pure-shear-dominated contraction in the diffuse zone of deformation (Teyssier et al. 1995). A two-sided N-NE trending fold and thrust belt is developed (fig. 6.3h), which possibly re-activates as well Cretaceous extensional faults or propagates on “easy-slip horizons” generated during Mesozoic folding (*chapter 5*). In the Otago Schist Belt the fold and thrust belt verges to the E, whereas in the Alpine Schist it verges to the W building up a large scale flower structure (fig. 6.3h). The initial flat-lying fold and thrust belt in the Alpine Belt is tilted to a steeper easterly dip by further reverse movement on continuously steepening faults (*chapter 5*). The pure-shear dominated uplift (Teyssier et al. 1995) is attended by continuous erosion resulting in an asymmetric flower structure (Casas et al. 2001). The steepening of the western wing of the fold and thrust belt is accompanied by the formation of backthrusts off the Alpine Fault to the E (Koons 1990, 1994, Cox & Findlay 1995). Reverse and dextral movement rotates the Alpine Fault to a more easterly trend than the N-NE trending fold and thrust belt (compare fig. 6.1 to 6.4d). Furthermore it causes the overthrusting of the Alpine Schist onto and the dextral offset of the Median Batholith and adjacent Eastern Province rocks – the Brook Street Group, the Dun Mountain–Maitai Group, the Caples Group and the Murihiku Group – in the central part of the South Island (fig. 6.3h, 6.1). The dextral strike-slip movement is partitioned on major N-NE trending steepened reverse faults east of the Alpine Fault (fig. 6.3h). An increased dextral strike-slip movement on these faults towards the Alpine Fault (Turnbull 2000) results in the strengthening of the Mesozoic bending of the Alpine and Otago Belt as well as adjacent units of the Eastern Province in the vicinity of the Alpine Fault (*chapter 5*).

## Appendix

### A.1. Mathematica subprogram written by Moore & Johnson (2000)

In this study the Mathematica subprogram written by Moore & Johnson (2000) is used to reconstruct the observed behaviour of folds and lineations during superposition of further fold generations. It is not taken the original FoldPlot program but the Mathematica built-in function ParametricPlot with its default settings because these surface plots with their gridlines better visualise the reconstructed deformations (fig. A.1).

```

axial[t_]:=Sin[-Pi t];
axial::"usage"=
" axial[t] generates the deformations used
  in axiZY, axiXZ etc.
  The default deformation function is sinusoidal:
  axial[t_] := Sin[-Pi t] .
  This should be overridden, when desired.";

axiZY::"usage"=axiZX::"usage"=axiYX::"usage"
=axiYZ::"usage"=axiXY::"usage"=axiXZ::"usage"=
"axiZY[ ][{x,y,z}] produces a deformation in
  the z-direction, which varies along the y-direction
  according to the function axial[y], to give {x,y,z+axial[y]}.
  axiZY[u][{x,y,z}] magnifies the deformation to give {x,y, z+u*axial[y]}.\n
  axiZY[u, v][{x,y,z}] rescales to give {x,y, z+u*axial[v*y]}.\n
  Variants axiZX , axiYX , axiYZ , axiXY , axiXZ deform along other axis
  directions.";

shrZY::"usage"= shrZX::"usage"=shrYX::"usage"=shrYZ::"usage"=
shrXY::"usage"=shrXZ::"usage"=
"shrZY[ ][{x,y,z}] produces a shear deformation in the Z-direction,
  which varies along the y-direction to give {x,y,z+y}.\n
  shrZY[u][{x,y,z}] rescales the shear to give {x,y, z+u*y} .\n
  Variants shrZX , shrYX , shrYZ , shrXY , shrXZ shear along other axis
  directions.";

rot::"usage"=
"rot[a,b,c][{x,y,z}] rotates the vector {x,y,z} by Euler-angles a, b, c
  measured in Degrees.";

axiZY[u_:1,v_:1]:=#1+{0,0,u axial[#1[[2]] v]}&;
axiZX[u_:1,v_:1]:=#1+{0,0,u axial[#1[[1]] v]}&;
axiYX[u_:1,v_:1]:=#1+{0,u axial[#1[[1]] v],0}&;
axiYZ[u_:1,v_:1]:=#1+{0,u axial[#1[[3]] v],0}&;
axiXY[u_:1,v_:1]:=#1+{u axial[#1[[2]] v],0,0}&;
axiXZ[u_:1,v_:1]:=#1+{u axial[#1[[3]] v],0,0}&;

<<Geometry`Rotations`

rot[a_:0,b_:0,c_:0]:=#1.N[RotationMatrix3D[a Degree,b Degree,c Degree]]&

shrZY[u_:1,v_:1]:=#1+{0,0,u #1[[2]]}&;
shrZX[u_:1,v_:1]:=#1+{0,0,u #1[[1]]}&;
shrYX[u_:1,v_:1]:=#1+{0,u #1[[1]],0}&;
shrYZ[u_:1,v_:1]:=#1+{0,u #1[[3]],0}&;
shrXY[u_:1,v_:1]:=#1+{u #1[[2]],0,0}&;
shrXZ[u_:1,v_:1]:=#1+{u #1[[3]],0,0}&;

```

**Fig. A.1:** Excerpt from the Mathematica subprogram FoldPlot written by Moore & Johnson (2000).

*This modified subprogram is adopted to reconstruct folds and lineations within this study.*

*For more information see Moore & Johnson (2000)*

The three dimensional parametric plot (ParametricPlot3D) is defined by one axis (axiZX, axiZY, axiYX, axiYZ, axiXY, axiXZ) and a finite plane (xy-plane, xz-plane, yz-plane; fig. A.2). Wavelength and amplitude of the fold can be determined (fig. A.2). Investigations are restricted to initial cylindrical folds (fig. A.3). Movement of points of one chosen plane (xy-, yz-, xz-plane) of the coordinate system x, y, z generates two cylindrical folds (fig. A.3a-c). Reconstructions are mostly done with cylindrical folds formed within the xy-plane along the ZX and ZY axis (fig.A.3a) because the observed folds in the Otago Belt plunge almost subhorizontally to gently. A problem of this subprogram is that the rotation of a chosen axis and plane is sometimes restricted. To generate folds in the ZX direction on the xy-plane every plunge can be chosen with the help of the Euler angle b of the function rot [a,b,c] (fig. A.2). Also the direction of the fold axis in the xy-plane can be determined with the Euler angle a of the function rot [a,b,c] (fig. A.2). Folds generated in the xy-plane parallel to the ZY axis can only be rotated within the xy-plane. Where it is necessary to generate the superposition of folds with arbitrary plunges, the third case of possible cylindrical folds is chosen (fig. A.2c).

The effect of shear imposed upon the ZX and ZY folds generated in the xy-plane is depicted in fig. A.4 and A.5. Commonly a shear perpendicular to the fold axis is chosen to reconstruct asymmetric or vergent folds (fig. A.4c, A.5c). The movement direction of the fold and shear direction lies within one plane, the xz- or the yz-plane.

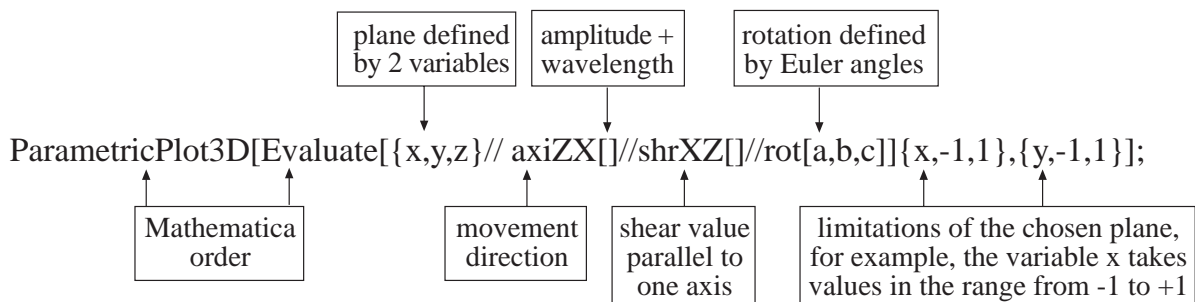
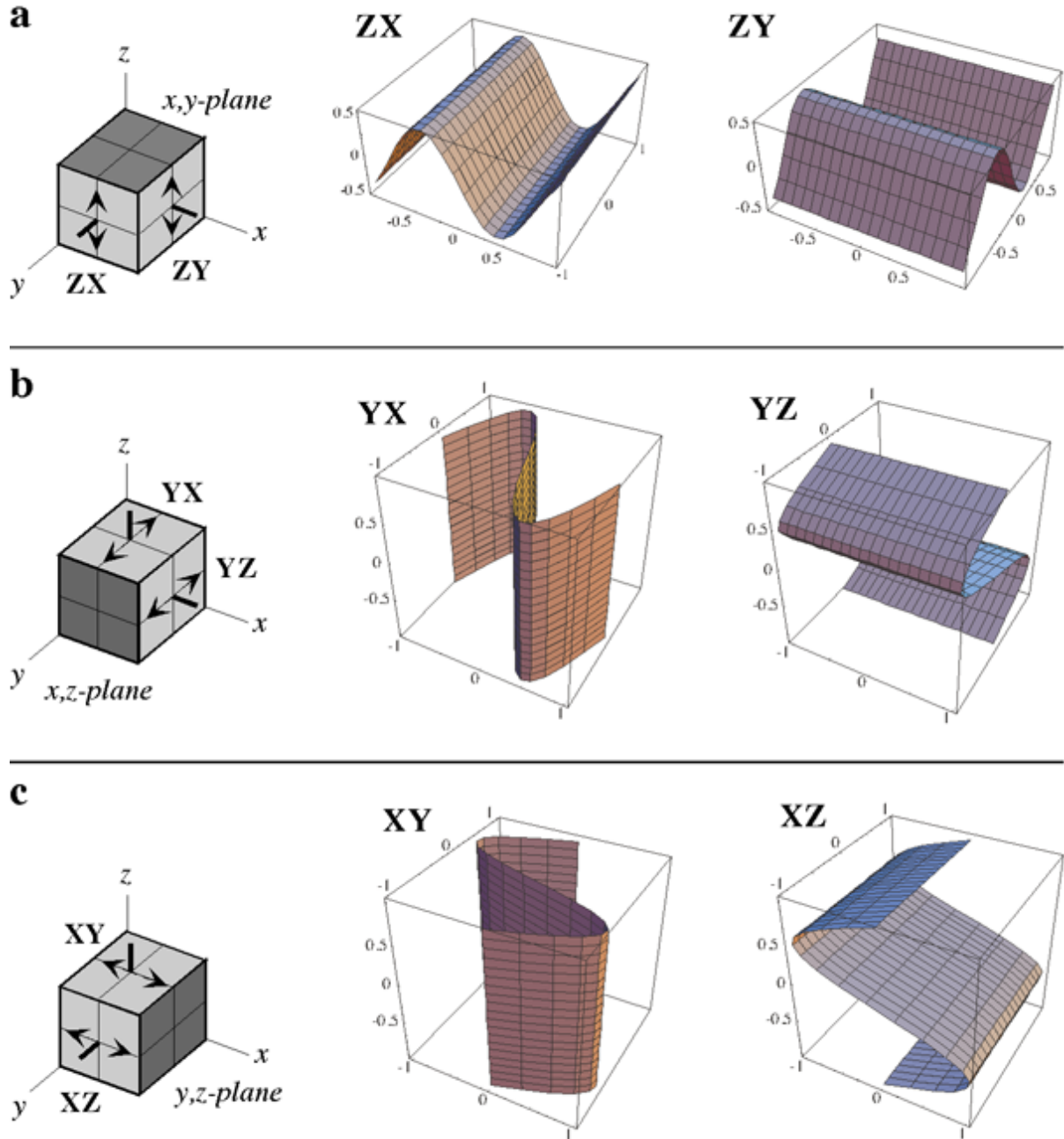


Fig. A.2: Explanation to the calculations of folds with the Mathematica subprogram.



**Fig. A.3 :** Three possibilities to reconstruct cylindrical folds: the box shows the chosen plane and the movement direction of the axis. The term ZX, for example, means that the axis lies within the xz-plane with the movement direction aligned subparallel to the z-axis. **a)** The ZX and ZY axes fold subhorizontally the xy-plane.

$(\text{axial}[t\_]:= \text{Sin}[-2 t]; \text{ParametricPlot3D}[\text{Evaluate}[\{x,y,0\}/\text{axiZX}[.5,2]],\{x,-1,1\},\{y,-1,1\}];$   
 $\text{ParametricPlot3D}[\text{Evaluate}[\{x,y,0\}/\text{axiZY}[.5,2]],\{x,-1,1\},\{y,-1,1\}];)$

**b)** The YX axis folds vertically the xz-plane, whereas the YZ axis arises subhorizontal folds  
 $(\text{axial}[t\_]:= \text{Sin}[-\text{Pi} t]; \text{ParametricPlot3D}[\text{Evaluate}[\{x,0,z\}/\text{axiYX}[1]],\{x,-1,1\},\{z,-1,1\}];$   
 $\text{ParametricPlot3D}[\text{Evaluate}[\{x,0,z\}/\text{axiYZ}[1]],\{x,-1,1\},\{z,-1,1\}];)$

**c)** The XY axis folds vertically the xz-plane, whereas the XZ axis arises subhorizontal folds  
 $(\text{axial}[t\_]:= \text{Sin}[-\text{Pi} t]; \text{ParametricPlot3D}[\text{Evaluate}[\{0,y,z\}/\text{axiXY}[1,1]],\{y,-1,1\},\{z,-1,1\}];$   
 $\text{ParametricPlot3D}[\text{Evaluate}[\{0,y,z\}/\text{axiXZ}[1,1]],\{y,-1,1\},\{z,-1,1\}];)$

Note that ZX, YX, XY and XZ folds can be rotated in every direction, whereas ZY and YZ folds can only be rotated in the xy-plane. No plunge of these folds is possible.

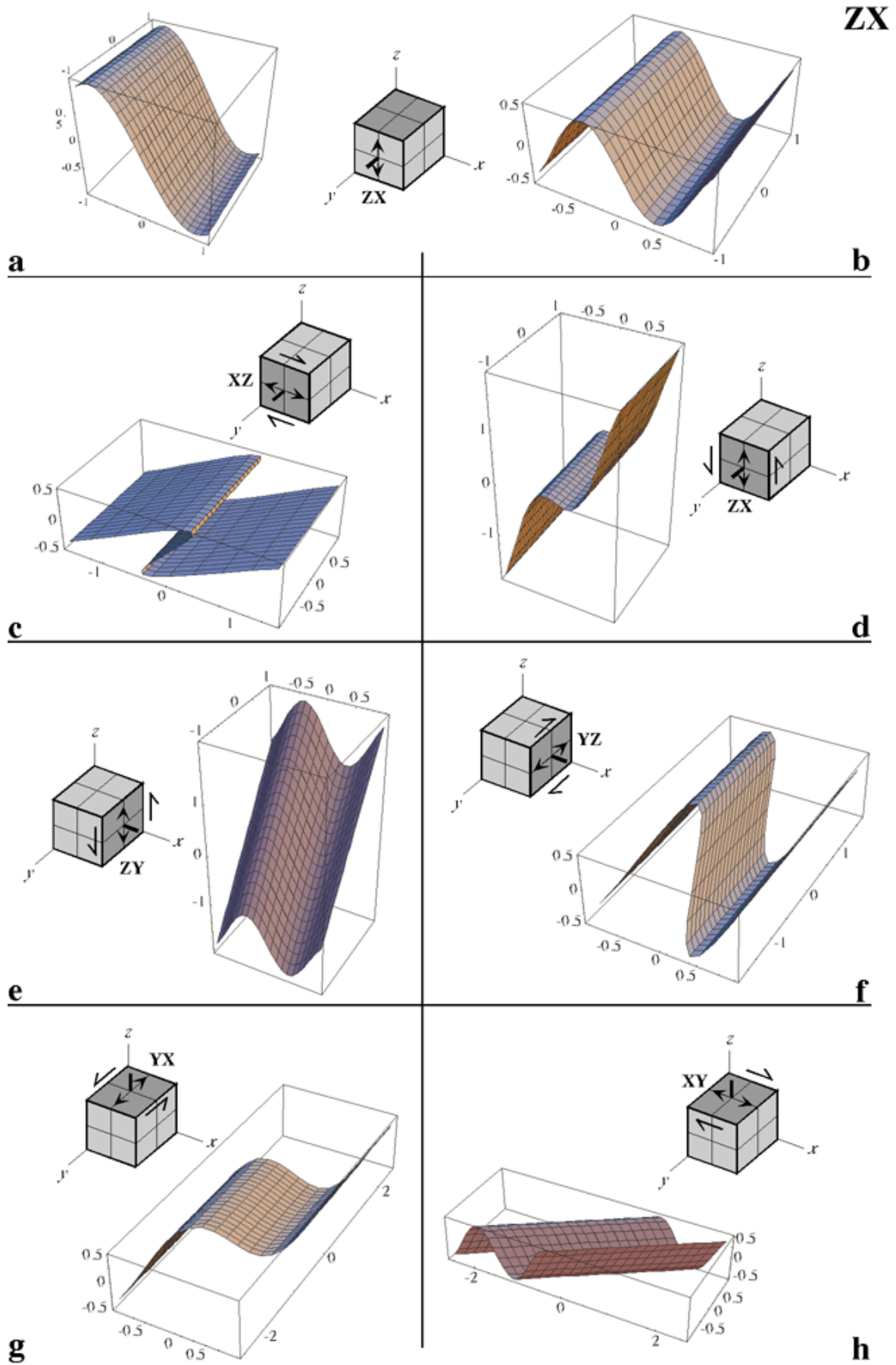


Fig. A.4: (see caption next page)

**Fig. A.4:** (see figure on previous page)

ZX folds generated with different shear opportunities ( $\text{axial}[t\_]=\text{Sin}[-2 t]$ ):

- a) Points of the  $xy$ -plane are moved along the  $z$ -axis in the  $xz$ -plane (ZX axis) leading to a fold axis parallel aligned to the  $y$ -axis ( $\text{ParametricPlot3D}[\text{Evaluate}[\{x,y,0\}/\text{axiZX}[1,1]],\{x,-1,1\},\{y,-1,1\}]$ );).
- b) The  $X$ -value determines the wavelength and the  $Z$ -value the amplitude of the fold ( $\text{ParametricPlot3D}[\text{Evaluate}[\{x,y,0\}/\text{axiZX}[,5,2]/\text{shrXZ}[0]],\{x,-1,1\},\{y,-1,1\}]$ );).
- c) Movement of the points along the  $x$ -axis in the  $xz$ -plane results in asymmetric folds (vergence) ( $\text{ParametricPlot3D}[\text{Evaluate}[\{x,y,0\}/\text{axiZX}[,5,2]/\text{shrXZ}[1.5]],\{x,-1,1\},\{y,-1,1\}]$ );).
- d) Movement of the points along the  $z$ -axis in the  $xz$ -plane causes an asymmetric fold, whose limbs are tilted ( $\text{ParametricPlot3D}[\text{Evaluate}[\{x,y,0\}/\text{axiZX}[,5,2]/\text{shrZX}[1.5]],\{x,-1,1\},\{y,-1,1\}]$ );).
- e) Movement of the points along the  $z$ -axis in the  $yz$ -plane leads to an increasing plunge of the fold axis, that means the fold is tilted as a whole one ( $\text{ParametricPlot3D}[\text{Evaluate}[\{x,y,0\}/\text{axiZX}[,5,2]/\text{shrZY}[1.5]],\{x,-1,1\},\{y,-1,1\}]$ );).
- f) Movement of the points along the  $y$ -axis in the  $yz$ -plane results in a sheared fold where the plane of inflection points remains constant ( $\text{ParametricPlot3D}[\text{Evaluate}[\{x,y,0\}/\text{axiZX}[,5,2]/\text{shrYZ}[1.5]],\{x,-1,1\},\{y,-1,1\}]$ );).
- g) Movement of the points along the  $y$ -axis in the  $xy$ -plane causes a fold with sheared limbs where the fold axial plane remains constant (rectangular), whereas the plane of inflection points is deformed into a parallelogram ( $\text{ParametricPlot3D}[\text{Evaluate}[\{x,y,0\}/\text{axiZX}[,5,2]/\text{shrYX}[1.5]],\{x,-1,1\},\{y,-1,1\}]$ );).
- h) Movement of the points along the  $x$ -axis in the  $xy$ -plane leads to a rotation of the fold axis in the  $xy$ -plane ( $\text{ParametricPlot3D}[\text{Evaluate}[\{x,y,0\}/\text{axiZX}[,5,2]/\text{shrXY}[1.5]],\{x,-1,1\},\{y,-1,1\}]$ );).

**Fig. A.5:** (see figure on next page)

ZY folds generated with different shear opportunities ( $\text{axial}[t\_]=\text{Sin}[-2 t]$ ):

- a) Points of the  $xy$ -plane are moved along the  $z$ -axis in the  $yz$ -plane (ZY axis) leading to a fold axis parallel aligned to the  $x$ -axis ( $\text{ParametricPlot3D}[\text{Evaluate}[\{x,y,0\}/\text{axiZY}[-1,1]/\text{shrXZ}[0]],\{x,-1,1\},\{y,-1,1\}]$ );).
- b) The  $Y$ -value determines the wavelength and the  $Z$ -value the amplitude of the fold ( $\text{ParametricPlot3D}[\text{Evaluate}[\{x,y,0\}/\text{axiZY}[,5,2]/\text{shrXZ}[0]],\{x,-1,1\},\{y,-1,1\}]$ );).
- c) Movement of the points along the  $y$ -axis in the  $yz$ -plane results in asymmetric folds (vergence) ( $\text{ParametricPlot3D}[\text{Evaluate}[\{x,y,0\}/\text{axiZY}[,5,2]/\text{shrYZ}[1.5]],\{x,-1,1\},\{y,-1,1\}]$ );).
- d) Movement of the points along the  $z$ -axis in the  $yz$ -plane causes an asymmetric fold, whose limbs are tilted ( $\text{ParametricPlot3D}[\text{Evaluate}[\{x,y,0\}/\text{axiZY}[,5,2]/\text{shrZY}[1.5]],\{x,-1,1\},\{y,-1,1\}]$ );).
- e) Movement of the points along the  $z$ -axis in the  $xz$ -plane leads to an increasing plunge of the fold axis, that means the fold is tilted as a whole one ( $\text{ParametricPlot3D}[\text{Evaluate}[\{x,y,0\}/\text{axiZY}[,5,2]/\text{shrZX}[1.5]],\{x,-1,1\},\{y,-1,1\}]$ );).
- f) Movement of the points along the  $x$ -axis in the  $xz$ -plane results in a sheared fold where the plane of inflection points remains constant ( $\text{ParametricPlot3D}[\text{Evaluate}[\{x,y,0\}/\text{axiZY}[,5,2]/\text{shrXZ}[1.5]],\{x,-1,1\},\{y,-1,1\}]$ );).
- g) Movement of the points along the  $x$ -axis in the  $xy$ -plane causes a fold with sheared limbs where the fold axial plane remains constant (rectangular), whereas the plane of inflection points is deformed into a parallelogram ( $\text{ParametricPlot3D}[\text{Evaluate}[\{x,y,0\}/\text{axiZY}[,5,2]/\text{shrXY}[1.5]],\{x,-1,1\},\{y,-1,1\}]$ );).
- h) Movement of the points along the  $y$ -axis in the  $xy$ -plane leads to a rotation of the fold axis in the  $xy$ -plane ( $\text{ParametricPlot3D}[\text{Evaluate}[\{x,y,0\}/\text{axiZY}[,5,2]/\text{shrYX}[1.5]],\{x,-1,1\},\{y,-1,1\}]$ );).

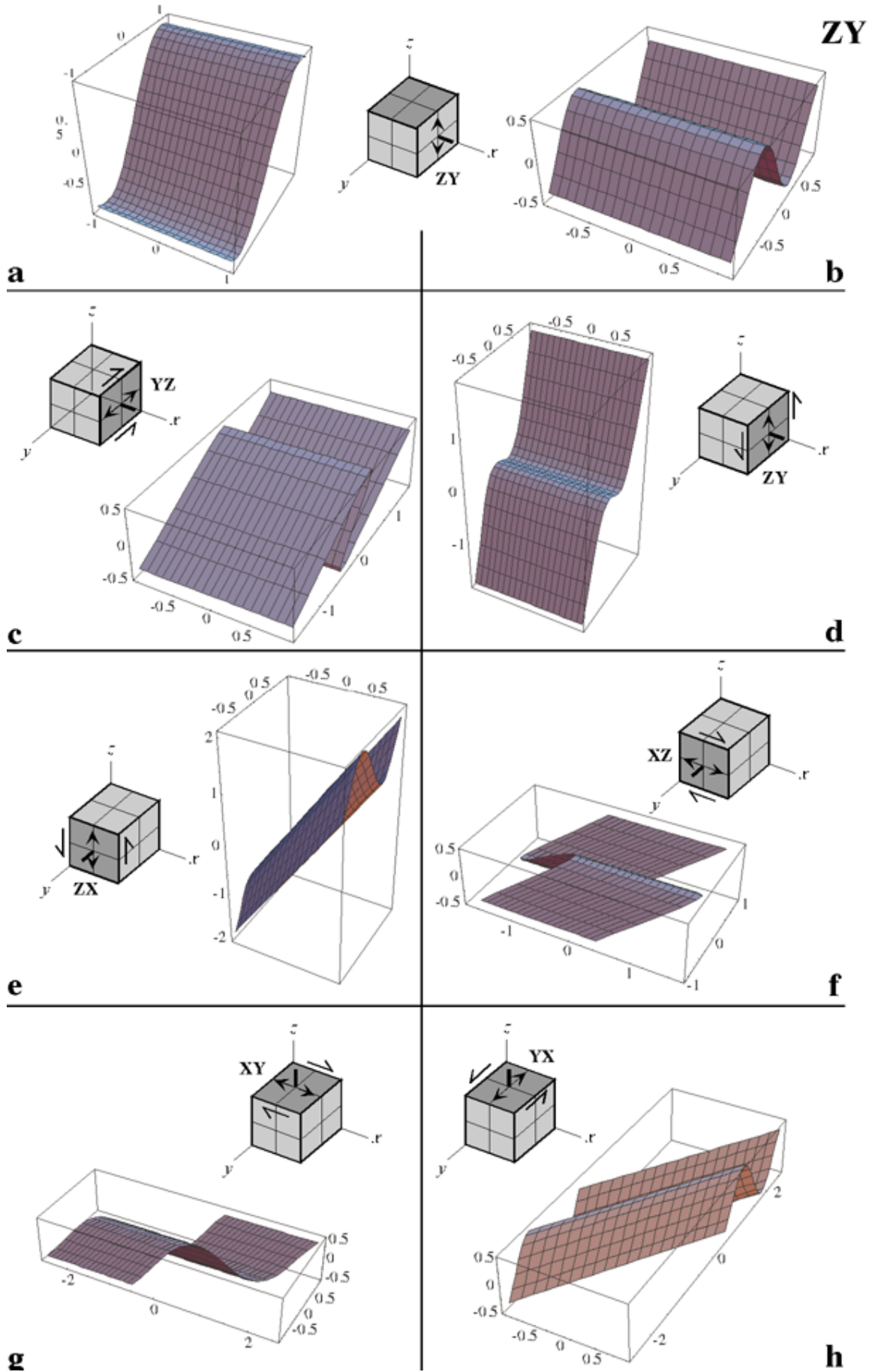


Fig. A.5: (see caption on previous page)



A.2. Calculations used in the thesis

Fig. 2.10b): axial[t\_]:=Sin[-2 t];  
 ParametricPlot3D[Evaluate[{x,y,0}]/axiZY[.1,1.5]/shrYZ[1.4]/axiZX[.58,1]/shrXZ[.8],  
 {x,-1.7,1.7},{y,-1.5,1.5},PlotPoints->{22,28},ViewPoint->{-1.079, -1.395, 3.165}];

Fig. 2.11b): axial[t\_]:=Sin[-2 t];  
 ParametricPlot3D[Evaluate[{x,y,0}]/axiZY[.25,1.8]/shrYZ[1]/axiZX[.4,1.5]/shrXZ[.5]/  
 shrYZ[.7],{x,-1.7,1.7},{y,-1.5,1.5},PlotPoints->{22,28},ViewPoint->{-1.079, -1.395,  
 3.165}]

Fig. 2.12.b): axial[t\_]:=Sin[-2 t];  
 ParametricPlot3D[Evaluate[{x,y,0}]/axiZY[.35,.9]/shrYZ[1.8]/rot[30,0,0]/  
 axiZX[.25,1.4]/  
 shrXZ[.6]/rot[10,10,0]],{x,-1.7,1.7},{y,-1.7,1.7},PlotPoints->22,28,ViewPoint->  
 {-1.358, -1.993, 2.704}];

Fig. 3.2: axial[t\_]:=Sin[-2 t];  
 a) ParametricPlot3D[Evaluate[{x,y,0}]/axiZY[.1,1.5]/shrYZ[1.4]/axiZX[.58,1]/shrXZ[.8],  
 {x,-1.7,1.7},{y,-1.5,1.5},PlotPoints->{22,28},ViewPoint->{-1.079, -1.395, 3.165}];  
 b) ParametricPlot3D[Evaluate[{x,y,0}]/axiZX[.3,1]/shrXZ[2]/rot[-20,0,0]/axiZY[.35,1]/  
 shrYZ[1]],{x,-1.7,1.7},{y,-1.5,1.5},AxesLabel[Rule]{"x","y","z"},  
 PlotPoints->{22,28},ViewPoint->{-1.576, -1.069, 3.083}]  
 c) ParametricPlot3D[Evaluate[{x,y,0}]/axiZY[.35,.9]/shrYZ[1.8]/rot[30,0,0]/  
 axiZX[.25,1.4]/  
 shrXZ[.6]/rot[10,10,0]],{x,-1.7,1.7},{y,-1.7,1.7},PlotPoints->22,28,ViewPoint->  
 {-1.358, -1.993, 2.704}];

Fig. 3.4: axial[t\_]:=Sin[-Pi t];  
 First row:  
 ParametricPlot3D[Evaluate[{x,y,0}]/axiZY[1,1.3]/shrYZ[1]/rot[170,-40,0]/axiZX[.3,1.5]/  
 /  
 rot[0,-10,0]],{x,-1,1},{y,-1,1},PlotPoints->30,30}]  
 ParametricPlot3D[Evaluate[{x,y,0}]/axiZY[1,1.3]/shrYZ[1]/rot[170,-40,0]/axiZX[.3,1.5]/  
 /  
 shrXZ[.7]/rot[0,-10,0]],{x,-1,1},{y,-1,1},PlotPoints->{20,25},ViewPoint->{1.795, -  
 2.147,  
 1.903}]  
 ParametricPlot3D[Evaluate[{x,y,0}]/axiZY[1.2,1.3]/shrYZ[1]/rot[170,-40,0]/  
 axiZX[.3,1.2]/  
 shrXZ[2]/rot[0,-10,0]],{x,-1,1},{y,-1,1}PlotPoints->{20,25}]

Second row:  
 ParametricPlot3D[Evaluate[{x,y,0}]/axiZY[1,1.3]/shrYZ[1]/rot[170,-40,0]/axiZX[.3,1.5]/  
 /  
 rot[0,-10,0]],{x,-1,1},{y,-1,1},PlotPoints->{30,30},ViewPoint->{-1.380, 2.799, 1.310}]  
 ParametricPlot3D[Evaluate[{x,y,0}]/axiZY[1,1.3]/shrYZ[1]/rot[170,-40,0]/axiZX[.3,1.5]/  
 /  
 shrXZ[.7]/rot[0,-10,0]],{x,-1,1},{y,-1,1},PlotPoints->{20,25},  
 ViewPoint->{-1.988, 2.370, 1.372}]  
 ParametricPlot3D[Evaluate[{x,y,0}]/axiZY[1.2,1.3]/shrYZ[1]/rot[170,-40,0]/  
 axiZX[.3,1.2]/  
 shrXZ[2]/rot[0,-10,0]],{x,-1,1},{y,-1,1},PlotPoints->{20,25},  
 ViewPoint->{-1.638, 2.624, 1.372}]

Fig. 3.5: axial[t\_]:=Sin[-Pi t];

First row:

```
ParametricPlot3D[Evaluate[{x,y,0}]/axiZY[.35,1.4]/shrYZ[.4]/rot[170,-40,0]/
  axiZX[.35,1.4]/shrXZ[.4]/rot[0,-10,0]],{x,-1,1},{y,-1,1},
  PlotPoints->{20,25},ViewPoint->{1.780,-2.130,2.103}]
ParametricPlot3D[Evaluate[{x,y,0}]/axiZY[.3,1.4]/shrYZ[.6]/rot[180,0,0]/axiZX[.2,1.4]],
  {x,-1,1},{y,-1,1},PlotPoints->{20,25},ViewPoint->{1.795,-2.147,1.903}]
ParametricPlot3D[Evaluate[{x,y,0}]/axiZY[.2,1.4]/rot[180,0,0]/axiZX[.2,1.4]],{x,-1,1},
  {y,-1,1},PlotPoints->{20,25},ViewPoint->{1.780,-2.130,2.103}]
```

Second row:

```
ParametricPlot3D[Evaluate[{x,y,0}]/axiZY[.35,1.4]/shrYZ[.4]/rot[170,-40,0]/
  axiZX[.35,1.4]/shrXZ[.4]/rot[0,-10,0]],{x,-1,1},{y,-1,1},PlotPoints->{20,25},
  ViewPoint->{-1.988,2.370,1.372}]
ParametricPlot3D[Evaluate[{x,y,0}]/axiZY[.3,1.4]/shrYZ[.6]/rot[180,0,0]/axiZX[.2,1.4]],
  {x,-1,1},{y,-1,1},PlotPoints->{20,25},ViewPoint->{-1.988,2.370,1.372}]
ParametricPlot3D[Evaluate[{x,y,0}]/axiZY[.2,1.4]/rot[180,0,0]/axiZX[.2,1.4]],{x,-1,1},
  {y,-1,1},PlotPoints->{20,25},ViewPoint->{-1.988,2.370,1.372}]
```

Fig. 3.7: axial[t\_]:=Sin[-1.8t];

First row:

```
ParametricPlot3D[Evaluate[{x,y,0}]/axiZX[.4,1.1]/shrXZ[1.8]/rot[-10,20,0]/
  axiZY[.4,1.1]/
  shrYZ[1.8]/rot[90,0,0]],{x,-1.7,1.7},{y,-1.5,1.5},PlotPoints->{22,28}];
ParametricPlot3D[Evaluate[{x,y,0}]/axiZX[.4,1.1]/shrXZ[1.8]/rot[-30,20,0]/
  axiZY[.4,1.1]/
  shrYZ[1.8]/rot[90,0,0]],{x,-1.7,1.7},{y,-1.5,1.5},PlotPoints->{22,28}];
ParametricPlot3D[Evaluate[{x,y,0}]/axiZX[.4,1.1]/shrXZ[1.8]/rot[-60,20,0]/
  axiZY[.4,1.1]/
  shrYZ[1.8]/rot[90,0,0]],{x,-1.7,1.7},{y,-1.5,1.5},PlotPoints->{25,28}];
```

Second row:

```
ParametricPlot3D[Evaluate[{x,y,0}]/axiZX[.4,1.1]/shrXZ[1.8]/rot[-10,20,0]/
  axiZY[.4,1.1]/
  shrYZ[1.8]/rot[90,0,0]],{x,-1.7,1.7},{y,-1.5,1.5},PlotPoints->{22,28},
  ViewPoint->{0.465,-0.455,3.321}]
ParametricPlot3D[Evaluate[{x,y,0}]/axiZX[.4,1.1]/shrXZ[1.8]/rot[-30,20,0]/
  axiZY[.4,1.1]/
  shrYZ[1.8]/rot[90,0,0]],{x,-1.7,1.7},{y,-1.5,1.5},PlotPoints->{22,28},
  ViewPoint->{0.465,-0.455,3.321}]
ParametricPlot3D[Evaluate[{x,y,0}]/axiZX[.4,1.1]/shrXZ[1.8]/rot[-60,20,0]/
  axiZY[.4,1.1]/
  shrYZ[1.8]/rot[90,0,0]],{x,-1.7,1.7},{y,-1.5,1.5},PlotPoints->{25,28},
  ViewPoint->{0.465,-0.455,3.321}]
```

Fig. 3.8:

a) axial[t\_]:=Sin[-2 t];

```
ParametricPlot3D[Evaluate[{x,y,0}]/axiZX[.4,1.4]/shrXZ[1]/rot[-90,0,0]/axiZY[.2,4]/
  shrYZ[.8]],{x,-1.7,1.7},{y,-1.5,1.5},PlotPoints->{90,20},
  ViewPoint->{2.986,-0.260,1.775}]
ParametricPlot3D[Evaluate[{x,y,0}]/axiZX[.4,1.4]/shrXZ[1]/rot[-100,0,0]/axiZY[.2,4]/
  shrYZ[.8]],{x,-1.7,1.7},{y,-1.5,1.5},PlotPoints->{90,20},
  ViewPoint->{2.986,-0.260,1.775}]
```

b) axial[t\_]:=Sin[-Pi t];

```
ParametricPlot3D[Evaluate[{0,y,z}]/axiXY[1,1]/shrXY[1.1]/rot[0,-90,0]/axiXZ[0.5,1]/
  shrXZ[1.5]/rot[0,0,0]],{y,-1,1},{z,-1,1}];
ParametricPlot3D[Evaluate[{0,y,z}]/axiXY[1,1]/shrXY[1.1]/rot[0,-84,0]/axiXZ[0.5,1]/
```

```

shrXZ[1.5]//rot[0,7,0]],{y,-1,1},{z,-1,1}];
ParametricPlot3D[Evaluate[{0,y,z}//axiXY[1,1]//shrXY[1.1]//rot[0,-75,0]//axiXZ[0.5,1]//
shrXZ[1.5]//rot[0,15,0]],{y,-1,1},{z,-1,1}];
ParametricPlot3D[Evaluate[{0,y,z}//axiXZ[1]//shrXZ[1.5]//rot[0,15,0]],{y,-1,1},{z,-1,1}];
ParametricPlot3D[Evaluate[{0,y,z}//axiXY[0.5,1]//shrXY[1.1]//rot[0,-75,0]],{y,-1,1},
{z,-1,1}];

```

Fig. 3.10:

```

axial[t_]:=Sin[-Pi t];
ParametricPlot3D[Evaluate[{x,y,0}//axiZY[.35,1.4]//shrYZ[.4]//rot[170,-40,0]//
axiZX[.35,1.4]//shrXZ[.4]//rot[0,-10,0]],{x,-1,1},{y,-1,1},PlotPoints->{20,25},
ViewPoint->{-1.988, 2.370, 1.372}]
a) axial[t_]:=Sin[-Pi t];
ParametricPlot3D[Evaluate[{x,y,0}//axiZX[.3,1.5]//shrXZ[2]//rot[60,0,0]],{x,-1,1},{y,-
1,1},
PlotPoints->{20,15}]
b) axial[t_]:=Sin[-Pi t];
ParametricPlot3D[Evaluate[{x,y,0}//axiZY[.3,1.5]//shrYZ[1]//rot[90,-20,0]],{x,-1,1},
{y,-1,1},PlotPoints->{20,15},ViewPoint->{1.854, -2.294, 1.659}]
c) axial[t_]:=Sin[-Pi t];
ParametricPlot3D[Evaluate[{x,y,0}//axiZY[1.2,1.3]//shrYZ[1]//rot[170,-40,0]
//axiZX[.3,1.2]//shrXZ[2]//rot[0,-10,0]],{x,-1,1},{y,-1,1},PlotPoints->{20,25},
ViewPoint->{-1.638, 2.624, 1.372}]
d) axial[t_]:=Sin[-Pi t];
ParametricPlot3D[Evaluate[{x,y,0}//axiZY[.3,1.4]//shrYZ[.6]//rot[180,0,0]//
axiZX[.2,1.4]],
{x,-1,1},{y,-1,1},PlotPoints->{20,25},ViewPoint->{-1.988, 2.370, 1.372}]
e) axial[t_]:=Sin[-2 t];
ParametricPlot3D[Evaluate[{x,y,0}//axiZX[.4,1.4]//shrXZ[1]//rot[-100,0,0]//axiZY[.2,4]//
shrYZ[.8]],{x,-1.7,1.7},{y,-1.5,1.5},PlotPoints->{90,20},
ViewPoint->{2.986, -0.260, 1.775}]

```

Fig. 4.6: axial[t\_]:=Sin[-\[Pi] t];

```

a) axial[t_]:=Sin[-2 t];a)
ParametricPlot3D[Evaluate[{x,y,0}//axiZY[.4,1.5]//shrYZ[2]//shrZY[-.25]],{x,-1,1},
{y,-1,4},ViewPoint->{3.283, -0.754, 1.335}];
b) axial[t_]:=Sin[-\[Pi] t];
ParametricPlot3D[Evaluate[{x,y,0}//axiZY[.3,1.2]//shrYZ[2]//rot[90,-20,0]],{x,-1,1},
{y,-1,1},PlotPoints->{20,20},ViewPoint->{1.583, -2.682, 2.419}]

```

Fig. 4.8: axial[t\_]:=Sin[-1.8t];

```

a) ParametricPlot3D[Evaluate[{x,y,0}//axiZX[.01,20]//rot[-30,0,0]//axiZY[.3,1]//
shrYZ[2.3]],
{x,-1.5,1.5},{y,-1.7,1.7},PlotPoints->{40,40},ViewPoint->{0.041, -0.033, 3.943}]
ParametricPlot3D[Evaluate[{x,y,0}//axiZX[.01,20]//rot[-30,0,0]//axiZY[.3,1]//shrYZ[4]],
{x,-1.2,1.2},{y,-1.2,1.2},PlotPoints->{40,40},ViewPoint->{0.041, -0.033, 3.943}];
b) ParametricPlot3D[Evaluate[{x,y,0}//axiZX[.015,20]//rot[-45,0,0]//axiZY[.3,1]//
shrYZ[2.3]],
{x,-1.5,1.5},{y,-2,2},PlotPoints->{40,40},ViewPoint->{0.041, -0.033, 3.943}]
ParametricPlot3D[Evaluate[{x,y,0}//axiZX[.015,20]//rot[-45,0,0]//axiZY[.3,1]//shrYZ[4]],
{x,-1.5,1.5},{y,-1.5,1.5},PlotPoints->{40,40},ViewPoint->{0.041, -0.033, 3.943}];

```

Fig. 4.9: axial[t\_]:=Sin[-1.8t];

```

a) ParametricPlot3D[Evaluate[{x,y,0}//axiZX[.015,20]//rot[60,0,0]//axiZY[.3,1]//
shrYZ[2.3]],
{x,-1.7,1.7},{y,-1.5,1.5},PlotPoints->{40,40},ViewPoint->{-0.036, -0.038, 3.943}]

```

```

ParametricPlot3D[Evaluate[{x,y,0} // axiZX[.015,20] // rot[60,0,0] // axiZY[.3,1] // shrYZ[4]],
  {x,-1.5,1.5},{y,-1.5,1.5},PlotPoints->{40,40},ViewPoint->{-0.036,-0.038,3.943}]
b) ParametricPlot3D[Evaluate[{x,y,0} // axiZX[.015,20] // rot[80,0,0] // axiZY[.3,1] //
shrYZ[2.3]],
  {x,-1.5,1.5},{y,-1.5,1.5},PlotPoints->{40,40},ViewPoint->{-0.036,-0.038,3.943}]
ParametricPlot3D[Evaluate[{x,y,0} // axiZX[.015,20] // rot[80,0,0] // axiZY[.3,1] // shrYZ[4]],
  {x,-1.5,1.5},{y,-1.5,1.5},PlotPoints->{40,40},ViewPoint->{-0.036,-0.038,3.943}]

```

Fig. 4.10: axial[t\_]:=Sin[-1.8t];

```

a) ParametricPlot3D[Evaluate[{x,y,0} // axiZX[.02,20] // rot[-30,0,0] // axiZX[-.3,1.4]
  // shrXZ[-2] // axiZY[.25,1.4] // shrYZ[2]],{x,-1.5,1.5},{y,-1.5,1.5},
  PlotPoints->{40,40},ViewPoint->{0.030,-0.043,3.943}]
b) ParametricPlot3D[Evaluate[{x,y,0} // axiZX[.025,20] // rot[-30,0,0] // axiZX[-.5,1.4]
  // shrXZ[-2] // rot[45,0,0] // axiZY[.08,.9] // shrYZ[2]],{x,-1.3,1.3},{y,-1.3,1.3},
  PlotPoints->{40,40},ViewPoint->{0.254,-0.137,3.933}]

```

Fig. 4.12: axial[t\_]:=Sin[-1.8t];

```

a) ParametricPlot3D[Evaluate[{x,y,0} // axiZX[.01,20] // shrYZ[2] // rot[-30,0,0]
  // axiZX[-.3,1.4] // shrXZ[-2] // axiZY[.25,1.4] // shrYZ[2]],{x,-1.5,1.5},{y,-1.5,1.5},
  PlotPoints->{40,40},ViewPoint->{0.030,-0.043,3.943}]
b) ParametricPlot3D[Evaluate[{x,y,0} // axiZX[.01,20] // shrYZ[2] // rot[-30,0,0]
  // axiZX[-.5,1.4] // shrXZ[-2] // rot[45,0,0] // axiZY[.08,.9] // shrYZ[2]],{x,-1.3,1.3},
  {y,-1.3,1.3},PlotPoints->{40,40},ViewPoint->{0.254,-0.137,3.933}]

```

Fig. 5.3:

```

axial[t_]:=Sin[-Pi t];
ParametricPlot3D[Evaluate[{x,y,0} // axiZY[.35,1.4] // shrYZ[.4] // rot[170,-40,0] //
  axiZX[.35,1.4] // shrXZ[.4] // rot[0,-10,0]],{x,-1,1},{y,-1,1},PlotPoints->{20,25},
  ViewPoint->{-1.988,2.370,1.372}]
a) axial[t_]:=Sin[-Pi t];
  ParametricPlot3D[Evaluate[{x,y,0} // axiZX[.3,1.5] // shrXZ[2] // rot[60,0,0]],{x,-1,1},{y,-
  1,1},
  PlotPoints->{20,15}]
b) axial[t_]:=Sin[-Pi t];
  ParametricPlot3D[Evaluate[{x,y,0} // axiZY[.3,1.5] // shrYZ[1] // rot[90,-20,0]],{x,-1,1},
  {y,-1,1},PlotPoints->{20,15},ViewPoint->{1.854,-2.294,1.659}]
c) axial[t_]:=Sin[-Pi t];
  ParametricPlot3D[Evaluate[{x,y,0} // axiZY[1.2,1.3] // shrYZ[1] // rot[170,-40,0]
  // axiZX[.3,1.2] // shrXZ[2] // rot[0,-10,0]],{x,-1,1},{y,-1,1},PlotPoints->{20,25},
  ViewPoint->{-1.638,2.624,1.372}]
d) axial[t_]:=Sin[-Pi t];
  ParametricPlot3D[Evaluate[{x,y,0} // axiZY[.3,1.4] // shrYZ[.6] // rot[180,0,0] //
  axiZX[.2,1.4]],
  {x,-1,1},{y,-1,1},PlotPoints->{20,25},ViewPoint->{-1.988,2.370,1.372}]
e) axial[t_]:=Sin[-2 t];
  ParametricPlot3D[Evaluate[{x,y,0} // axiZX[.4,1.4] // shrXZ[1] // rot[-100,0,0] // axiZY[.2,4] //
  shrYZ[.8]],{x,-1.7,1.7},{y,-1.5,1.5},PlotPoints->{90,20},
  ViewPoint->{2.986,-0.260,1.775}]

```

Fig. 5.7: axial[t\_]:=Sin[-2 t];

```

a) ParametricPlot3D[Evaluate[{x,y,0} // axiZY[.3,9] // shrYZ[1.4] // axiZX[.6,1]
  // shrXZ[.5]],{x,-1.7,1.7},{y,-1.8,1.8},PlotPoints->{22,28},
  ViewPoint->{-1.358,-1.993,2.704}];
  ParametricPlot3D[Evaluate[{x,y,0} // axiZY[.3,9] // shrYZ[1.4] // axiZX[.7,1]
  // shrXZ[.5] // rot[0,50,0]],{x,-1.7,1.7},{y,-1.8,1.8},PlotPoints->{22,28},
  ViewPoint->{-1.358,-1.993,2.704}];

```

b) ParametricPlot3D[Evaluate[{x,y,0} //axiZY[.5,1] //shrYZ[1.4] //axiZX[.6,1] //shrXZ[.5]],{x,-1.7,1.7},{y,-1.8,1.8},PlotPoints->{22,28}, ViewPoint->{2.471, 2.661, 1.537}];  
 ParametricPlot3D[Evaluate[{x,y,0} //axiZY[.5,1] //shrYZ[1.4] //axiZX[.6,1] //shrXZ[.5] //rot[0,-50,0]],{x,-1.7,1.7},{y,-1.8,1.8},PlotPoints->{22,28}, ViewPoint->{2.301, 2.478, 0.109}];

Fig. 5.12: axial[t\_]:=Sin[-2 t];

a) ParametricPlot3D[Evaluate[{x,y,0} //axiZY[.35,.9] //shrYZ[1.8] //rot[30,0,0] //axiZX[.25,1.4] //shrXZ[.6] //rot[10,10,0]],{x,-1.7,1.7},{y,-1.8,1.8},PlotPoints->{22,28}, ViewPoint->{-1.358, -1.993, 2.704}];

b) ParametricPlot3D[Evaluate[{x,y,0} //axiZY[.35,.9] //shrYZ[2.2] //rot[30,10,0] //axiZX[.25,1.4] //shrXZ[.7] //rot[10,40,0]],{x,-1.7,1.7},{y,-1.7,1.7}, PlotPoints->{22,28}, ViewPoint->{-1.358, -1.993, 2.704}];

Fig. 5.15b: axial[t\_]:=Sin[-2 t];

ParametricPlot3D[Evaluate[{x,y,0} //axiZX[1,1] //rot[-90,0,0] //axiZY[.5,10]],{x,-1.6,1.6},{y,-1.5,1.5},PlotPoints->{90,20}, ViewPoint->{-2.481, -1.314, 1.889}];

ParametricPlot3D[Evaluate[{x,y,0} //axiZX[1.5,2] //rot[-90,0,0] //axiZY[.5,10]],{x,-1.6,1.6},{y,-1.5,1.5},PlotPoints->{70,20}, ViewPoint->{-2.481, -1.314, 1.889}];

ParametricPlot3D[Evaluate[{x,y,0} //axiZX[1.7,3] //rot[-90,0,0] //axiZY[.5,10]],{x,-1.6,1.6},{y,-1.5,1.5},PlotPoints->{90,20}, ViewPoint->{-2.481, -1.314, 1.889}];

## References

- Abassi, M. R. & Mancktelow, N. S. 1990. The effect of initial perturbation shape and symmetry on fold development. *Journal of Structural Geology* 12, 273-282.
- Adams, C. J. & Gabites, J. E. 1985. Age of metamorphism and uplift of the Haast Schist Group at Haast Pass, Lake Wanaka and Lake Hawea, South Island, New Zealand. *New Zealand Journal of Geology and Geophysics* 28, 85-96.
- Adams, C. J., Bishop, D. G. & Gabites, J. E. 1985. Potassium-argon studies of a low grade, progressively metamorphosed greywacke sequence, Dansey Pass, South Island, New Zealand. *Journal of Geological Society London* 141, 339-349.
- Adams, C. J. & Robinson, P. 1993. Potassium-Argon age studies of metamorphism/ uplift/ cooling in Haast Schist coastal sections of Dunedin, Otago, New Zealand. *New Zealand Journal of Geology and Geophysics* 36, 317-325.
- Adams, C. J. & Graham, I. J. 1997. Age of metamorphism of Otago Schist in eastern Otago and determination of protoliths from initial strontium isotope characteristics. *New Zealand Journal of Geology and Geophysics* 40, 275-286.
- Aitchison, J. C. & Landis, C. A. 1990. Sedimentology and tectonic setting of the Late Permian – Early Triassic Stephens Subgroup, Southland, New Zealand: an island arc-derived mass flow apron. *Sedimentary Geology* 68(1-2), 55-74.
- Allis, R. G. 1986. Mode of crustal shortening adjacent to the Alpine Fault, New Zealand. *Tectonics* 5(1), 15-32.
- Alsop, G. I. & Holdsworth, R. E. 1999. Vergence and facing patterns in large-scale sheath folds. *Journal of Structural Geology* 21, 1335-1349.
- Andrews, P. B., Bishop, D. G., Bradshaw, J. D. & Warren, G. 1974. Geology of the Lord Range, central Southern Alps, New Zealand. *New Zealand Journal of Geology and Geophysics* 17, 271-299.
- Andrews, C. B., Speden, I. G. & Bradshaw, J. D. 1976. Lithological and paleontological content of the Carboniferous-Jurassic Canterbury suite, South Island, New Zealand. *New Zealand Journal of Geology and Geophysics* 19, 791-819.
- Ballance, P. F., Heming, R. F. & Sameshima, T. 1981. Petrography of the youngest known Miurihiku Supergroup, New Zealand. Latest Jurassic arc volcanism on the southern margin of Gondwana. In: Cresswell, M. M. & Vella, P. (Eds.), *Gondwana Five*. Balkema, Rotterdam, 161-166.
- Ballance, P. F. & Campbell, J. D. 1993. The Murihiku arc-related basin of New Zealand (Triassic - Jurassic). In: Ballance, P. F. & Hsu, K.J. (Eds.), *South Pacific Sedimentary Basins in Sedimentary Basins of the World*. Elsevier, Amsterdam, 21-33.

- Batt, G. E., Kohn, B. P., Braun, J., McDougall, I. & Ireland, T. R. 1999. New insight in to the dynamic development of the Southern Alps of New Zealand, from detailed thermochronological investigation of the Mataketake Range pegmatites. In: Ring, U., Brandon, M. T., Lister, G. S. & Willett, S. (Eds.), *Exhumation Processes: Brittle Faulting, Ductile Flow and Erosion*, 154. Special Publication, Geological Society London, 261-282.
- Beanland, S. & Barrow-Hurlbert, S. A. 1988. The Nevis-Cardrona fault system, central Otago, New Zealand: Late Quaternary tectonics and structural development. *New Zealand Journal of Geology and Geophysics* 31(337-352).
- Beanland, S. & Berryman, K. R. 1989. Style and episodicity of Late Quaternary activity on the Pisa-Grandview fault zone, central Otago, New Zealand. *New Zealand Journal of Geology and Geophysics* 32(451-461).
- Beaven, J., Moore, M., Pearson, C., Henderson, M., Parsons, B., Bourne, S., England, P., Walcott, D., Blick, G., Darby, D. & Hodkinson, K. 1999. Crustal deformation during 1994-1998 due to oblique continental collision in the central Southern Alps, New Zealand, and implications for seismic potential of the Alpine Fault. *Journal of Geophysical Research* 104(B11), 25,233-25,255.
- Bell, T. H. & Forde, A. 1995. On the significance of foliation patterns preserved around folds by mineral overgrowth. *Tectonophysics* 246(1-3), 171-181.
- Berryman, K. 1979. Active faulting and derived PHS directions in the South Island, New Zealand. *The Royal Society of New Zealand Bulletin* 18, 29-34.
- Bishop, D. G. 1972. Transposition structures associated with cleavage formation in the Otago schists. *New Zealand Journal of Geology and Geophysics* 15, 360-371.
- Bishop, D. G. 1974. Stratigraphic, structural and metamorphic relationships in the Dansey Pass area, Otago, New Zealand. *New Zealand Journal of Geology and Geophysics* 17, 301-335.
- Bishop, D. J. 1992. Extensional tectonism and magmatism during middle Cretaceous to Paleocene, North Westland, New Zealand. *New Zealand Journal of Geology and Geophysics* 35, 81-91.
- Bishop, D. G. & Turnbull, I. M. 1996. *Geology of the Dunedin area*. Institute of Geological & Nuclear Sciences 1:250 000 geological map 21. Institute of Geological & Nuclear Sciences, Lower Hutt, New Zealand.
- Bishop, D. G. 1994. *Geology of the Forgotten River area*. Scale 1: 50 000. Institute of Geological & Nuclear Science geological map 15. Institute of Geological & Nuclear Science Ltd., Lower Hutt.
- Boyer, S. E. & Elliot, D. 1982. Thrust systems. *American Association of Petroleum Geologists bulletin* 66, 1196-1230.

- Bradshaw, J. D., Adams, C. J. & Andrews, B. P. 1981. Carboniferous to Cretaceous on the Pacific margin of Gondwana: The Rangitata phase of New Zealand. In: Cresswell, M. M. & Vella, P. (Eds.), *Gondwana Five*. Balkema, A.A., Rotterdam, 217-221.
- Bradshaw, J. D. 1989. Cretaceous geotectonic pattern in the New Zealand region. *Tectonics* 8, 803-820.
- Bradshaw, J. D. 1993. A review of the Median Tectonic Zone: terrane boundaries and terrane amalgamation near the Tectonic Line. *New Zealand Journal of Geology and Geophysics* 36, 117-125.
- Bradshaw, J., Weaver, S. & Muir, R. 1996. Mid Cretaceous oroclinal bending of New Zealand terranes. *New Zealand Journal of Geology and Geophysics* 39, 461-468.
- Brown, E. H. 1968. Metamorphic structures in part of the eastern Otago schists. *New Zealand Journal of Geology and Geophysics* 11, 41-65.
- Butler, R. W. H. 1982. The terminology of structures in thrust belts. *Journal of Structural Geology* 4, 239-245.
- Campbell, J. D. & Coombs, D. S. 1966. Murihiku Supergroup (triassic- Jurassic) of Southland and South Otago. *New Zealand Journal of Geology and Geophysics* 9, 99-137.
- Campbell, J. D. & Force, E. R. 1972. Stratigraphy of Mount Potts Group at Rocky Gully, Rangitata Valley, Canterbury. *New Zealand Journal of Geology and Geophysics* 15, 157-167.
- Carter, R. M. & Norris, R. J. 1976. Cainozoic history of southern New Zealand; an accord between geological observations and plate tectonic predictions. *Earth Planetary Science Letters* 31, 85-94.
- Carter, R. M., Hicks, M. D., Norris, R. J. & I.M., T. 1978. Sedimentation patterns in an ancient Arc-Trench-Ocean basin complex: Carboniferous to Jurassic Rangitata Orogeny, New Zealand. In: Stanley, D. J. & Kelling, G. (Eds.), *Sedimentation in Submarine Canyons, Fans and Trenches*. Dowden, Hutchison and Ross, Stroudsburg, Pennsylvania, 340-361.
- Casas, A. M., Gapais, D., Nalpas, T., Besnard, K. & Roman-Berdiel, T. 2001. Analogue models of transpressive systems. *Journal of Structural Geology* 23, 733-743.
- Chamberlain, C. P., Zeitler, P. K. & Cooper, A. F. 1995. Geochronologic constraints of the uplift and metamorphism along the Alpine Fault, South Island, New Zealand. *New Zealand Journal of Geology and Geophysics* 38, 515-523.
- Cobbold, P. R., Gapais, D. & Rossello, E. A. 1991. Partitioning of transpressive motions within a sigmoidal fold belt: the Variscan Sierras Australes, Argentina. *Journal of Structural Geology* 13, 743-758.
- Coombs, D. S., Landis, C. A., Norris, R. J., Sinton, J. M., D.J., B. & Craw, D. 1976. The Dun Mountain Ophiolite Belt, New Zealand, its tectonic setting constitution and origin, with special reference to the southern portion. *American Journal of Science* 276, 561-603.



- Cooper, A. F. 1974. Multiphase deformation and its relationship to metamorphic crystallisation at Haast River south Westland, New Zealand. *New Zealand Journal of Geology and Geophysics* 17, 855-880.
- Cooper, A. F. 1976. Concentrically zoned ultramafic pods from the Haast schist zone, South Island, New Zealand. *New Zealand Journal of Geology and Geophysics* 19, 603-623.
- Cooper, A. F. 1980. Petrograde alteration of chromian kyanite in metachert and amphibolite white schist from the Southern Alps, New Zealand, with implications for uplift on the Alpine Fault. *Contribution to Mineralogy and Petrology* 75, 153-164.
- Cooper, A. F., Barrierio, B. A., Kimbrough, D. C. & Mattinson, J. M. 1987. Lampophyre dike intrusion and the age of the Alpine Fault, New Zealand. *Geology* 15, 941-944.
- Cosgrove, J. W. 1976. Formation of crenulation cleavage. *Journal of Geological Society London* 132, 155-178.
- Cosgrove, J. W. 1980. The tectonic implications of some small scale structures in the Mona Complex of Holy Isle, North Wales. *Journal of Structural Geology* 2, 383-396.
- Cox, S. C. 1991. The Aspiring/Caples terrane boundary: The translation surface of an early nappe structure in the Otago Schist. *New Zealand Journal of Geology and Geophysics* 34, 73-82.
- Cox, S. C. & Findlay, R. H. 1995. The Main Divide fault zone and its role in formation of the Southern Alps, New Zealand. *New Zealand Journal of Geology and Geophysics* 38, 489-499.
- Craw, D. 1985. Structure of schist in the Mt. Aspiring region, northwestern Otago, New Zealand. *New Zealand Journal of Geology and Geophysics* 28, 55-75.
- Craw, D. & Norris, R. J. 1991. Metamorphogenic Au-W veins and regional tectonics: Mineralisation throughout the uplift history of the Haast Schist, New Zealand. *New Zealand Journal of Geology and Geophysics* 34, 373-383.
- Craw, D., Rattenbury, M. S. & Johnstone, R. D. 1994. Structures within greenschist facies, Alpine Schist, central Southern Alps, New Zealand. *New Zealand Journal of Geology and Geophysics* 37, 101-111.
- Craw, D. 1998. Structural boundaries and biotite and garnet 'isograds' in the Otago and Alpine Schists, New Zealand. *Journal of Metamorphic Geology* 16(395-402).
- Davey, F. J., Henyey, T., Kleffmann, S., Melhuish, A., Okaya, D., Stern, T. A. & Woodward, D. J. 1995. Crustal reflections from the Alpine Fault Zone, South Island, New Zealand. *New Zealand Journal of Geology and Geophysics* 38, 601-604.
- Davey, F. J., Henyey, T., Holbrook, W. S., Okaya, D., Stern, T. A., Melhuish, A., Henrys, S., Anderson, H., Eberhart-Phillips, D., McEvelly, T., Uhrhammer, R., Wu, F., Jiracek, G. R., Wannamaker, P. E., Caldwell, G. & Christensen, N. 1998. Preliminary results from a geophysical study across a modern continent-continent collisional plate boundary - the Southern Alps, New Zealand. *Tectonophysics* 288, 221-235.

- Davis, T. E., Johnson, M. R., Rankin, P. C. & Stull, R. Y. 1980. The Dun Mountain belt in east Nelson. In: *Ophiolites: Proceedings of the International Ophiolite Symposium*. Cyprus Geological Survey Department, Cyprus 1979, 480-496.
- Davis, D., Suppe, J. & Dahlen, F. A. 1983. Mechanics of fold-and thrust-belts and accretionary wedges. *Journal of Geophysical Research* 88, 1153-1172.
- DeMets, C., Gordon, R. G., Argus, D. F. & Stein, S. 1990. Current plate motions. *International Journal of Geophysics* 101, 425-478.
- DeMets, C., Gordon, R. G., Argus, D. F. & Stein, S. 1994. Effect of recent revisions to the geomagnetic reversal time scale on estimates of current plate motions. *Geophysical Research Letters* 21, 2191-2194.
- Department of Conservation 1999. *Aoraki / Mount Cook - the ancestor of Ngai Tahu*. Department of Conservation (Te Papa Atawhai), Private Bag 4715, Christchurch, New Zealand.
- Dewey, J. F., Holdsworth, R. E. & Strachan, R. A. 1998. Transpression and transtension zones. In: Holdsworth, R. E., Strachan, R. A. & Dewey, J. F. (Eds.), *Continental Transpressional and Transtensional Tectonics*, 135. Geological Society Special Publications, 1-14.
- Elliott, D. 1981. The strength of thrust sheets. *EOS* 62, 397.
- Findlay, R. H. & Spörli, K. B. 1984. Structural geology of the Mount Cook Range and Main Divide, Hooker Valley region, New Zealand. *New Zealand Journal of Geology and Geophysics* 27, 257-276.
- Findlay, R. H. 1987. Structure and interpretation of the Alpine schists in Copland and Cook River valleys, South Island, New Zealand. *New Zealand Journal of Geology and Geophysics* 30, 117-138.
- Fisher, D. & Byrne, T. 1987. Structural evolution of underthrust sediments, Kodiak Islands, Alaska. *Tectonics* 6(6), 775-793.
- Fisher, D. & Byrne, T. 1992. Strain variation in an ancient accretionary complex: implications for forearc evolution. *Tectonics* 11, 330-347.
- Fleming, C. A. 1970. Two new deep-water Mollusca from the Tarakohe mudstone (lower Miocene) of Nelson, New Zealand. *New Zealand Journal of Geology and Geophysics* 13(3), 676-683.
- Fossen, H. & Tikoff, B. 1998. Extended models of transpression and transtension, and application to tectonic settings. In: Holdsworth, R. E., Strachan, R. A. & Dewey, J. F. (Eds.), *Transpressional and Transtensional Tectonics*, Special Publications. Geological Society, London, 15-33.
- Ghosh, S. K. & Ramberg, H. 1968. Buckling experiments on intersecting fold patterns. *Tectonophysics* 5, 89-105.

- Ghosh, S. K. 1970. A theoretical study of intersecting fold patterns. *Tectonophysics* 9, 559-569.
- Ghosh, S. K. 1974. Strain distribution in superposed buckling folds and the problem of reorientation of early lineation. *Tectonophysics* 21, 249-272.
- Ghosh, S. K. & Chatterjee, A. 1985. Patterns of deformed early lineations over late folds formed by buckling and flattening. *Journal of Structural Geology* 7, 651-666.
- Ghosh, S. K., Mandal, N., Sengupta, S., Deb, S. K. & Khan, D. 1993. Superposed buckling in multilayers. *Journal of Structural Geology* 15(1), 95-111.
- Ghosh, S. K. 1993. *Structural Geology - Fundamentals and modern developments*. Pergamon Press, Oxford, 598p.
- Ghosh, S. K., Deb, S. K. & Sengupta, S. 1996. Hinge migration and hinge replacement. *Tectonophysics* 263(1-4), 319-337.
- Graham, I. J. & Mortimer, N. 1992. Terrane characterisation and timing of metamorphism in the Otago Schist, New Zealand, using Rb-Sr and K-Ar geochronology. *New Zealand Journal of Geology and Geophysics* 35, 391-401.
- Grapes, R. H. & Palmer, K. 1984. Magma type and tectonic setting of metabasites, Southern Alps, New Zealand, using immobile elements. *New Zealand Journal of Geology and Geophysics* 27, 21-25.
- Grapes, R. H. & Watanabe, T. 1992. Metamorphism and uplift of Alpine Schist in the Franz-Josef -Fox area of the Southern Alps, New Zealand. *Journal of Metamorphic Geology* 10, 171-180.
- Gray, D. R. & Durney, D. W. 1979. Crenulation cleavage differentiation; implications of solution-deposition processes. *Journal of Structural Geology* 1(1), 73-80.
- Gray, D. R. 1979. Geometry of crenulation-folds and their relationship to crenulation cleavage. *Journal of Structural Geology* 1(3), 187-205.
- Gray, D. R., Gregory, R. T., Norris, J. R. & Cox, S. C. 1995. Regional scale sheath-folding and heterogeneously distributed shear strain in an evolving nappe pile, Otago Schist, New Zealand. *Geological Society of Australia Abstracts* 40, 53.
- Grindley, G. W. 1963. Structure of the Alpine Schists of South Westland, Southern Alps, New Zealand. *New Zealand Journal of Geology and Geophysics* 6(5), 872-930.
- Grujic, D. 1993. The influence of initial fold geometry on Type 1 and Type 2 interference patterns: an experimental approach. *Journal of Structural Geology* 15(3-5), 293-307.
- Grujic, D., Walter, T. R. & Gärtner, H. 2002. Shape and structure of (analogue models of) refolded layers. *Journal of Structural Geology* 24, 1313-1326.
- Gunn, B. M. 1960. Structural feature of the Alpine Schists of the Franz Josef - Fox Glacier region. *New Zealand Journal of Geology and Geophysics* 3, 287-308.

- Harding, T. P. 1985. Seismic characteristics and identification of negative flower structures, positive flower structures and positive structural inversion. *American Association of Petroleum Geologists Bulletin* 69(4), 582-600.
- Harland, W. B., Cox, A. V., Llewellyn, P. G., Pickton, C. A. G., Smith, A. G. & Walters, R. 1982. *A geologic time scale*. Cambridge University Press, New York.
- Haston, R., Luyendyk, B. P., Landis, C. A. & Coombs, D. S. 1989. Paleomagnetism and the question of the original location of the Permian Brook Street Terrane, New Zealand. *Tectonics* 8, 791-801.
- Holcombe, R. J. & Little, T. A. 2001. A sensitive vorticity gauge using rotated porphyroblasts, and its application to rocks adjacent to the Alpine Fault, New Zealand. *Journal of Structural Geology* 23, 979-989.
- Holm, D., Norris, R. J. & Craw, D. 1989. Brittle and ductile deformation in a zone of rapid uplift: Central Southern Alps, New Zealand. *Tectonics* 8, 153-168.
- Houghton, B. F. & Landis, C. A. 1989. Sedimentation and volcanism in a Permian arc-related basin, southern New Zealand. *Bulletin of Volcanology* 51(6), 433-450.
- Howell, D. G. 1980. Mesozoic accretion of exotic terranes along the New Zealand segment of Gondwanaland. *Geology* 8, 487-491.
- Hudleston, P. J. & Lan, L. 1993. Information from fold shape. *Journal of Structural Geology* 15(3-5), 253-264.
- Hunt, T. 1978. Stokes Magnetic Anomaly System. *New Zealand Journal of Geology and Geophysics* 21, 595-606.
- Jackson, J. & Molnar, P. 1990. Active faulting and block rotation in the western transverse ranges, California. *Journal of Geophysical research* 95(B13), 22,073-22,087.
- Jamison, W. R. 1991. Kinematics of compressional fold development in convergent wrench terranes. *Tectonophysics* 190, 209-232.
- Johns, M. K. & Mosher, S. 1996. Physical models of regional fold superposition: the role of competence contrast. *Journal of Structural Geology* 18(4), 475-492.
- Johnson, M. R. H. 1956. Conjugate fold system in the Moine Thrust Zone in the Lochcarran and Coulin Forest areas of Wester Ross. *Geological Magazine* 93(4), 345-352.
- Jones, D. L., Howell, D. G., Coney, P. J. & Monger, J. W. H. 1982. Recognition, character and analysis of tectonostratigraphic terranes in western North America. In: Hashimoto, M. & Uyeda, S. (Eds.), *Accretion tectonics in the circum-Pacific regions*. D.Riedel Publishing Co., Boston, 21-36.
- Jones, R. R. & Tanner, P. W. G. 1995. Strain partitioning in transpression zones. *Journal of Structural Geology* 17, 793-802.

- Kamp, P. J. J. 1986a. The mid-Cenozoic Challenger Rift System of western New Zealand and its implications for the age of Alpine Fault inception. *Bulletin of the Geological Society of America* 97, 255-281.
- Kamp, P. J. J. 1986b. Late Cretaceous- Cenozoic tectonic development of the southwest Pacific region. *Tectonophysics* 121, 225-251.
- Kamp, P. J. J. 1987. Age and origin of the New Zealand orocline in relation to Alpine Fault movement. *Journal of Geological Society London* 144, 641-652.
- Kamp, P. J. J., Green, P. F. & White, S. H. 1989. Fission track analysis reveals character of collisional tectonics in New Zealand. *Tectonics* 8, 169-195.
- Karig, D., Lawrence, M. B., Moore, G. F. & Curray, J. R. 1980. Structural framework of forearc basin, NW Sumatra. *Journal of the Geological Society, London* 137, 77-91.
- Kidan, T. W. & Cosgrove, J. W. 1996. The deformation of multilayers by layer-normal compression: an experimental investigation. *Journal of Structural Geology* 18(4), 461-474.
- Kimbrough, D. L., Mattinson, J. M., Coombs, D. S., Landis, C. A. & Johnston, M. R. 1992. Uranium- Lead ages from the Dun Mountain Ophiolite Belt and Brook Street Terranes, South Island, New Zealand. *Geological Society of America Bulletin* 104, 429-443.
- Kimbrough, D. L., Tulloch, A. J., Coombs, D. S., Johnston, M. R. & Mattinson, J. M. 1994. Uranium-Lead zircon ages from the Median Tectonic Zone, South Island, New Zealand. *New Zealand Journal of Geology and Geophysics* 37, 393-419.
- Kimura, G. & Ludden, J. 1995. Peeling oceanic crust in subduction zones. *Geology* 23(3), 217-220.
- Koehn, D., Hilgers, C., Bons, P. D. & Passchier, C. W. 2000. Numerical simulation of fibre growth in antitaxial strain fringes. *Journal of Structural Geology* 22, 1311-1324.
- Koons, P. O. 1990. The two-sided orogen: collision and erosion from the sandbox to the Southern Alps, New Zealand. *Geology* 18, 679-682.
- Koons, P. O. 1994. Three-dimensional critical wedges: tectonics and topography in oblique collisional orogens. *Journal of Geophysical Research* 99(B6), 12301-12315.
- Koons, P. O. & Henderson, C. M. 1995. Geodetic analysis of model oblique collision and comparison to the Southern Alps of New Zealand. *New Zealand Journal of Geology and Geophysics* 38, 545-552.
- Korsch, R. J. & Wellman, H. W. 1988. The geological evolution of New Zealand and the New Zealand region. In: Nairn, A. E. M., Stehli, F. G. & Uyeda, S. (Eds.), *The Ocean Basins and Margins*, 7B. Plenum Publishing Corporation, 411-482.
- Lamb, S. H. 1988. Tectonic relations about vertical axes during the last 4Ma in part of the New Zealand plate boundary zone. *Journal of Structural Geology* 10, 875-893.
- Lan, L. & Hudleston, P. J. 1991. Finite-element models of buckle folds in non-linear materials. *Tectonophysics* 199, 1-12.

- Landis, C. A. & Coombs, D. S. 1967. Metamorphic belt and orogenesis in southern New Zealand. *Tectonophysics* 4, 501-518.
- Landis, C. A. & Bishop, D. G. 1972. Plate tectonics and regional stratigraphic metamorphic relations in the southern part of the New Zealand geosyncline. *Geological Society of America Bulletin* 83, 2267-2284.
- Landis, C. A. 1980. Little Ben Sandstone, Maitai Group (Permian): nature and extent in the Hollyford-Eglinton region, South Island, New Zealand. *New Zealand Journal of Geology and Geophysics* 23(5-6), 551-567.
- Lillie, A. R., Gunn, B. M. & Robinson, P. 1957. Structural observation on Central Alpine region of New Zealand. *Royal Society of New Zealand transactions* 85, 113-129.
- Lisle, R. J. 1999. A new Variscan deformation map of England and Wales. *Tectonophysics* 309, 27-39.
- Little, T. A. & Roberts, A. P. 1997. Distribution and mechanism of Neogene to present-day vertical axis rotations, Pacific-Australian plate boundary zone, South Island, New Zealand. *Journal of Geophysical Research* 102(B9), 20,447-20,468.
- Little, T. A., Mortimer, N. & McWilliams, M. 1999. An episodic Cretaceous cooling model for the Otago-Marlborough Schist, New Zealand, based on  $40\text{ Ar}/^{39}\text{ Ar}$  white mica ages. *New Zealand Journal of Geology and Geophysics* 42, 305-325.
- Little, T. A. & Mortimer, N. 2001. Rotation of ductile fabrics across the Alpine Fault and Cenozoic bending of the New Zealand orocline. *Journal of the Geological Society, London* 158(2001), 745-756.
- Little, T. A., Holcombe, R. J. & Ilg, B. R. 2002a. Ductile fabrics in the zone of active convergence near the Alpine Fault, New Zealand: identifying the neotectonic overprint. *Journal of Structural Geology* 24, 193-217.
- Little, T. A., Holcombe, R. J. & Ilg, B. R. 2002b. Kinematics of oblique collision and ramping inferred from microstructures and strain in middle crustal rocks, central Southern Alps, New Zealand. *Journal of Structural Geology* 24, 219-239.
- Luyendyk, B. P. 1995. Hypothesis for Cretaceous rifting of East Gondwana caused by subducted slab capture. *Geology* 23, 373-376.
- MacKinnon, T. C. 1983. Origin of the Torlesse terrane and coeval rocks, South Island, New Zealand. *Geological Society of America Bulletin* 94, 967-985.
- Madin, I. 1988. Geology and neotectonics of the upper Manuherikia basin, Central Otago, New Zealand. *New Zealand Geological Survey Record* 27, 32.
- Makgill, K. P. & Norris, R. J. 1983. Recent movement on the Akatore Fault, east Otago, and its relationship to regional tectonics. Abstracts. In: *Pacific Science Conference*, 1, Dunedin, 158.

- Malavieille, J. 1987. Extensional shearing deformation and kilometer-scale 'a'-type folds in a Cordilleran metamorphic core complex (Raft River Mountains, northwestern Utah). *Tectonics* 6(4), 423-448.
- Markley, M. & Norris, R. J. 1999. Structure and neotectonics of the Blackstone Hill Antiform, Central Otago, New Zealand. *New Zealand Journal of Geology and Geophysics* 42, 205-218.
- Mayer, W. 1969. Petrology of the Waipapa Group near Auckland, New Zealand. *New Zealand Journal of Geology and Geophysics* 12, 412-435.
- Means, W. D. 1963. Mesoscopic structure and multiple deformation in the Otago Schist. *New Zealand Journal of Geology and Geophysics* 6, 801-816.
- Means, W. D. 1966. A macroscopic recumbent fold in schist near Alexandra, central Otago. *New Zealand Journal of Geology and Geophysics* 9(3), 173-194.
- Miller, J. M. & Gray, D. R. 1996. Structural signature of sediment accretion in a Paleozoic accretionary complex, southeastern Australia. *Journal of Structural Geology* 18, 1245-1258.
- Molnar, P., Atwater, T., Mammerickx, J. & Smith, S. M. 1975. Magnetic anomalies, bathymetry and the tectonic evolution of the South Pacific since the late Cretaceous. *Geophysical Journal of Royal Astronomical Society* 40, 383-420.
- Moore, R. R. & Johnson, S. E. 2000. Three-dimensional reconstruction and modelling of complexly folded surfaces using Mathematica.  
In: <http://www-texdev.mpce.mq.edu.au/GeoMath/>
- Mortimer, N. & Roser, B. P. 1992. Geochemical evidence for the position of the Caples-Torlese boundary in the Otago Schist, New Zealand. *Journal of Geological Society London* 149, 967-977.
- Mortimer, N. 1993a. Geology of the Otago Schist and adjacent rocks. Institute of Geological & Nuclear Sciences 1:500 000 geological map 7. Institute of Geological & Nuclear Sciences, Lower Hutt, New Zealand.
- Mortimer, N. 1993b. Jurassic tectonic history of the Otago Schist, New Zealand. *Tectonics* 12, 237-244.
- Mortimer, N. 1995. Triassic to early Cretaceous tectonic evolution of New Zealand terranes: A summary of recent data and integrated model. In: Mauk, J. L. & St. Gorge, J. D. (Eds.), *Proceedings of the 1995 PACRIM Congress*, Australian Institute of Mining & Metallurgy, Carlton, Victoria, Australia.
- Mortimer, N., Gans, P. B., Calvert, A. & Walker, N. W. 1999a. Geology and geochronometry of the east edge of the Median Batholith (Median Tectonic Zone): a new perspective on Permian to Cretaceous crustal growth of New Zealand. *The Island Arc* 8(3), 404-425.
- Mortimer, N., Tulloch, A. J., Spark, R. N., Walker, N. W., Ladley, E., Allibone, A. &

- Kimbrough, D. C. 1999b. Overview of the Median Batholith New Zealand: a new interpretation of the geology of the Median Tectonic Zone and adjacent rocks. *Journal of African Earth Science* 29, 257-268.
- Mortimer, N. 2000. Metamorphic discontinuities in orogenic belts: example of the garnet-biotite-albite zone in the Otago Schist, New Zealand. *Geologische Rundschau* 89, 295-306.
- Mortimer, N., Davey, F. J., Melhuish, A. & Yu, J. *subm.* Crustal structure across an extended Phanerozoic convergent orogen: Eastern Province and Median Batholith, New Zealand. *subm. to New Zealand Journal of Geology and Geophysics.*
- Muir, R. J., Weaver, S. D., Bradshaw, J. D., Eby, G. N. & Evans, J. A. 1995. The Cretaceous Separation Point batholith, New Zealand: granitoid magmas formed by melting of mafic lithosphere. *Journal of Geological Society London* 152, 689-701.
- Müller, R. D., Gaina, C., Roest, W. R. & Hansen, D. L. 2001. A recipe for microcontinent formation. *Geology* 29(3), 203-206.
- Needham, D. T. & MacKenzie, J. S. 1988. Structural evolution of the Shimanto Belt accretionary complex in the area of Gokase River, Kyushu, SW Japan. *Journal of the Geological Society London* 145, 1-10.
- Norris, R. J. & Cooper, A. F. 1977. Structure and metamorphism of the Haast Schist in the Kawarau Gorge and at Lake Hawea. *Geological Society of New Zealand, Queenstown Conference Field Trip Guides C1-C4.*
- Norris, R. J., Carter, R. M. & Turnbull, I. M. 1978. Cainozoic sedimentation in basins adjacent to a major continental boundary in southern New Zealand. *Journal of the Geological Society London* 135, 191-205.
- Norris, R. J. 1979. A geometrical study of finite strain and bending in the South Island. In: Walcott, R. I. & Creswell, M. M. (Eds.), *Origin of the Southern Alps*. Royal Society of New Zealand Bulletin 18, 21-28.
- Norris, R. J. & Craw, D. 1987. Aspiring terrane: an oceanic assemblage from New Zealand and its implications for terrane accretion in the southwest Pacific. In: Leitch, E. C. & Scheibner, E. (Eds.), *Terrane accretion and orogenic belts*. American Geophysical Union Geodynamic Series 19, 169-178.
- Norris, R. J., Koons, P. O. & Cooper, A. F. 1990. The obliquity-convergent plate boundary in the South Island, New Zealand: implications for ancient collision zones. *Journal of Structural Geology* 12, 715-725.
- Norris, R. J. & Bishop, D. G. 1990. Deformed metaconglomerates and textural zones in the Otago Schists, South Island, New Zealand. *Tectonophysics* 174, 331-349.
- Norris, R. J. & Cooper, A. F. 1995. Origin of small scale segmentation and transpressional thrusting along the Alpine Fault. *Geological Society of America Bulletin* 107, 231-240.



- Norris, R. J. & Cooper, A. F. 1997. Erosional control on the structural evolution of a transpressional thrust complex on the Alpine Fault, New Zealand. *Journal of Structural Geology* 19, 1323-1342.
- Norris, R. J. & Cooper, A. F. 2001. Late Quaternary slip rates and slip partitioning on the Alpine Fault, New Zealand. *Journal of Structural Geology* 23, 507-520.
- Odonne, F. & Vialon, P. 1987. Hinge migration as a mechanism of superimposed folding. *Journal of Structural Geology* 9, 835-844.
- Park, R. G. 1969. Structural correlation in metamorphic belts. *Tectonophysics* 7, 323-338.
- Passchier, C. W., Urai, J. L., van Loon, J. & Williams, P. F. 1981. Structural geology of the central Sesia Lanzo Zone. *Geologie en Mijnbouw* 60(4), 497-507.
- Passchier, C. W. & Trouw, R. A. W. 1996. *Microtectonics*. Springer, Berlin, 289p.
- Paull, R. K., Campbell, J. D. & Coombs, D. S. 1996. New information on the age and thermal history of probably Early Triassic siltstone near Kaka Point, South Island, New Zealand. *New Zealand Journal of Geology and Geophysics* 39, 581-584.
- Piazolo, S. & Passchier, C. W. 2002. Controls on lineation development in low to medium grade shear zones: a study from the Cap de Creus peninsula, NE Spain. *Journal of Structural Geology* 24(1), 25-44.
- Platt, J. P., Legget, J. K., Young, J., Raza, J. & Alam, S. 1985. Large-scale sediment underplating in the Makran Accretionary Prism, Southwest Pakistan. *Geology* 13, 507-511.
- Platt, J. P. 1986. Dynamics of orogenic wedges and the uplift of high-pressure metamorphic rocks. *Geological Society of America Bulletin* 97(9), 1037-1053.
- Pumpelly, R., Woff, J. E. & Dale, T. N. 1894. *Geology of the Green Mountains, Part III, Mount Greylock: its areal and structural geology*. U.S. Geological Survey Mon. 22, p.158.
- Ramberg, H. 1955. Natural and experimental boudinage and pinch-and-swell structures. *Journal of Geology* 63, 512-526.
- Ramberg, H. 1964. Selective buckling of composite layers with contrasted rheological properties, a theory for simultaneous formation of several orders of folds. *Tectonophysics* 1, 307- 341.
- Ramberg, H. & Ghosh, S. K. 1977. Rotation and strain of linear and planar structures in 3-dimensional progressive deformation. *Tectonophysics* 40, 309-337.
- Ramsay, J. G. 1960. The deformation of early linear structures in areas of repeated folding. *Journal of Geology* 68(1), 75-93.
- Ramsay, J. G. 1967. *Folding and fracturing of rocks*. Mc-Graw-Hill Books Co., New York, 568p.
- Ramsay, J. G., Casey, M. & Kligfield, R. 1983. Role of shear in development of the Helvetic fold-thrust belt of Switzerland. *Geology* 11, 439-442.

- Ramsay, J. & Huber, M. 1987. The techniques of modern structural geology. Volume 2: Folds and fractures. Academic Press, London, 309-700.
- Ramsay, J. G. & Lisle, R. J. 2000. The techniques of Modern Structural Geology. Volume 3: Applications to continuum mechanics in structural geology. Academic Press London, 701-1061.
- Rattenbury, M. S., Cooper, R. A. & Johnston, M. R. 1998. Geology of the Nelson area. Institute of Geological & Nuclear Sciences 1:250 000 geological map 9, Lower Hutt.
- Reilly, W. I. 1986. Crustal bending in Otago, New Zealand, from the evidence of geodetic measurements. In: Reilly, W. I. & Harford, B. E. (Eds.), Recent Crustal Movements of the Pacific Region, 24. Bulletin of the Royal Society of New Zealand, 65-73.
- Retallak, G. J. 1979. Middle Triassic coastal outwash deposits in Tank Gully, Canterbury, New Zealand. Journal of Royal Society of New Zealand 9, 397-414.
- Retallak, G. J. 1985. Triassic fossil plants from shallow marine rocks of the Murihiku Supergroup, New Zealand. Journal of the Royal Society of New Zealand 15, 1-26.
- Roser, B. P., Mortimer, N., Turnbull, I. M. & Landis, C. A. 1993. Geology and geochemistry of the Caples Terrane, Otago, New Zealand: compositional variations near a Permo-Triassic arc margin. In: Ballance, P. F. (Eds.), South Pacific Sedimentary Basins in Sedimentary Basins of the World, 2, 3-19.
- Roser, B. P. & Korsch, R. J. 1999. Geochemical characterization, evolution and source of a Mesozoic accretionary wedge: the Torlesse terrane, New Zealand. Geological Magazine 136, 493-512.
- Sample, J. C. & Fisher, D. M. 1986. Duplex accretion and underplating in an ancient accretionary complex, Kodiak Islands, Alaska. Geology 14, 160-163.
- Sample, J. C. & Moore, J. C. 1987. Structural style and kinematics of an underplated slate belt, Kodiak and adjacent islands, Alaska. Geological society of America Bulletin 99, 7-20.
- Sanderson, D. J. & Marchini, W. R. D. 1984. Transpression. Journal of Structural Geology 6, 449-458.
- Sengör, A. M. C. & Dewey, J. F. 1991. Terranology: vice or virtue? In: Dewey, J. F., Gass, I. G., Curry, G. B., Harris, N. B. W. & Sengör, A. M. C. (Eds.), Allochthonous Terranes. Cambridge University Press, 1-21.
- Skinner, D. N. B. 1972. Subdivision and petrology of the Mesozoic rocks of Coromandel (Manaia Hill Group). New Zealand Journal of Geology and Geophysics 15, 203-227.
- Skjernaas, L. 1975. Experiments on superimposed buckle folds. Tectonophysics 27, 255-270.
- Smith, E. G. C., Stern, T. & O'Brien, B. 1995. A seismic velocity profile across the central South Island, New Zealand, from explosion data. New Zealand Journal of Geology and Geophysics 38, 565-570.

- Spörli, K. B. 1978. Mesozoic tectonics, North Island, New Zealand. *Geological society of America Bulletin*. 89, 415-425.
- Spörli, K. B. 1979. Structure of the South Island Torlesse in relation to the origin of the Southern Alps. In: Walcott, R. I. & M.M., C. (Eds.), *The origin of the Southern Alps*. The Royal Society of New Zealand Bulletin 18, Wellington, 99-104.
- Spörli, K. B. & Ballance, P. F. 1988. Mesozoic ocean floor/continent interaction and terrane configuration, southwest Pacific area around New Zealand. In: Ben-Avraham, Z. (Eds.), *The Evolution of Pacific Ocean Margins*. Oxford Monographs on Geology and Geophysics 8, 176-190.
- Stock, J. & Molnar, P. 1987. Revised history of early Tertiary plate motion in the south-west Pacific. *Nature* 325, 495-499.
- Suggate, R. P. 1963. The Alpine Fault. *Transaction Royal Society of New Zealand Geology* 2, 105-129.
- Suggate, R. P. 1978. *The Geology of New Zealand*. New Zealand Government Printer, Wellington, 343.
- Sutherland, R. 1999. Cenozoic bending of New Zealand basement terranes and Alpine Fault displacement: a brief review. *New Zealand Journal of Geology and Geophysics* 42, 295-301.
- Sutherland, R. & Hollis, C. 2001. Cretaceous demise of the Moa plate and strike-slip motion at the Gondwana margin. *Geology* 29(3), 279-282.
- Sylvester, A. G. 1988. Strike-slip faults. *Geological Society of America Bulletin* 100, 1666-1703.
- Teyssier, C., Tikoff, B. & Markley, M. 1995. Oblique plate motion and continental tectonics. *Geology* 23(5), 447-450.
- Thiessen, R. L. & Means, W. D. 1980. Classification of fold interference patterns. *Journal of Structural Geology* 2, 311-316.
- Thiessen, R. L. & Haviland, T. 1986. A technique for the analysis of re-fold structures. *Journal of Structural Geology* 8(2), 191-200.
- Tikoff, B. & Teyssier, C. 1994. Strain modelling of displacement-field partitioning in transpressional orogens. *Journal of Structural Geology* 16(1575-1588).
- Tikoff, B. & Peterson, K. 1998. Physical experiments of transpressional folding. *Journal of Structural Geology* 20(6), 661-672.
- Treagus, S. H. 1973. Buckling instability of a viscous single-layer system, oblique to the principal compression. *Tectonophysics* 19, 271-289.
- Tulloch, A. J. & Rabone, S. D. C. 1993. Mo-bearing granodiorite porphyry plutons of the Early Cretaceous Separation Point Suite west Nelson, New Zealand. *New Zealand Journal of Geology and Geophysics* 36, 401-408.

- Turnbull, I. M. 1979a. Stratigraphy and sedimentology of the Caples terrane of the Thomson Mountains, northern Southland, New Zealand. *New Zealand Journal of Geology and Geophysics* 22, 555-574.
- Turnbull, I. M. 1979b. Petrography of the Caples terrane of the Thomson Mountains, northern Southland, New Zealand. *New Zealand Journal of Geology and Geophysics* 22, 709-727.
- Turnbull, I. M. 1981. Contortions in the schists of the Cromwell district, Central Otago, New Zealand. *New Zealand Journal of Geology and Geophysics* 24, 65-86.
- Turnbull, I. M. 1988. Sheet S133 – Cromwell. Geological map of New Zealand. Scale 1:63 360. Department of Scientific and Industrial Research, Wellington.
- Turnbull, I. M., Craw, D. & Norris, R. J. 1993. Pre-Miocene and post-Miocene deformation in the Bannockburn basin, central Otago, New Zealand. *New Zealand Journal of Geology and Geophysics* 36, 107-115.
- Turnbull, I. M. 2000. Geology of the Wakatipu area. Institute of Geological & Nuclear Sciences 1:250 000 geological map 17. Institute of Geological & Nuclear Sciences, Lower Hutt, New Zealand.
- Turnbull, I. M., Mortimer, N. & Craw, D. 2001. Textural zones in the Haast Schist - a reappraisal. *New Zealand Journal of Geology & Geophysics* 44, 171-183.
- Turner, F. J. & Weiss, L. E. 1963. Structural analysis of metamorphic tectonites. McGraw-Hill Book Co.
- Tünker, M. E. & Ring, U. 2001. Large-scale folding in the Otago Belt, New Zealand. *Journal of Conference Abstracts (EUGXI)* 6, 630.
- Vitaliano, C. J. 1968. Petrology and structure of the south-eastern Marlborough Sounds, New Zealand. *Bulletin of the New Zealand Geological Survey* 74.
- Waight, T. E., Weaver, S. D., Maas, R. & Eby, G. N. 1999. French Creek Granite and Hohonu mafic dike swarm, South Island, New Zealand: Late Cretaceous alkaline magmatism and the opening of the Tasman Sea. *Australian Journal Earth Science* 45, 823-835.
- Walcott, R. I. 1978. Present tectonics and late Cenozoic evolution of New Zealand. *Geophysical Journal of Royal Astronomical Society* 52, 137-164.
- Walcott, R. I. 1979. Plate motion and shear strain rates in the vicinity of the Southern Alps. *Bulletin of the Royal Society of New Zealand* 18, 5-12.
- Walcott, R. I. & Cresswell, M. M. 1979. The origin of the Southern Alps. *Bulletin of the Royal Society of New Zealand* 18, 147pp.
- Walcott, R. I. 1998. Modes of oblique compression: late Cenozoic tectonics of the South Island, New Zealand. *Review of Geophysics* 36, 1-26.
- Wandres, A. M., Weaver, S. D., Shelley, D. & Bradshaw, J. D. 1998. Change from calc-alkaline to adakitic magmatism recorded in the Early Cretaceous Darran Complex, Fjordland, New Zealand. *New Zealand Journal of Geology and Geophysics* 41, 1-14.

- Ward, C. M. & Spörli, K. B. 1978. Exceptionally large steeply plunging folds in the Torlesse terrane, New Zealand. *Journal of Geology* 87, 187-193.
- Watkinson, A. J. 1981. Patterns of fold interference: influence of early fold shapes. *Journal of Structural Geology* 3, 19-23.
- Weiss, L. E. 1959. The geometry of superposed folding. *Geological Society of America Bulletin* 70, 91-106.
- Wellman, W. H. 1955. New Zealand Quaternary tectonics. *Geologische Rundschau* 43, 238-257.
- Wellman, W. H. 1979. An uplift map for the South Island of New Zealand, and a model for uplift of the Southern Alps. *Bulletin of the Royal Society of New Zealand* 18, 13-20.
- White, S. 1996. Composition and zoning of garnet and plagioclase in Haast Schist, northwest Otago, New Zealand: implications for progressive regional metamorphism. *New Zealand Journal of Geology and Geophysics* 39, 515-532.
- Williams, P. F. 1985. Multiply deformed terrains - problems of correlation. *Journal of Structural Geology* 7, 269-280.
- Wilson, G. 1961. The tectonic significance of small-scale structures and their importance to the geologist in the field. *Annuaire de Société Géologique de Belgique* 84, 424-548.
- Winsor, C. N. 1991a. The relationship between the Hyde-Macraes Shear Zone, deformation episodes, and gold mineralization potential in eastern Otago, New Zealand. *New Zealand Journal of Geology and Geophysics* 34, 237-245.
- Winsor, C. N. 1991b. Low-angle shear zones in Central Otago, New Zealand - their regional extent and economic significance. *New Zealand Journal of Geology and Geophysics* 34, 501-516.
- Wood, B. L. 1963. Structure of the Otago Schists. *New Zealand Journal of Geology and Geophysics* 6(5), 641-680.
- Wood, B. L. 1978. The Otago schist megaculmination: its possible origins and tectonic significance in the Rangitata orogen of New Zealand. *Tectonophysics* 47, 339-368.
- Woodcock, N. H. 1977. Specification of fabric shapes using an eigenvalue method. *Geological Society of America Bulletin* 88, 1231-1236.
- Woodward, D. J. & Hatherton, T. 1975. Magnetic anomalies over southern New Zealand. *New Zealand Journal of Geology and Geophysics* 18, 65-82.
- Woodward, D. J. 1979. The crustal structure of the Southern Alps, New Zealand, as determined by gravity. *The Royal Society of New Zealand Bulletin* 18, 95-98.
- Wright, T. O. & Platt, L. B. 1982. Pressure dissolution and cleavage in the Martinsburg Shale. *American Journal of Science* 282(2), 122-135.
- Yardley, B. W. D. 1982. The early metamorphic history of the Haast Schists and related rocks of New Zealand. *Contribution to Mineralogy and Petrology* 81, 317-327.

## Acknowledgement

*Meinst du denn alles, was du sagst?  
Meinst du denn ernstlich, was du fragst?  
Wen kümmerts, was ich meine und sage:  
Denn alles Meinen ist nur Frage.  
(Johann Wolfgang von Goethe)*

I want to thank every-one, who has helped to get together this thesis  
- you know who you are.

## Curriculum Vitae

Maren Edda Tünker, geboren am 19.07.1971 in Mülheim an der Ruhr

1991 Abitur am Otto Pankok Gymnasium, Mülheim an der Ruhr

1991 Aufnahme des Geologie-Studiums an der Ruhr-Universität Bochum

1993 erster Teil des Vordiploms Geologie,

Aufnahme des Hauptstudiums mit Schwerpunkt Ingenieurgeologie/  
Hydrogeologie

1994 zweiter Teil des Vordiploms Geologie,

Aufnahme des Hauptstudiums mit Schwerpunkt Endogene Geologie

1995 Diplomkartierung "Geologie der Sole- und Glencoul Thrust südlich des  
Loch Glencoul, Schottland"

1997 Diplomarbeit "Die strukturelle Entwicklung der Phyllit-Quarzit Einheit  
im Raum Kondokinigi, SW Kreta, Griechenland"

1998 Diplom der Geologie der Ruhr-Universität Bochum

1999 Aufnahme des Promotionsstudiums an der Johannes Gutenberg-Universität

Mainz mit dem vorläufigen Titel "Tektonometamorphe Analyse großmaßstäblicher  
Deckenfalten im Otago Akkretionskeil, Neuseeland"